

Corrosion inhibition of mild steel in 15 wt% HCl solution by synthetic and green compounds

Ajayi Olorunfemi Michael

A thesis submitted to the University of Nottingham for the degree of Doctor of Philosophy

November 2018

Abstract

Registration, Evaluation, Authorization, and restriction of CHemicals (REACH) legislation, in conjunction with Paris Commission (PARCOM) recommendations (1991), are driving research into environmentally friendly alternatives to currently-used corrosion inhibitors. The main focus of this thesis is on compounds of plant-origin because they contain components which can be extracted by simple procedures. These plant extracts are relatively benign in their environmental impact compared to the highly toxic compounds, including propargyl alcohol (PA) and 2- mercaptobenzimidazole (MI), which are currently in use to mitigate the corrosion of oil and gas wells during acidizing treatment.

The four 'green' corrosion inhibitors, chosen for this research, were extracts from durum wheat (DW), aloe vera gel (AV), inulin (IN; extracted from Jerusalem artichoke), and broccoli (BC).

The corrosion inhibition performance of PA, MI, DW, BC, IN and AV for mild steel (MS), immersed in 15wt% HCl solution in the absence and presence of the inhibitors, has been investigated. Weight loss and electrochemical (open circuit potential (OCP), potentiodynamic polarization and linear polarization resistance) were used to determine the corrosion inhibition performance of the inhibitors with a variation of concentration of the inhibitors, solution temperature (20-60°C) and immersion time (5- 192 h). Also, gas chromatography-mass spectrometry (GC- MS) and Fourier transform infrared (FTIR) spectroscopy were further employed to characterize all the chemical compounds to determine their main constituents and functional groups. The as-received MS surfaces were analyzed after immersion in uninhibited and inhibited solutions using scanning electron microscopy (SEM), energy dispersive X-ray spectroscopy (EDS),

and 3D profilometry. X-ray photoelectron spectroscopy (XPS) was performed to determine the nature and composition of the protective film formed at the MS/HCl solution interface.

Potentiodynamic polarization results showed that all the studied inhibitors suppressed both the anodic dissolution of MS and cathodic hydrogen evolution – this implies that they can be classified as mixed- type corrosion inhibitors in the corrosive environment investigated.

Concentration studies showed that the corrosion rate of MS decreased with increase in the concentration of all the inhibitors until a point where a further increase in strength did not markedly change the corrosion rate. AV required significant concentration (100 g/L) in the electrolyte to be effective. The study also showed that the corrosion inhibition performance of PA was stable with an increase in temperature (over 99% IE), which indicated that the inhibition performance of PA in 15 wt% HCl was not temperature dependent. However, the corrosion inhibition performance of MI, DW, and BC decreased with an increase in solution temperature.

The inhibition performance of IN and AV decreased significantly with the increase in temperature especially at 60°C after 24 h immersion. At 20°C, the corrosion inhibition performance of PA (99%), MI (over 84%) and IN (80%) remained stable with prolonged immersion time (up to192 h). However, DW, BC, and AV decreased slightly at the onset but were later stable throughout the immersion time.

The adsorption of both the synthetic and 'green' inhibitors onto the MS surface followed the Langmuir adsorption isotherm. Thermodynamic parameters suggested that PA, MI and DW interacted with the MS surface at 20°C via both physical and

chemical adsorption, while BC, IN and AV were physically adsorbed onto the MS surface.

SEM/EDS examinations revealed that the MS surfaces treated with different inhibitors were less corroded compared to the uninhibited surface. 3D profilometry showed that MS surfaces, after immersion in 15wt% HCl in the presence of various inhibitors, have lower surface roughness values. MS exposed to PA inhibited solution had the lowest surface roughness. XPS studies showed that the studied inhibitors adsorbed at the MS/solution interface, then formed a protective layer.

The corrosion inhibition performance of the synthetic inhibitors (PA and MI) were better than the 'green' inhibitors for the protection of MS in 15wt % HCl. However, DW and BC performed better than other 'green' inhibitors in all the experimental conditions studied. Hence, they may be promising candidate inhibitors. PA performed much better than all the inhibitors investigated, while AV poorly protected MS against corrosion in the environment/conditions studied.

The economic analysis of the inhibitors showed that DW and BC were cheaper than the commercial inhibitors (PA and MI), while IN and AV were costlier. The high concentration (100 ml/L HCl) and the cost of AV are pointers that it may not currently be economically viable on an industrial scale.

List of conferences

- Ajayi Olorunfemi Michael, Nicola Everitt, and Katy Voisey (2017), "**Corrosion inhibition of mild steel in 15wt% HCl by durum wheat**". **EUROCORR2017:**20th International Corrosion Congress and Process Safety Congress, 3 -7 September 2017, Prague, Czech Republic. (*Poster presentation*)

- Katy Voisey, Ajayi Olorunfemi Michael, and Nicola Everitt (2016), "**Evaluation of inulin and aloe vera as green corrosion inhibitors for mild steel in 15wt% HCl**" **EUROCORR2016**: Advances in linking science to engineering, 11-15 September 2016, Montpellier, France. (*Poster presentation*)

Dedication

This PhD thesis is dedicated to the liberation commission for the wisdom, knowledge and understanding.

To Him alone be all the glory!

Acknowledgements

I want to express my sincere appreciation to my supervisors, Dr. Katy Voisey, and Dr. Nicola Everitt, for their valuable inputs and significant contributions towards the completion of this research. I have learned a lot from you during the period of my study at the University of Nottingham.

I would also like to use this medium to thank all members of staff at Wolfson building- Martin Roe and Dr Deen Zang for the technical support and training offered during my experiments. Also, I thank Dr. Emily Smith for the XPS training sessions and her continuous guidance when I was analysing my XPS data. Thanks to Dr Mick Cooper for the GC-MS training.

I am also grateful to my loving and caring wife (**Dr AJAYI Ifeoluwa Leah**) and my son (**Nathaniel**) for their understanding and support throughout my PhD programme.

I sincerely appreciate the University of Nottingham for offering me the prestigious Dean of Engineering scholarship to carry out this research.

Table of Contents

Abstract ..... **i**
List of conferences ..... **iv**
Dedication ..... **v**
Acknowledgements ..... **vi**
Table of Contents ..... **vii**
List of Figures ..... **xii**
List of Tables ..... **xvi**
List of abbreviations and symbols ..... **xviii**
CHAPTER ONE GENERAL INTRODUCTION **1**
1.0 Introduction 2
1.1 Objectives 4
1.2 Thesis structure 5
CHAPTER TWO LITERATURE REVIEW **7**
2.1 Introduction 8
2.2 Basics of corrosion 8
2.3 Electrochemical aqueous corrosion 9
2.4 Corrosion in the oil and gas industry 12
2.4.1 Types of corrosion in the oil and gas industry 14
2.4.2 Acidizing (acid treatment) 16
2.5 Economics of corrosion 18
2.6 Corrosion control measures 20
2.6.1 Inspection and monitoring 20
2.6.2 Proper material selection 21
2.6.3 Coatings 21
2.6.4 Cathodic protection 22
2.6.5 Corrosion inhibition 23
2.7 Adsorption isotherm 34
2.8 Currently used corrosion inhibitors for acid treatment operations 36
2.8.1 Propargyl alcohol (PA) 40
2.8.2 2-mercaptobenzimidazole (MI) 44
2.8.3 Mixed corrosion inhibitors 48
2.8.4 Natural products as corrosion inhibitors in HCl solution 49

2.9 Factors influencing the performance of corrosion inhibitors 60
2.9.1 Inhibitor concentration 60
2.9.2 Immersion time 62
2.9.3 Solution temperature 63
CHAPTER THREE 66
EXPERIMENTAL METHODOLOGY 66
3.1 Introduction 67
3.2 Materials 69
3.2.1 Synthetic inhibitors 69
3.2.2 Green inhibitors 70
3.2.3 Test solution 71
3.3 Sample preparation 72
3.4 Corrosion testing 74
3.4.1 Weight loss measurements 74
3.4.2 Electrochemical measurements 75
3.5 Material characterisation 77
3.5.1 X-ray photoelectron spectroscopy (XPS) 77
3.5.2 Scanning electron microscopy (SEM) and energy dispersive X-ray spectroscopy (EDS) 79
3.5.3 Gas Chromatography-Mass Spectroscopy (GC-MS) 80
3.5.4 Attenuated total reflectance-Fourier transform infrared (ATR-FTIR) Spectroscopy 82
CHAPTER FOUR 84
ESTABLISHING CORROSION INHIBITION EFFECT OF THE INHIBITORS 84
4.1 Introduction 85
4.2 Determination of suitable acid volume per sample 85
4.3 Effect of concentration on corrosion inhibition 86
4.4 Effect of temperature on corrosion of MS 90
4.4.1 Weight loss results 91
4.4.2 Electrochemical results 95
4.5. Effect of immersion time on corrosion of MS 104
4.6 Characterization of MS sample surfaces 110
4.6.1 Scanning electron microscopy (SEM) 110
4.6.2 Energy dispersive spectroscopy (EDS) of the MS surfaces 112
4.6.3 Topography measurements 112

CHAPTER FIVE ADSORPION ISOTHERM AND CHEMICAL ANALYSIS 115

5.1 Introduction..... 116

5.2 Adsorption isotherms 116

5.3 Activation energy studies 122

5.4 Chemical composition analysis of the inhibitors 124

5.4.1 FTIR of different inhibitors..... 124

5.4.2 Gas–Chromatography Mass Spectrometry (GC-MS)..... 129

CHAPTER SIX ANALYSIS OF THE NATURE/COMPOSITION OF THE ADSORBED FILM..... 140

6.1 X-ray photoelectron spectroscopy (XPS) 141

6.2 FTIR analysis of the adsorbed inhibiting film 157

CHAPTER SEVEN 160

DISCUSSION OF INDIVIDUAL CORROSION INHIBITOR..... 160

7.1 Overview 161

7.2 Propargyl alcohol (PA)..... 162

7.2.1 Effect of concentration on PA performance..... 162

7.2.2 Effect of immersion time on PA performance 163

7.2.3 Effect of temperature on PA performance 164

7.2.4 Surface characterization of MS treated with PA 166

7.2.5 Corrosion inhibition mechanism of PA 167

7.2.6 Summary 173

7.3 2-Mercaptobenzimidazole (MI) 174

7.3.1 Effect of MI concentration on MS corrosion inhibition 174

7.3.2 Effect of immersion time on inhibition performance of MI..... 177

7.3.3 Effect of temperature on the inhibition performance of MI..... 179

7.3.4 Surface characterization of MS in the presence of MI 181

7.3.5 Corrosion inhibition mechanism of MI..... 182

7.3.6 Summary 188

7.4 Inulin (IN)..... 189

7.4.1 Effect of concentration on IN performance..... 189

7.4.2 Effect of immersion time on inulin performance 191

7.4.3 Effect of temperature on IN performance 192

7.4.4 Surface characterization of MS surface in the presence of IN 194

7.4.5 Corrosion inhibition mechanism of IN 195

7.4.6 Summary 200
7.5 Durum wheat extract 201
7.5.1 Effect of concentration on durum wheat extract performance 201
7.5.2 Effect of immersion time on DW performance 202
7.5.3 Effect of temperature on the inhibition performance of DW 204
7.5.4 Surface characterization of MS surface in the presence of DW extracts .. 206
7.5.5 Corrosion inhibition mechanism of DW extracts 207
7.5.6 Summary 211
7.6 Broccoli 212
7.6.1 Effect of concentration on broccoli performance 212
7.6.2 Effect of immersion time on BC performance 214
7.6.3 Effect of temperature on BC performance 215
7.6.4 Surface characterization of MS in the presence of BC extracts 216
7.6.5 Corrosion inhibition mechanism of BC extracts 217
7.6.6 Summary 221
7.7 Aloe vera gel 222
7.7.1 Effect concentration on aloe vera gel performance 222
7.7.2 Effect of immersion time on aloe vera gel performance 223
7.7.3 Effect of temperature on aloe vera gel performance 223
7.7.4 Surface characterization of MS surface treated with aloe vera gel 224
7.7.5 Corrosion inhibition mechanism of aloe vera gel 225
7.7.6 Summary 228
CHAPTER EIGHT 229
GENERAL DISCUSSION 229
8.1 Introduction 230
8.2 Effect of Temperature 232
8.3 Effect of time on inhibition performance 233
CHAPTER NINE 235
ECONOMIC AND ENVIRONMENTAL IMPACTS OF GREEN INHIBITORS 235
9.1 Introduction 236
9.2 Economics of corrosion inhibitors 236
9.3 Durum wheat inhibitor 238
9.3.1 Environmental impact 238
9.3.2 Economic impact 238

9.4 Inulin 238
9.4.1 Environmental impact 238
9.4.2 Economic impact 239
9.5 Broccoli inhibitor 240
9.5.1 Environmental impact 240
9.5.2 Economic impact 240
9.6 Aloe vera inhibitor 241
9.6.1 Environmental impact 241
9.6.2 Economic impact 241
CHAPTER TEN 242
CONCLUSIONS AND FUTURE WORK 242
10.1 CONCLUSIONS 243
10.2 FUTURE WORK 246
References 248

List of Figures

Figure 2-1 Basic corrosion cell. 10
Figure 2-2 A schematic representation of the corrosion on a steel surface in an acidic solution showing both the anodic and cathodic sites of the steel. 12
Figure 2-3 An offshore platform showing some likely corrosion sources including acidizing 13
Figure 2-4 Annual total corrosion cost breakdown in the oil and gas industry 19
Figure 2-5 Global corrosion inhibitors market volume share in 2012 24
Figure 2-6 Physical adsorption of a corrosion inhibitor on a metal surface due to electrostatic interaction (Van der Waals forces) 26
Figure 2-7 Chemical adsorption of a corrosion inhibitor on a metal surface due to covalent bond. 27
Figure 2-8 A general classification of corrosion inhibitors 28
Figure 2-9 Potentiodynamic polarisation curves showing the electrochemical behaviour of a metal in a solution in the presence of an anodic inhibitor 31
Figure 2-10 Potentiodynamic polarisation curves showing the electrochemical behaviour of a metal in a solution in the presence of a cathodic inhibitor 32
Figure 2-11 Potentiodynamic polarisation curves showing the electrochemical behaviour of a metal in a solution in the presence of a mixed inhibitor (a) and in the absence of inhibitor (b). 33
Figure 2-12 Chemical structure of propargyl alcohol 40
Figure 2-13 Chemical structure of MI 44
Figure 2-14 Chemical structure of IN 56
Figure 2-15 Variation of inhibition efficiency with different concentrations of marigold flower extracts by weight loss and electrochemical measurements 61
Figure 3-1 Overview of the experimental methods used in this work. 68
Figure 3-2 Chemical molecular structures of (a) PA and (b) MI. 69
Figure 3-3 (a) Aloe vera plant; (b) Extracted gel; (c) 15% HCl solution with aloe vera gel 71
Figure 3-4 Photograph of the as-received MS sample used for the weight loss test... 73
Figure 3-5 (a) Schematic diagram and (b) a photograph of the working electrode used for the electrochemical tests. 74

Figure 3-6 A schematic representation of a three-cell electrochemical set-up 76
Figure 3-7 A schematic representation of the basic components of XPS..... 78
Figure 3-8 Interaction volume of the incident beam of electrons with a sample [161].
Figure 3-9 A schematic represenatton of GC-MS system. 81
Figure 3-10 Schematic illustration of ATR-FTIR principle. 83
Figure 4-1 The variation in weight loss of the as-received MS with volume of 15 wt. % HCl after 1, 2 and 6 h of immersion at 20°C 86
Figure 4-2 Dependence of corrosion inhibition performance on different concentrations of PA, MI, DW, BC and IN for MS in 15 wt.% HCl at 20°C after 5 h 89
Figure 4-3 Dependence of corrosion inhibition performance on different concentrations of AV for MS in 15 wt.% HCl solution at 20°C after 5 h 90
Figure 4-4 Variation of inhibition efficiency with temperature (20, 40 and 60°C) for MS in 15 wt. % HCl containing 7g/L (PA, MI, and DW), 10 g/L (BC and IN) and 100 g/L AV after 5 h immersion 92
Figure 4-5 Temperature dependence of inhibition efficiency for MS in 15 wt.% HCl containing 7 g/L (PA, MI, and DW), 10 g/L (BC and IN) and 100 g/L AV for 24 h immersion 95
Figure 4-6 Variation of OCP as a function of time recorded for MS immersed 15 wt.% HCl in the absence and presence of PA, MI, DW, BC and IN at 20°C after 1 h immersion 96
Figure 4-7 Variation of OCP as a function of time recorded for MS immersed 15 wt.% HCl in the absence and presence of PA, MI, DW, BC and IN at 40°C after 1 h immersion..... 97
Figure 4-8 Variation of OCP as a function of time recorded for MS immersed 15 wt.% HCl in the absence and presence of PA, MI, DW, BC and IN at 60°C after 1 h immersion..... 98
Figure 4-9 Effect of temperature on the potentiodynamic polarisation curves for MS in 15 wt% HCl solution in the absence and presence of various inhibitors in the temperature range of 20-60°C 100
Figure 4-10 Effect of immersion time (5-192h) on inhibition efficiency for MS in 15 wt.% HCl in the presence of PA, MI, DW, BC and IN at 20°C. 105
Figure 4-11 Effect of immersion time (5-24h) on inhibition efficiency for MS in 15 wt.% HCl in the presence of 100 g/L at 20 °C..... 106

Figure 4-12 Effect of immersion time on inhibition efficiency for MS in 15 wt.% HCl in the presence of optimum concentrations of inhibitors at 40°C. 107
Figure 4-13 Effect of immersion time on inhibition efficiency for MS in 15 wt. % HCl in the presence of different inhibitors at 60°C 109
Figure 4-14 SEM images of MS specimens in 15 wt% HCl. (a) before immersion, (b) after immersion 111
Figure 4-15 3-D profiles obtained by profilometer 114
Figure 5-1 Langmuir adsorption isotherm plot for MS in 15 wt.% HCl containing different concentrations of PA, MI, DW, BC and at 20, 40 and 60°C. 119
Figure 5-2 Langmuir isotherm plot for the adsorption of AV on the MS surface in 15 wt. % HCl at 20°C after 5 h immersion. 120
Figure 5-3 Arrhenius plots for MS corrosion in the absence and presence of optimum concentrations PA, MI, DW, BC, IN and AV in 15wt% HCl solution after 24 h 123
Figure 5-4 FTIR absorption spectrum of as-received PA. 124
Figure 5-5 FTIR absorption spectrum of as-received MI. 125
Figure 5-6 FTIR absorption spectrum of as-received DW. 126
Figure 5-7 FTIR absorption spectrum of BC. 127
Figure 5-8 FTIR absorption spectrum of IN. 128
Figure 5-9 FTIR absorption spectrum of AV. 129
Figure 5-10 GC-MS chromatogram of hexane extract of IN. 130
Figure 5-11 Molecular structures of the major components in inulin hexane extract131
Figure 5-12 GC-MS chromatogram of hexane extract of BC. 132
Figure 5-13 Molecular structures of different major constituents in broccoli hexane extract
Figure 5-14 GC-MS chromatogram of the hexane extract of AV gel 134
Figure 5-15 Molecular structures of different major constituents in the hexane extract of Aloe Vera gel 136
Figure 5-16 GC-MS chromatogram of hexane extract of DW. 138
Figure 5-17 Molecular structures of different major constituents in durum wheat hexane extract 139
Figure 6-1 XPS survey scan for MS surface after 5 h immersion in 15 wt.% HCl in the absence and presence of optimum concentration of PA, MI, DW, BC and IN at 20°C 144

Figure 6-2 XPS deconvoluted profile of Fe 2p core level for MS in 15 wt.% HCl in the absence and presence of inhibitors showing different oxidation states..... 146
Figure 6-3 XPS deconvoluted profile of C 1s for MS in 15 wt.% HCl..... 150
Figure 6-4 XPS deconvoluted profile of O 1s core level for MS in 15 wt% HCl 152
Figure 6-5 XPS deconvoluted profile of N 1s for MS in 15 wt% HCl..... 155
Figure 6-6 FTIR spectra of (a) as-received PA; (b) film formed at the MS immersed in 15wt% HCl..... 158
Figure 7-1 Schematic representation of possible corrosion inhibition mechanism for MS in 15wt% HCl solution containing 7 g/L PA..... 172
Figure 7-2 possible schematic representation of the effect of concentration on the corrosion rate of MS in 15wt% HCl. 175
Figure 7-3 Time-dependence of inhibition efficiency of MI for MS in 15wt% HCl solution..... 178
Figure 7-4 Protonation of MI in acidic solution..... 185
Figure 7-5 Schematic representation of the likely inhibition corrosion mechanism of MS in 15wt% HCl in the presence of MI after 5 h..... 187
Figure 7-6 Possible schematic representation of the effect of inulin concentration on corrosion inhibition performance 191
Figure 7-7 Inulin-HCl solution (a) before degradation (b) after the weight loss test at 60°C 193
Figure 7-8 Schematic illustration of possible physical adsorption mechanism 199
Figure 7-9 Dependence of corrosion rate and inhibition efficiency on immersion time for MS in 15wt% HCl containing 7g/l DW at 20°C..... 203
Figure 7-10 DW-HCl solution (a) before heating (b) after heating to 60°C for 24 h. 205
Figure 7-11 Schematic representation of the adsorption strength of BC on the MS surface with increasing concentration resulting in a decrease of the corrosion rate. 213
Figure 7-12 Possible adsorption mechanism for the inhibition of MS corrosion. 220
Figure 7-13 Proposed schematic representation of aloe vera gel adsorption mechanism on the MS surface..... 227

List of Tables

Table 2-1 Inhibition efficiencies and/or corrosion rate for different materials in different acidic solutions. 38
Table 2-2 Summary of work on propargyl alcohol as corrosion inhibitors..... 43
Table 2-3 Summary of work on 2-mercaptobenzimidazole as corrosion inhibitors. .. 47
Table 2-4 Inhibition efficiencies of different plant extracts used as corrosion inhibitors in various HCl solutions for different metals as reported in the articles 53
Table 2-5 Corrosion inhibition efficiency of IN for N-80 steel in 15wt% HCl solution at 65 °C 57
Table 3-1 Chemical compositional information of the reference synthetic inhibitors. 69
Table 3-2. The chemical composition of the as-received mild steel specimen..... 72
Table 4-1 Weight loss and corrosion rate data of MS in 15 wt.% HCl in the absence and presence of different concentrations of PA, MI, DW, BC, IN and AV after 5 h of immersion at 20°C. 87
Table 4-2 Corrosion rate data of MS in 15 wt. % HCl in the absence and presence of different inhibitors at a temperature range from 20-60°C after 5 h immersion 91
Table 4-3 Effect of temperature on the corrosion rate of MS in 15 wt. % HCl without and with different inhibitors (PA, MI, DW, BC, IN and AV) after 24 h..... 93
Table 4-4 Electrochemical polarisation parameters for MS in 15 wt% HCl in the absence and presence of PA, MI, DW, BC and IN in the temperature range of 20- 60°C 101
Table 4-5 Linear polarisation resistance data recorded for MS in 103
15 wt.% HCl in various inhibitors at 20, 40 and 60°C after 1 h OCP. 103
Table 4-6 EDS data of MS in 15 wt. % HCl in the absence and presence of optimum concentrations of PA, MI, DW, IN, BC and AV gel at 60°C after 5 h. 112
Table 4-7 Mean surface roughness (S_a) of unexposed and exposed MS in uninhibited and inhibited 15wt% HCl at 60°C after 5 h of immersion..... 113
Table 5-1 Equilibrium constant (K_{ads}) and Gibbs free energy of adsorption (..... 121
Table 5-2 Activation parameter for MS in 15wt% HCl in the absence and presence of an optimum concentration of PA, MI, DW, BC, IN and AV after 24 h..... 123
Table 5-3 Identified constituents from a hexane extract of IN. 130
Table 5-4 Identified components from a hexane extract of BC 132

Table 5-5 Identified constituents of the hexane extract of AV gel. 135
Table 5-6 Identified constituents from the hexane extract of DW. 138
Table 6-1 XPS composition for MS immersed in 15 wt.% HCl in the absence and presence of 7 g/L (PA, MI, DW) and 10 g/L IN at 20°C after 5 h immersion. 145
Table 6-2 Relative intensity (%) of Fe 2p core level for untreated and treated MS sample. 148
Table 6-3 Binding energies (eV), (relative intensity) and their assignment for deconvoluted O 1s profile 153
Table 6-4 Binding energies, relative intensity and their assignment for deconvoluted N 1s profile 156
Table 7-1 Comparison of the inhibition efficiency at a different concentration of PA obtained in the present work with those reported in the literature 163
Table 7-2 Comparison of the inhibition efficiency of MI obtained in this work with literature. 176
Table 7-3 Comparison of the variation of temperature on the inhibition performance of MI. 181
Table 7-4 Comparison of the ΔG_{ads} obtained for MI in this work, and that reported in the literature 183
Table 7-5 Comparison of inhibition efficiency of IN in this work with previous studies. 190
Table 7-7 Apparent activation energy values and adsorption mechanism obtained in the present work and those reported in the literature. 197
Table 7-8 Comparison of the corrosion rate of the present work with plant corrosion inhibition reported for MS in HCl solution. 201
Table 7-9 Comparison of the activation energy for DW and other green inhibitors in HCl medium. 208
Table 7-13 Possible adsorption sites of the major constituents of BC 217
Table 8-2 Effect of temperature on inhibition performance for different inhibitors after 24 h immersion 232
Table 9-1 The cost of optimum concentration of inhibitor per liter of 15wt% HCl solution. 237

List of abbreviations and symbols

AV	Aloe vera gel extract
At%	Atomic percent
BC	Broccoli extract
CI_s	Corrosion inhibitors
Cl	Chlorine
DW	Durum wheat extract
E_a	Activation energy
E_{cor}	Corrosion potential
EDS	Energy dispersive spectroscopy
eV	electron volts
Fe	Iron
FTIR	Fourier transform infrared spectroscopy
GCMS	Gas spectroscopy mass spectrometry
GDP	Gross domestic product
g/L	gram per litre
HCl	Hydrochloric acid
h	hour
IN	Inulin
K_{ads}	Equilibrium adsorption constant
kV	kilovolts
M	Molarity
MI	2-Mercaptobenzimidazole
mL	Millilitre
MS	Mild steel
OCP	Open circuit potential
PA	Propargyl alcohol
ppm	parts per million
SE	Secondary electron

S_a	surface roughness
XPS	X-ray photoelectron spectroscopy
θ	Surface coverage
ø	Diameter
η	Inhibition efficiency
°C	Celsius
β_a	Tafel anodic slope
β_c	Tafel cathodic slope

CHAPTER ONE

GENERAL INTRODUCTION

1.0 Introduction

Corrosion is the degradation process that results from the reaction of a material such as a metal with its environment [1]. It has a significant effect on safety, environment, and the economy. The global cost of corrosion was estimated to be US$2.5 trillion, which is about 3.4% of the Gross Domestic Product (GDP) of the world [2]. The investigation of corrosion problems in the oil and gas industry is vital because the total annual cost incurred on corrosion is about $1.37 billion [3]. Acidizing is one of the stimulation techniques employed to enhance the productivity of an oil and gas well. The acidizing treatment is achieved by pumping 5-28wt% HCl solution into an oil well to open new flow channels in the rock formation or enlarge the existing ones [3, 4]. However, a standard 15wt% HCl is commonly employed because most primary inhibitors are soluble in it [4]. Also, 15wt% HCl solution is used to remove iron oxides, and carbonate minerals in a wellbore at a temperature up to 60°C [4, 5].

Low-grade carbon steel is used widely in oil field applications because of its low cost and excellent mechanical properties including high tensile strength, ductility, malleability [6]. However, exposure of this material to an aggressive environment during the acidizing process results in severe corrosion. Consequently, inhibitors are introduced into an oil well to protect this material against corrosion. Synthetic organic compounds containing heteroatoms such as nitrogen (N), sulphur (S), oxygen (O) atoms as well as multiple bonds are effective corrosion inhibitors [7-9]. However, these synthetic inhibitors are highly toxic [10, 11]. For example, Gloria and Nick [11] reported that PA irritates the eyes and the skin; and that it is dangerous to life when ingested because it produces highly toxic vapour even with short term exposure. Hence, their use is highly discouraged. The development of environmentally friendly (green)

inhibitors, especially of plant-origin is an area of continuous research in the academia and industry because plants are biodegradable, non-toxic, renewable, readily available as well as contain incredible phytochemicals which can be extracted by simple procedures [12, 13].

The aim of this thesis is to investigate the possibility of using extracts of durum wheat (DW), broccoli (BC), aloe vera gel (AV) as well as inulin (extract from Jerusalem artichoke) as green corrosion inhibitors for mild steel (MS) corrosion inhibition, applicable in the oilfield aggressive environment (15wt% HCl solution) and compared with the standard industrial inhibitors.

DW was selected as one of the green inhibitors because it contains electron-rich oxygen and nitrogen atoms as well as pi-electrons in its double bond that can donate electrons to the vacant d-orbital of iron atoms. BC was chosen due to the presence of oxygen, sulphur, and pi-electrons in the double bonds present in its constituents. IN was selected as one of the green inhibitors because it has several oxygen atoms in its molecular structure which can act as nucleophiles [14]. Also, IN has been reported as an effective corrosion inhibitor in 15wt% HCl solution, but the analysis of the corrosion inhibition mechanism and sample characterisation were not done [15]. Lastly, the presence of constituents like proteins (lectin), amino acids, carbohydrates (manna cellulose) having several oxygen and nitrogen atoms as well as pi-electrons in its aromatic ring that can act as adsorption centres for binding to the vacant d-orbital of iron atom makes AV a suitable candidate [16].

1.1 Objectives

The following specific objectives are defined to achieve the aim of the research:

1. To select green corrosion inhibitors that would be effective in oilfield conditions, based on a review of the current literature.
2. To determine the performance of the candidate green inhibitors compared to the commercially used corrosion inhibitors, propargyl alcohol (PA) and 2- mercaptobenzimidazole (MI) and also the effect of some factors including temperature and time of immersion on the effectiveness of corrosion inhibition using chemical (weight loss) and electrochemical measurements (open circuit potential (OCP), potentiodynamic polarisation (PDP) and linear polarisation resistance (LPR).
3. To characterise the adsorbed film formed at the MS/solution interface using X- ray photoelectron spectroscopy (XPS), scanning electron microscopy (SEM) and energy dispersive spectroscopy (EDS).
4. To establish the economic and environmental impacts of green inhibitors.

1.2 Thesis structure

This thesis has 10 chapters. The content of each chapter is presented below:

Chapter 1 presents the corrosion problems encountered during the acidizing process of oil well, the total annual cost incurred on corrosion in the oil and gas industry, and the possibility of using plant-based inhibitors to mitigate MS corrosion in the oil and gas corrosive environment.

Chapter 2 outlines the basics of corrosion, the corrosion problems faced in the oil field applications, and literature review on the commercial and green inhibitors that are presently used in the oil and gas industry to protect MS against corrosion.

Chapter 3 reports the experimental procedures used for evaluating the corrosion behaviour of MS in the absence and presence of different inhibitors as well as the material characterisation techniques.

Chapter 4 presents the basic results establishing corrosion inhibition effect of PA, MI, DW, BC, IN and AV using chemical (weight loss) and electrochemical (open circuit potential (OCP), potentiodynamic polarization and linear polarization resistance) as well as characterization of the inhibiting film formed on the MS surface using SEM and EDS.

Chapter 5 describes the chemical analysis of the selected candidate plant-based inhibitors (DW, BC, IN and AV) using FTIR and GCMS as well as the adsorption isotherm analysis of the different inhibitors investigated.

Chapter 6 elucidates the results of the analysis of the adsorbed film by XPS after exposure of the MS in 15wt% HCl solution in the absence and presence of different inhibitors using weight loss measurements after 5 h immersion at 20°C.

Chapter 7 presents a discussion on the effect of concentration, immersion times and solution temperature on the inhibition performance of each of the inhibitors. Also, the surface characterisation of the MS surface treated with each inhibitor and the corrosion inhibition mechanism are discussed.

Chapter 8 describes the economic and environmental impacts of the selected candidate plant-based inhibitors (DW, BC, IN and AV) in the present study.

Chapter 9 presents the general discussion on the inhibition performance of the commercially available and the plant-based inhibitors.

Chapter 10 presents the conclusions of the undertaken research and the recommended future work.

CHAPTER TWO

LITERATURE REVIEW

2.1 Introduction

The literature review chapter presents the basics of corrosion, the economics of corrosion, an overview of corrosion inhibitors, the mechanism of corrosion inhibition in the presence of inhibitors and the environmental factors that affect the performance of corrosion inhibitors. This chapter also covers currently used corrosion inhibitors and the need for environmentally friendly alternatives. Also, the effect of acidization on metallic structures, especially in the oil and gas industry was discussed. An overview of the synthetic (PA and MI) and green (DW, BC, IN, and AV) inhibitors used in this research was explained.

2.2 Basics of corrosion

Corrosion is the destruction of a material, usually metal, due to its reaction with the environment [17]. In the case of metals, it is a natural process that occurs when a metal reverts to its chemically combined form (ore) at a lower energy state [17, 18]. The magnitude and forms of corrosion are dependent on the reactivity of the metal and the nature of the environment the metal is exposed to, such as acids, brine, air and moisture, gases (hydrogen sulphide, carbon dioxide), among others [1, 18]. Corrosion is a worldwide challenging problem that has significant consequences on health, safety, environment as well as the economy despite the advancement in corrosion science and technology [4].

The two main classifications of corrosion are general (uniform) and localized corrosion. In general corrosion, the destructive attack occurs over the entire surface of metal evenly. In this type of corrosion, the extent of corrosion or the life of a metallic structure and equipment can be predicted and measured using a simple immersion test. In localized corrosion, the

destructive attack occurs at some specific sites of the metal exposed to the corrosive environment. Corrosion failure due to localized corrosion can be severe because it is difficult to predict and detect the areas of breakdown [19, 20]. This form of corrosion is possibly due to the heterogeneity of the material's microstructure arising from imperfections (voids, inclusions, and dislocations) or environmental factors such as the concentration of dissolved oxygen, temperature, flow rate, electrolyte's pH and concentration of aggressive species [19].

2.3 Electrochemical aqueous corrosion

The corrosion of metals in an aqueous solution is electrochemical because it involves the transfer of electrons (loss and gain of electrons). This corrosion process can be represented by two half-reactions: anodic and cathodic reactions [18]. For electrochemical corrosion to occur, four essential components (anode, cathode, an electrolyte, and electrical path) must be present in a corrosion cell as presented in Figure 2-1 [21].

Anode: Corrosion occurs at this electrode with loss of electrons from the neutral metallic atom and moves into the electrolytic solution in the form of metallic ions.

Cathode: This electrode consumes the electrons that are produced at the anode by a gain of electrons. The reduction reaction occurs at the cathode.

Electrolyte: This is an electrically conductive solution that must be present for corrosion to occur.

Metallic path: This is a metallic conductor that connects the anode to the cathode for the flow of current.

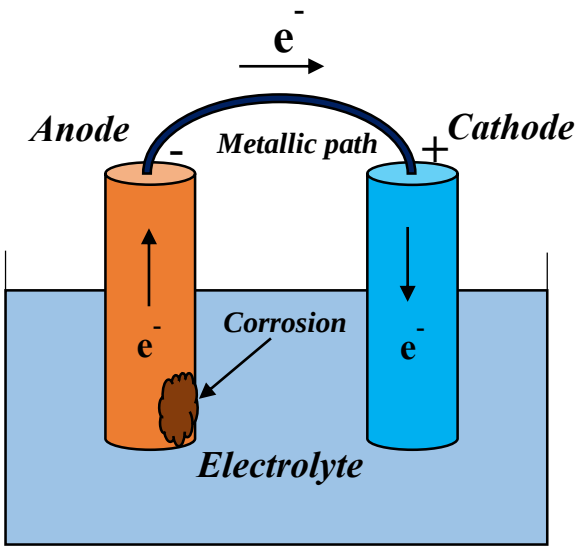


Figure 2-1 Basic corrosion cell.

At the anodic site, electrically neutral metal atom (M) loses electrons to become positively charged ions (cations). These ions may either react with other species at the metal-electrolyte interface, forming corrosion products on the surface of the metal (depending on the environment) or into the electrolyte. Corrosion occurs at the anodic site of the metal, and the general anodic reaction is represented by the following equation [22, 23]:

$$M_{(s)} \rightarrow M^{n+} + n^{e-} \qquad \textbf{(Oxidation reaction)} \qquad \text{Eqn 2-1}$$

where M is a neutral metal atom, n is the number of valence electrons (depending on the nature of the metal) and e^- represents an electron [22, 23].

The partial or two half-reactions for the corrosion of iron in aerated HCl solution is of interest in this study and given as:

$$Fe_{(s)} \rightarrow Fe^{2+} + 2e^{-} \text{ (}\textit{oxidation reaction}\text{)} \qquad \text{Eqn 2-2}$$

At the cathode site, the electrons released at the anode are consumed at the cathode which involves the gain of electrons. The cathodic reaction for metals immersed in acidic solutions are given in the following equations and is dependent on the nature of the solution which the metal is exposed. (e.g. absence or presence of dissolved oxygen)[22]:

$$2H^{+} + 2e^{-} \rightarrow H_2 \text{ (}\textit{Hydrogen evolution}\text{)} \qquad \text{Eqn 2-3}$$

Overall reaction:

$$Fe + 2H^{+} \rightarrow Fe^{2+} + H_2 \qquad \text{Eqn 2-4}$$

Cathodic reaction of an acidic solution containing dissolved oxygen:

$$O_2 + 4H^{+} + 4e\text{-} \rightarrow 2H_2O \qquad \text{Eqn 2-5}$$

Overall reaction:

$$Fe + O_2 + 4H^{+} \rightarrow Fe^{2+} + 2H_2O \qquad \text{Eqn 2-6}$$

The oxidation and reduction reactions must simultaneously occur at the surface of the metal during corrosion to achieve a state of dynamic equilibrium. In other words, the rate at which electron is produced at the anode must be equal to its consumption at the cathode.

The electrochemical reactions occurring at the anodic and cathodic sites of steel in an acid solution is presented in **Figure 2-2.** Details of previous research into corrosion inhibition in this environment are presented in **section 2.4.2**.

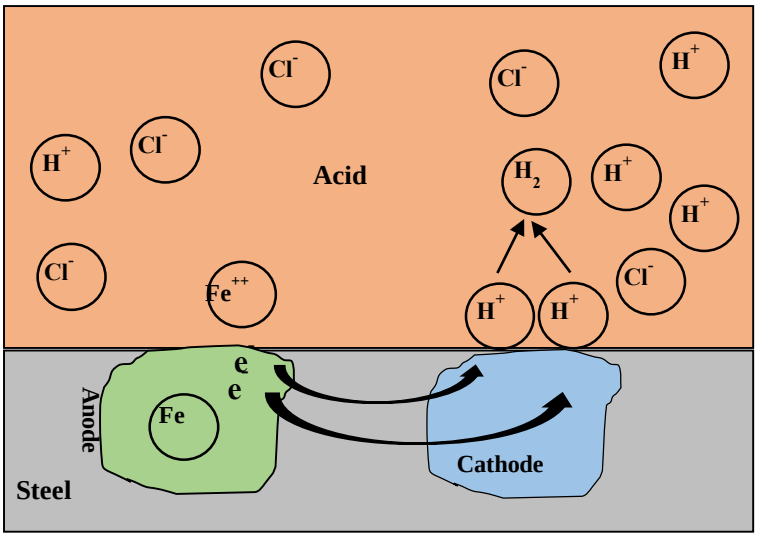


Figure 2-2 A schematic representation of the corrosion on a steel surface in an acidic solution showing both the anodic and cathodic sites of the steel.

2.4 Corrosion in the oil and gas industry

This thesis is particularly aimed at inhibitors which might be useful for the oil and gas industry. Oil and gas structures corrode when they are exposed to the aggressive solution during exploration and production, refinery, transportation and storage. Hence, appropriate corrosion control technologies must be employed to mitigate the effect of corrosion on the economy, safety and the environment. A large portion of the total costs incurred in the oil and gas industry

is attributed to corrosion induced problems [4]. Formation fluids (oil, gas and water) contain corrosive species including salt water, hydrogen sulphide (H_2S), carbon dioxide (CO_2), which can react together to form highly aggressive environments, resulting in the corrosion of oilfield facilities [4]. Figure 2-3 presents the schematic diagram of some likely sources of corrosion during oilfield applications.

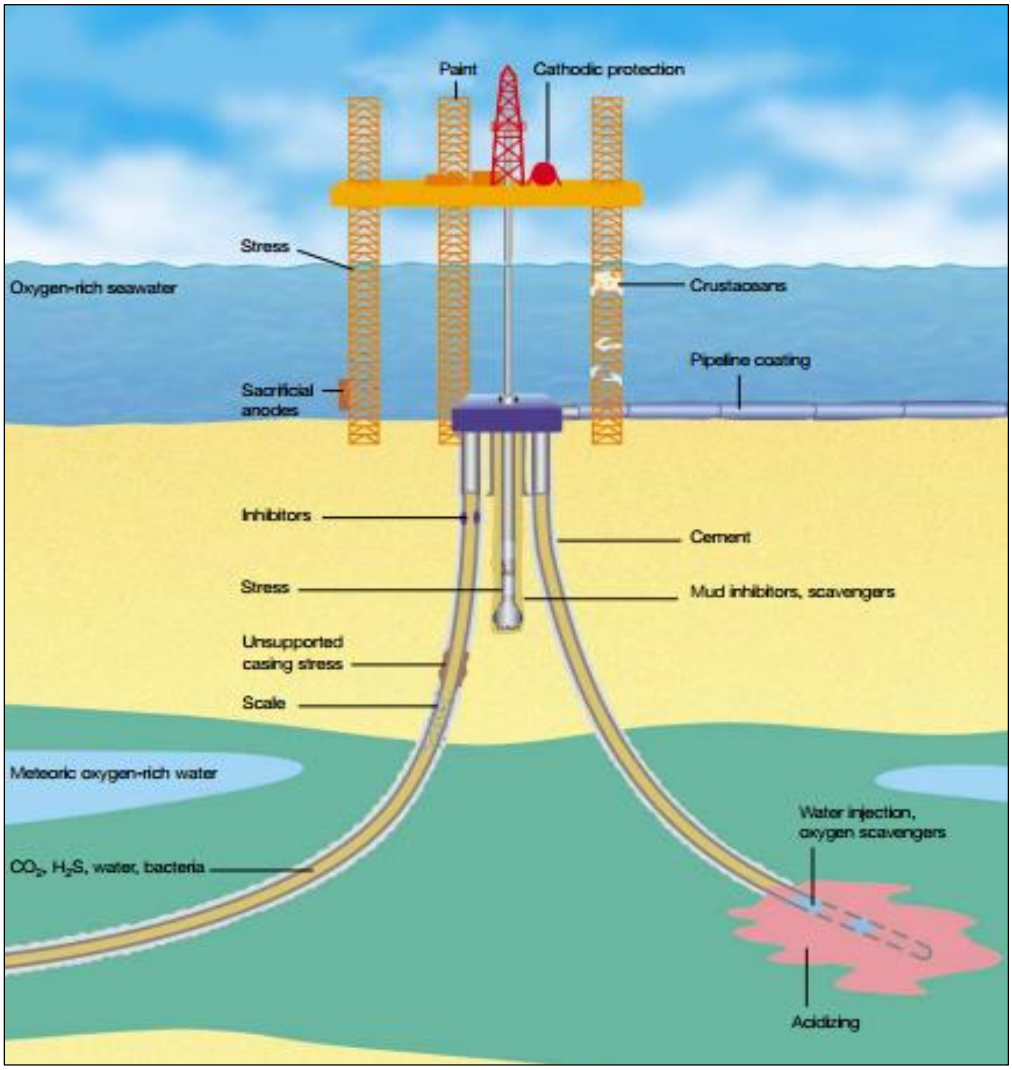


Figure 2-3 An offshore platform showing some likely corrosion sources including acidizing [24].

2.4.1 Types of corrosion in the oil and gas industry

The primary cause of corrosion in the oil and gas industry is due to the presence of dissolved gases such as carbon dioxide, hydrogen sulphide and oxygen in a stream of fluid [24].

2.4.1.1 Carbon dioxide (CO_2)/sweet corrosion

Carbon dioxide corrosion is one of the major forms of corrosion in oil field applications. It is reported that 60% of all oil and gas equipment failures are attributed to CO_2 corrosion [25]. The severity of this type of corrosion is influenced by the concentration of CO_2, an increase in pH, temperature, pressure, material type, water chemistry, flow conditions, etc. CO_2 is injected into an oil reservoir to increase its productivity. The reaction of carbon dioxide with water leads to the formation of carbonic acid (H_2CO_3) [4, 26].

Further reaction of carbonic acid with steel can result in the formation of iron carbonate ($FeCO_3$) as given in the equations below:

The reaction of carbon dioxide with water produces carbonic acid:

$$\mathbf{CO_2 + H_2O \rightarrow H_2CO_3 \ (carbonic\ acid)} \qquad \text{Eqn 2-7}$$

Carbonic acid dissociates into carbonate and bicarbonate ions because it is a weak acid:

$$\mathbf{H_2CO_3 \rightarrow H^+ + HCO_3^-} \qquad \text{Eqn 2-8}$$

As pH rises, bicarbonate dissociates to carbonate:

$$\mathbf{HCO_3^- \rightarrow H^+ + CO_3^{2-}} \qquad \text{Eqn 2-9}$$

The general reaction of steel with carbon dioxide containing environment corrosion can be represented as given below:

$$\mathbf{Fe + CO_2 + H_2O \rightarrow FeCO_3 + H_2} \qquad \text{Eqn 2-10}$$

The precipitation of iron carbonate can occur when the concentrations of Fe^{2+} and $\boldsymbol{CO_3^{2-}}$ ions exceed the solubility limit:

$$\boldsymbol{Fe^{2+} + CO_3^{2-} \rightarrow FeCO_{3(s)}} \qquad \text{Eqn 2-11}$$

One of the most important factors governing the rate of corrosion is the precipitation of iron carbonate on a metallic surface. The breakdown of ferrous carbonate ($FeCO_3$) film from a steel surface can result in the initiation of pits, followed by propagation and eventually failure [26]. Carbon dioxide corrosion causes severe damage because it is difficult to predict and detect [25, 26].

2.4.1.2 Hydrogen sulphide (H_2S) or sour corrosion

Hydrogen sulphide occurs naturally in crude oil and natural gas. It is produced by the breakdown of organic materials, animal waste and other sulphate reducing bacteria. It is colourless, flammable and heavier than air [27]. Hydrogen sulphide is not corrosive in its dry form but becomes severely corrosive when it dissolves in water.

Hydrogen sulphide induced corrosion occurs when iron/carbon steel dissolves in water containing a high concentration of hydrogen sulphide, leading to the evolution of hydrogen that penetrates the metal. The effects of hydrogen entry into the metal can cause blistering or sulphide stress cracking [27].

The equation expresses the general equation for the reaction of carbon steel in hydrogen sulphide containing environment:

Hydrogen sulphide dissociates when it dissolves in water:

$$H_2S_{(aq)} \rightarrow HS_{(aq)} + H^+_{(aq)} \qquad \text{Eqn 2-12}$$

The attack of carbon steel by hydrogen sulphide yields:

$$Fe_{(s)} + H_2S_{(aq)} \rightarrow FeS_{(s)} + H_{2(g)}\uparrow \qquad \text{Eqn 2-14}$$

The type of iron sulphide (FeS) film formed on the carbon steel surface and the extent of corrosion is dependent on temperature, H_2S concentration, H_2S partial pressure, water chemistry, pH and exposure time [28].

2.4.1.3 Oxygen-induced corrosion

One of the problems encountered in the oil and gas industry is due to the presence of dissolved oxygen in production fluid [24]. The ingress of oxygen into the production fluid could occur through leakage of pump seals, casing and process vents, among others [24, 29]. Severe damage could occur even at a low dosage of oxygen of about 1 ppm because electrons are consumed at the cathode, hence enhancing corrosion rate [4, 24]. Oxygen-induced corrosion is usually overcome by the introduction of scavengers (oxygen removal chemical) into the system [29, 30].

2.4.2 Acidizing (acid treatment)

Historically, the productivity of oil and gas wells was enhanced by exploding rock formations using torpedoes [3, 4]. However, this technique was discontinued because rock formations were not properly disintegrated. Consequently, acids are used to enhance the flow of hydrocarbons from rock formations was discovered in 1896 by Herman Frasch [31].

Acidizing is a process employed to enhance the productivity of an oil and gas reservoir. This is achieved by pumping acids through the wellbore to enlarge existing pores in the rock formation or create new pathways for the flow of formation fluids (oil, gas and water)[32]. Acidizing can be performed on unproductive wells to restore their productivity and new wells to maximize their production capacity. The main types of acid treatments employed to increase the productivity of hydrocarbon reservoir are matrix acidizing, fracture acidizing and acid wash.

In matrix acidizing, acid is injected into the pores of rock formation through the wellbore below the reservoir fracture pressure to dissolve the materials that are hindering the permeability of the rock, hence enlarging the existing pores and increasing the flow of hydrocarbons into the well [32, 33].

Fracture acidizing is performed by injecting highly pressurized acid (usually HCl) into a carbonate formation such as limestone and dolomite above the formation fracturing pressure in order to dissolve the materials in the rock formation and open new channels, thereby increasing the permeability of the well and the flow of hydrocarbons into the wellbore [33].

Acid wash is employed to remove scale or deposits on tubings after completion of oil and gas well [5]. Scale removal treatments are often carried out to remove iron oxides and carbonate minerals using 15 wt% HCl at 60°C [4, 5]. The treatment fluid (15wt% HCl) is not pumped into the reservoir formation in this process [4, 5].

The drawback of the stimulation techniques is that oil and gas metallic materials (casings, tubings, pipelines and other components) are severely damaged when exposed to the aggressive environment which often results in the depletion of resources and loss of lives [5].

Consequently, it becomes imperative to inhibit acid solution with effective inhibitors before being pumped into a wellbore.

2.4.2.1 Acids used for acidizing treatment

Different acids ranging from organic and inorganic are employed for acidizing of oil and gas wells. Examples of common conventional acids used for stimulation are hydrochloric, hydrofluoric, acetic, formic, sulfamic and chloro-acetic acids [3, 4, 34]. However, these conventional acids can also be mixed with sulphuric, methanesulphonic, nitric, sulphamic and phosphoric acids, depending on the characteristics of the rock formation [34, 35]. HCl is the most common acid used for acidizing treatment because the reaction of metal with HCl forms metal chlorides, which are soluble in the aqueous phase compared to nitrates, sulphates and phosphates [4, 35, 36]. Although most of the acidizing treatment is carried out using 5-28wt% HCl, a standard 15wt% HCl had been chosen since 1960 because of its solubility in the primary inhibitor (arsenic inhibitor) used at that time [37]. Even though other acids had been tested in acidizing treatments of oil and gas wells, they were not so effective as HCl. Consequently, HCl is the most common acid employed for acidizing treatment [3, 4].

2.5 Economics of corrosion

Corrosion problems significantly affect the safety and the economy of almost all sectors including oil and gas, health, aviation, nuclear power plants etc. Although corrosion is inevitable, it can be minimized through proper corrosion management techniques [29].

The annual total direct cost of corrosion of five major sectors: utilities, transportation, production and manufacturing, infrastructure, and government in the United States reported by

the Federal Highway Administration (FWHA) was estimated to be $ 276 billion, which is approximately 3.1 % Gross Domestic Product (GDP) of the United States [29]. These costs do not include the indirect cost of corrosion incurred due to loss of productivity, downtime, failures, among others [29]. In Canada, the cost of corrosion incurred in the mining sector was $CAN 1450 million, while £187.5 million was spent on corrosion costs in the farming industry in the United Kingdom [29]. The total annual corrosion cost in the oil and gas industry was estimated to be $ 1.372 billion by the National Association of Corrosion Engineers (NACE), and this cost is broken down as shown in Figure 2-4.

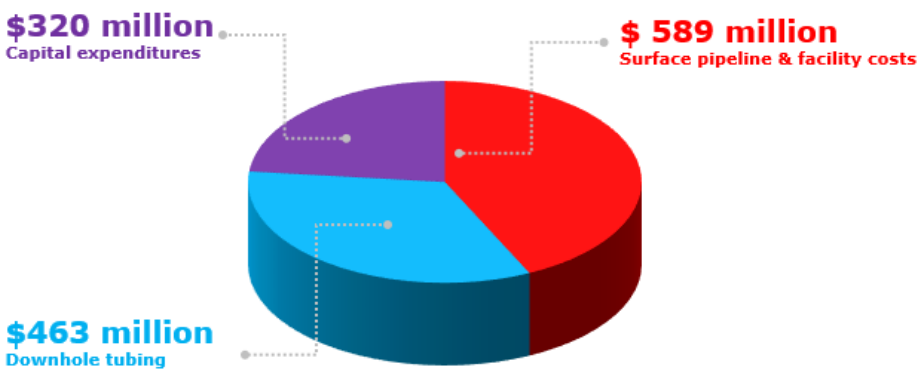


Figure 2-4 Annual total corrosion cost breakdown in the oil and gas industry [2].

On a global scale, the cost of corrosion in industrialized nations was estimated to be 3- 4% of the GDP [38]. According to the National Association of Corrosion Engineers (NACE), the direct and indirect global corrosion cost was US$ 552 billion annually in 2001, which increased to US$ 1.3 trillion in 2009. In 2013, these costs were estimated to be US$ 2.5 trillion, which is equivalent to almost 3.4 % of the GDP. However, 15 to 35 % (US$ 375 and $ 875 billion) of the mentioned total cost of corrosion could be saved annually on a global basis by

implementing appropriate corrosion control technologies. These costs do not include savings due to safety or environmental effects [39].

Schmitt et al. [40] reported that 25-30 % of the total annual cost of corrosion could be reduced in the U.S. if appropriate and optimum corrosion management is employed. It is imperative that economically useful measures must be put in place to minimize the effect of corrosion. Otherwise, huge costs will be incurred on corrosion induced problems.

2.6 Corrosion control measures

Corrosion is a natural process that has a severe impact on the economy, safety and environment, among others[18]. Although corrosion is inevitable, it can be controlled or minimised by employing appropriates techniques such as proper material selection, cathodic protection, inspection and monitoring, application of coatings, and corrosion inhibitors to prolong the life of metallic components that are exposed to an aggressive environment [18, 22, 30].

2.6.1 Inspection and monitoring

Inspection plays a significant role in preventing sudden failure of structure/equipment, which could lead to severe damage to assets worth billions of dollars, environmental pollution and even loss of lives. It helps in providing relevant data and information necessary to evaluate existing structures in an aggressive environment [41]. Inspection can be carried out by visual examination, fiberscope, borescope, calliper tools etc.

Monitoring also plays a vital role in corrosion control because it involves following up inspected facilities, to ensure they are in good working condition. It gives an early signal about the failure of a structure [22, 41]. One of the ways to monitor equipment is by using either

electrical or mechanical probes such as linear polarisation, electrical resistance, galvanic probes, etc.

Inspection is usually carried out on a short-term once-off measurement, based on the maintenance and inspection schedule, while monitoring involves long term measurement of the corrosion damage to understand the fluctuation of corrosion over time as well as the cause of the failure [22, 41].

2.6.2 Proper material selection

The selection of any material for a specific application is always integrated at the design stage. Corrosion and wear behaviour, physical (electrical conductivity, thermal conductivity), mechanical (such as tensile strength, density, ductility, fracture toughness, etc.) properties, as well as the cost, are some of the factors that are considered before selecting a material [4, 22]. Carbon steels (CS) are the most common engineering materials used for several industrial applications due to their low cost, but because they are susceptible to corrosion, corrosion resistant alloys (CRA) such as austenitic or duplex stainless steel are used in some special applications [4]. However, the high cost of CRA has led to the use of CS in combination with chemical treatments (corrosion inhibitors), which is still cost-effective in corrosion control [4].

2.6.3 Coatings

A coating is a thin material which is deposited on a substrate surface to improve its surface properties and create a protective barrier against deterioration due to exposure to an environment. Effective coatings must have low porosity, good adhesion to the substrate, corrosion resistant, uniform appearance, chemically resistant to the environment for which it is exposed, sufficient thickness (the higher the thickness, the higher the higher the resistance), fire and heat resistant, abrasion resistant as well as low cost [22]. Coatings can be classified

into organic (paints, lacquers, epoxy, polyurethane, polyvinyl chloride), inorganic (enamels, ceramics and glass) and metallic (nickel, titanium, aluminium and chromium coatings) [30, 42]. The failure of coatings may be attributed to water absorption, blistering due to gas or air inclusion, surface contamination, surface defects, temperature differentials, among others [22, 42].

2.6.4 Cathodic protection

Cathodic protection is one of the methods of corrosion control. Generally, the electrons produced at the anode are consumed at the cathode in a corrosion cell. If additional electrons are supplied to the metallic structure to be protected from an external source, the metal dissolution will be suppressed, while the rate of hydrogen evolution will increase [22]. In other words, cathodic protection forces current to flow to the metallic structure to be protected and suppresses the corrosion current that causes corrosion [41]. Cathodic protection can be achieved in two ways. Firstly, if the electrons are supplied to the metallic surface (e.g. iron) by other metal which is more active (zinc, magnesium or aluminium), then the metallic structure will become the cathode while the more active metal (sacrificial anode) will act as the anode (corrodes). The sacrificial anodes are easy to install, relatively inexpensive and can be used without an external power supply[22]. Secondly, cathodic protection can be achieved by generating electrons from an external direct current (dc) power source to the metal surface to be protected. This will enhance the speed of the cathodic reactions, while the metal dissolution (corrosion) will be suppressed [22].

Cathodic protection is often employed to protect underground and undersea structures such as cables, oil and gas pipelines, submarines, marine facilities and water tank storage [30].

2.6.5 Corrosion inhibition

Corrosion inhibitors have been used to prevent the dissolution of metals in the aggressive environment since the nineteenth century. The first patent on corrosion inhibitor was given by Baldwin who used molasses and vegetable oils to inhibit the corrosion of pickling sheet steel in acids [43].

A corrosion inhibitor is a chemical substance that when added (continuously or intermittently) in small concentration to an aggressive environment inhibits the corrosion rate of the exposed metal effectively [4, 44]. It can either be in the liquid or vapour form.

Corrosion inhibitors are used widely in several applications such as cooling water systems, refinery units, chemical processing plants, power generation, chemical plant, oil and gas production units etc. The use of corrosion inhibitors is one of the most economically viable, effective, and practical methods to prevent metal dissolution and acid consumption [22]. The concentration and amount of corrosion inhibitor injected into a system is dependent on the type of the acid and its strength, the metal type, pH of the solution, temperature and the exposure time [4]. The corrosion inhibitors that are effective under some certain conditions might behave poorly in another set of conditions. An inhibitor is considered to be efficient if it is environmentally compatible, economical and achieves the desired corrosion inhibition effect when added in small concentrations [23]. Most of the effective inhibitors are organic compounds containing most of the elements in the Group V or VI of the Period Table including nitrogen, phosphorus, sulphur etc. [45]. For an inhibitor to be effective, it must have an anchoring group (OH, NH_2, SH, NH etc.) which binds onto the metal surface; a substituent group (provides further adsorption strength), and a backbone (bears both the anchoring and the substituent groups) [21]. The adsorption strength of an inhibitor onto a metal surface depends

on the electron density of the anchoring and substituent groups as well as the orientation of the inhibitor molecule on the metal surface [21].

The global corrosion inhibitors market volume share was estimated to be US$ 5.2 billion in 2012 and expected to reach a value of US$ 7.14 billion by the end of 2019 as reported by transparency market research intelligence company (TMRIC). The global demand for corrosion inhibitors based on different industries is shown in Figure 2-5.

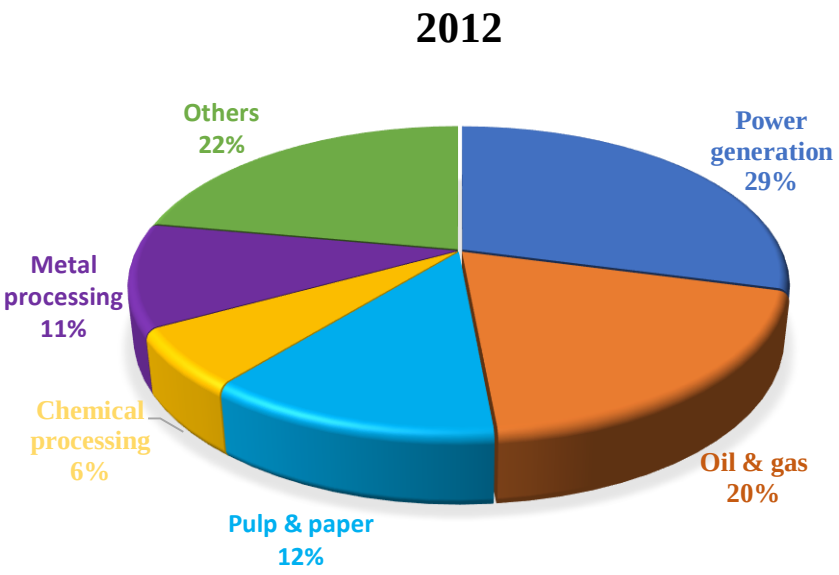


Figure 2-5 Global corrosion inhibitors market volume share in 2012 [46].

2.6.5.1 Performance of corrosion inhibitors

The performance of a corrosion inhibitor is evaluated by calculating the inhibition efficiency (IE) as given in eqn 2-13:

$$\boldsymbol{IE}\ (\%) = \left(\frac{\boldsymbol{CR_o - CR_i}}{\boldsymbol{CR_o}}\right) \times \mathbf{100} \qquad \text{Eqn 2-13}$$

where CR_o and CR_i represent the corrosion rate in the absence and presence of the inhibitor, respectively.

The corrosion rate can be determined by either using chemical (weight loss) or electrochemical measurements.

2.6.5.2 Mechanism of corrosion inhibition

The primary steps in the inhibitive mechanism of most organic inhibitors can be attributed to the transportation of the inhibitor molecules from the bulk solution and adsorption onto the metal surface [29]. The adsorption of these inhibitors takes place after the initially adsorbed water molecules on the metal surface desorbed as given in Eqn 2-15. The displacement occurred because the lateral energy between the inhibitor molecule and the metal surface is higher than that of the water molecules [47].

$$\boldsymbol{Org_{(sol)} + yH_2O_{(ads)} \leftrightarrow Org_{(ads)} + yH_2O_{(sol)}} \qquad \text{Eqn 2-15}$$

where $Org_{(sol)}$ is the organic compound in the aqueous solution, $H_2O_{(ads)}$ is the water molecules that adsorb on the electrode surface, y represents the number of water molecules replaced by one organic inhibitor, and $Org_{(ads)}$ is the organic inhibitor that adsorbed on the electrode surface.

Generally, the protection efficiency of an inhibitor molecule is dependent on the extent of the adsorption of the inhibitor molecules with a metallic surface, and this adsorption can be physical /and or chemical adsorption.

2.6.5.2.1 Physical adsorption (physisorption)

This type of adsorption is due to weak intermolecular interactions between the ionic charges or dipoles on the adsorbed inhibitor and the electrically charged metal surface as shown in Figure 2-6. The interaction between the organic corrosion inhibitor and the metal surface is weak (Van der Waals forces) and can desorb easily by an increase in temperature. Consequently, the corrosion inhibition performance of the inhibitor molecule decreases.

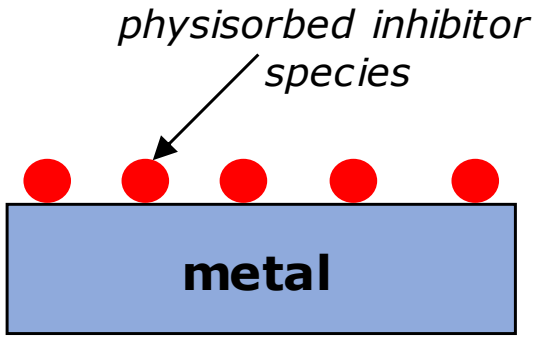


Figure 2-6 Physical adsorption of a corrosion inhibitor on a metal surface due to electrostatic interaction (Van der Waals forces).

2.6.5.2.2 Chemical adsorption (chemisorption)

This type of adsorption involves charge transfer or sharing from the organic corrosion inhibitor with a metal, which leads to the formation of a coordinate covalent bond as shown in Figure 2- 7. Chemical adsorption may take place between lone pair electron of organic corrosion inhibitor having electron rich heteroatoms (N, O, S or P) and pi-electrons in the

multiple bonds or aromatic ring of the inhibitor with the metal. The adsorption strength is dependent on the electron density and polarity of the corrosion inhibitor. Increase in temperature may increase the protection efficiency of the corrosion inhibitor. Example of the type of inhibitor that exhibits this behaviour is PA. Chemical adsorption is usually irreversible because it has higher adsorption energy than physical adsorption.

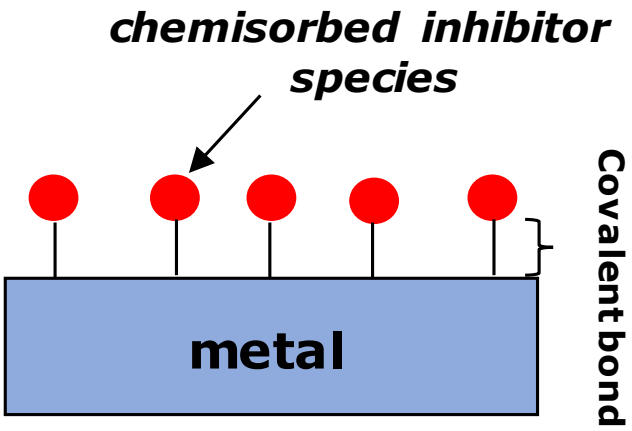


Figure 2-7 Chemical adsorption of a corrosion inhibitor on a metal surface due to covalent bond.

2.6.5.3 Types of corrosion inhibitors

Corrosion inhibitors are classified into interface inhibitors and environmental conditioners based on their mechanism of inhibition as shown in Figure 2-8. Environmental conditioners are corrosion inhibitors, which remove the corrosive ions (e.g., chloride and hydrogen ions) in an aggressive environment. Examples of environmental scavengers are hydrazine and sodium sulphite. Interface inhibitors are corrosion inhibitors, which form an inhibiting or protective

film between metal and solution interface. The two classifications of corrosion inhibitors are liquid and vapour-phase.

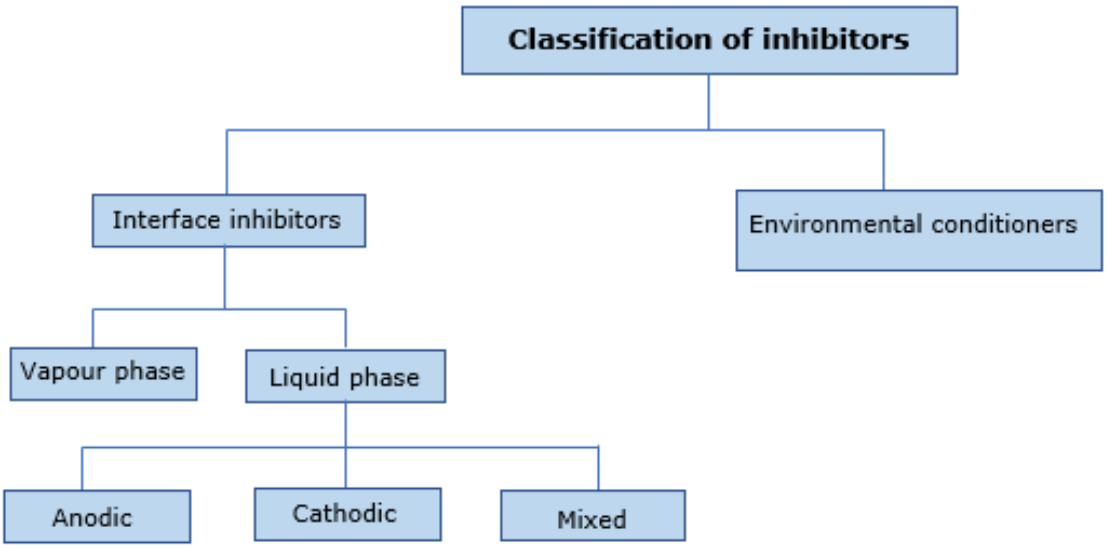


Figure 2-8 A general classification of corrosion inhibitors [21]

2.6.5.3.1 Vapour-phase inhibitors

Vapour-phase inhibitors (VPIs) are chemical compounds that are transported in the vapour phase to the surface of a metal (ferrous and non-ferrous) and then form a protective layer on the metallic material against atmospheric corrosion, especially in a closed system [22, 48]. These inhibitors must have high passivating properties and strong tendencies toward surface adsorption to be effective. These types of inhibitor are also called volatile corrosion inhibitors. Examples of these corrosion inhibitors are amine and Dicyclohexylamine Nitrile [22, 48].

2.6.5.3.2 Liquid phase inhibitors

Liquid-phase inhibitors are chemical compounds that inhibit the corrosion of a metallic material exposed to corrosive solution in the liquid phase. They can be classified into anodic, cathodic or mixed (based on their corrosion inhibition mechanism), depending on the electrochemical reaction(s) they inhibit. The primary focus of this thesis is the type of inhibitor that can be managed in a liquid flow.

Corrosion potential (E_{cor}) is the potential of a working electrode in an electrolyte relative to a reference electrode without the application of an external load (i.e. with no flow of electric current) [29]. Corrosion potential is also known as rest potential, free- corroding potential or open-circuit potential.

Corrosion current density (I_{cor}) is the dissolution current at the corrosion potential.

2.6.5.3.2.1 Anodic inhibition mechanism

Anodic corrosion inhibitors are compounds that reduce the corrosion rate of a metal (anodic metal dissolution) by forming an insoluble passivating film on the metal surface, which blocks the anodic reaction. Furthermore, the addition of these inhibitors to a corrosive environment cause the corrosion potential to shift to a more positive direction and decreases the value of the corrosion current density as shown in Figure 2.9. Anodic inhibitors are also called passivating inhibitors because they force the surface of the metal into the passivation region by the anodic shift of the corrosion potential [30]. The two types of anodic inhibitors are oxidizing anions (e.g., chromates and nitrites) which are effective in the absence of oxygen and non-oxidizing ions (phosphate, tungstate, and molybdate) which require the presence of oxygen to be effective. The dosage of the anodic inhibitor must be sufficient in the solution. Otherwise, the surface of the metal will not be fully covered by the inhibiting film, leading to the localized corrosion of the exposed sites of metal [49].

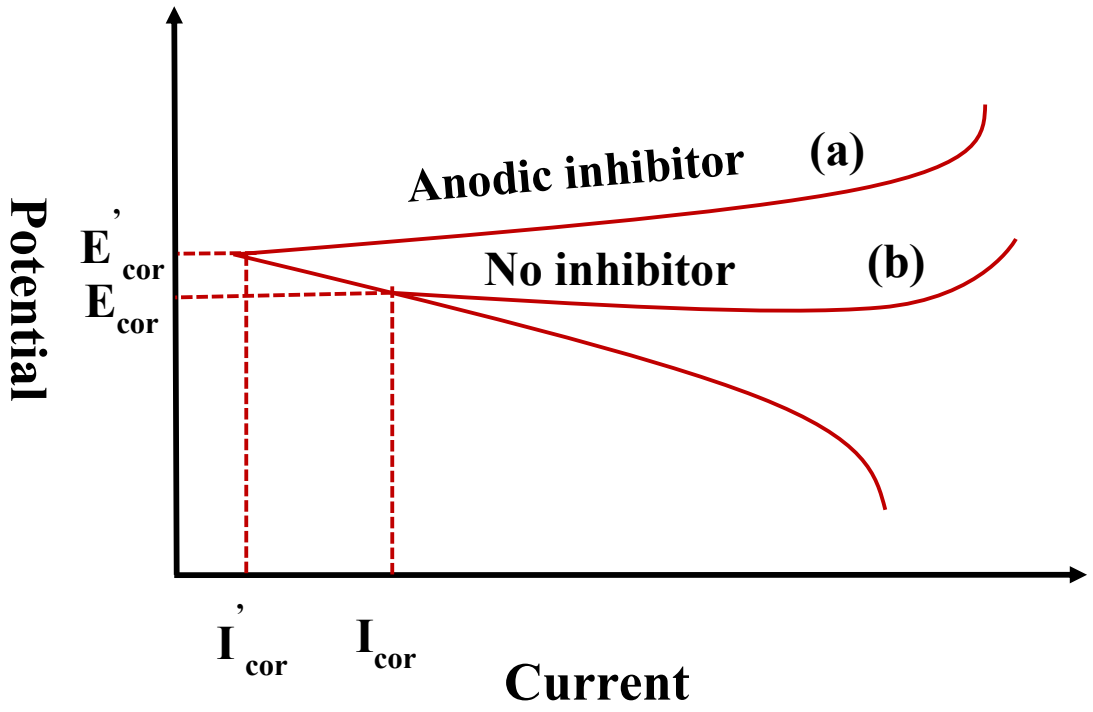


Figure 2-9 Potentiodynamic polarization curves showing the electrochemical behaviour of a metal in a solution in the presence of an anodic inhibitor (a) and the absence of inhibitor (b).

2.6.5.3.2.2 Cathodic inhibition mechanism

Cathodic corrosion inhibitors are compounds which function either by retarding the evolution of hydrogen gas or by selectively precipitating insoluble compounds at the cathodic sites (cathodic precipitators), thereby increasing the resistance of the metal surface and restricting the diffusion of reducible species such as hydrogen ions and oxygen to the cathodic sites of the metal [49]. The addition of cathodic inhibitors to the aggressive solution shifts the corrosion potential to more negative direction and decrease the corrosion current density as shown in Figure 2-10.

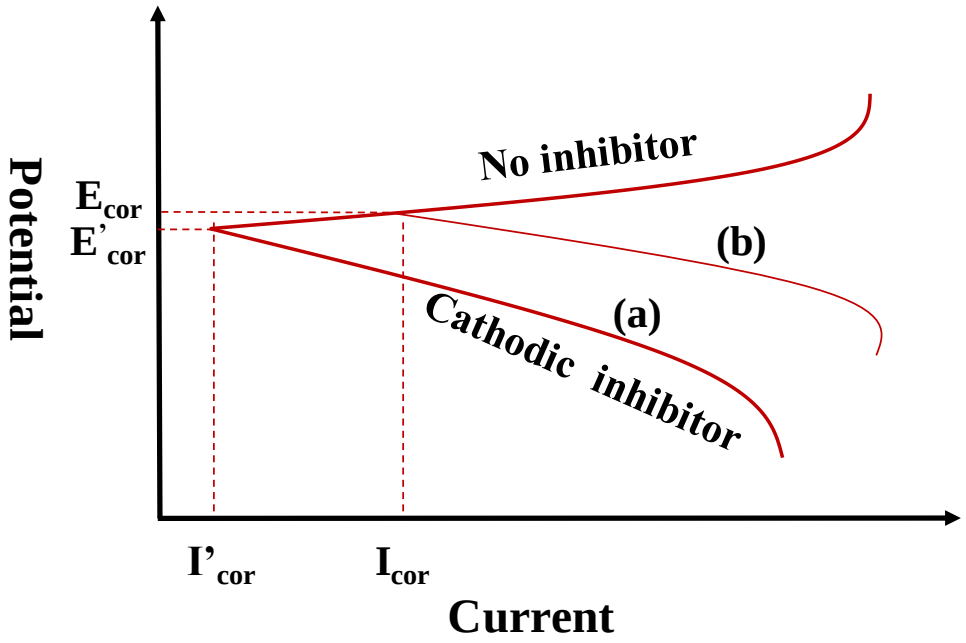


Figure 2-10 Potentiodynamic polarization curves showing the electrochemical behaviour of a metal in a solution in the presence of a cathodic inhibitor (a) and the absence of inhibitor (b).

2.6.5.3.2.3 Mixed inhibitors

In this thesis, mixed inhibitors are referred to as the type of inhibitors that retard anodic dissolution of metal and cathodic hydrogen ion reduction. The author does not necessarily mean a combination of two or more inhibitors.

Mixed inhibition mechanism type of inhibitors are mostly organic compounds (80%) that reduce the anodic dissolution of metal and retard the cathodic evolution of hydrogen gas [22]. The corrosion protection ability of these inhibitors is dependent on the extent of their adsorption and coverage on the metal surface. The adsorption of a mixed inhibitor depends on nature and surface charge on the metal surface (positively or negatively charged), the structure of the inhibitor, and the solution type [50]. The

mode of their corrosion inhibition may be physisorption, chemisorption or both. Most of the mixed corrosion inhibitors are organic inhibitors such as silicates, phosphates, PA, aldehydes, MI, ascorbic acid, and extracts of plant materials**. Figures 2-11** shows a decrease of the corrosion current density from I_{cor} to I'_{cor}, whilst the corrosion potential remains unchanged after the addition of the mixed corrosion inhibitor into the solution.

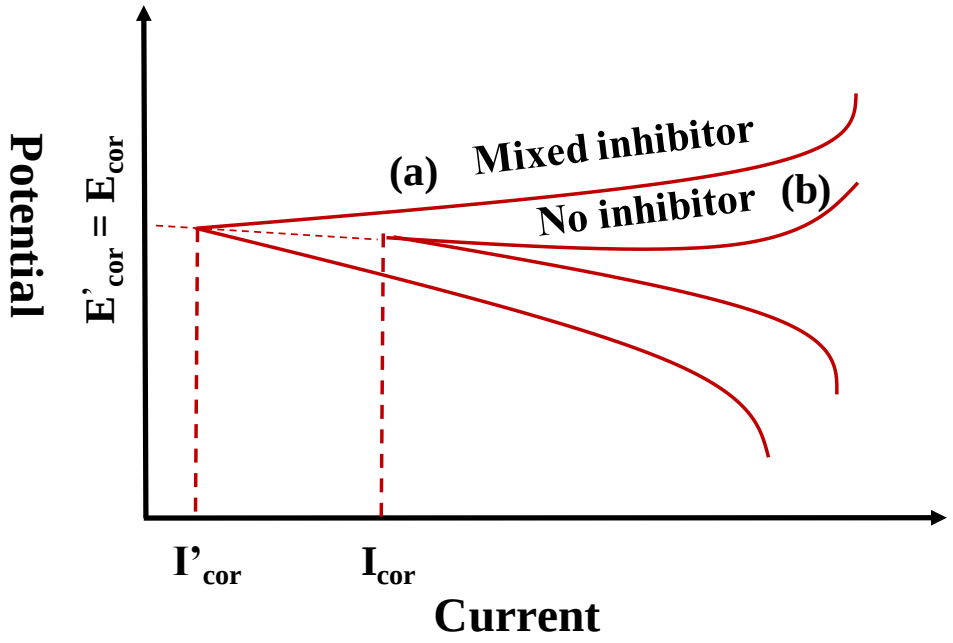


Figure 2-11 Potentiodynamic polarization curves showing the electrochemical behaviour of a metal in a solution in the presence of a mixed inhibitor (a) and the absence of inhibitor (b).

2.7 Adsorption isotherm

Generally, the adsorption of inhibitor molecules on a metallic surface is the first step before corrosion inhibition [51]. The adsorption isotherm gives necessary information about the interaction between inhibitor molecules and a metal surface [52]. It defines the degree of surface coverage (θ) of an adsorbate (inhibitor) on the adsorbent (metal surface) at a given temperature. Generally, it is assumed that the degree of the metal surface covered by the inhibitor is directly proportional to the concentration of the inhibitor. That is, the surface coverage increases as the concentration of the inhibitor in the bulk solution increases. In addition, a complete monolayer is assumed to be formed when the surface coverage is 1. The fractional inhibition efficiency (E) is related to the surface coverage as given in eqn 2-16:

$$\boldsymbol{E = \left(\frac{CR_o - CR_i}{CR_o}\right) = \theta} \qquad \text{Eqn 2-16}$$

Several adsorption isotherm models including Langmuir, Temkin, Frumkin and Freundlich are usually tested to determine the best model that explains the adsorption behaviour of a corrosion inhibitor on a metal surface as given by the following equations [12, 53]:

$$\textbf{Langmuir: } \boldsymbol{\frac{C_{inh}}{\theta} = \frac{1}{K_{ads}} + C_{inh}} \qquad \text{Eqn 2-17}$$

$$\textbf{Temkin: } \boldsymbol{e^{(-2a\theta)} = K_{ads} C_{inh}} \qquad \text{Eqn 2-18}$$

$$\textbf{Frumkin: } \boldsymbol{\left(\frac{\theta}{1-\theta}\right) e^{(-2a\theta)} = K_{ads} C_{inh}} \qquad \text{Eqn 2-19}$$

$$\textbf{Freundlich: } \boldsymbol{\theta = K_{ads} C_{inh}} \qquad \text{Eqn 2-20}$$

where C_{inh} represents the concentration of the inhibitor, θ is the fraction of the surface covered by the inhibitor, K_{ads} is the adsorption equilibrium constant and a is the lateral interaction constant.

The adsorption equilibrium constant is related to the standard free energy (ΔG°_{ads}) of adsorption by the following equation:

$$K_{ads} = \frac{1}{C_{sol}} e^{\left(\frac{-\Delta G^{\circ}_{ads}}{RT}\right)} \qquad \text{Eqn 2-21}$$

where R is the molar gas constant, T is the absolute temperature and $\mathbf{C_{sol}}$ is the molar concentration of the solvent (water is used in this experiment) in the solution (1000 g/L).

Several authors have used the adsorption isotherm and the standard free energy of adsorption to explain the adsorption behaviour of corrosion inhibitors on a metal surface. For example, Li et al. [54] studied the inhibition effect of methyl violet on the corrosion of cold rolled steel (CRS) in 3.5wt% HCl at 293K. They reported that the adsorption of methyl violet on the CRS obeyed Langmuir adsorption isotherm. The value of ΔG°_{ads} of methyl violet was -40.7 kJ/mol which indicates that the inhibitor adsorbed on the CRS mainly by the formation of a coordinate covalent bond (chemisorption). Also, Yadav et al.[55] reported that the adsorption of spiropyrimidinethiones (SM) on mild steel in 15wt% HCl solution in the temperature range from 303 to 333K.The adsorption of SM on mild steel followed Langmuir adsorption isotherm. The calculated values of ΔG°_{ads} were in the range of - 36.2 to - 39.0 kJ/mol, which demonstrates that SM adsorbed on the substrate via both physical and chemical mechanism.

2.8 Currently used corrosion inhibitors for acid treatment operations

Billions of dollars need to be spent yearly by the oil and gas industry on preventing corrosion induced failures of structures. Proper corrosion management and technologies such as the use of corrosion inhibitors will reduce not only the cost but also the effect of corrosion on safety, health and the environment. Some of the corrosion inhibitors used to minimise the loss of metals during acidizing treatment are described below:

Vishwanatham and Haldar [56] studied the methoxyl phenol (MPH) and nonylphenol (NPH) as corrosion inhibitors for N80 steel in 15wt% HCl at 90°. They reported that the maximum inhibition efficiencies of NPH and MPH were 83 and 78% at 75 mM concentration after 6 h. The higher inhibition efficiency of NPH compared to MPH is attributed to the larger molecular area covered on the metal surface and long hydrophobic chain present in NPH.

Migahed and Nassar [34] studied the corrosion inhibition effect of 6-methyl-5-[m-nitrolsytryl]-3-mercapto-1,2,4-triazine for mild steel in 12wt% HCl at 50°C. They reported that the inhibition efficiency of this inhibitor increased from 55.21 to 88.4% with increasing concentration from 75 to 375 ppm using weight loss measurements.

Sathiya et al.[57] studied the corrosion inhibition of 1-Cinnamylidine-3-thiocarbohydrazide and 1, 1'-Dicinnamylidine-3-thiocarbohydrazide for carbon steel (CS) in 15wt% HCl solution at 30-110°C. They reported that the inhibition efficiency increases with increasing concentration of the inhibitors. The inhibition performance of 1,1'-Dicinnamylidine-3-thiocarbohydrazide was more than 1-Cinnamylidine-3-thiocarbohydrazide.

Jayaperumal [36] studied the corrosion inhibition of mild steel in 15wt% HCl containing 1 wt% propargyl alcohol at 30 and 105℃ after 6 h using weight loss measurements. They reported that the inhibition efficiencies of PA were 100% (CR= 0.4 mm/y) and 99% (CR= 3mm/y) at 30 and 105℃. PA was classified as a mixed type inhibitor because it suppressed anodic and cathodic reactions. Similarly, this same author also reported in the same paper that the inhibition efficiencies of octyl alcohol were 87% (CR=21 mm/y) and 82% (CR=77 mm/y) at 30 and 105℃ for mild steel in 15wt% HCl containing 1 wt% octyl alcohol.

Yadav et al.[58] studied 1-(2-aminoethyl)-2-Oley-imidazole (AEOI) and 1- (2- Oleyamidoethyl)-2-Oley-imidazole (OAEOI) as corrosion inhibitors for N80 steel in 15wt% HCl at 25°C. They showed that the inhibition efficiency of the inhibitors increases with increasing concentration. The inhibition efficiencies of OAEOI increased from 69.25 to 96.23%, and that of AEOI increased from 64.25% to 90.26% with increasing concentration from 10 to 150 ppm. The higher inhibition efficiency offered by OAEOI was attributed to its larger molecular size and the presence of more active groups. The tested compounds were classified as mixed type inhibitors.

Yadav et al.[59] studied the corrosion inhibition of N80 steel in 15wt%HCl using thiadiazoles derivatives at 30°C after 6 h exposure time. They showed that the inhibition efficiency has the following order:2-amino-5-(4-methoxyphenyl)-1,3,4-thiadiazole (AMPT)>2-Amino-5-phenyl-1,3,4-thiadiazole (APT)>2-Amino-5-(4-chlorophenyl)-1,3,4-thiadiazole (ACPT). The authors claimed that these organic compounds act as mixed-type inhibitors.

The summary of the organic compounds used as acid inhibitors is given in Table 2-1.

Table 2-1 Inhibition efficiencies and/or corrosion rate for different materials in different acidic solutions.

Inhibitor	Material	Medium	Inhibitor concentration	Test conditions and technique	Corrosion rate (CR) & inhibition efficiency (%)	Ref
Propargyl alcohol (PA)	MS	15wt% HCl	200 - 1000 mg/L	TP, WL and EIS at 35-105°C	97-100%	[36]
Octyl alcohol	MS	15wt% HCl	200 - 1000 mg/L	TP, WL and EIS at 35-105°C	97-100%	[36]
Cinnamaldehyde	N80 steel	20 wt% HCl	1000 mg/L	WL at 90°C	CR=6.3g/m2h	[60]
Cinnamaldehyde + 10% PA	N80 steel	20wt% HCl	1000 mg/L	WL at 90°C	CR=2.9 g/m2h	[60]
Benzalacetone	N80 steel	20wt% HCl	1000 mg/L	WL at 90°C	CR=116g/m2h	[60]
1-cinnamylidine-3-thiocarbohydrazine	Carbon steel	15wt% HCl	500-2000 mg/L	WL at 30-110°C	CR=0.71-255.96mm/y	[57]
1,1-dicinnamylidine-3-thiocarbohydrazide	Carbon steel	15wt% HCl	500-2000 mg/L	WL at 30-110°C	CR=0.39-140.31mm/y	[57]
3-(deca-9-ene)-4-aryl-5-mercapto-1,2,4-triazole	MS	15wt% HCl	500-5000mg/L	WL at 105°C	51.42-99.14%	[61]
6-methyl-5-mercapto-1,2,4-triazine	MS	12wt%HCl	75-375 mg/L	TP at 50°C	57.3-89.4%	[34]
5-Benzoyl-1,3-dioxane	J55 steel	15wt% HCl	2000 mg/L	WL at 65°C	56.6%	[35]
Dicinnamaldehyde acetone	N80 steel	15wt% HCl	1000-5000 mg/L	WL at 105°C	62.1-96%; CR=115-1088mm/y	[62]

Note TP – Tafel polarization measurement, WL – weight loss measurements and EIS - electrochemical impedance spectroscopy.

Table 2-1 (Continued)

But-3-yn-1-ol	Carbon steel	4 M HCl	30 mM	WL at 100°C	99.2%	[63]
But-3-yn-2-ol	Carbon steel	4 M HCl	30 mM	WL at 100°C	99.4%	[63]
Hex-1-yn-3-ol	Carbon steel	4 M HCl	30 mM	WL at 100°C	99.8%	[63]
Non-1-yn-3-ol	Carbon steel	4 M HCl	30 mM	WL at 100°C	99.7%	[63]
Dipropargyl ether	Carbon steel	4 M HCl	30 mM	WL at 100°C	99.4%	[63]
But-2-yn-1,4-diol	Carbon steel	4 M HCl	30 mM	WL at 100°C	99.4%	[63]
2-methyl) but-3-yn-2-ol	Carbon steel	4 M HCl	30 mM	WL at 100°C	93.1%	[63]
Hex-1-yne	Carbon steel	4 M HCl	30 mM	WL at 100°C	4.8%	[63]
Crotonaldehyde	Carbon steel	2 M HCl	10 mM	WL at 80°C	44.4%	[63]
Cinnamaldehyde	Carbon steel	2 M HCl	10 mM	WL at 80°C	93.9%	[63]
3-methylbutanal	Carbon steel	2 M HCl	10 mM	WL at 60°C	36.4%	[63]
Furfural	Carbon steel	2 M HCl	10 mM	WL at 60°C	44.5%	[63]
Benzaldehyde	Carbon steel	2 M HCl	10 mM	WL at 60°C	36.6%	[63]

2.8.1 Propargyl alcohol (PA)

Historically, the acetylenic alcohols including propargyl alcohol were discovered to be excellent corrosion inhibitors in the 1940s [64]. It is one of the most extensively studied classes of acid inhibitors. The excellent corrosion inhibition behaviour of acetylenic alcohols has been attributed to the formation of a protective polymeric film on a metallic surface [29, 51, 63].

Propargyl alcohol (2-Propyn-1-ol) [HC≡C-CH_2-OH] belongs to the class of unsaturated organic compounds called acetylenic compounds and is a standard commercial corrosion inhibitor used for acidizing treatment and other industrial applications (acid pickling, acid cleaning, etc.) [65]. It offers excellent corrosion inhibition against the corrosion of metals and alloys, especially at elevated temperatures (110°C) and pressures [4, 65]. PA has a triple bond and a hydroxyl group in its molecules as shown in **Figure 2-12**.

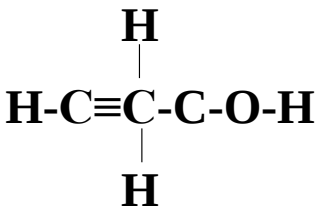


Figure 2-12 Chemical structure of propargyl alcohol (PA).

PA has been employed in conditions where the concentrations of HCl solution is in the range of 5-28wt%, but most notably in 15wt% HCl. The corrosion inhibition performance of PA is better in HCl solution because of the adsorption or polymerisation of PA on a metal surface.

2.8.1.1 Corrosion inhibition mechanism of PA

The corrosion inhibition of PA on metals, especially in iron or steel, in hydrochloric and sulphuric acid solutions was attributed to two possible mechanisms:

The chemical adsorption of PA through the pi-electrons of its triple bond (highly reactive) with the vacant d-orbital of the transition metals, which is further strengthened by the presence of the hydroxyl (OH) group in the molecule [63-65].

The corrosion inhibition due to polymerisation of PA on the metallic surface results in the formation of the adherent, insoluble and hydrophobic polymeric protective film [66- 70]. The polymeric film is composed of hydroxyl, carbonyl, carboxylate and saturated hydrocarbon material [68].

Some of the reviewed corrosion inhibition papers for metals in acidic solutions containing PA are summarised below:

Singh et al. [67] studied the corrosion inhibition efficiency of mild steel in 10wt% HCl containing 200 ppm at 30°C after 3 h. They showed that the inhibition efficiency of PA was 95% at 200 ppm. Furthermore, the inhibition efficiency of PA was not affected (95%) with increasing temperature from 30 to 90°C.

Aramaki and Fujioka [71] studied the inhibiting effect of PA against iron corrosion in 0.5 M HCl solution at 25°C after 1 h. The authors showed that the inhibition efficiency

of PA was 38% at a concentration of 1x 10^{-2} M. They concluded that the inhibition performance was due to the coverage of PA on the iron surface.

Quraishi and Jamal [72] investigated the corrosion inhibition of PA for mild steel in 15wt% HCl at 105±2°C for 30 minutes. The authors reported that the inhibition efficiency of PA increased from 12.22% (CR=12,628 mm/y) to 99.70% (CR=43 mm/y) with increasing concentration from 1000 to 5000 ppm. The corrosion protective properties were attributed to the formation of adherent and protective film on the metallic substrate, which isolated the substrate from the corrosive ions.

The summary of other reviewed work on PA in both acidic and neutral media is presented in Table 2-2.

Table 2-2 Summary of work on propargyl alcohol as corrosion inhibitors

Inhibitor	Medium	Concentration	Optimum inhibition efficiency	Material	Reference
PA	15 wt% HCl	100 – 900 ppm	96.79% (30˚C), 95.13 (40°C), 92.33% (50°C) and 90.98% (60˚C)	N-80 steel	[73]
PA	15 wt% HCl	0-1000 ppm	30˚C: WL (100%), TP (99%) and EIS (89%);105°C: WL (99%), PTP (99%),	Mild steel	[36]
PA	5 wt% HCl	0-100 ppm	WL: 30°C(100%) & 90 °C (97%)	Mild Steel	[74]
PA	1 M Phosphoric acid	50 mM	50°C: TP (98.2%) and EIS (98%)	Mild steel	[75]
PA	15wt%HCl	1000-5000 ppm	105°C: WL (99.7%)	Mild steel	[76]
PA	15wt%HCl	0-500 ppm	35°C: 98.29%	Mild steel	[76]
PA	0.5M H_2SO4	0.5-20 mM	94%	Mild steel	[46]
PA	0.2% acetic acid	200-1000 ppm	110˚C: 96.4%	Super13Cr steel	[77]
PA	0.5 M H_2SO_4	1.25-10 mM	TP (93.3%)	Low alloy Cr steel	[78]
PA	0.5 M HCl	0.01 M	TP (90%) at 70°C	Iron	[66]
PA	10 wt% HCl	200 ppm	WL at 30°C 95%	Mild steel	[67]

Note PP- potentiodynamic polarization, EIS- electrochemical impedance spectroscopy and WL- weight loss.

2.8.2 2-mercaptobenzimidazole (MI)

Heterocyclic compounds are organic compounds that have a ring structure containing nitrogen (N), sulphur (S) or oxygen (O) atoms, apart from carbon [79]. Examples of heterocyclic compounds are pyridine, pyrrole, furan, thiophene, 2- mercaptobenzimidazole, among others. These compounds have been widely used as corrosion inhibitors in different aggressive environments [34, 79-82] as well as in many biological fields [83]. The inhibitive efficiency of heterocyclic compounds depends on (i) the electronic structure of the molecule, which determines the electron density at the active centre of the molecule and (ii) the chemical structure, which is determined by the molecular volume and surface area as well as the steric distribution of the substituents [84].

2-mercaptobenzimidazole is one of the common heterocyclic compounds and is of major interest in this thesis, because it has been widely used as a corrosion inhibitor for metallic materials in different corrosive solutions such as phosphoric acid [85, 86], HCl [79, 87-90], sulphuric acid [87] and sodium chloride[91]. In addition, it is used for several biological activities such as anti-inflammatory [92], anti-convulsant [92], anti-microbial [92], and anti-oxidants [93].+96

MI has a pentagonal nitrogen ring (imidazole), a benzene ring and thiol group as shown in **Figure 2-13.**

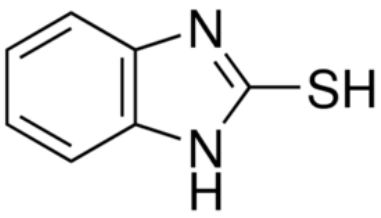


Figure 2-13 Chemical structure of MI [79].

MI has been widely reported to be an effective corrosion inhibitor in low HCl concentration [79, 88-90, 94-96]. However, little or no work has been done in a highly aggressive environment (15wt% HCl), which is of main interest in this thesis.

Some of the work reported on the inhibition effect of MI is summarised below:

Aljourani et al. [79] studied the corrosion inhibition efficiency of benzimidazole and its derivatives for mild steel in 1 M HCl containing 250 ppm of these compounds at 25°C. They showed that the inhibition efficiency is in this order: 2- mercaptobenzimidazole (88.76%) > 2-methyl benzimidazole (57.1%) > benzimidazole (52.2%). The corrosion inhibitive properties of these compounds are attributed to their adsorption on the metal surface, followed by blocking anodic dissolution and hydrogen evolution. They found that increasing temperature (25 to 55°C) decreased the corrosion inhibition efficiency of MI due to desorption from the metal surface.

Benabdellah et al. [97] investigated the inhibitive performance of 2- mercaptobenzimidazole (MI) for mild steel in 1 M HCl at 35°C after 6 h exposure time. They showed that the inhibition efficiency of MI was 98% at a concentration of 10^{-3} M and that this inhibitor acted as a mixed inhibitor by suppression both anodic and cathodic reactions on the steel surface. They further demonstrated that increasing temperature (25 to 80°C), decreased the performance of the inhibitor due to its desorption from the metal surface.

On the other hand, Popova et al. [50] found that MI effectiveness was not affected with increasing temperature (20 to 60°C) for mild steel immersed in 1 M HCl.

Morales-Gil et al. [88] investigated the corrosion inhibition of mild steel in 0.01M-1M HCl using 2mM 2-mercaptobenzimidazole (MI) after 4 h by linear polarisation resistance (LPR). They showed that the corrosion rate of mild steel decreased with

decreasing HCl concentration containing 2 mM MI. For example, 0.4 mm/y (2mM MI/1M HCl), 0.2 mm/y (2mM MI/0.1M HCl) and 0.1 mm/y (2Mm/0.01 HCl). They further demonstrated that MI impeded both the anodic and cathodic electrode reactions by its adsorption on the MS surface. **Table 2-3** shows the summary of some research work on the corrosion inhibition of metals in the presence of 2- mercaptobenzimidazole in acidic medium.

Table 2-3 Summary of work on 2-mercaptobenzimidazole as corrosion inhibitors.

Medium	Material	Concentration	Temperature	Inhibition efficiency (optimum)	Reference
1 M HCl	MS	150 ppm	35°C	WL (98%), EIS (95%) & TP (97%)	[97]
1 M HCl	MS	300 ppm	Room temp	LPR (98%)	[88]
0.1 M HCl	MS	300 ppm	Room temp	LPR (97%)	[88]
0.01 M HCl	MS	300 ppm	Room temp	LPR (92%)	[88]
1 M HCl	Carbon steel	250 ppm	25°C	TP (89%)	[87]
1 M HCl	MS	250 ppm	25°C	TP (88.7%)	[79]
1 M HCl	API 5L X52	200 ppm	Room temp	EIS (99%)	[90]
3 M H_3PO_4	MS	1.50 ppm	30°C	WL (98%)	[85]
3 wt% NaCl	Armco iron	750 ppm	25°C	WL (92.3%)	[91]
1 M H_2SO_4	Steel (API 5L X52)	25 ppm	Not stated	LPR (98.5%)	[98]
1 M H_2SO_4	Steel (API 5L X52)	25 ppm	Not stated	TP (99%)	[99]
1 M H_2SO_4	Carbon steel	25 ppm	25°C	TP (90.1%)	[87]
0.5 M HCl	Cu	150 ppm	40 °C	WL (91.6%)	[100]
1 M HNO_3	Cu	150 ppm	25 °C	WL (87.65%)	[101]

Note: LPR – Linear polarization resistance

2.8.3 Mixed corrosion inhibitors

In industrial applications, a single organic compound may not be able to achieve the desired corrosion inhibition of metallic structures and components, especially in highly aggressive conditions [29, 65, 102]. Consequently, some components such as intensifiers, surfactants, solvents, sol-gels are added to the corrosion inhibitors (active ingredient) to achieve the corrosion inhibitor effectiveness desired. The blend of the corrosion inhibitor formulation to be employed is dependent on the immersion time, type of acid and concentration, temperature and pressure and the type of metal.

Several authors have reported that the addition of other compounds such as halides to an inhibitor enhanced the inhibition performance [4, 102, 103]. For example, Heydary et al. [78] demonstrated that the addition of 0.01 wt% potassium iodide (KI) to 10 mM PA increased the inhibition efficiency from 93 to 97% for low alloy Cr steel in 0.5 M H_2SO_4. They claimed that the presence of KI stabilised the adsorption of PA on the steel surface. Zhang et al. [104] argued that the addition of 0.5 mM KI to 2- mercaptobenzimidazole (MI) 0.5 M H_2SO_4 inhibited solution enhanced the inhibition performance from 63 to 94%. The inhibition action was attributed to the initial adsorption of the iodide ions on the copper surface, which facilitated the adsorption of protonated MI. Larabi et al. [105] also corroborated this by demonstrating that the addition of 0.1 wt% KI to 100 mg/L poly (4-vinyl pyridine) (P4VP) enhanced the corrosion inhibition efficiency from 90 to 97% for mild steel in 1 M HCl. The authors attributed this behaviour to the chemisorption of P4VP on the mild steel surface, which was stabilised by the introduction of iodide ions into the solution.

2.8.4 Natural products as corrosion inhibitors in HCl solution

Overview

Natural products have been widely used as effective corrosion inhibitors to prevent or minimise the corrosion of several metals such as aluminium [106, 107], mild steel, zinc, copper in both acidic and neutral media [108]. The following review gives a summary of the research on the corrosion inhibitive performance of plant extracts for steel in acidic medium.

Chauhan and Gunasekaran [109] studied zanthoxylum plant extract as a corrosion inhibitor for mild steel in 5 and 15wt% HCl at 30°C. They found that zanthoxylum plant extract (24000 ppm) offers 95.0 % IE and 91 %IE in 5 and 15wt% HCl, respectively. The inhibitive performance of this inhibitor was attributed to the formation of a protective film on the steel surface, thereby blocking anodic and cathodic reactions.

Deng and Li [110] reported the use of ginkgo leaves extract (GLE) as a corrosion inhibitor for cold rolled steel in 5 M HCl solution at 25°C. They found that the corrosion inhibition efficiency of GLE was 61.7% at a concentration of 100 mg/L. The corrosion inhibition performance was due to the presence of flavonoids, ginkgolides and amino acids in GLE extract. This inhibitor was classified as a mixed-type inhibitor.

El-Etre [111] investigated aqueous extract of olive leaves as a corrosion inhibitor for carbon steel in 2 M HCl. He found that the inhibition efficiency of this extract was 91% at a concentration of 900 ppm. The author further concluded that the inhibitive properties were dependent on concentration, temperature. The extract was classified as a mixed inhibitor because it impeded both anodic and cathodic electrode reactions.

Da Rocha et al. [112] investigated orange, mango, passion fruit, and cashew peels as corrosion inhibitors for mild steel in 1 M HCl solution at 25◦C after 1 h. They demonstrated that all the fruit peels have inhibitive efficiency this order: orange (86%) >passion fruit (76%)> cashew (71%)>mango (67%). The authors attributed the inhibitive properties of these fruit peels to the adsorption of the hydroxyl groups in the extracts onto the steel surface. Also, the inhibition efficiency depends on both the temperature and concentration of the extract. These fruit peel extracts were classified as mixed-type inhibitors as they blocked both anodic and cathodic reactions.

Pereira et al. [113] studied the corrosion inhibition of garlic peels as a corrosion inhibitor for mild steel in 1 M HCl solution at 25◦C after 24 h exposure time. They found that the inhibition efficiency increased from 92% to 97% with increasing concentration of the extract from 100 to 400 mg/L. The authors also showed that the inhibition efficiency increased with increasing temperature and that the inhibitive performance was due to the presence of the organic sulphur compounds including, diallyl disulphide and methyl trisulphide that adsorbed on the metal surface, hence isolating the steel from the corrosion ions.

Ostovari et al.[12] investigated the corrosion inhibition performance of henna extract as a corrosion inhibitor for mild steel in 1 M HCl at 25◦C. The authors demonstrated that the inhibition efficiency increases with increasing concentration of the extract, reaching a maximum value of 92% at 1.2 g/L. The corrosion inhibitive performance was attributed to the formation of an insoluble complex compound by the lawsone (hennotannic acid) molecules in the extract with the metal cations. They also reported that the inhibitor acted as a mixed-type inhibitor.

Abiola and James [114] reported aloe vera extract as a corrosion inhibitor for zinc in 2 M HCl at 30◦C after 30 minutes. They found that the inhibition efficiency increased with increasing concentration (1-10% v/v) until a maximum value of 67% at a concentration of 10% v/v. They further showed that the inhibition efficiency of aloe vera decreased with increase in temperature and is due to physical adsorption of heteroatoms in different organic compounds (aloin, aloe-emodin, saponins, and steroids) in aloe vera on the steel surface.

Behpour et al.[115] reported two oleo- gum resins (Ferula assa-foetida and Dorema ammoniacum) as corrosion inhibitors for mild steel in 2M HCl. They demonstrated that the inhibition efficiencies of these extracts were 96% and 91%, respectively at a concentration of 0.8 g/L. The better corrosion inhibition efficiency offered by Ferula assa-foetida was attributed to stronger dipole-dipole interactions of the constituents in this compound and the metal surface. The inhibition efficiency of the extracts was found to depend on concentration (0.2-0.8 g/L) and temperature (30-60°C). Phytochemical screening showed that tannins, proteins, amino acids, and alkaloids were the primary constituents present in the extracts.

Khaled et al.[116] studied 16 amino acids as corrosion inhibitors for Armco iron in 1M HCl at 35°C. The best inhibition efficiencies exhibited by methionine (72%), cysteine (58%), cysteine (61%) and glycine (36%) were attributed to adsorption of the sulphur atom in their molecular structure on the metal surface. The best inhibition efficiency of methionine was due to the formation of a protective film on the iron surface, which impeded the electrochemical reactions.

Amin et al.[117] investigated alanine (Ala), S-methyl cysteine (S-MCys) and cysteine (Cys) as corrosion inhibitors for mild steel in 1M HCl at 25±2°C. They reported that

Cys was the most effective inhibitor due to the presence of the mercapto group in its molecule structure. They further claimed that Cys blocked more corrosion sites on the surface than the other compounds.

Bentrah et al.[118] showed that the inhibition efficiency of a natural polymer gum arabic increased with increasing concentration, reaching a maximum value of 92% at a concentration of 2 g/L for API 5L X42 in 1 M HCl solution at 25°C. Gum arabic was classified as a mixed-type inhibitor, and the mechanism of adsorption was due to physisorption.

The summary of the literature review for the corrosion inhibition of metals in acidic media is presented in Table 2-4.

Table 2-4 Inhibition efficiencies of different plant extracts used as corrosion inhibitors in various HCl solutions for different metals as reported in the articles.

Plant extracts	Inhibitor concentration	Medium	Material	Test methods and conditions	Inhibition efficiency	Reference
Garlic peel	10 – 1000 mg/L	1 M HCl	Carbon steel	WL at 25°C	32-96%	[113]
Geissospermum leaves alkaloid	10-100 mg/L	1 M HCl	Carbon steel	EIS at 25°C	80-90%	[119]
Phyllanthus leaves	0.1-4000 mg/L	2 M HCl	Mild steel	WL at 30°C	86-94%	[53]
Phyllanthus seeds	0.1-4000 mg/L	2 M HCl	Mild steel	WL at 30°C	61-80%	[53]
Phyllanthus leaves and seeds	0.1-4000 mg/L	2 M HCl	Mild steel	WL at 30°C	73-87%	[53]
Phyllanthus leaves	0.1-4000 mg/L	5 M HCl	Mild steel	GS at 40°C	27-75%	[53]
Phyllanthus seeds	0.1-4000 mg/L	5 M HCl	Mild steel	GS at 40°C	18-66%	[53]
Phyllanthus leaves and seeds	0.1-4000 mg/L	5 M HCl	Mild steel	GS at 40°C	59-74%	[53]
Zenthoxylum alatum	100-2400 mg/L	5 M HCl	Mild steel	EIS at 30°C	52-91%	[109]
Zenthoxylum alatum	100-2400 mg/L	5% HCl	Mild steel	EIS at 30°C	63-95%	[109]
Salvia officinalis leaves	500 -2000 mg/L	1 M HCl	Stainless steel	WL at 25°C	72-96%	[120]
Salvia officinalis leaves	2000 mg/L	1 M HCl	Stainless steel	WL at 25-65°C	96-97%	[120]
Gum arabic	400 -2000 mg/L	1 M HCl	API 5L X42	Tafel extrapolation at 25°C	68-93%	[118]
Justicia gendarussa	10-150 mg/L	1 M HCl	Mild steel	EIS at 25°C	79-86%	[121]
Justicia gendarussa	400 mg/L	1 M HCl	Mild steel	EIS at 60 and 70°C	94% and 91%	[121]
Occimum viridis	10-50 v/v%	2 M HCl	Mild steel	GS at 30°C	66-71%	[122]

Telferia accidentalis	10-50 v/v%	2 M HCl	Mild steel	GS at 30°C	83-94%	[122]
Hibiscus sabdariffa	10-50 v/v%	2 M HCl	Mild steel	GS at 30°C	57-90%	[122]
Azadirachta indica	10-50 v/v%	2 M HCl	Mild steel	GS at 30°C	94-95%	[122]
Garcinia kola	10-50 v/v%	2 M HCl	Mild steel	GS at 30°C	81-93%	[122]
Occimum vriridis	10-50 v/v%	2 M HCl	Mild steel	GS at 60°C	56-65%	[122]
Telferia accidentalis	10-50 v/v%	2 M HCl	Mild steel	GS at 60°C	28-40%	[122]
Azadirachta indica	10-50 v/v%	2 M HCl	Mild steel	GS at 60°C	89-96%	[122]
Hibiscus sabdariffa	10-50 v/v%	2 M HCl	Mild steel	GS at 60°C	48-73%	[122]
Garcinia kola	10-50 v/v%	2 M HCl	Mild steel	GS at 60°C	75-80%	[122]
Ripe banana peel	100-300 mg/L	1 M HCl	Mild steel	EIS at 26±1°C	66-82%	[123]
Water melon seed	100 -2000 mg/L	1 M HCl	Mild steel	Tafel polarization at 25°C	63-83%	[124]
Pectin (Citrus peel)	2000 mg/L	1 M HCl	Mild steel	WL at 15-45°C	90-94%	[125]
Jasminum leaves	1000 mg/L	1 M HCl	Aluminium	WL at 25-35°C	93-72%	[126]
Coffee	400 mg/L	1 M HCl	Carbon steel	WL at 25-55°C for 2 h	76-91%	[127]
Alkaloid extract of oxandra asbeckii	5-100 mg/L	1 M HCl	Carbon steel	Tafel polarization at 25°C	81-92%	[128]
Alkaloid extract of Neolamarckia cadamba	1-5 mg/L	1 M HCl	Mild steel	EIS at 30 ± 2°C	33-83%	[129]
Neolamarckia cadamba bark	1-5 mg/L	1 M HCl	Mild steel	EIS at 30 ± 2°C	64-82%	[129]
Neolamarckia cadamba leaves	1-5 mg/L	1 M HCl	Mild steel	EIS at 30 ± 2°C	67-84%	[129]
Bamboo leaves	10-100 mg/L	1 M HCl	Cold rolled steel	Tafel polarization at 20°C	61-89%	[130]
Mango peel	200-600 mg/L	1 M HCl	Carbon steel	EIS at 25± 2°C	80-91%	[112]
Orange peel	200-400 mg/L	1 M HCl	Carbon steel	EIS at 25± 2°C	63-95%	[112]

Passion fruit peel	200-500 mg/L	1 M HCl	Carbon steel	EIS at 25± 2°C	62-90%	[112]
Cashew peel	100-800 mg/L	1 M HCl	Carbon steel	EIS at 25± 2°C	56-80%	[112]
Mango peel	400 mg/L	1 M HCl	Carbon steel	WL at 25± 2°C from 1-24 h	67-96%	[112]
Orange peel	400 mg/L	1 M HCl	Carbon steel	WL at 25± 2°C from 1-24 h	86-95%	[112]
Passion fruit peel	400 mg/L	1 M HCl	Carbon steel	WL at 25± 2°C from 1-24 h	76-96%	[112]
Cashew peel	400 mg/L	1 M HCl	Carbon steel	WL at 25± 2°C from 1-24 h	71-93%	[112]
Dendrocalamus brandishii leaves extract	0.1-1 g/L	1 M HCl	Aluminium	Tafel polarization at 20°C	41-90%	[131]
Alkaloid extract from Aniba rosaeodara plant	25-200 mg/L	1 M HCl	Mild steel	EIS at 25°C	91-95%	[132]
Aloe vera extract	1-10 v/v%	2 M HCl	Zinc	WL at 40°C	30-59%	[114]
Zenthoxylum alatum	0.4-2.8 g/L	5% HCl	Mild steel	EIS at 30°C	64-69%	[109]
Ginger roots extract	0.05 – 0.2 g/L	1 M HCl	Carbon steel	WL at 25°C for 90 min	89.5-94.9%	[133]
Ginger roots extract	0.2 g/L	1 M HCl	Carbon steel	WL at 25-55°C for 90 min	94.9-62.85%	[133]
Osmanthus fragran leaves extract	0.034-0.34 g/L	1 M HCl	Carbon steel	Tafel polarization at 45°C	60.6-96.6%	[134]

Note: EIS =Electrochemical impedance spectroscopy, WL= weight loss measurements and GS = gasometric measurements.

Even though natural products have been used as corrosion inhibitors (CIs) to effectively prevent or minimize the dissolution of metals in acidic media, only a few papers have investigated the inhibitive properties of natural products in strongly acidic solution (15wt% HCl). Consequently, the main interest of this research work is to investigate the possibility of using natural products, specifically plant extracts, as a corrosion inhibitor for acidizing operations.

2.8.4.1 Inulin

Inulin (IN) is a naturally occurring polysaccharide and belongs to the class of carbohydrate known as fructans [14]. It can be found in various plants such as chicory roots, Jerusalem artichoke, asparagus, dahlia tuber, leeks, bananas, and garlic. Inulin can be used a fat or sugar replacer, prebiotic, i.e., promotes the growth of intestinal microorganisms, texture modifier, among others [14]. It is a polymer composed of several fructose units that are linked to one glucose unit by β (2, 1) at its terminal end as shown in **Figure 2-14 [14]**.

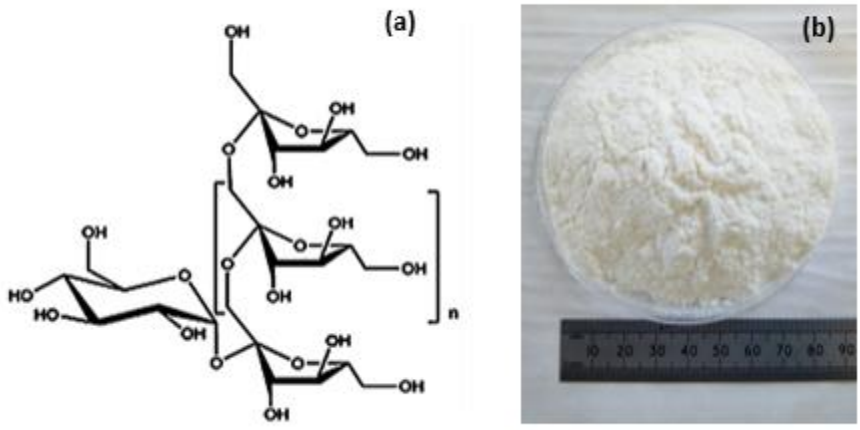


Figure 2-14 Chemical structure of IN (a) and a photograph of inulin powder (b) [14].

Hydrolysis of inulin occurs at low pH and high temperature, and in the highly acidic environment [14]. Inulin was selected as a candidate corrosion inhibitor because it is eco-friendly, biodegradable and has several hydroxyl (OH) groups in its molecule that can adsorb onto a metal surface by donating the lone pair electrons in the several hydroxyl groups of its molecule.

Choudary et al.[15] were the first to report the corrosion inhibitive properties of inulin for N-80 steel in 15wt% HCl solution. Although, the authors reported that IN inhibited the corrosion of N-80 steel in the strong acidic medium investigated, the mechanism of corrosion inhibition and characterisation of the inhibiting film were not investigated. An attempt has been made in this thesis in section 7.4.5 to discuss the corrosion inhibition mechanism. The results of IN as a corrosion inhibitor as reported in the literature is presented in Table 2-5.

Table 2-5 Corrosion inhibition efficiency of IN for N-80 steel in 15wt% HCl solution at 65 °C.

Medium	Inhibitor	Concentration (g/L)	Immersion time (h)	IE (%)	Reference
15wt% HCl	IN	3.6	6	55	[15]
15wt% HCl	IN	10.0	6	84	[15]
15wt% HCl	IN	20.0	3	43	[15]

2.8.4.2 Broccoli

Broccoli belongs to the cruciferous vegetable family, and its botanical name is Brassica oleracea. It grows when exposed to an average temperature between 18 and 23°C [135]. The chemical compounds present in broccoli are ascorbic acid, glucosinolates, phenolics, carotenoid, protein, carbohydrates [135, 136].

Broccoli was chosen as a candidate corrosion inhibitor because it is non-toxic, biodegradable, cheap and readily available; Also, because of the presence of heteroatoms in its compounds such as nitrogen (N), sulphur (S) and oxygen (O) which are possible reaction centres for anchoring onto the surface of a metal by donating their lone pair electrons. To the best knowledge of the author of this thesis, the corrosion inhibition performance of broccoli has not been reported for metals in either acidic or neutral medium.

2.8.4.3 Aloe vera

Aloe vera plants belong to the Liliaceae family, and its botanical name is called Aloe barbadensis miller. It has three layers: (i) the inner layer composed of gel (ii) the middle layer of the latex composed of glycosides and anthraquinones and (iii) the thick outer layer containing carbohydrates and protein [137, 138]. Aloe vera is used in several industrial applications due to its healing properties, antiviral and anti-tumour activity, anti-inflammatory action, laxative, moisturising and anti-ageing and antiseptic effects [137, 138].

Aloe vera gel is a viscous liquid that contains water, amino acids, phenolics, polysaccharides, vitamins, enzymes, among others [137].

Aloe vera has been studied previously as a corrosion inhibitor for metals in acidic media and reported in the literature [114, 139-141]. For example, Singh et al.[140] reported that the corrosion inhibition efficiency of aloe vera increases with increase in concentration (30-200 ppm), reaching a maximum value of 88% at a concentration of 200 ppm. The authors further showed that the inhibition efficiency of aloe vera gel depends on acid concentration and temperature. The decrease of inhibition efficiency of aloe vera gel with increasing temperature was due to its desorption from the mild steel surface. The mechanism of inhibition performance of aloe vera gel was attributed to its physical adsorption onto the mild steel surface. Eddy and Odoemelam [142] demonstrated that the inhibition efficiency of aloe vera extract for mild steel in 2.5 M H_2SO_4 also increases with concentration but decreases with increasing temperature. Similar decreasing inhibition performance of aloe vera gel with temperature (27 -80°C) for copper in 2 M HCl has been reported by Hart and James [139]. The authors claimed that corrosion inhibition action could be attributed to the synergistic effect of the compounds present in the extract.

2.8.4.4 Durum wheat

Durum wheat belongs to the family of Poaceae, and its botanical name is Triticum durum [143]. It is cultivated in the Mediterranean basin and other regions having similar climatic conditions[144]. The major chemical compounds in durum wheat are proteins (gliadins and glutenin), vitamins (vitamin B1, vitamin B6, vitamin A, and vitamin E), phenolics (trans-ferulic acid, anthocyanidins, flavanols), fibres (lignin and inulin) and minerals (selenium, magnesium, etc.) [144]. Durum wheat is used for bread, semolina, pasta, couscous, and other food products [144]. It has not been reported as a corrosion inhibitor for metals in both acidic and neutral media. Organic compounds having

heteroatoms such as N, O or S as well as multiple bonds or aromatic rings in their structures have been reported to be effective corrosion inhibitors [121, 127, 145-147]. Consequently, durum wheat was selected as a candidate green corrosion inhibitor in the current study because of the several reaction/active centres in the nitrogen atoms present in gliadin and glutenin, and the presence of aromatic rings, and hydroxyl groups that could bind onto a metallic surface, hence mitigating its corrosion.

2.9 Factors influencing the performance of corrosion inhibitors

The inhibition performance of corrosion inhibitors is attributed to the ease of the initial step of transportation of the inhibitor from the bulk solution before interacting with the metal surface[3, 29]. The influence of some factors may change the inhibition mechanism action of the organic compounds and affect its performance [29].

Some of these factors are inhibitor concentration, immersion time, temperature [3].

2.9.1 Inhibitor concentration

It is generally accepted that the corrosion rate of metal decreases and the inhibition efficiency increases with increase in the concentration of a corrosion inhibitor [12, 44, 148]. An example is shown in **Figure 2-15** [149].

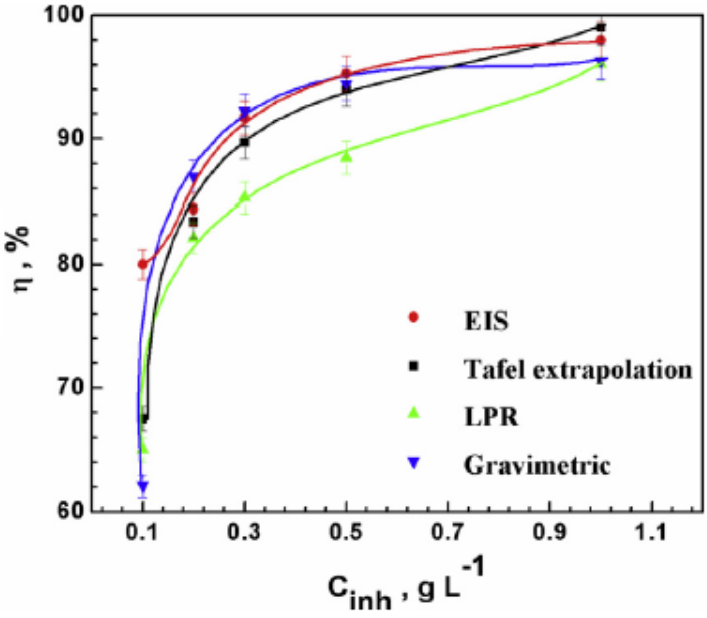


Figure 2-15 Variation of inhibition efficiency with different concentrations of marigold flower extracts by weight loss and electrochemical measurements [149].

The increase in inhibition efficiency has been attributed to increasing of the surface covered by the adsorbate (inhibitor) on the adsorbent (metal), thereby preventing the further attack of the metal by the corrosive ions [3, 12, 29, 150]. Some authors reported that an optimum inhibition performance could be achieved when there is complete coverage of an inhibitor molecule on a metallic surface [29, 151].

According to Yadav et al.[55], the corrosion rate of mild steel in 15wt% HCl decreased from 6.58 to 0.91 mm/y and the inhibition efficiency increased from 67.4 to 95.5% at 30°C with increasing concentration of spiropyrimidinethiones from 25 to 250 ppm. The increasing inhibition efficiency was attributed to an increase in the adsorption and surface coverage of the inhibitor on the mild steel surface.

Chauhan and Gunasekaran [109] have reported an increase in inhibition performance of Zanthoxylum alatum plant extract with increasing concentration from 400 to 2400 ppm due to increasing in the surface coverage of the extract on the steel surface.

Bentrah et al. reported that the inhibition efficiency of gum arabic increased sharply with increasing concentration (0.1-2g/L). However, a further increase in the concentration beyond 2 g/L did not influence the inhibition performance [118].

2.9.2 Immersion time

One of the ways to appraise the stability of inhibitor molecules on a metal surface is by varying the immersion time. Generally, the inhibition performance of most green CIs decreases with increasing immersion due to desorption of the pre-adsorbed inhibitor from a metallic surface [127, 152]. However, some authors reported that the protective film formed on the metal surface is strengthened at longer immersion time [153, 154].

D' Elia et al.[127] reported that the inhibition efficiency of coffee ground extract decreases (97 to 80%) with an increase in immersion time from 24 to 72 h for mild steel in 1 M HCl solution. They attributed the decreasing inhibition behaviour to desorption of the protective film formed on the steel surface.

On the other hand, Arockiasamy et al.[153] studied the effect of immersion time on the corrosion inhibition performance of Mollugo cerviana extracts for mild steel in 1M HCl at room temperature. They found that the inhibition efficiency of this extract increase (64 to 92%) with increasing immersion time from 1 to 72 h. The increasing inhibition performance was attributed to the increasing adsorption of the extract on the metal surface with time. In addition, Lebrini et al.[128] demonstrated that the corrosion inhibition efficiency of alkaloids extract of Geissospermum leaves for mild steel 1 M

HCl increases with time from 1 to 24 h due to increase in the adsorptive film with time, and then remained stable between 24 -72 h because of the formation of maximal thickness protective layer on the steel surface.

Solani et al.[120] reported that the inhibition performance of Salivia officinalis leaves extract for stainless steel in 1 M HCl did not change with an increase in immersion time (2-12 h) due to the formation of a stable and protective film on the metal surface.

From previous studies, it can be deduced that the corrosion inhibition performance of green CIs could be enhanced, decrease or remain unaffected depending on the stability and adherence of the adsorbed layer on a metallic surface.

2.9.3 Solution temperature

Temperature is an important kinetic factor that could affect the corrosion behaviour of metals and change the adsorption strength of inhibitors on metal surfaces [150]. It has a great effect on the rate of metal corrosion, and its variation is useful for studying and clarifying the adsorption mechanism of an inhibitor [155]. For example, chemisorption type of adsorption occurs when increasing temperature leads to increase in the inhibition performance [127, 156], whilst physisorption occurs when the inhibition performance decreases with increase in temperature [12, 150, 157]. The effect of temperature on an inhibited/metal reaction is highly complex due to several changes that occur on the metal surface such as (i) desorption or adsorption of adsorbed inhibitor molecules from or on the metal surface, and (ii) decomposition of the inhibitor molecules and re-arrangement of some inhibitor molecules from the metal surface [3, 29, 79]. The change in temperature could increase, decrease or have no influence on the corrosion inhibition performance of an organic compound [29]. Several authors

have reported the corrosion inhibition performance of green CI for metals in an acidic media. For example, Satapathy [121] reported that the inhibition efficiency of Justicia gendarussa plant extract (JGPE) decreased with increasing temperature from 25 to 75°C for mild steel in 1 M HCl due to the decomposition of the compounds present in JGPE. Furthermore, Souad et al.[158] found that the inhibition efficiency of amino-tris(methylene phosphonic) acid (ATMP) decreases (87 to 67%) with increasing temperature from 30 to 60°C for carbon steel in 1 M HCl solution. This behaviour was attributed to decreases in the adsorption strength of ATMP on the steel surface, and this is suggestive of physical adsorption mode.

Abiola and James [114] studied the effect of temperature on the corrosion inhibition performance of aloe vera extract for zinc in 2 M HCl. They claimed that the inhibition efficiency decreased from 67 to 59% with an increase in temperature from 30 to 40°C. They further reported that the aloe vera extract was weakly adsorbed (physisorbed) on the zinc surface, hence easily desorbed from the substrate. Gunasekaran and Chauhan [109] also reported the inhibition efficiency of Zenthoxylum alatum plant extract decreases and the corrosion rate of mild steel increases with increase in temperature from 30 to 80°C due to a decrease in the strength of the extract adsorption.

On the other hand, D'Elia et al.[127] found that the inhibition efficiency of coffee ground extract increases with increasing temperature from 25 to 55°C for carbon steel in 1 M HCl and the increases inhibitive performance was attributed to the strong chemisorptive bond between the steel surface and the compounds (alkaloids and phenolics) in the extract.

Recently, Qiang et al.[150] found that temperature (25-45°C) did not influence the inhibition performance of ginkgo leaves extract (GLE) for X70 steel in 1M HCl because the protective film remained stable at high temperature.

It was observed that little research had been done on the effect of temperature on green corrosion inhibitors, especially plant extracts, for mild steel in a strong acid medium (15wt% HCl) at elevated temperatures. One of the aims of this thesis is to investigate the influence of temperature on the selected green inhibitors used for acidizing treatment application.

CHAPTER THREE

EXPERIMENTAL METHODOLOGY

3.1 Introduction

This chapter presents the experimental protocols employed for the preparation of the various inhibitors and the MS samples used for this work. Also, the experimental procedures for the corrosion tests (weight loss and electrochemical) and the surface characterization were presented. Surface micrographs were obtained using scanning electron microscopy (SEM). The nature and composition of the adsorbed layer formed at the MS surface after weight loss measurements were investigated using X-ray photoelectron spectroscopy (XPS) and attenuated total reflectance Fourier transform infrared spectroscopy (ATR-FTIR) was used to identify the functional groups in the inhibitors. The chemical constituents in the green inhibitors were investigated by gas chromatography-mass spectroscopy (GC-MS). The overview of the experimental methodology was presented in **Figure 3-1**.

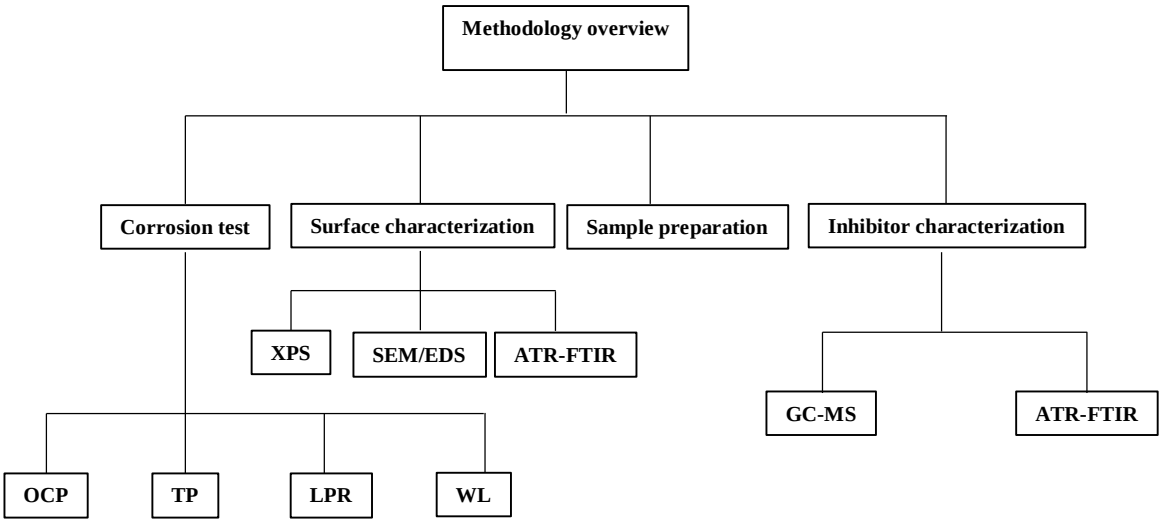


Figure 3-1 Overview of the experimental methods used in this work.

OCP: Open circuit potential

TP: Tafel polarization

LPR: Linear polarization resistance

WL: Weight loss

XPS: X-ray photoelectron spectroscopy

SEM: Scanning electron microscopy

EDS: Energy dispersive spectroscopy

GC-MS: Gas-chromatography mass spectrometry

ATR-FTIR: Attenuated total reflectance Fourier transform infrared

3.2 Materials

3.2.1 Synthetic inhibitors

Propargyl alcohol (PA) (Sigma-Aldrich, UK) and 2-mercaptobenzimidazole (MI) (Sigma-Aldrich, UK) used as reference inhibitors in this research were used as supplied without further purification and the chemical information are summarised in Table 3- 1. The chemical structures of PA and MI are shown in Figure 3-2.

Table 3-1 Chemical compositional information of the reference synthetic inhibitors.

Material	Molecular formula	Molecular weight (g/mol)	Form	Product Number
PA	C_3H_4O	150.2	Liquid	P50803
MI	$C_7H_6N_2S$	56.1	Powder	M3205

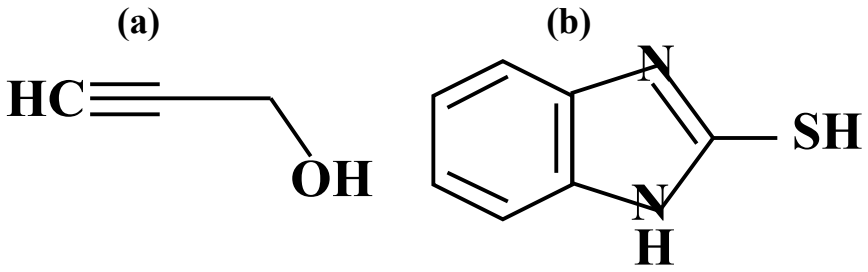


Figure 3-2 Chemical molecular structures of (a) PA and (b) MI.

3.2.2 Green inhibitors

3.2.2.1 Durum wheat inhibited solution

Different amount (1, 4, 7 and 10 g) of commercial durum wheat powder (East end foods, Nottingham) having particle size 0.782 µm was added to 600 mL distilled water, stirred for 10 minutes, before adding 400 mL HCl solution to prepare the durum wheat inhibited HCl solution in the concentration range from 1 – 10 g/L.

3.2.2.2 Broccoli inhibited solution

Fresh broccoli heads (Lidl, Nottingham) were chopped and dried in an oven at 80°C for 3 h to remove excess water. Then, the dried broccoli was pulverized using a blender before it was sieved using a 0.8 mm mesh. 20 g sample of the broccoli powder was added to water (100 ml / 10 g), refluxed in a round flask at 40°C for 2 h and then allowed to cool down for 3 h. The refluxed solution was filtered using an electric vacuum filter, and different concentration of the stock solution (1, 4, 7 and 10 g) was added to the HCl solution to prepare the broccoli inhibited solution in the range from 1 - 10 g/L.

3.2.2.3 Aloe vera gel inhibited solution

Aloe vera leaves (IKEA, Nottingham) shown in Figure 3-3(a) with approx. 10 to 25 cm in length, 2 to 2.5 cm in width and 1.5 cm thickness were washed under running water to remove dirt. Then, the aloe vera leaves were cut open with a knife, and its gel was squeezed out through a muslin cloth. 331 g of the gel was obtained from 855 g aloe vera leaves, and the gel was used within 30 minutes of extraction. Different concentrations of aloe vera gel (4, 7, 10, 50, 100 and 110 g) was added to 4.5 M HCl solution to prepare aloe vera inhibited solution of concentration in the range from 4 to 110 g/L.

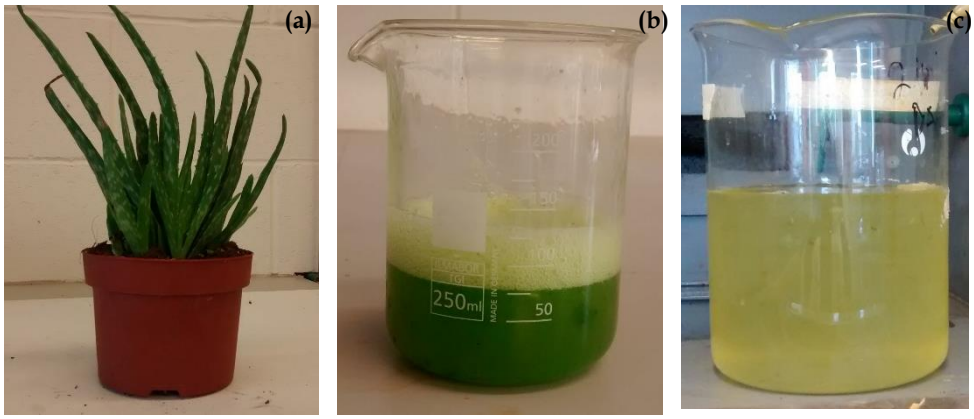


Figure 3-3 (a) Aloe vera plant; (b) Extracted gel; (c) 15% HCl solution with aloe vera gel

3.2.2.4 Inulin

Different quantities (1, 4, 6 and 10 g) of inulin powder from Jerusalem artichoke (Swanson Health products, UK) were added to 600 mL ml of distilled water and stirred for 10 minutes. Subsequently, 400 mL of 12 M HCl solution was added to already stirred inulin solution to obtain inulin inhibited HCl solution over the concentration range of 1 – 10 g/L.

3.2.3 Test solution

The acidic test solution (15 wt% HCl) used throughout this experiment was prepared by adding 400 mL of 37 wt. % HCl analytical reagent (AR) grade (Thermo- Scientific, U.K.) to 600 mL double distilled water. A fresh solution was prepared for each experiment.

3.3 Sample preparation

Weight loss measurements were carried out using rectangular as-received mild steel specimens (Smith metals, Nottingham) of size 6 cm × 4 cm × 0.3 cm having composition shown in Table 3-2. The elemental composition of the as-received mild steel substrates was determined using an optical emission spectrometer (FOUNDRY- MASTER UV, Oxford Instruments, UK).

Table 3-2. The chemical composition of the as-received mild steel specimen.

Element	Composition (wt.%)
C	0.06
Mn	0.32
S	0.01
P	0.01
Cu	0.02
Si	0.03
Cr	0.01
Ni	0.02
Fe	99.52

The samples were degreased in acetone, then rinsed thoroughly with distilled water and dried with hot air. Also, the edges and bottom of the specimens were carefully painted with acid resistant lacquer (composed of toluene, xylene, isobutyl methyl ketone, butanone, 2-methoxy-1-methyl-acetate, and 1-methoxy-2-propanol) leaving the exposed surface area of ~ 20 cm^2. Then the specimens were dried again, weighed on an analytical balance (Sartorius PRACTUM213-1S, Germany) with an accuracy of ± 0.1 mg and stored in a desiccator before use. The average surface roughness (R_a) of the as-received MS sample was 1.343 µm, obtained via a Bruker NP FLEX surface 3D profilometer with a vertical resolution of < 0.15 nm.

It should be noted that the acid resistant lacquer may come off the sample at high temperature during the experiments, thereby exposing the initially covered part of the sample to the aggressive solution and increasing the corrosion rate.

Figure 3-4 shows the photograph of the sample used for the weight loss test.

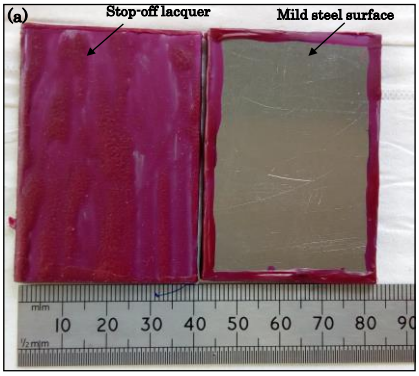


Figure 3-4 Photograph of the as-received MS sample used for the weight loss test.

For electrochemical measurements, mild steel specimens of size 2 cm × 2 cm × 0.3 cm were embedded in a non-conductive epoxy resin and masked with lacquer, leaving an exposed surface area of 1 cm^2 to the electrolyte. The preparation and cleaning procedures of the specimens were carried out as described for weight loss measurements. The mild steel samples were used in the as-received condition as a representative of the ideal service conditions for all the experiments.

Figure 3-5 shows the photograph and schematic diagram of the working electrode used for the electrochemical measurements.

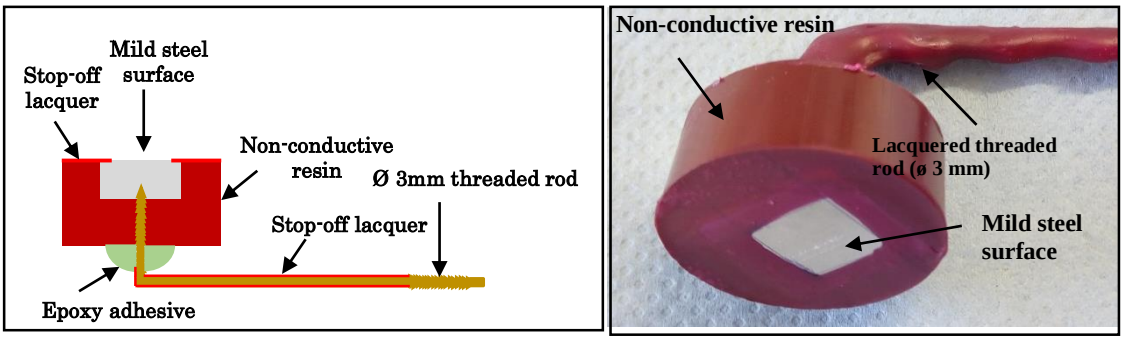


Figure 3-5 (a) Schematic diagram and (b) a photograph of the working electrode used for the electrochemical tests.

3.4 Corrosion testing

3.4.1 Weight loss measurements

Three pre-weighed MS samples were immersed completely in a 5 L beaker containing 3000 mL test solutions (15 wt. % HCl) without and with different concentrations of each inhibitor. The temperature of the test solutions (20-60 ± 1 °C) was controlled using a water bath and monitored with a digital K- type thermocouple for immersion times of 5 – 192 h at 20°C and 5- 24 h at 40 and 60°C, respectively. After completion of the tests, the specimens were taken out, thoroughly washed with distilled water and blown dry, before they were re-weighed.

The corrosion rate (CR) was calculated using eq 3-1 [54, 110, 125, 159]:

$$\mathbf{CR} = \frac{\Delta W}{S \times t} \qquad \text{Eq 3-1}$$

where ΔW is the average weight loss, S is the exposed surface area of the MS sample, and t is the immersion time.

The inhibition efficiency (η) was calculated from the corrosion rate values according to eq 3-2 [54, 110, 125, 159]:

$$\boldsymbol{\eta = \frac{C_R^O - C_R^i}{C_R^O} \times 100} \qquad \text{Eq 3-2}$$

where $\boldsymbol{C_R^O}$ and $\boldsymbol{C_R^i}$ represents the corrosion rate of the mild steel specimens without and with different concentrations, respectively.

3.4.2 Electrochemical measurements

A three-electrode glass cell (1L) assembly with MS sample as the working electrode, platinum wire as the auxiliary/counter electrode and a silver/silver chloride electrode (3 M KCl) as the reference electrode was used for all the electrochemical measurements. Before each test, the open circuit potential (OCP) of the MS sample was monitored for 1 h to ensure that a steady state condition was achieved.

Tafel polarisation (TP) measurements were carried out from a cathodic potential of – 250 mV to the anodic potential of + 250 mV for the OCP at a scan rate of 1 mV/s. Linear polarization resistance (LPR) measurements were carried out by applying a potential scan in the range of ±10 mV with respect to the corrosion potential at a scan rate of 0.1 mV/s.

All electrochemical measurements described above were carried out in a glass cell containing 500 ml of 15 wt. % HCl in the absence and presence of the studied inhibitors. A potentiostat (Volta Lab PGZ 100, UK) connected to a personal computer was used for the Tafel polarization measurements, and the data were analysed using VoltaMaster4 software.

LPR measurements were performed using a PalmSens3 (Netherlands) and analyzed with PS TRACE 4 software.

The solution temperature was maintained at 20, 40 and 60 ± 1°C. The results presented are the average of three different measurements.

The schematic diagram of the electrochemical set-up is presented in Figure 3-6.

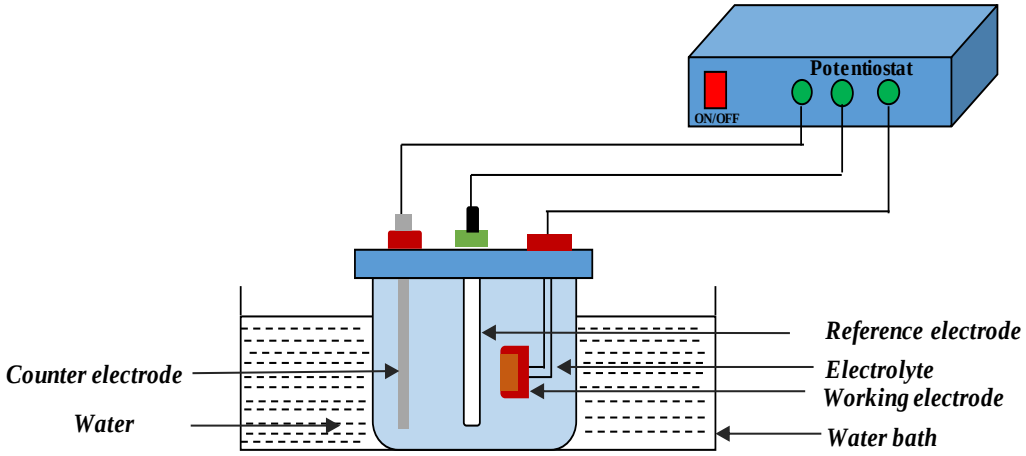


Figure 3-6 A schematic representation of a three-cell electrochemical set-up.

For the potentiodynamic polarisation measurements, the Tafel anodic and cathodic curves were extrapolated to the corrosion potential (E_{corr}) to determine the electrochemical parameters including corrosion current densities (i_{corr}).

The inhibition efficiency (η %) was calculated using equation 3-3 [54, 110, 129, 160]:

$$\eta\% = \left(\frac{i^{o}_{corr} - i_{corr}}{i^{o}_{corr}}\right) \times 100 \qquad \text{Eq 3-3}$$

where i_{corr}^{o} and i_{corr} are the corrosion current densities in the absence and presence of the studied inhibitors, respectively.

For the linear polarization resistance measurements, the inhibition efficiency was calculated using Equation 3-4:

$$\boldsymbol{\eta\% = \left(\frac{R_p^i - R_p^o}{R_p^i}\right) \times 100} \qquad \text{Eq 3-4}$$

where $R_p^o \ and \ R_p^i$ are the polarization resistances in the absence and presence of the inhibitors.

3.5 Material characterization

3.5.1 X-ray photoelectron spectroscopy (XPS)

XPS is a useful analytical technique for probing the surface chemistry of sample(s) up to 10 nm. In this process, samples to be analyzed are irradiated with X-ray photons (hv) in an ultra-high vacuum (UHV) chamber to minimize photoelectron scattering and reduce the amount of contamination on the surface, amongst others, thereby causing photoelectrons to be emitted from the sample surface. The electron energy analyzer measures the kinetic energy of the emitted photoelectrons, and the binding energy can be determined from Eq 3.5.

$$\mathbf{E_B = hv - E_K - \phi} \qquad \text{Eq 3-5}$$

Where E_B is the binding energy of the electrons, hv is the energy of the incident X-ray photon, E_K is the kinetic energy and ϕ represents the work function of the spectrometer. The schematic of the basic components of XPS is represented in Figure 3-7.

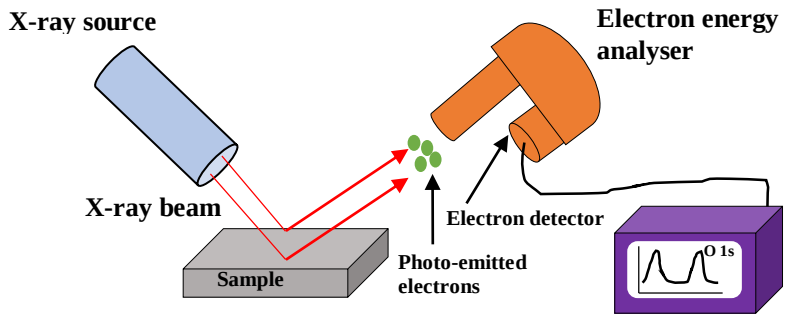


Figure 3-7 A schematic representation of the basic components of XPS.

In this study, XPS analyses were carried out on mild steel samples (1 cm × 1 cm) immersed in 15 wt.% HCl solution without (control) and with an optimum concentration of the studied inhibitors at 20ºC. After 5 h of immersion of weight loss measurements, the samples were removed from the solution, washed with ultrapure water to prevent contamination and dried. Then, the samples were mounted on sample bars with copper clips and put in an ultra-high vacuum chamber at a pressure of 8×10^{-9} torr. The sample surface (0.3 mm × 0.7 mm) was then analyzed with a Kratos AXIS ULTRA spectrometer having a monochromatic Al Kα X-ray source of 1486.6 eV, emission current of 10 mA and anode potential of 12 kV. The survey and high- resolution scans were performed at pass energies of 80 eV (step size of 0.5 eV) and 20 eV (step size of 0.1 eV), at three different positions on each sample. The photoelectrons emitted from the sample surface were collected with an electrostatic

lens, and survey scans performed within 10- 20 mins and high-resolution scans were run for approximately 10 minutes. The elemental atomic % values of various elements detected on the sample surface were determined from the peak areas of the survey scan data. All XPS spectra were charge corrected with reference to C 1s peak at a binding energy of 285 eV to compensate for the adventitious carbon contamination due to exposure of the samples to the atmosphere before transferring them to the vacuum chamber. The sample surface was analyzed at a probe depth of 10 nm, and the data were processed with CasaXPS software.

3.5.2 Scanning electron microscopy (SEM) and energy dispersive X-ray spectroscopy (EDS)

The interaction of a focused, energetic beam of electrons with sample results in the production of several signals such as secondary electrons (SE), backscattered electrons (BSE), characteristic X-rays, continuous X-rays, and fluorescence X-rays [161] as shown in Figure 3-8. BSE is produced when incident electrons interact with the atomic nucleus of a sample, and these electrons deflect elastically through an angle of about 180°. In this type of interaction, the kinetic energy loss is negligible. The higher atomic number of a sample leads to a higher amount of an elastically scattered BSE, resulting in a brighter image. In other words, the heavier the elements present, the brighter the region of the BSE image. BSE gives information about the elemental composition of a sample[161].

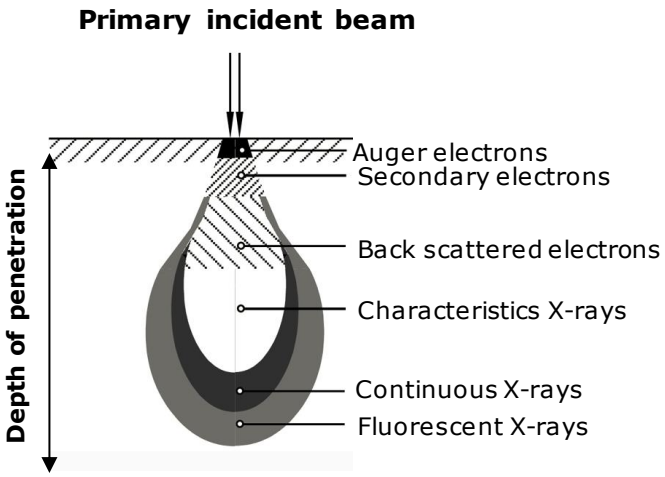


Figure 3-8 Interaction volume of the incident beam of electrons with a sample [161].

Secondary electrons (SEs) are produced when an incident beam of electrons elastically collides with an atom, resulting in the ejection of a loosely bound valence electron of the K-orbital of the atom. The ejected electrons are known as SEs having a kinetic energy of less than 50 eV [161]. Secondary and backscattered electrons are the two signals that are commonly used to produce images.

In this study, the MS samples were analyzed using PHILIPS XL30 SEM at an accelerating voltage of 20 kV and a spot size of 5. Subsequently, the elemental composition of the MS samples was obtained using the EDS system with INCA X-ray microanalysis software.

3.5.3 Gas Chromatography-Mass Spectroscopy (GC-MS)

GC-MS is a combination of two analytical techniques for separating, identifying and quantifying the components of a sample, which must be volatile and thermally stable [162]. The sample was introduced into a heated injector (200 -300 °C) of the GC, where it was vaporized and carried by a carrier gas (usually helium (He) because it is an inert gas and does not react with the sample components) into the capillary column [162]. Then, the individual components in the mixture were separated in the column due to

the interaction with the stationary phase and later eluted from the column to the detector at different times (retention times). At the detector, the eluted components were converted to ions by a beam of the electron (electron ionization). Subsequently, the ionized molecules were accelerated to the mass analyzer and separated according to their mass-to-charge ratios (m/z) [162]. The different components in the mixture were then analyzed and presented in the form of a mass spectrum, and the unknown components were compared with the library database. It should be noted that the yield of phytocompounds is dependent on the GC-MS sample preparation or solvent type used for extraction (e.g., hexane or water-based) [163].

The schematic illustration of a typical GC- MS system is presented in Figure 3-9.

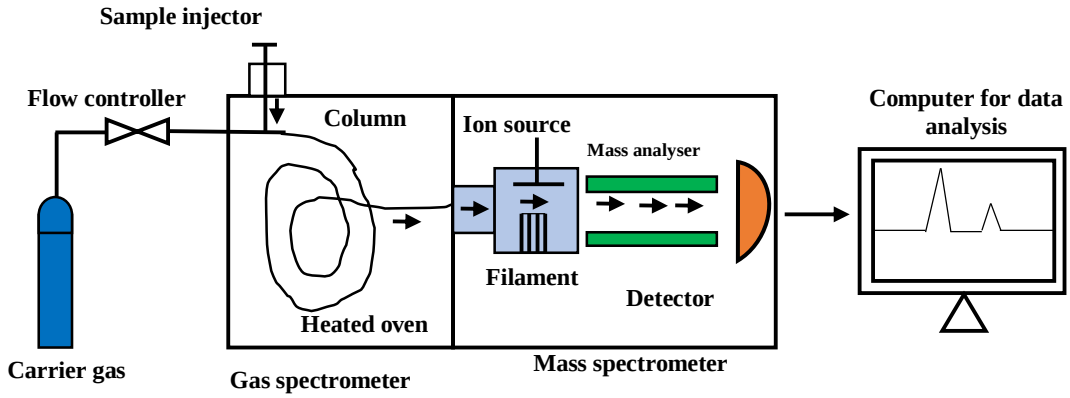


Figure 3-9 A schematic representation of GC-MS system.

In this study, GC-MS analysis of the extracts of various natural products was carried out using Agilent 7890B (Agilent Technologies Inc., Wilmington, USA) GC equipped with DB-5MS capillary column (30 m in length, 0.25 mm in diameter, and 25 µm film thickness) and a JEOL mass spectrometer with ionisation energy of 70 eV. The oven temperature was programmed to 50°C for 4 min and then increased to 350°C at 10°C/min. The inlet temperature was maintained at 200°C, and pure helium (99.99%)

was used as the carrier gas at a flow rate of 1 mL/min. The acquisition mass range was 50-500 Da. 3g (approx., weighed accurately) of the natural product (broccoli, durum wheat, inulin, and aloe vera) were placed in an 8-dram vial, and 20mL hexane was added. The vial was sealed (using an aluminium foil barrier over the plastic top to prevent contamination through solvent leaching) and shaken for 10 min. Shaking was repeated every hour during the working day, and the samples were then allowed to stand overnight. An aliquot (1.5mL) of the supernatant was taken and the solvent allowed to evaporate at ambient temperature under a stream of dry nitrogen. The dried extract was then resolvated with 30 µL hexane, and 1 µL was injected into the GC- MS for analysis [164]. The peaks observed in the chromatograms from the GC- MS analysis of each of the hexane extracts were matched with NIST 14 (National Institute of Standards and Technology) mass spectral library.

3.5.4 Attenuated Total Reflectance-Fourier transform infrared (ATR-FTIR) Spectroscopy

ATR-FTIR is a good technique for analysing samples because it requires little or no further sample preparation. This is achieved by passing an infrared (IR) beam onto an optically dense ATR crystal having a high refractive index (usually a diamond or germanium) at a specific angle of incidence. The internal reflection of the IR beam at the surface of the ATR crystal creates an evanescent wave that extends into the sample at a certain depth of penetration (D_p), usually between 0.5-5 µm. The magnitude of D_p depends on the wavelength of IR light, the angle of incidence and the refractive index of the ATR crystal. The internally reflected beam exits the crystal and then collected by a detector, where it is analyzed and displayed as an ATR-FTIR spectrum[165]. The basic principle of ATR-FTIR is schematically represented in **Figure 3-10**.

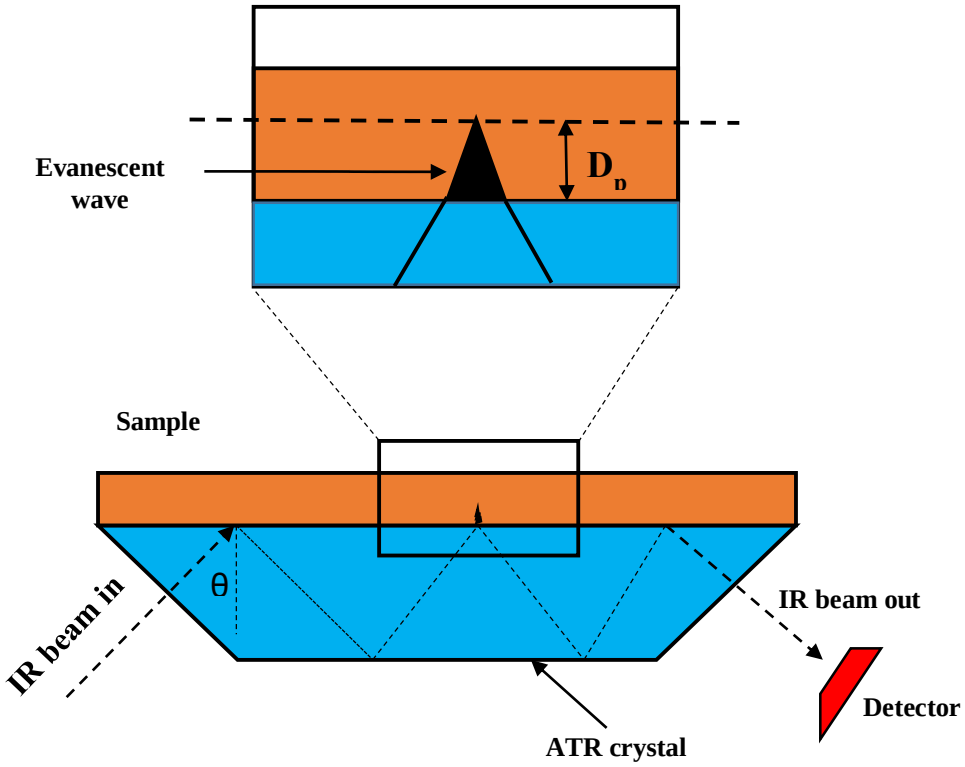


Figure 3-10 Schematic illustration of ATR-FTIR principle.

In this study, ATR-FTIR analysis was carried out to identify the organic functional groups present in the natural products. Samples of the studied natural products were placed on a diamond crystal, and all spectra were collected at a resolution of 4 cm^{-1} in the wavenumber range of 4000-550 cm^{-1} using a Bruker Tensor FTIR spectrometer coupled with an Attenuated Total Reflectance (ATR) accessory. The samples were scanned over the average of 32 scans, and each spectrum was processed and analyzed using OPUS software.

CHAPTER FOUR

ESTABLISHING CORROSION INHIBITION EFFECT OF THE INHIBITORS

4.1 Introduction

This chapter presents the results of the corrosion inhibition efficiencies of the reference inhibitors (propargyl alcohol (PA) and 2-mercaptobenzimidazole (MI)) and the plant-based inhibitors: durum wheat (DW), broccoli (BC), inulin (IN) and aloe vera gel (AV). The specific results are presented in the sub-sections below.

4.2 Determination of suitable acid volume per sample

The adequate amount of HCl solution per sample test was determined to know the appropriate quantity of the test solution to use throughout this work and to show that the results obtained were independent of volume used.

Figure 4-1 shows the variation in weight loss of a standard size (60 mm × 40 mm × 3 mm) MS sample as a function of the volume of HCl solution at 20°C after different immersion times (1, 2 and 6 h). As illustrated in the figure, the weight loss of MS decreases as the volume of the test solution increased from 500 to 1000 ml, and then remained almost constant with further increase in the volume of the test solution from 1000 to 2000 ml. This trend was observed for the different immersion times (1, 2 and 6 h) investigated. The results indicated that 1000 mL of the test solution per sample was enough for the test. Therefore, 1000 mL of 15 wt% HCl solution/sample was used throughout this work.

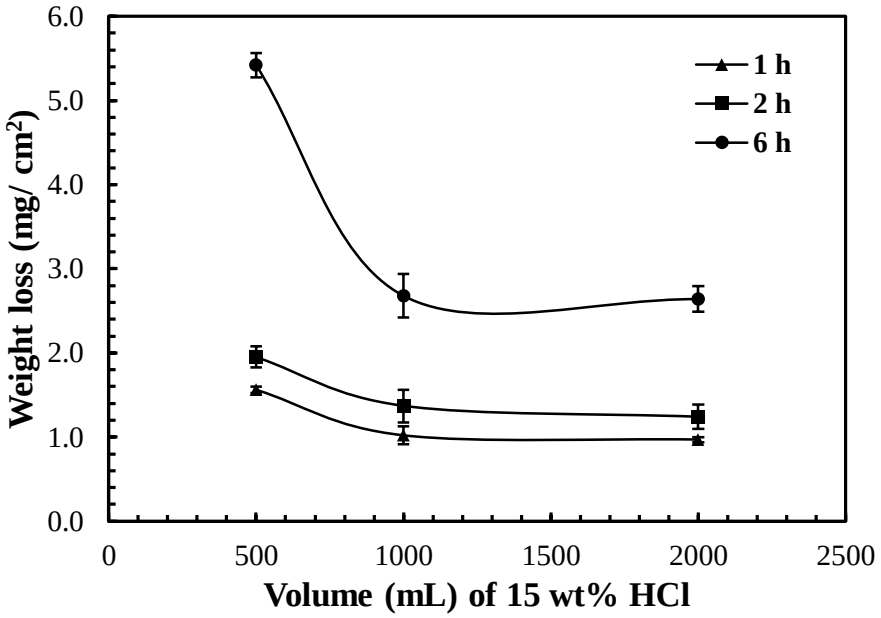


Figure 4-1 The variation in weight loss of the as-received MS with volume of 15 wt. % HCl after 1, 2 and 6 h of immersion at 20°C. Error bars show standard deviations of the three measurements. The solid line is included as a guide to the eye and does not represent a model of the experimental data.

4.3 Effect of concentration on corrosion inhibition

Table 4-1 shows the corrosion rates of MS immersed in 15 wt.% HCl in the absence and presence of different concentrations of PA, MI, DW, BC, IN and AV at 20°C after 5 h. The corrosion rate of MS decreases with increasing concentration for both synthetic and green inhibitors until a point where a further increase in concentration did not change the corrosion rate markedly. It was noted that the different inhibitors studied have different optimal concentrations - a point where there was no significant change in the corrosion rate. The optimal concentrations were 7 g/L for PA, MI and DW, 10 g/L BC and IN, while AV had 100 g/L. Hence, these optimum concentrations were used throughout this work.

Table 4-1 Weight loss and corrosion rate data of MS in 15 wt.% HCl in the absence and presence of different concentrations of PA, MI, DW, BC, IN and AV after 5 h of immersion at 20°C.

Inhibitor	Concentration (g/L)	Weight loss (mg/cm^2)	Corrosion rate (mg/cm^2h)
Control	0.0	13.510 ± 0.200	2.704 ± 0.040
PA	1.0	0.234 ± 0.005	0.047 ± 0.001
	4.0	0.132 ± 0.048	0.026 ± 0.010
	7.0	0.045 ± 0.029	0.009 ± 0.003
	10.0	0.045 ± 0.018	0.009 ± 0.002
MI	1.0	0.855 ± 0.123	0.171 ± 0.025
	4.0	0.605 ± 0.018	0.121 ± 0.004
	7.0	0.452 ± 0.048	0.095 ± 0.010
	10.0	0.490 ± 0.021	0.098 ± 0.005
DW	1.0	1.753 ± 0.569	0.351 ± 0.114
	4.0	0.421 ± 0.110	0.084 ± 0.022
	7.0	0.352 ± 0.043	0.065 ± 0.009
	10.0	0.333± 0.038	0.067 ± 0.008
BC	1.0	5.281 ± 0.197	1.056 ± 0.039
	4.0	2.338 ± 0.074	0.468 ± 0.015
	7.0	1.455 ± 0.294	0.360 ± 0.059
	10.0	1.507 ± 0.073	0.312 ± 0.021
IN	1.0	6.07 ± 0.482	1.214 ± 0.964
	4.0	3.79 ± 0.090	0.757 ± 0.017
	7.0	3.27 ± 0.120	0.655 ± 0.025
	10.0	2.76 ± 0.110	0.551 ± 0.023
	11.0	2.82 ± 0.100	0.564 ± 0.021
AV	4.0	12.308 ± 0.198	2.462 ± 0.040
	7.0	11.782 ± 0.562	2.356 ± 0.112
	10.0	10.537 ± 0.475	2.107 ± 0.095
	50.0	4.973 ± 0.442	0.995 ± 0.088
	100.0	1.985 ± 0.293	0.397 ± 0.059
	110.0	2.000 ± 0.023	0.400 ± 0.038

Figures 4-2 and **4-3** show the effect of different concentrations of the studied inhibitors on their inhibition efficiencies for MS immersed in 15 wt.% HCl at 20°C after 5 h immersion using weight loss measurements. Figure 4-2 revealed that there is no significant change in the inhibition efficiency of PA with increasing concentration. However, the inhibition efficiency of MI increases with increase in concentration from 1 to 7 g/L, and the inhibition efficiency slightly decreased beyond 7g/L. For the plant- based inhibitors, the inhibition efficiencies of DW increase with an increase in concentration up to 7 g/L. For both BC and IN, the inhibition efficiency increases with increase in the concentration from 1 to 10 g/L, while the inhibition efficiency of AV increases with concentration up to 100 g/L. It is evident that a significantly higher concentration of AV is required to achieve high inhibitive performance compared to other inhibitors. The graph of AV was plotted separately because of its higher concentrations. The inhibition efficiencies of PA, MI, DW are 99.7±0.2%, 96.5±0.4%, 97.8±0.3% at 7 g/L, whilst that of BC and IN are 88.4±0.9% and 79.6±0.5% at 10g/L. The inhibition efficiency of AV was 84.4±2.0% at a concentration of 100 g/L.

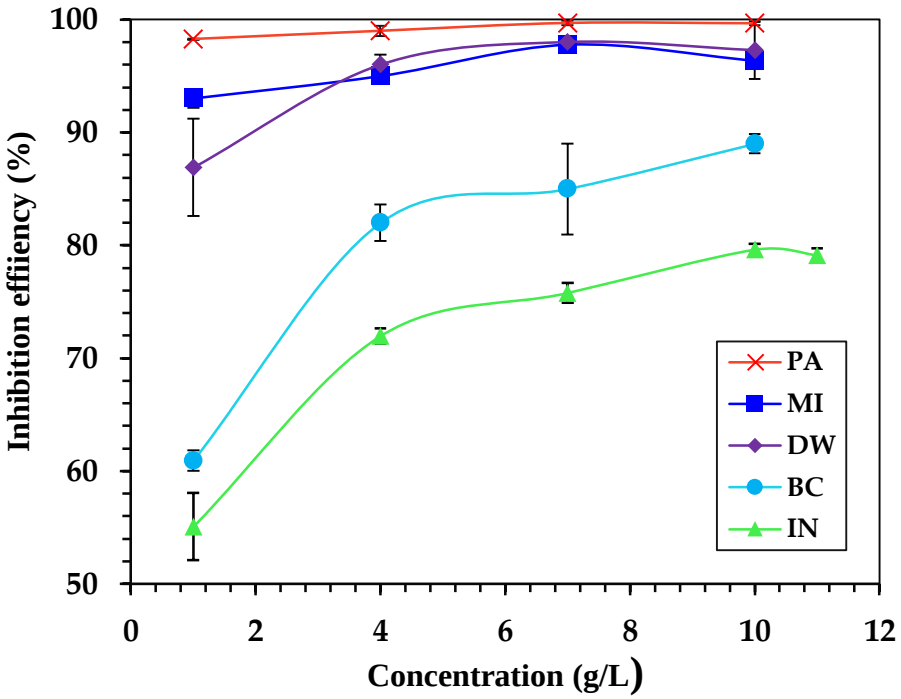


Figure 4-2 Dependence of corrosion inhibition performance on different concentrations of PA, MI, DW, BC and IN for MS in 15 wt.% HCl at 20°C after 5 h. Error bars represent standard deviations of three measurements.

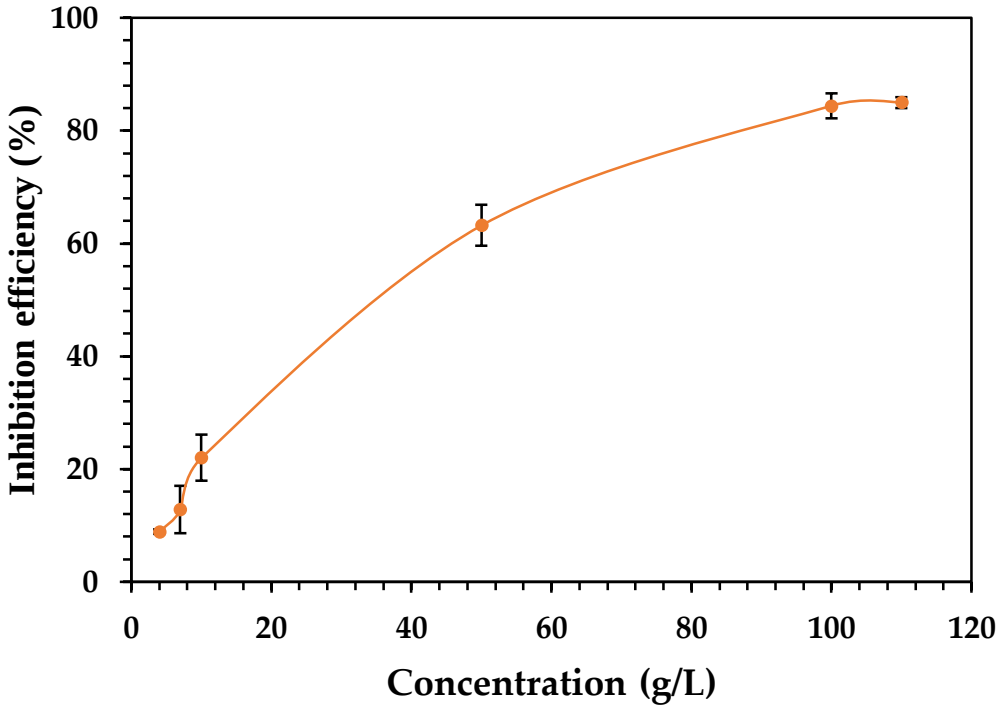


Figure 4-3 Dependence of corrosion inhibition performance on different concentrations of AV for MS in 15 wt.% HCl solution at 20°C after 5 h. Aloe vera was plotted differently because of its range of concentration (4-110 g/L). Error bars represent the standard deviation of three measurements.

4.4 Effect of temperature on corrosion of MS

Temperature is one of the factors that affect the corrosion rate of metals and the stability of inhibitor molecules at the surface of metal [50]. Hence, the influence of temperature on the inhibition performance of the studied inhibitors for MS in 15 wt.% HCl solution was investigated using weight loss, potentiodynamic polarization, and linear polarization resistance measurements.

4.4.1 Weight loss results

As shown in Table 4-2, the corrosion rate increased with increasing temperature from 20 to 60˚C for MS immersed in both inhibitor-free solutions (control) and the presence of the inhibitors, except for PA that the corrosion rate decreased from 20-40˚C and then increased at 60˚C. Furthermore, the addition of all the inhibitors into the electrolyte reduced the corrosion rate of MS significantly compared to the uninhibited MS sample at all the studied temperatures. Among all the inhibitors, PA had the lowest corrosion rate in the temperature range investigated. The corrosion rate of MS in the presence of all inhibitors at 60°C follows this order: AV>BC>DW>MI>IN>PA.

Table 4-2 Corrosion rate data of MS in 15 wt. % HCl in the absence and presence of different inhibitors at a temperature range from 20-60°C after 5 h immersion. Error bars show standard deviations of three measurements.

Medium	Corrosion rate (mg/cm^2h)		
	20°C	40°C	60°C
Control	2.70 ± 0.04	17.66 ± 0.35	65.35± 0.39
PA	0.01± 0.001	0.004 ±0.001	0.03 ± 0.01
MI	0.09 ± 0.01	1.09 ± 0.03	8.07 ± 0.94
DW	0.07± 0.01	1.65 ± 0.41	8.19 ± 0.24
BC	0.31 ± 0.02	2.73 ± 0.26	11.26 ± 0.06
IN	0.55 ± 0.02	1.82 ± 0.03	7.89± 0.65
AV	0.42 ± 0.06	4.61 ± 0.12	14.56± 0.27

Figure 4-4 shows the inhibition efficiencies of MS in 15 wt% HCl solution in the presence of 7 g/L PA, MI and DW; and 10 g/L (BC and IN) and 100 g/L AV at 20, 40 and 60°C after 5 h immersion. In this figure, the inhibition efficiency of PA was not affected (99%) - independent of the temperature of the environment which demonstrates the stability of PA in the temperature range studied. However, the

inhibition efficiencies of MI, DW, and BC decreases with increasing temperature. For IN, the inhibition efficiency increased from 80±0.5% to 90±0.2% as the temperature increased from 20-40ºC and then decreased as the temperature increased from 40 to 60ºC. The inhibition efficiency of AV decreased from 84±2 % to 74±1% with increased temperature from 20-40°C and then increased as the temperature decreased from 40- 60°C. PA inhibited the corrosion of MS the most (99±1%), whilst AV showed the lowest inhibition efficiency (77±0.4%) at 60°C after 5 h.

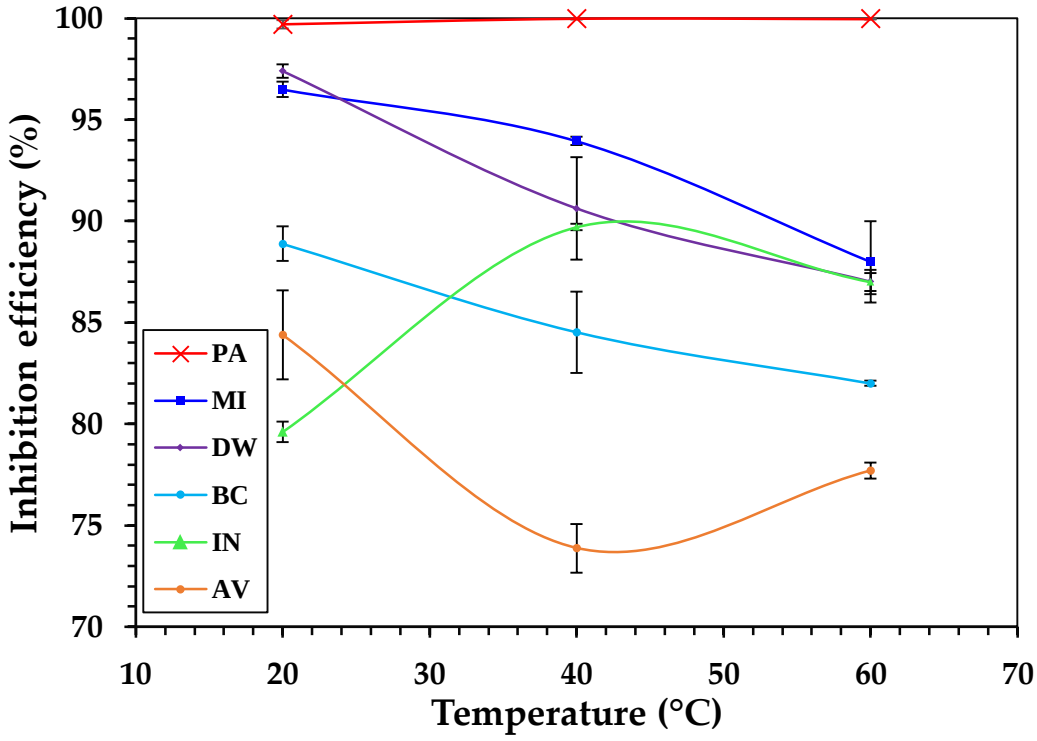


Figure 4-4 Variation of inhibition efficiency with temperature (20, 40 and 60°C) for MS in 15 wt. % HCl containing 7g/L (PA, MI, and DW), 10 g/L (BC and IN) and 100 g/L AV after 5 h immersion. Error bars represent standard deviations of three measurements.

It is evident from the data presented in Table 4-3 that the corrosion rate of MS increased with increasing temperature from 20-60°C in both the uninhibited and inhibited solutions after 24 h, apart from MS immersed in PA solution where the corrosion rate was constant between 40 and 60°C. However, the addition of all the inhibitors into 15 wt. % HCl decreased the corrosion rate again compared to the uninhibited sample. PA had the lowest corrosion rate again as previously mentioned at 5 h, whilst that of AV was the highest. For example, the corrosion rate of MS in inhibited free solution is 48.58 ± 0.77 mg/cm^{2}h at 60°C. In the presence of all the inhibitors, the corrosion rates were 0.034 ± 0.009 mg/cm^{2}h, 5.90± 0.83 mg/cm^{2}h, 10.86 ± 0.26 mg/cm^{2}h, 12.18±0.31 mg/cm^{2}h, 17.53 ± 1.25 mg/cm^{2}h, and 32.29 ± 0.50 mg/cm^{2}h for PA, MI, DW, BC, IN and AV at 60°C, respectively.

Table 4-3 Effect of temperature on the corrosion rate of MS in 15 wt. % HCl without and with different inhibitors (PA, MI, DW, BC, IN and AV) after 24 h. Error bars show standard deviations of three measurements

Inhibitor	Corrosion rate (mg/cm^{2}h)		
	20°C	40°C	60°C
Control	2.33 ± 0.03	21.13 ± 0.74	48.58 ± 0.77
PA	0.006 ± 0.002	0.03 ± 0.01	0.03 ± 0.01
MI	0.08± 0.02	1.24± 0.10	5.90 ± 0.83
DW	0.35 ± 0.05	3.22 ± 0.05	10.86 ± 0.26
BC	0.34 ± 0.01	2.90 ± 0.15	12.18 ± 0.31
IN	0.51 ± 0.03	2.68 ± 0.20	17.53 ± 1.25
AV	0.52 ± 0.05	6.64 ± 0.34	32.29± 0.49

The results presented in Figure 4-5 show that the inhibition efficiency of PA remains unchanged (over 99.9 %) with increasing temperature from 20 to 60℃ after 24 h. However, the inhibition efficiencies of MI and DW decreased slightly as the temperature increased from 20-60℃. In the case of BC, the inhibition efficiency remained unchanged from 20 to 40℃ but decreased from 40 to 60℃. The inhibition efficiency of IN and AV significantly decreased from 40 to 60℃ compared to other inhibitors (MI, DW, and BC). However, the inhibition performance of AV was much more affected – it decreased the most.

The inhibition efficiency of PA was the highest, while that of AV was the lowest in the temperature range investigated as obtained before. A similar trend was reported in the previous section. The inhibition performance of PA, MI, DW, BC, IN and AV were 99.9±0.2%, 88± 2%, 78± 0.3%, 75±1%, 64±3% and 32±1.4% respectively at 60˚C.

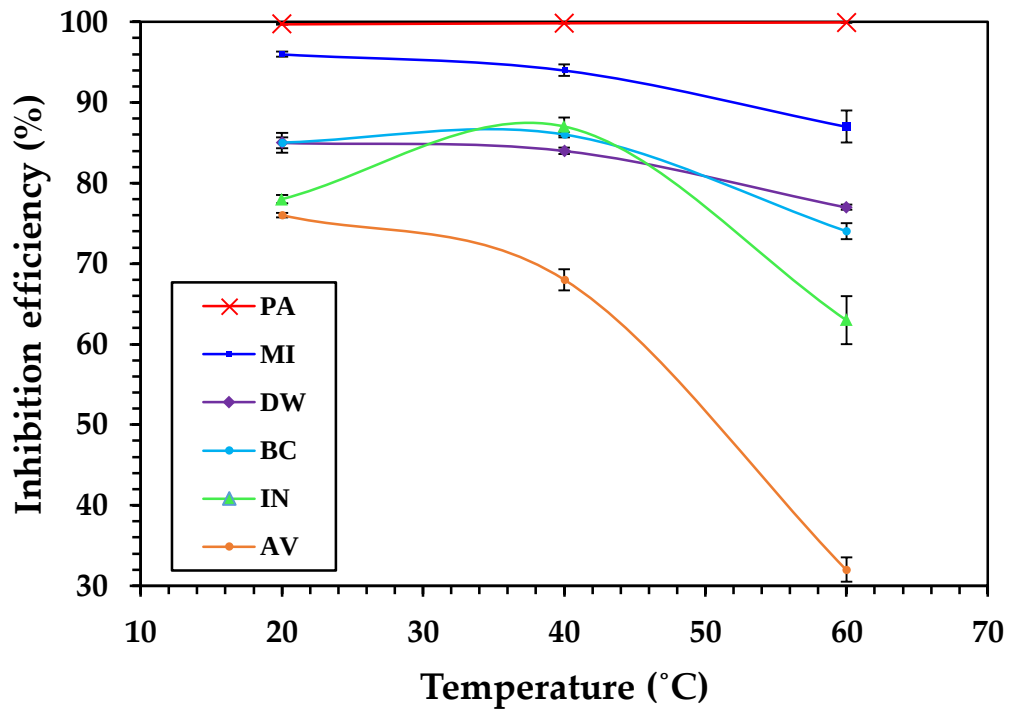


Figure 4-5 Temperature dependence of inhibition efficiency for MS in 15 wt.% HCl containing 7 g/L (PA, MI, and DW), 10 g/L (BC and IN) and 100 g/L AV for 24 h immersion. Error bars represent the standard deviation of three measurements.

4.4.2 Electrochemical results

4.4.2.1 Open circuit potential (OCP)

Figure 4-6 shows the OCP behaviour of MS immersed in 15 wt.% HCl in the absence and presence of 7 g/L (PA, MI, and DW), 10 g/L (BC and IN) at 20°C after 1 h. The results demonstrated that the uninhibited MS (control) achieved steady OCP of - 423 mV vs Ag/AgCl after about 20 minutes. MS immersed in PA solution exhibited a nobler potential from the onset, while MS immersed in DW, MI, BC and IN exhibited more negative onset potentials. MI achieved the most negative OCP value of -515 mV

vs. Ag/AgCl. Electrochemical measurements did not investigate the corrosion inhibition performance of AV because of its high concentration (100 g/L).

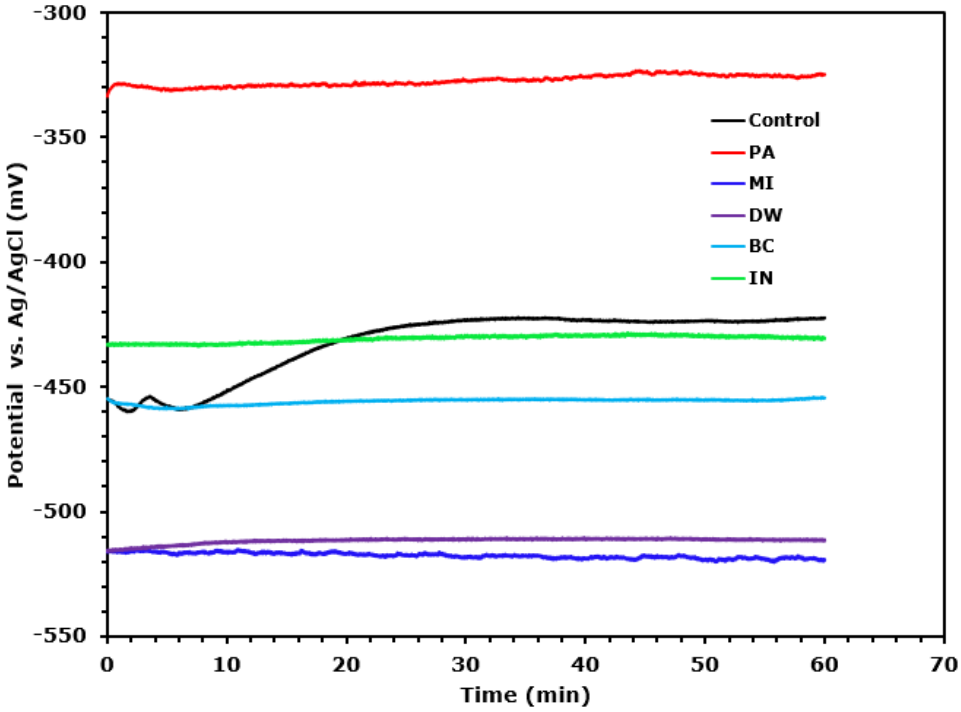


Figure 4-6 Variation of OCP as a function of time recorded for MS immersed 15 wt.% HCl in the absence and presence of PA, MI, DW, BC and IN at 20°C after 1 h immersion

Figure 4-7 presents the variation of OCP with time for MS samples in 15 wt.% HCl in the absence and presence of PA, MI, DW, BC and IN at 40°C recorded after 1 h. The result showed that the OCP of the uninhibited MS sample (control) increased with increasing time and then achieved a steady OCP of -422 mV with respect to Ag/AgCl after 10 minutes. MS samples treated with PA, DW, and IN shifted to more positive potentials, with PA showing the noblest behaviour. The OCP of MS treated with BC decreases with time and then reaches a stable state. MS treated with MI and BC shifted to more negative potentials.

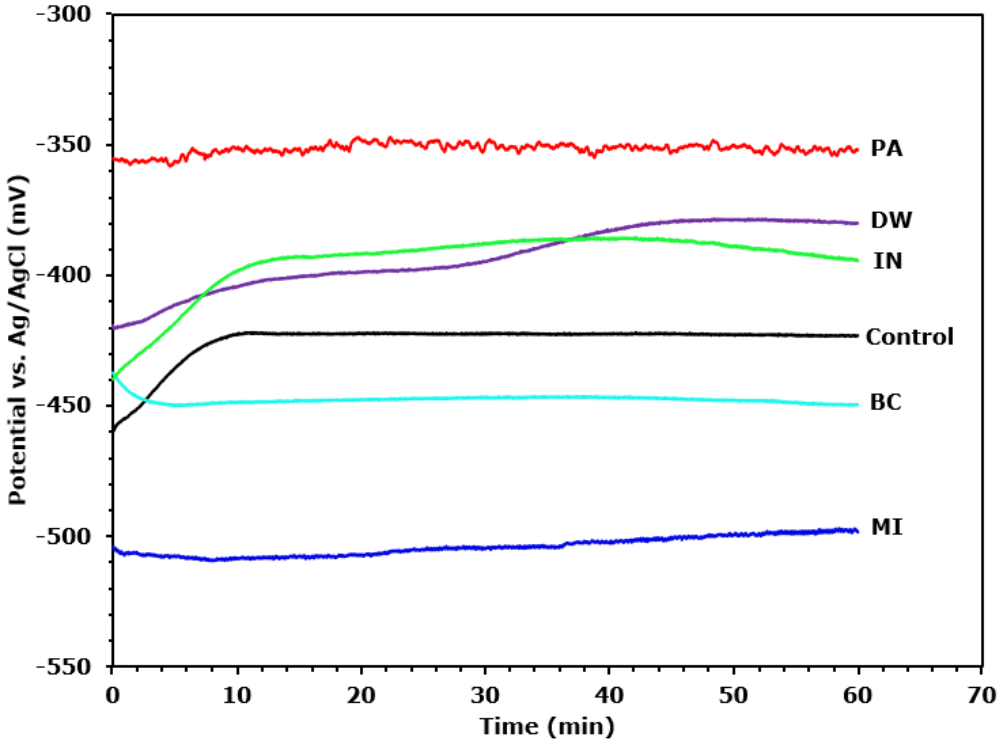


Figure 4-7 Variation of OCP as a function of time recorded for MS immersed 15 wt.% HCl in the absence and presence of PA, MI, DW, BC and IN at 40°C after 1 h immersion.

Comparison of OCP variation with time for MS samples in 15 wt.% HCl in the absence and presence of PA, MI, DW, BC and IN after 1 h immersion at 60°C is presented in Figure 4-8. MS immersed in uninhibited 15 wt.% HCl achieved steady OCP of - 426 mV (vs. Ag/AgCl) quickly after 2 minutes of immersion. The addition of PA and DW to the test solution shifted the OCP values to a more positive direction (i.e. they exhibited noble behaviour). PA reached onset steady OCP. The steady OCP values for PA and DW were -382 mV and -404 mV, respectively. On the other hand, the addition of IN, BC, and MI to the test solution shifted the OCP values towards the more negative direction. The OCP values of MS treated with DW, BC and IN increased with

immersion and then achieved a steady state. The sample treated with PA exhibited the noblest behaviour, whilst MS treated with MI has the lowest OCP value of -477 mV.

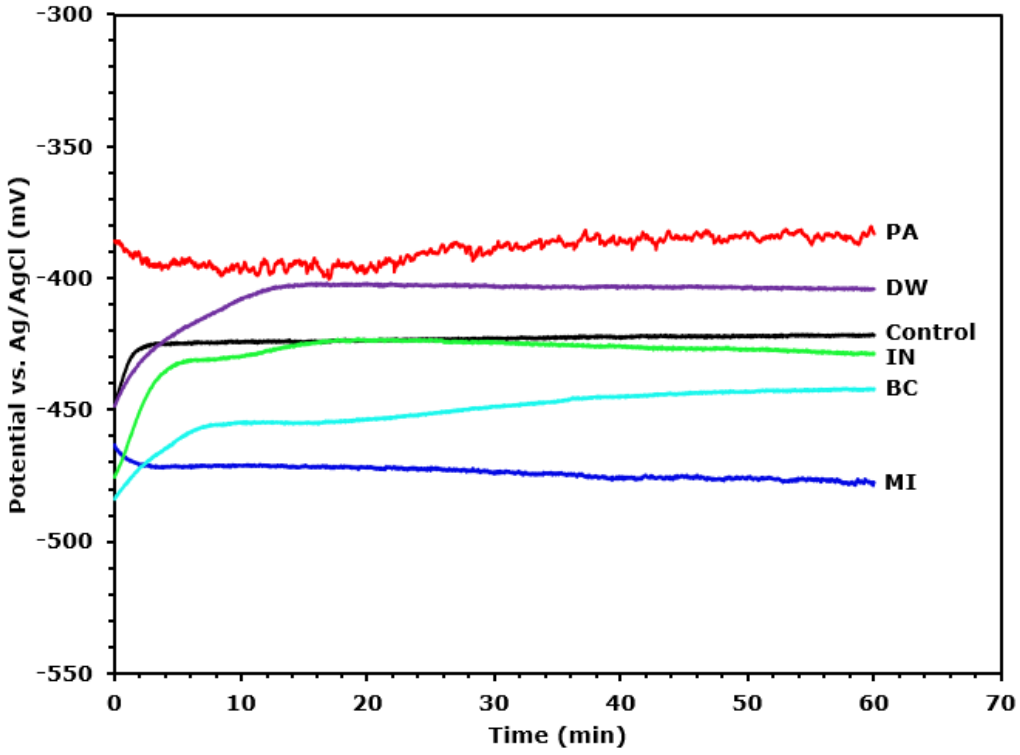


Figure 4-8 Variation of OCP as a function of time recorded for MS immersed 15 wt.% HCl in the absence and presence of PA, MI, DW, BC and IN at 60°C after 1 h immersion.

4.4.2.2 Potentiodynamic polarization

Figure 4-9 shows the potentiodynamic polarization curves for MS in 15 wt% HCl in the absence and presence of PA, MI, DW, BC and IN in the temperature range 20 to 60°C. The polarization parameters including anodic and cathodic Tafel slopes (βa and βc), corrosion potential (E_{corr}), corrosion current density (i_{corr}) and inhibition efficiency (η) were extracted from the polarization curves and summarized in Table 4-4. As shown in the table, it is clear that the corrosion current densities of MS increased with increasing temperature both in the uninhibited and inhibited HCl solutions. However,

the corrosion current densities of MS decreased significantly in the presence of all the studied inhibitors with respect to the uninhibited sample. In other words, the presence of all the studied inhibitors retarded the anodic dissolution of MS and cathodic hydrogen evolution reaction.

The corrosion current densities of MS in the presence of the commercial inhibitors (PA and MI) decreased more compared to the plant-based materials (DW, BC and IN) in the temperature range studied. The corrosion current density of MS immersed in PA inhibited solution was the lowest (0.127 ± 0.029 mA/cm^2), while that of BC was the highest (19 ± 0.7 mA/cm^2) at 60°C.

In the absence of inhibitors (blank), E_{corr} shifted towards more negative potentials with increasing temperature (20-60°C). On the other hand, E_{corr} shifts considerably towards more positive potentials in the presence of PA, MI, DW, BC, and IN at each temperature compared to the absence of inhibitors.

As shown in Table 4-4, PA maintains its high protective efficiency of over 99% at all temperatures (i.e., the inhibition efficiency of PA was temperature-independent). In the presence of MI, the inhibition efficiency decreased from 98 to 93% with an increase in temperature from 20 to 40°C and then increased to 96% at 60°C. For the plant-based inhibitors, the inhibition efficiencies of DW and BC decreased as the temperature increased from 20 to 40˚C, and are nearly constant from 40 to 60°C. In the presence of IN, the inhibition efficiency decreased from 91 to 77% as the temperature increased from 20 to 40°C, and then increased to 88% at 60°C.

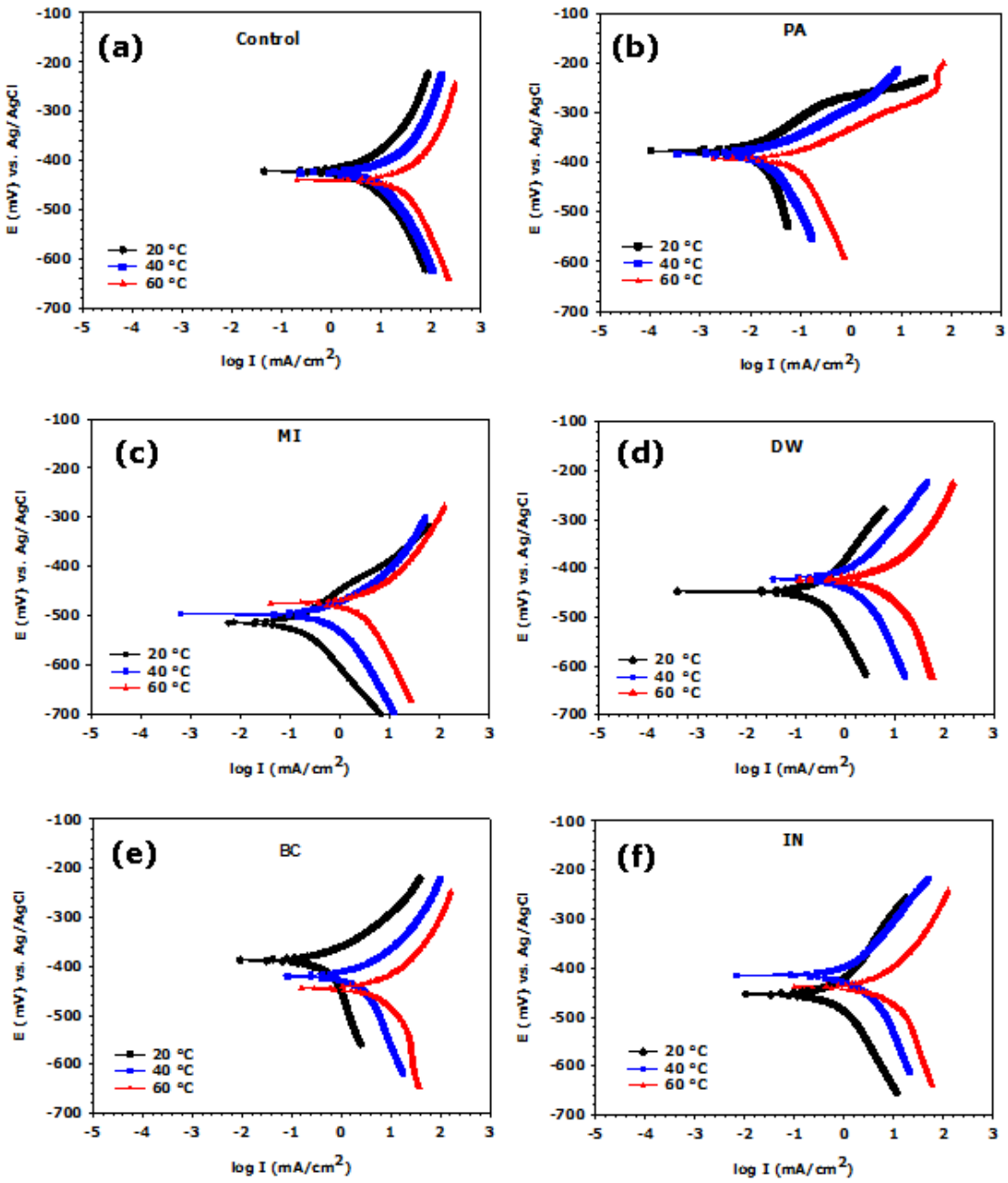


Figure 4-9 Effect of temperature on the potentiodynamic polarization curves for MS in 15 wt% HCl solution in the absence and presence of various inhibitors in the temperature range of 20-60°C (a) uninhibited; (b) 7 g/LPA; (c) 7 g/L MI; (d) 7/L DW; (e) 10 g/L BC; and (f) 10 g/L IN.

Table 4-4 Electrochemical polarization parameters for MS in 15 wt% HCl in the absence and presence of PA, MI, DW, BC and IN in the temperature range of 20- 60°C. Error bars show standard deviations of three measurements.

20 °C						
System	**Conc (g/L)**	**E_{corr} (mV)**	**β_a (mV/dec)**	**β_c (mV/dec)**	**i_{corr} (mA/cm^2)**	**η (%)**
Blank	0.0	-419 ± 10	182 ± 7	-220 ± 5	9 ± 1	-
PA	7.0	-367 ± 17	68 ± 28	-217 ± 86	0.013 ± 0.002	99.9
MI	7.0	-516 ± 2	82 ± 13	-119 ± 3	0.193 ± 0.023	97.9
DW	7.0	-458 ± 40	136 ± 16	-174 ± 23	0.314 ± 0.018	96.5
BC	10.0	-388 ± 1	59 ± 6	-207 ± 19	0.379 ± 0.056	95.8
IN	10.0	-456 ± 17	158 ± 28	-177 ± 6	0.798 ± 0.168	91.1
40 °C						
Blank	0.0	-424 ± 3	147 ± 20	-222 ± 2	14.298 ±2.018	-
PA	7.0	-389 ± 6	56 ± 1	-173 ± 8	0.026 ±0.005	99.8
MI	7.0	-497 ± 2	90 ± 4	-184 ± 9	1.072 ±0.079	92.5
DW	7.0	-405 ± 8	142 ± 12	-222 ± 19	1.871 ±0.478	86.9
BC	10.0	-416 ± 2	93 ± 5	-231 ± 5	2.922 ±0.285	79.6
IN	10.0	-414 ± 5	177 ± 19	-237 ± 8	3.279 ±0.639	77.1
60 °C						
Blank	0.0	-434 ± 11	366 ± 10	-489 ± 48	86.139±3.579	-
PA	7.0	-400 ± 7	62 ± 11	-225 ± 15	0.127 ± 0.029	99.9
MI	7.0	-471 ± 3	95 ± 1	-222 ± 10	3.579 ± 0.482	95.9
DW	7.0	-426 ± 9	166 ± 9	-322 ± 51	11.159±1.919	87.1
BC	10.0	-447 ± 2	197 ± 9	-211 ± 19	19.0±0.700	78.0
IN	10.0	-441 ± 6	185 ± 3	-120 ± 13	10.223±1.07	88.1

Note: η – Inhibition efficiency

4.4.2.3 Linear polarisation resistance (LPR)

Table 4-5 shows the linear polarisation results for MS in 15 wt.% HCl solution in the absence and presence of PA, MI, DW, BC and IN at 20, 40 and 60˚C after 1 h OCP. The results show that the polarisation resistance (R_p) increased considerably in the presence of PA, MI, DW, BC and IN at each temperature investigated with respect to the uninhibited sample. The polarisation resistance of MS in the presence of PA was the highest at all temperature studied. Also, it is clear that with an increase in temperature from 20-60°C, the polarisation resistance decreased for all inhibitors, except IN that the polarization resistance was constant between 40 and 60°C. The inhibition efficiencies of PA and DW were almost unaffected with increasing solution temperature from 20 to 60°C, while that of MI and BC inhibited samples decreased with temperature. The inhibition efficiency of IN decreased from 85% to 77% as the temperature increased from 20-40°C and then increased to 91% at 60°C (This trend is consistent with potentiodynamic polarisation results as shown in Table 4- 6). Comparing the inhibition efficiencies of the commercial inhibitors (PA and MI) with the possible green alternatives (DW, BC and IN), the inhibition efficiency follows this trend at the highest temperature studied (60˚C): PA>DW>MI>IN>BC.

Table 4-5 Linear polarisation resistance data recorded for MS in 15 wt.% HCl in various inhibitors at 20, 40 and 60°C after 1 h OCP.

20°C				
Medium	**Concentration (g/L)**	**R_p (Ω cm^2)**	**Cr (mm/year)**	**η (%)**
Control	0.0	8.3±1.9	48.5±9.8	-
PA	7.0	1583±222	0.25±0.03	99.48
MI	7.0	174±14	2.25±0.18	95.23
DW	7.0	115±15	3.55±0.50	92.78
BC	10.0	92.4±20	4.34±0.88	91.05
IN	10.0	56.0±9.3	7.07±1.17	85.42
40°C				
Control	0.0	2.6±0.2	149±13.1	-
PA	7.0	275.7±63.7	1.5±0.3	99.00
MI	7.0	28.7±3.5	13.7±1.6	90.94
DW	7.0	32.6±1.4	12.0±0.5	91.95
BC	10.0	19.6±0.6	19.9±0.6	86.64
IN	10.0	11.2±0.6	34.7±2.0	76.79
60°C				
Control	0.0	0.97±0.01	403.5±6.4	-
PA	7.0	165.67±6.66	2.36±0.10	99.41
MI	7.0	5.48±0.34	71.3±4.4	83.30
DW	7.0	14.60±1.55	27.0±2.9	93.35
BC	10.0	5.3±0.9	76.0±12.0	81.70
IN	10.0	11.03±1.01	35.6±3.3	91.21

Note: *R_p means the polarization resistance, Cr is the corrosion rate, and η is the inhibition efficiency.*

4.5. Effect of immersion time on corrosion of MS

In this section, the dependence of inhibition efficiency on different immersion times of MS in 15 wt.% HCl solution containing PA, MI, DW, BC, IN and AV was investigated to determine the stability of the inhibitors, and the time it takes each inhibitor to achieve maximum protection. The variation of inhibition efficiency of these inhibitors as a function of immersion time (5-192 h) at 20 °C is presented in Figure 4-10. From the figure, the inhibition efficiencies of PA, MI and IN were almost unchanged throughout the immersion times (5-192). DW achieved stable inhibition efficiency between 10 to 192 h, while the inhibition efficiency of BC was virtually unaffected from 24 to 192 h. It is evident that the inhibition efficiencies of the synthetic inhibitors (PA and MI) were higher than the plant-based extracts (DW, BC and IN) throughout the time scale investigated. However, the plant-based materials also have high inhibitive performance with prolonged immersion. The inhibition efficiencies of PA, MI, DW were 99.9±0.2%, 94.8±1.7%, 84.4±2.7% at 7 g/L, while those for BC and IN were 83.2±3.6% and 82.1±1.3% at 10 g/L respectively after 192 h immersion. It is clear that PA outperformed other inhibitors under the experimental conditions studied.

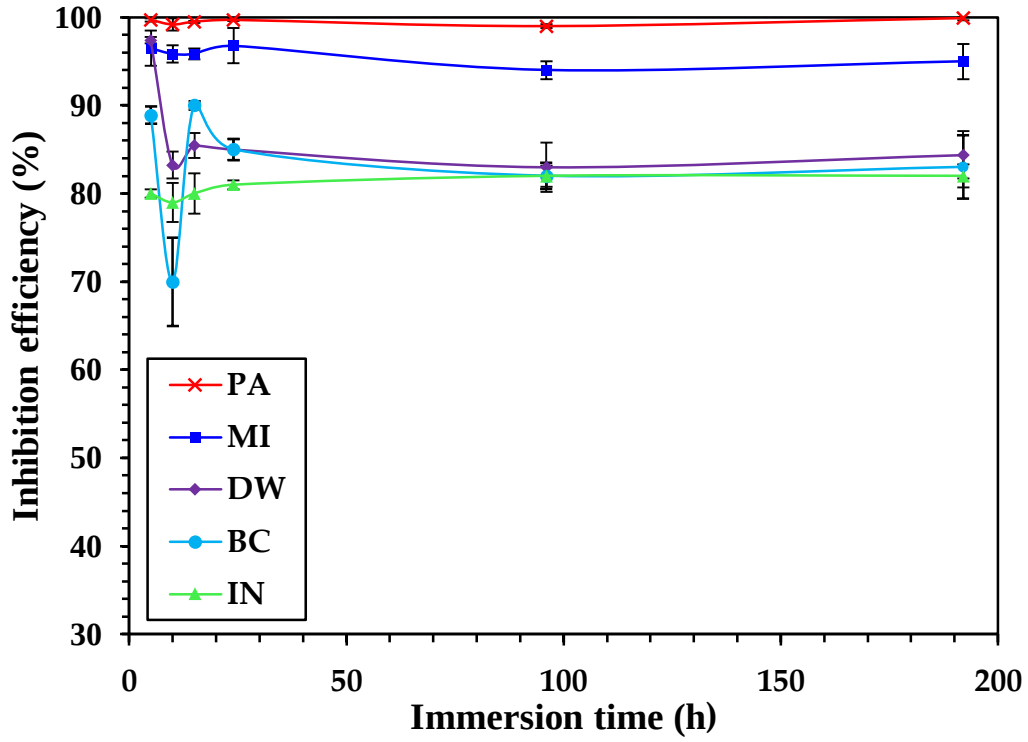


Figure 4-10 Effect of immersion time (5-192h) on inhibition efficiency for MS in 15 wt.% HCl in the presence of PA, MI, DW, BC and IN at 20°C. Error bars represent standard deviation (n=3). The solid line is included to guide the eye and does not represent a model of the experimental data.

Figure 4-11 shows the dependence of inhibition efficiency of AV on time after 5 h immersion period at 20°C. The inhibition efficiency of AV decreased with increased immersion time from 5 to 10 h and then remained almost unchanged between 10 and 24 h. The time dependence of AV was only carried out between 5 and 24 h because of its significant amount of concentration (100 g/L). AV was not plotted in Figure 4-10 because the investigated immersion time was carried out between 5 and 24 h.

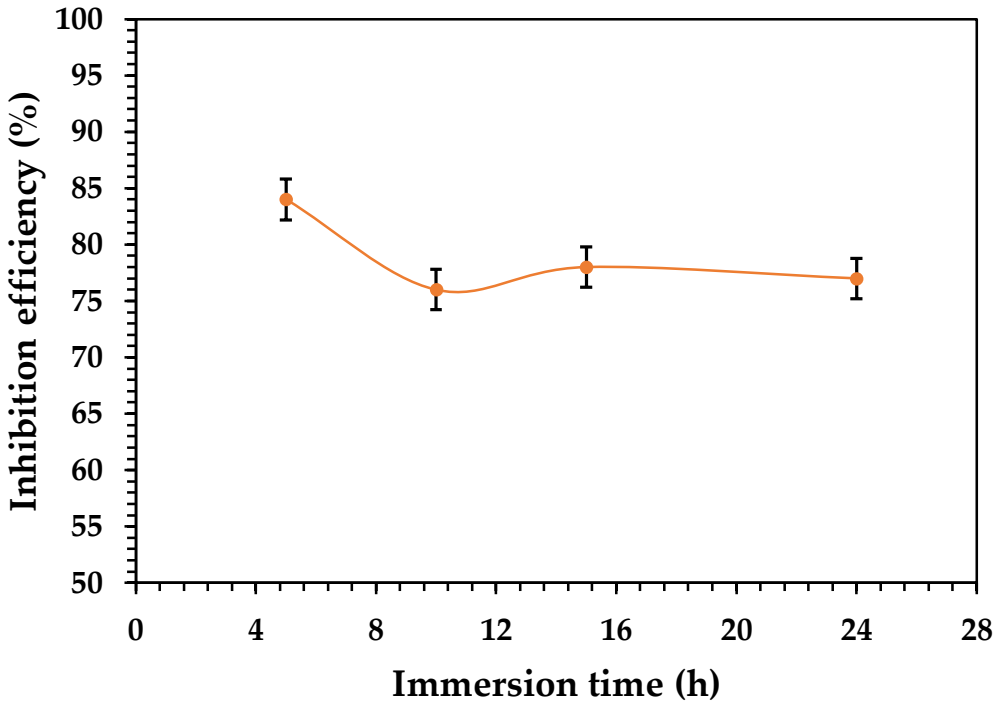


Figure 4-11 Effect of immersion time (5-24h) on inhibition efficiency for MS in 15 wt.% HCl in the presence of 100 g/L at 20 °C. The solid line is included to guide the eye and does not represent a model of the experimental data.

Figure 4-12 shows the variation of inhibition efficiency with different immersion times (5-24 h) for MS in 15 wt % HCl solution in the presence of PA, MI, DW, BC, IN and AV at 40ºC. It is evident from the figure that the inhibition efficiency of PA remains unchanged (99%) with increasing immersion time (i.e., the inhibition performance of PA is time-independent). It was observed that as immersion time increased from 5 to 10 h, the inhibition efficiency of MI also increased from 94% to 96%, and then decreased to 94% after 24 h immersion. MI reached maximum inhibition efficiency of 96±0.3% after 10 h of its application into the test solution. The corrosion inhibition efficiencies of DW, BC, and IN were slightly affected with increasing immersion time from 5 to 24 h. Among the plant-based inhibitors, IN performed better and was more stable than other green inhibitors in the immersion time investigated as shown in

Figure 4-12. The inhibition efficiency of AV significantly decreased from 75.8±1% to 30.10±0.30% as time increased from 10 to 15 h before it later increased to 68.6±1.3% after 24 h. The inhibition efficiencies of PA, MI, DW, BC, IN and AV were 99.8±1%, 94.1±0.7%, 84.8±0.6%, 86.3±0.3%, 87.3±1.1% and 68.6±1.3%, respectively after

24 h. It is clear from these results that the corrosion inhibition efficiencies of the synthetic inhibitors (PA and MI) were higher than the green inhibitors (DW, BC, IN and AV).

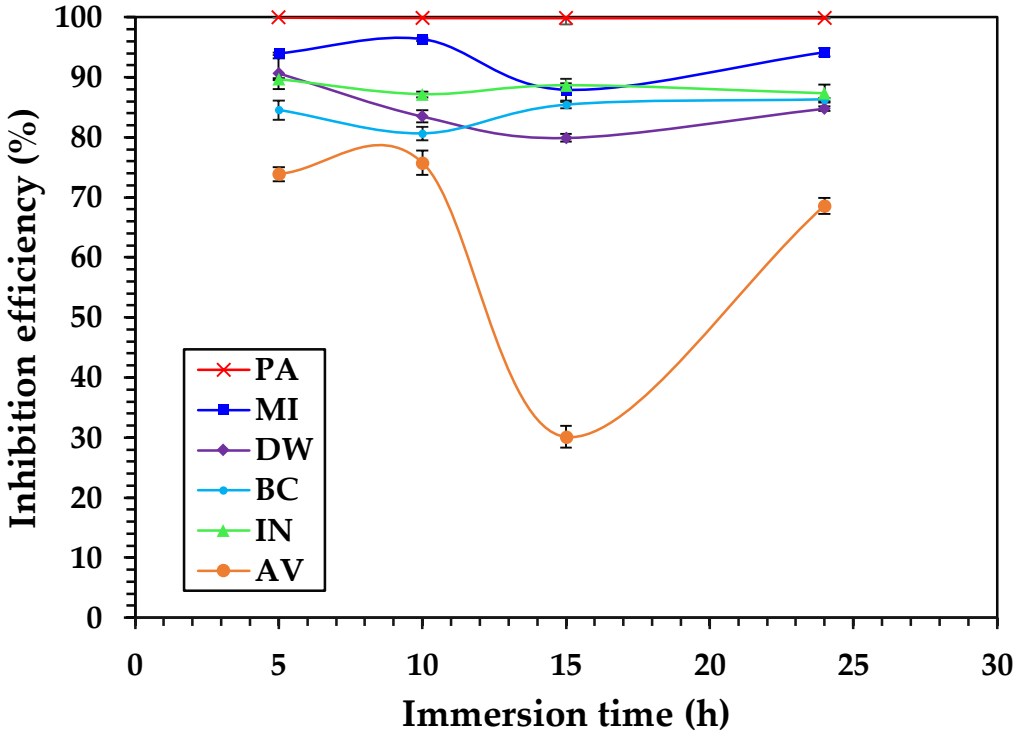


Figure 4-12 Effect of immersion time on inhibition efficiency for MS in 15 wt.% HCl in the presence of optimum concentrations of inhibitors at 40°C. Error bars represent standard deviation (n=3).

Figure 4-13 shows the time-dependent behaviour of PA, MI, DW, BC, IN and AV for MS in 15 wt.% HCl solution at 60ºC. The results show that the inhibition efficiency of PA remains constant throughout the investigated immersion times. On the other hand, the inhibition efficiency of MI increased from 88±2% to 94±0.5% as the immersion time increased from 5 to 10 h and then decreased to 81±2% after 15 h and then increased to 88±1.6% after 24 h. The maximum inhibition efficiency of 94±0.5% was achieved after 10 h. With regards to the green inhibitors, the inhibition efficiencies of DW and IN decreased with increasing immersion time, except between 10 and 15 h. DW and IN achieved the maximum inhibition efficiency of 87.5±0.4% and 87.9±0.6% after the first 5 h of immersion. However, the inhibition efficiency of AV decreased with increasing immersion time from 5 to 24 h. In the presence of BC, the corrosion inhibition efficiency decreased from 83±0.13% to 77±2% as the immersion time increased from 5 to 10 h and then decreased to 75±1% after 24 h. The results show that the inhibition efficiencies of the synthetic inhibitors (PA and MI) were higher than those of the green inhibitors (DW, BC, IN and AV) but the DW outperformed BC, IN and AV.

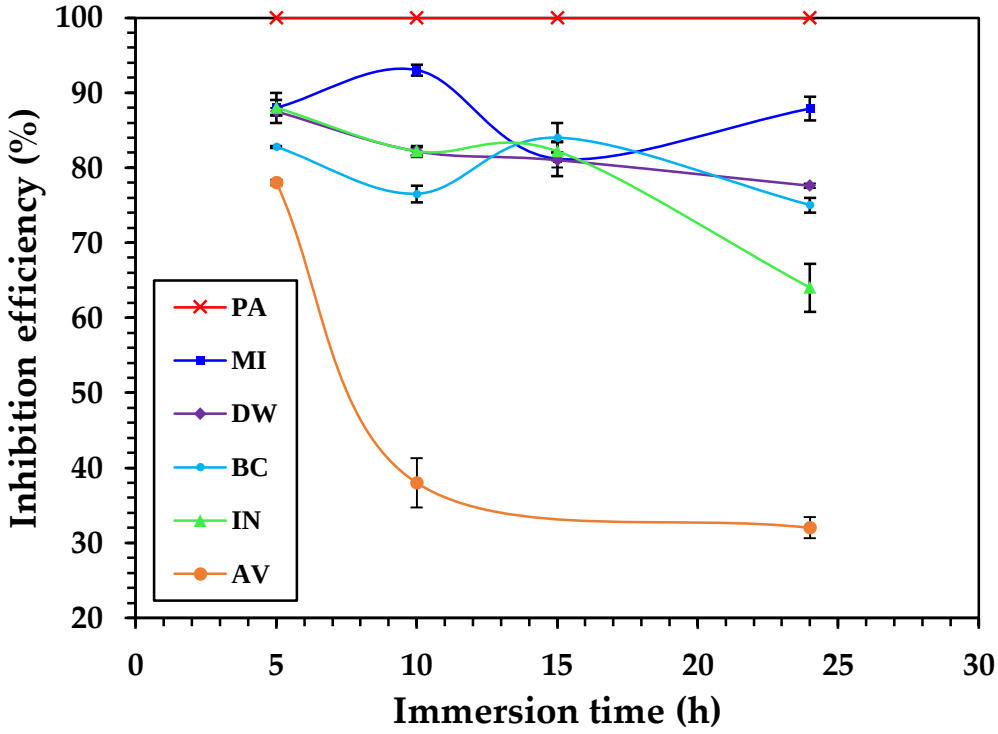


Figure 4-13 Effect of immersion time on inhibition efficiency for MS in 15 wt. % HCl in the presence of different inhibitors at 60°C. Error bars represent standard deviation (n=3). The solid line is included to guide the eye and does not represent a model of the experimental data.

4.6 Characterization of MS sample surfaces

4.6.1 Scanning electron microscopy (SEM)

Figures 4-14 show the secondary electron (SE) images of MS sample surfaces after 5 h of immersion in aerated 15 wt % HCl without and with an optimum concentration of PA, MI, DW, IN, BC and AV at 60°C after 5 h. The MS surface immersed in the uninhibited 15 wt % HCl (control) as shown in Figure 4-14 b was severely corroded and extremely rough compared to the unexposed sample (Figure 4-14a). However, MS surfaces treated with the different inhibitors were less corroded and smoother as shown in Figures 4-14 (c-h). MS surface treated with PA appears to be the least corroded compared to other MS surfaces treated with inhibitors. SEM examinations do not provide quantitative information about the surface roughness. Hence, 3D profilometry has been carried out for further investigation of the surface roughness and is presented in **section 4.6.3**

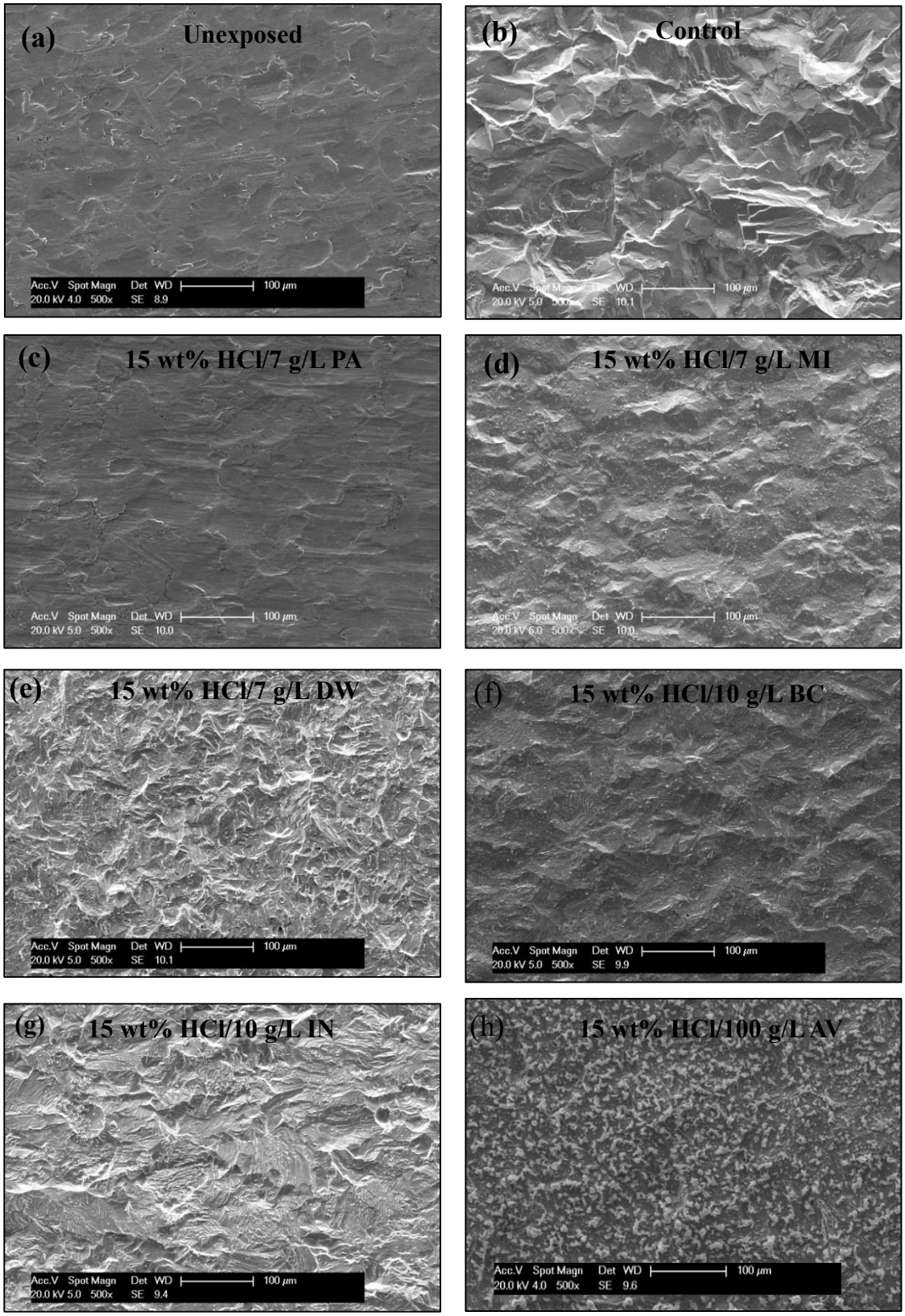


Figure 4-14 SEM images of MS specimens in 15 wt% HCl. (a) before immersion, (b) after immersion (b) uninhibited solution (c) inhibited 7g/L solution PA (d) inhibited 7g/L MI (e)inhibited 7g/L DW (f) inhibited 10 g/L BC (g) inhibited 10 g/l IN and (h) inhibited 100 g/L AV.

4.6.2 Energy dispersive spectroscopy (EDS) of the MS surfaces

EDS was employed to characterise the elemental composition of the MS surfaces in the absence and presence of 7 g/L (PA, MI, and DW), 10 g/L (BC and IN) and 100 g/L AV. The EDS data presented in Table 4-6 shows that the uninhibited MS has a significant amount of chloride ions (4.38 wt%). However, chloride ions and oxygen were suppressed significantly for the MS surfaces treated with all the inhibitors (Table 4-6). Also, MS in the inhibitor-free solution showed a much higher amount of oxygen (37.65 wt %), confirming the oxidation of the sample.

Table 4-6 EDS data of MS in 15 wt. % HCl in the absence and presence of optimum concentrations of PA, MI, DW, IN, BC and AV gel at 60°C after 5 h.

Medium	Composition (weight %)						
	Fe	C	O	Cl	Al	Ni	Mn
Unexposed	92.23	6.40	2.04	-	-	-	-
Control	46.68	11.21	37.65	4.38	0.16	0.17	-
PA	86.67	12.19	1.11	0.07	-	-	-
MI	84.88	8.32	6.46	0.34	-	-	-
DW	87.89	9.79	2.20	0.12	-	-	-
BC	87.47	10.10	2.17	0.20	-	-	0.20
IN	87.79	10.31	1.63	0.20	-	-	0.23
AV	92.61	3.30	3.52	0.58	-	-	-

4.6.3 Topography measurements

The 3D-profiles of MS in 15 wt% HCl solution in the absence and presence of different inhibitors after 5 h immersion at 60°C is presented in Figure 4-15. From the figure, the MS sample exposed to the uninhibited solution appears to be the roughest compared to the samples in 15 wt% HCl containing different inhibitors. PA-treated MS surface was the smoothest compared to other samples treated with MI, DW, IN, and BC under the same experimental conditions. The mean surface roughness (Sa) values of the

unexposed and exposed MS in 15 wt% HCl solution in the absence and presence of different inhibitors at 60°C after 5 h immersion is presented in Table 4-7. It is clear from the results that the sample exposed to the uninhibited solution had the highest S_a value (6.55 ± 0.58 µm) compared to the samples immersed in the inhibited solutions. However, the S_a values of samples immersed in the inhibited solutions were considerably decreased compared to the uninhibited sample. Among the MS surfaces treated with different inhibitors, the S_a value of PA was the lowest (1.43 ±0.04 µm) whilst that of BC was the highest (3.49±0.06 µm). The S_a values of MS in the presence of different inhibitors follow this order: BC>DW>MI>IN>PA.

Table 4-7 Mean surface roughness (S_a) of unexposed and exposed MS in uninhibited and inhibited 15wt% HCl at 60°C after 5 h of immersion. The results presented are the average of three measurements.

S/N	System	Average surface roughness (Sa), µm
1.	Unexposed	1.59 ± 0.03
2.	15 wt% HCl alone	6.55 ± 0.58
3.	15 wt% HCl + PA	1.43 ± 0.04
4.	15 wt% HCl + MI	2.34 ± 0.02
5.	15 wt% HCl + DW	2.55 ± 0.06
6.	15 wt% HCl + BC	3.49 ±0.06
7.	15 wt% HCl + IN	2.00 ±0.02

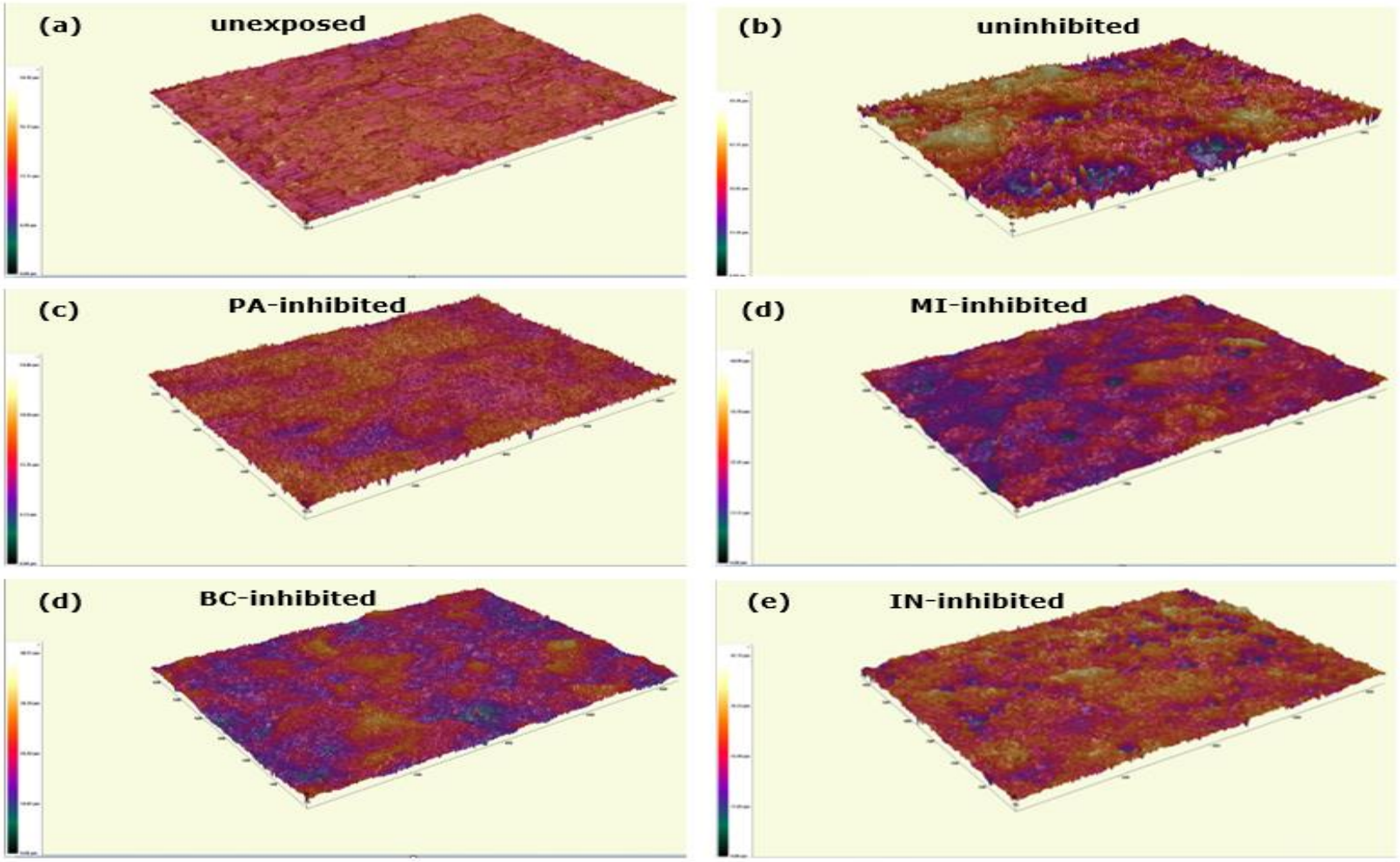


Figure 4-15 3-D profiles obtained by profilometer for (a) unexposed MS; and MS in 15wt% HCl at 60°C after 5 h (b) uninhibited (b) PA-inhibited (c) MI inhibited (d) BC-inhibited and (e) IN-inhibited using weight loss measurements.

CHAPTER FIVE

ADSORPTION ISOTHERM AND CHEMICAL ANALYSIS

5.1 Introduction

In this chapter, the interaction between the studied inhibitors and the MS surfaces was studied by adsorption isotherm models. Also, the activation parameters of the uninhibited and inhibited MS surfaces were analyzed to determine the adsorption behaviour of the studied inhibitors.

The chemical analysis of both the synthetic and green inhibitors was analysed using Fourier transform infrared (FTIR) and Gas chromatography-mass spectroscopy (GCMS), which are also presented in this chapter.

5.2 Adsorption isotherms

Adsorption isotherms provide necessary information about the interaction between an inhibitor molecule and a metal surface [150, 166] which is achieved by fitting the obtained experimental data to different adsorption isotherm models, and the model that gives the best linearity describes the adsorption behaviour of an inhibitor at the interface of a metal/solution.

In this study, the experimental data (Figure 4-2) obtained from weight loss measurements after 5 h immersion were fitted graphically to the Langmuir, Temkin, Florry-Huggins and Frumkin isotherms. The best fit was obtained for Langmuir adsorption isotherm (Eqn 5-1 [8, 147, 167]) and the plots are presented in Figures 5-1 and 5-2. The Langmuir plot for AV was plotted separately because of the range of its concentration (4 to 100 g/L). Majority of the adsorption behaviour of inhibitors on a metallic surface has been attributed to Langmuir adsorption isotherm [55, 127, 150, 154, 168]

$$\boldsymbol{\theta}=\left(\frac{\boldsymbol{K_{ads}\,C}}{\boldsymbol{1+K_{ads}}}\right) \qquad \text{Eqn 5-1}$$

The linearized form gives:

$$\frac{C}{\theta} = \frac{1}{K_{ads}} + C \qquad \text{Eqn 5-2}$$

where K_{ads} is the equilibrium constant of the adsorption process (calculated from the intercepts of the straight lines of the plots in Figures 5-1 and 5-2), C is the concentration of the inhibitors and θ is the fractional surface coverage (θ=η/100). The plot of $\frac{C}{\theta}$ against C showed straight lines with linear regression coefficients (R^2) around 1 (Table 5-1), indicating that the adsorption behaviour of both the synthetic (PA and MI) and green inhibitors (DW, BC, IN and AV) on the MS surfaces modelled Langmuir adsorption isotherm well.

The values of the Gibbs free energy of the adsorption (ΔG_{ads}) were obtained from the following equation [8, 150, 167] to determine the adsorption mode of the inhibitors at the MS/solution interface:

$$\Delta G_{ads} = -RT \ln(C_{H_2O} K_{ads}) \qquad \text{Eqn 5-3}$$

where R is the universal gas constant, T is the absolute temperature and C_{H_2O} is the water concentration in the solution (1000 g/L). The unit of C_{H_2O} is expressed in 1000 g/L instead of 55.5 mol/L for consistency with K_{ads} units (L/g). The obtained K_{ads} values were used to calculate ΔG_{ads} as summarized in Table 5-1.

The adsorption and thermodynamic parameters of PA, MI, DW, BC and IN for MS immersed in 15 wt.% HCl from 20 to 60°C after 5 h immersion are shown in Table 5- 1. The adsorption equilibrium constant and Gibbs free energy were only obtained for AV at 20°C only, because of its high concentration (100 g/L) as mentioned previously.

From data presented in Table 5-1, the values of ΔG_{ads} in the presence of PA are -26.5, -33.9 and – 41 kJ/mol at 20, 40 and 60°C, respectively. Hence, at 20 and 40°C, the adsorption of PA on MS surface was due to both physisorption and chemisorption. However, the adsorption mechanism was solely chemisorption at 60°C (Detailed explanation is given in section 7.2.5 - page 166).

Turning to MI, the ΔG_{ads} values are -25.3, -27.0 and – 18.4 kJ/mol in the range of temperature from 20 to 60°C (Table 5-1) which shows that the adsorption of MI on the surface of MS at 20 and 40°C were both physisorption and chemisorption. On the other hand, the adsorption mechanism was physisorption at 60°C.

The values of ΔG_{ads} in the presence of DW are between -23 and -22 kJ/mol over the temperature range 20 to 60°C, which demonstrated that DW adsorbed on MS surface via both physisorption and chemisorption.

The values of ΔG_{ads} in the presence of BC is in the range of -18 to -21 kJ/mol and that of IN is from – 17 kJ/mol to -21 kJ/mol from 20 to 60°C, this shows that the adsorption of BC and IN on the surface of MS at all temperature occurred by physisorption. Lastly, the value of ΔG_{ads} for AV was -7.3 kJ/mol at 20°C, and it means that the adsorption mechanism was due to physisorption (Table 5-1).

Generally, if the value of ΔG_{ads} -20 kJ/mol or less negative, the adsorption of an inhibitor on the metal surface is considered to be physisorption, while the value of ΔG_{ads} that is -40 kJ/mol or more negative is suggestive of chemisorption [123, 169, 170].

The negative values of ΔG_{ads} in the presence of all the studied inhibitors indicate the spontaneity of the adsorption process of the inhibitors on MS surfaces at all temperatures as shown in Table 5-1 [117, 171, 172].

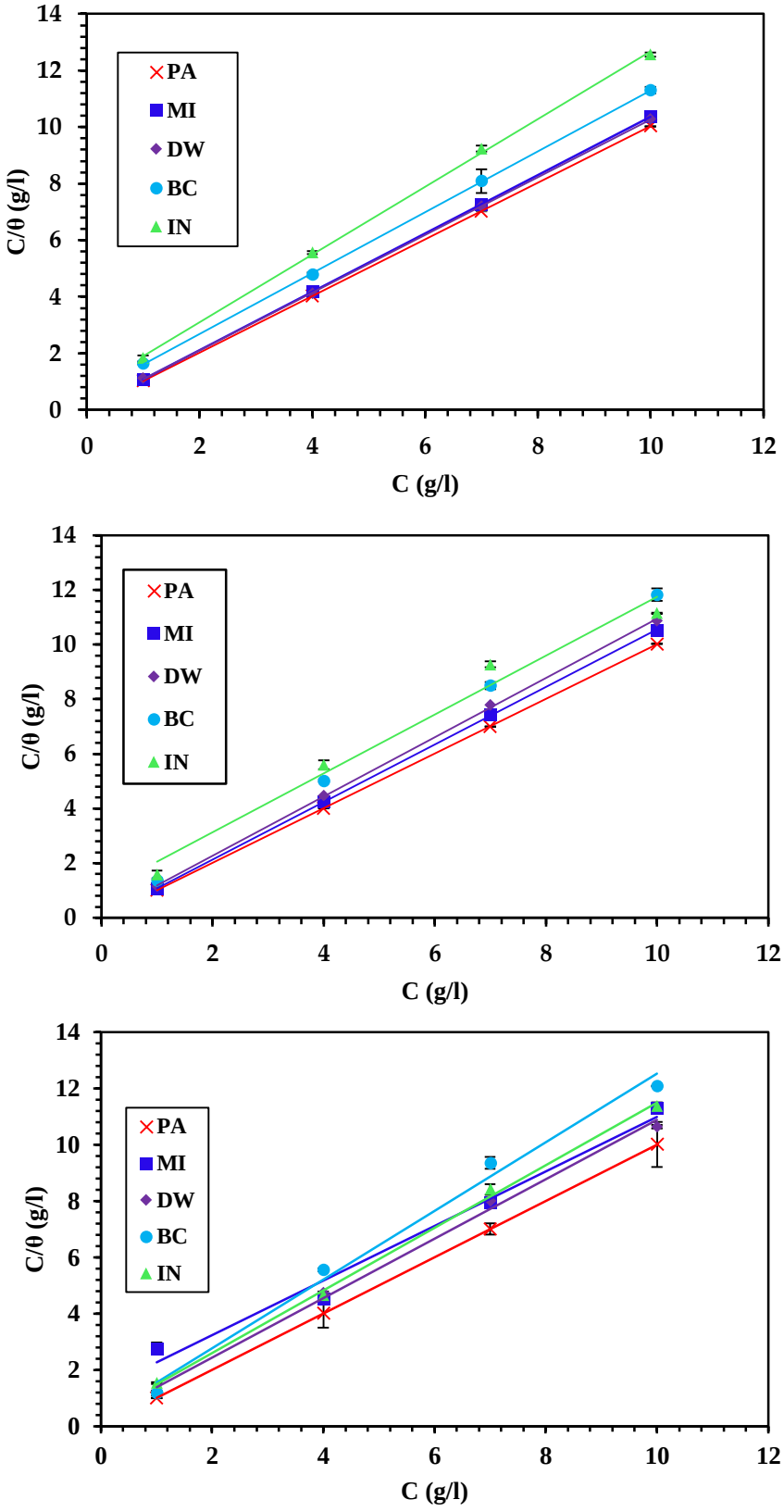


Figure 5-1 Langmuir adsorption isotherm plot for MS in 15 wt.% HCl containing different concentrations of PA, MI, DW, BC and at 20, 40 and 60°C. Error bars represent standard deviations.

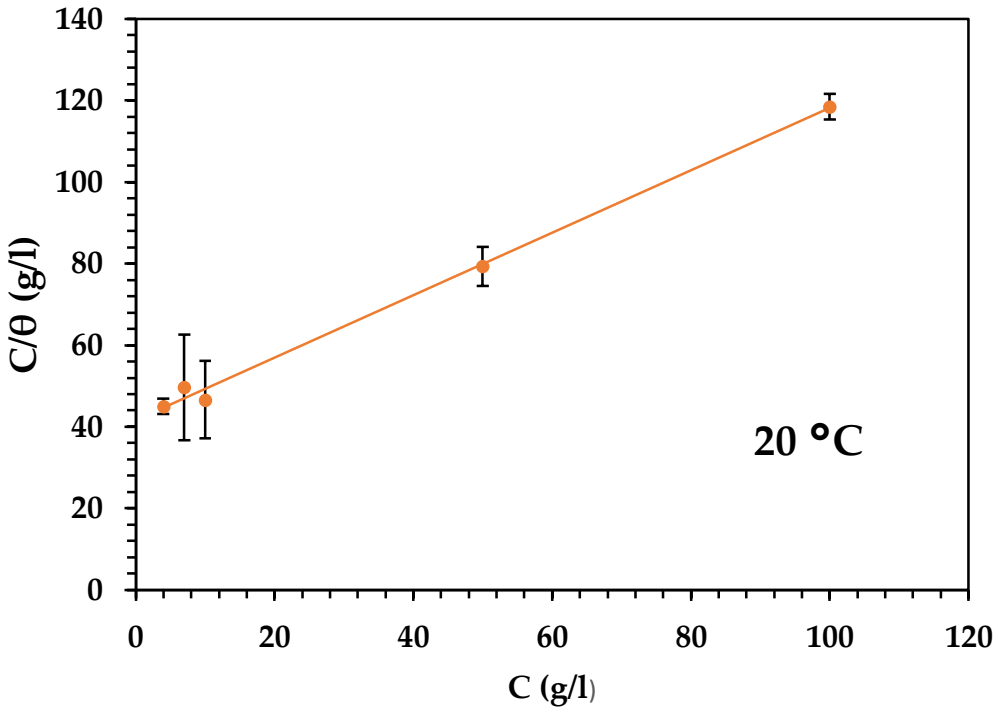


Figure 5-2 Langmuir isotherm plot for the adsorption of AV on the MS surface in 15 wt. % HCl at 20°C after 5 h immersion. Error bars represent the standard deviation of three measurements.

Table 5-1 Equilibrium constant (K_{ads}) and Gibbs free energy of adsorption (ΔG_{ads}) for MS in 15wt% HCl solution in the presence of optimum concentrations of PA, MI, DW, BC, IN and AV. The presented data were obtained from weight loss measurements after graphically fitting the results with Langmuir adsorption isotherm at different temperatures.

Temperature (°C)	Inhibitors	R^2	K_{ads} (L/g)	$-\Delta G_{ads}$ (kJ/mol)
20	PA	0.9999	52.91	26.50
	MI	0.9999	32.47	25.31
	DW	0.9999	14.66	23.37
	BC	0.9999	1.88	18.37
	IN	0.9993	1.40	17.65
	AV	0.9683	0.02	7.30
40	PA	0.9999	454.54	33.90
	MI	0.9999	29.67	27.00
	DW	0.9996	9.26	23.77
	BC	0.9996	3.43	21.18
	IN	0.9766	1.02	18.03
60	PA	0.9999	2500	41.00
	MI	0.9818	0.76	18.38
	DW	0.9958	2.91	22.08
	BC	0.9897	1.22	19.68
	IN	0.9981	2.57	21.74

Note: R^2 means a correlation coefficient

5.3 Activation energy studies

The dependence of the corrosion kinetics of MS in the absence and presence of different inhibitors in 15 wt% HCl after 24 h immersion by weight loss measurements on Arrhenius behaviour was investigated:

$$C_r = Ae^{\left(-\frac{E_a}{RT}\right)} \quad \text{Eqn 5-4}$$

The linearized form of the equation gives:

$$lnC_r = ln\,A - \left(\frac{E_a}{RT}\right) \quad \text{Eqn 5-5}$$

where A is the Arrhenius pre-exponential factor, E_a is the apparent activation energy of the corrosion process, R is the universal gas constant, and T is the absolute temperature.

Figure 5-3 shows the Arrhenius plots for MS in the absence and presence of PA, MI, DW, BC, IN and AV in 15wt% HCl solution after 24 h immersion from weight loss measurements data (Table 4-3) and their apparent activation energies are summarised in Table 5-2. From the table, it can be seen that the apparent activation energies of the corrosion process calculated from the slopes of the plots increase with the addition of the inhibitors (MI, DW, BC, IN, and AV) into the test solution compared to the inhibitor-free solution. This demonstrates an increase in the energy barrier of the corrosion process in the presence of the additives; except for PA-inhibited solution that the apparent activation energy of the corrosion process was lower compared to the uninhibited solution.

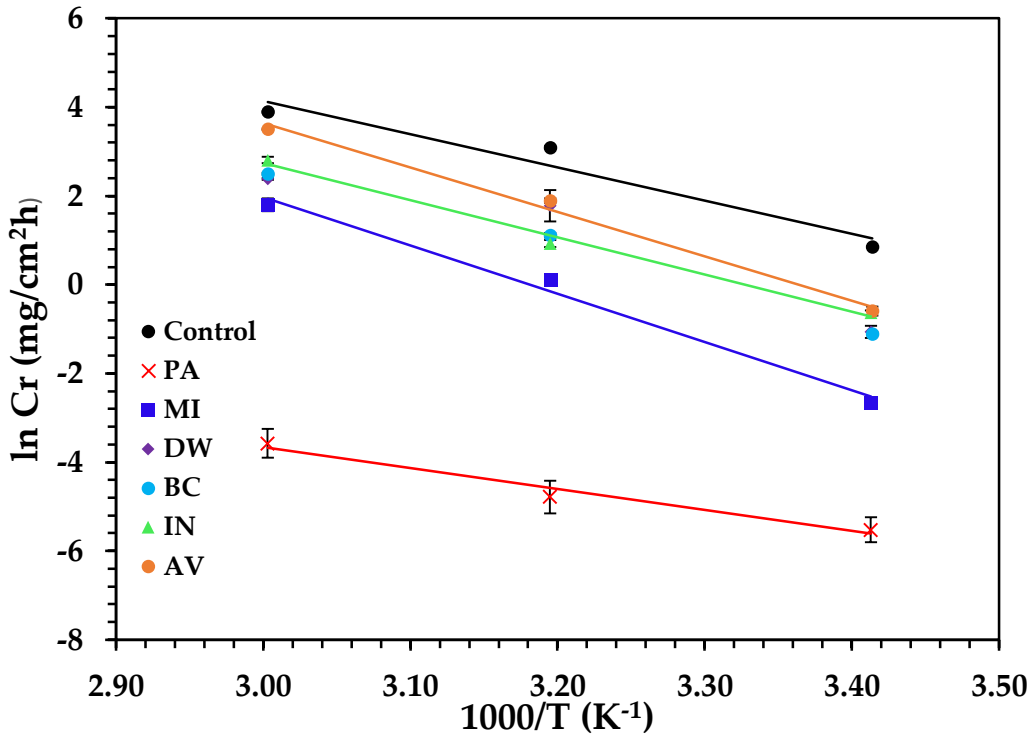


Figure 5-3 Arrhenius plots for MS corrosion in the absence and presence of optimum concentrations PA, MI, DW, BC, IN and AV in 15wt% HCl solution after 24 h immersion using weight loss measurements data.

Table 5-2 Activation parameter for MS in 15wt% HCl in the absence and presence of an optimum concentration of PA, MI, DW, BC, IN and AV after 24 h immersion at different temperatures.

Acid solution/inhibitor	Activation energy (kJ/mol)	Slope
15 wt% HCl + 0 g/L	62.1±0.1	-7.47
15 wt% HCl + 7 g/L PA	40.8±0.1	-4.90
15 wt% HCl + 7 g/L MI	89.0±2.8	-10.31
15 wt% HCl + 7 g/L DW	70.3±2.5	-8.46
15 wt% HCl + 10 g/L IN	71.7±2.5	-8.62
15 wt% HCl + 10 g/L BC	72.5±0.6	-8.72
15wt% HCl + 100 g/l AV	84.8±2.1	-10.00

5.4 Chemical composition analysis of the inhibitors

5.4.1 FTIR of different inhibitors

The FTIR spectrum of PA is presented in Figure 5-4. The absorption bands at 3290, 2122 and 638 cm^{-1} show the presence of acetylenic groups (-C≡C-) [68]. A shoulder peak at 3345 cm^{-1} corresponds to an -OH group. The bands at 2931, 2875, 1424, 1362 and 1232 were attributed to CH_2 stretching vibrations [68]. Finally, the peaks at 1024 and 938 cm^{-1} were assigned to C-O and C-C stretching vibrations, respectively [68].

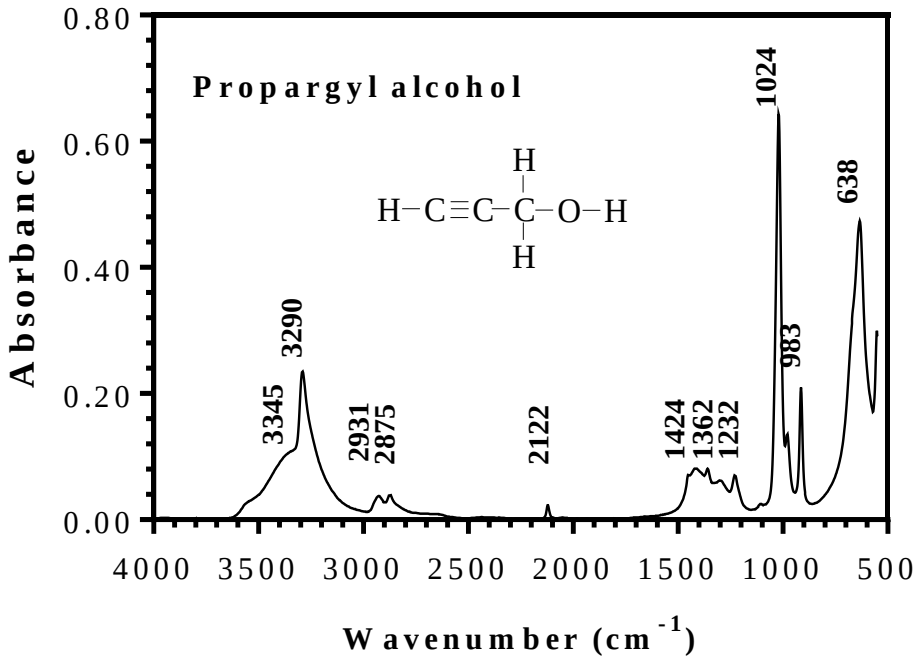


Figure 5-4 FTIR absorption spectrum of as-received PA.

Figure 5-5 shows the FTIR spectrum of MI. The absorption bands at 3109 and 2570 cm^{-1} were attributed to the stretching vibrations of N-H and thiol (SH) groups [173]. The band at 1619 cm^{-1} was assigned to the presence of imidazole C=N stretching vibration [173]. The last two bands observed at 1510 and 659 cm^{-1} were due to the presence of C=C stretching aromatic and C-S, respectively [173].

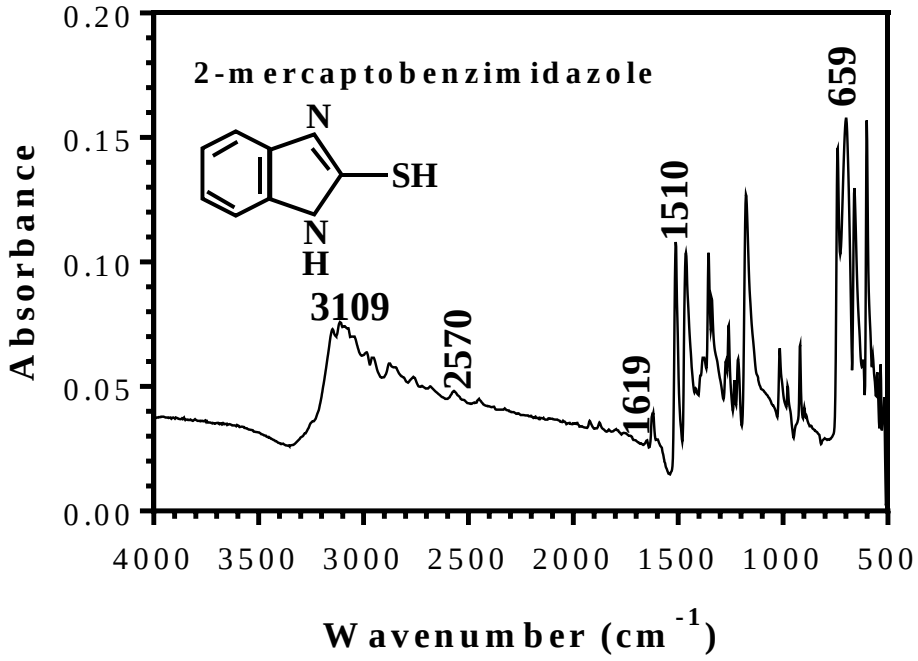


Figure 5-5 FTIR absorption spectrum of as-received MI.

Figure 5-6 shows the FTIR spectrum of DW. The broadband at 3287 cm^{-1} was assigned to the presence of NH stretching vibration [174]. The two bands at 2925 and 2855 cm^{-1} are attributed to CH stretching vibration [174]. The absorption band at 1646 cm^{-1} corresponds to the stretching vibration of C=O (amide I) while the shoulder band at 1541 cm^{-1} is due to the presence of CN and NH bending vibration mode (amide II) [174]. The band at 1077 cm^{-1} was assigned to the presence of C-C stretching vibration

[174]. The absorption band at 996 cm^{-1} is due to the stretching vibration of C-O [174]. These results indicate that durum wheat contains electron rich O and N atoms as well pi-electrons in the carbon double bonded to oxygen which makes durum wheat meet the requirements of being screened as a potential corrosion inhibitor.

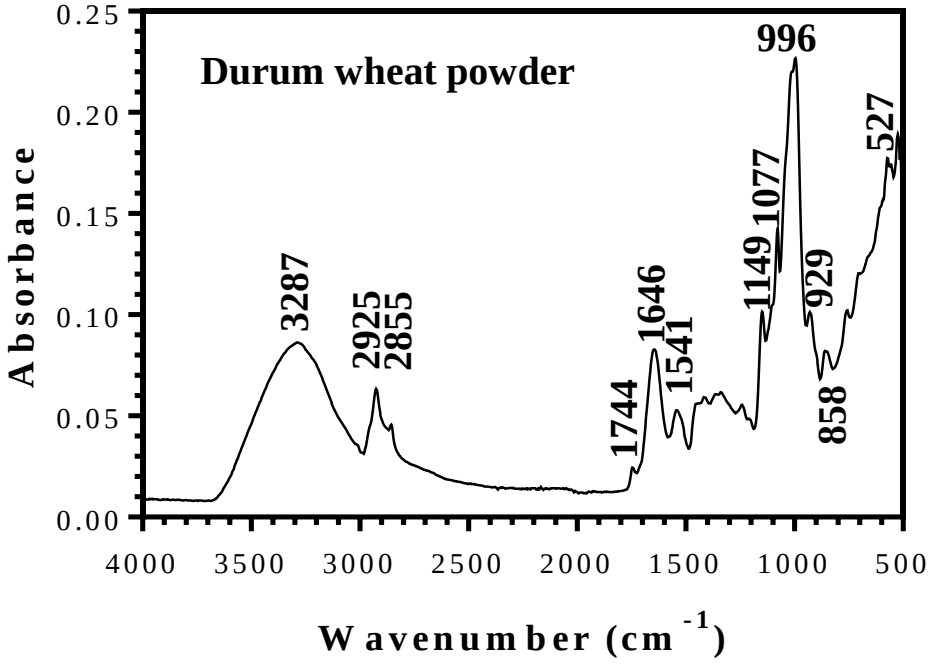


Figure 5-6 FTIR absorption spectrum of as-received DW.

The FTIR spectrum of BC powder is presented in Figure 5-7. The broad absorption band observed at 3277 cm^{-1} was due to the vibration of phenol O-H stretching mode. The absorption bands at 2918 and 2850 cm^{-1} were due to the presence of C-H stretching vibration mode [175]. The band at 1621 cm^{-1} was related to C=O group, and the band that appeared at 1047 cm^{-1} was assigned to sulfoxide stretch (S=O)[175].

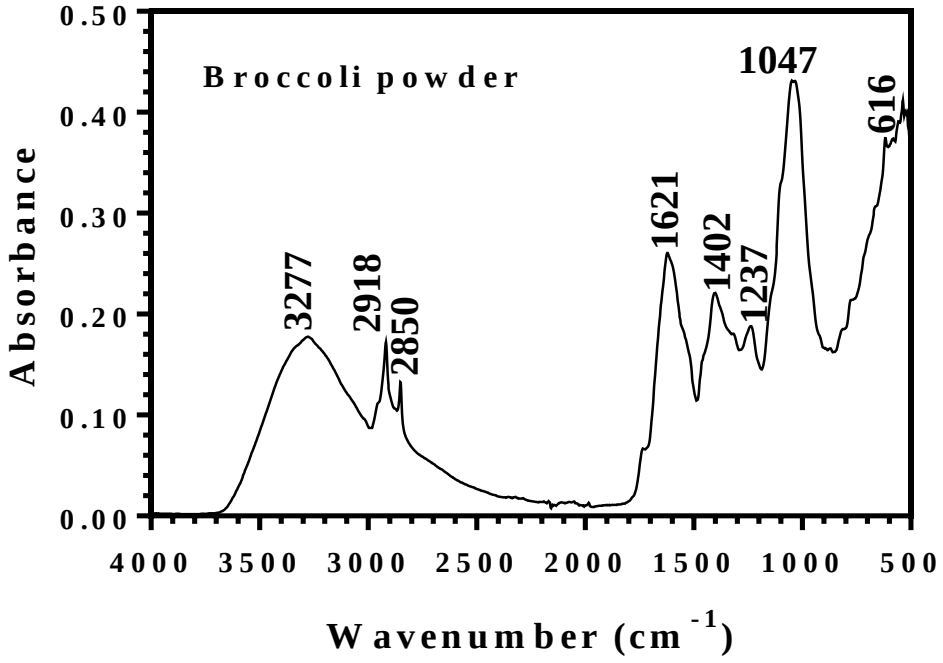


Figure 5-7 FTIR absorption spectrum of BC.

Figure 5-8 shows the FTIR spectrum of IN. The broad absorption peak at 3285 cm^{-1} corresponds to the stretching vibrations of hydroxyl groups (- OH) of carbohydrates [176, 177]. The peak at 2918 was assigned to the vibration of C-H asymmetric of CH2 and a shoulder peak at 2851 cm^{-1} was assigned to the presence of C-H symmetric stretching of CH_3 [176, 178]. Furthermore, the peak at 1639 cm^{-1} was attributed to a carbonyl group(C=O) that is in fructose and glucose structure [179]. The band that appeared at 1575 cm^{-1} was attributed to C=C vibration, and the two peaks at 1418 and 1334 cm^{-1} were attributed to the vibrations of CH and CH_2 and OH groups from fructose ring. The absorption bands at 1119 and 1015 cm^{-1} are characteristics of strongly coupled stretching vibrations of C-C, C-O, C-O-H and C-O-C bonds of oligo and polysaccharides [178, 180]. Lastly, the peak at 927 cm^{-1} was assigned to the presence of β-(2,1) glycosidic bond [181]. The results demonstrate that IN has several

oxygen atoms and pi-electrons which meet the characteristics of a promising corrosion inhibitor.

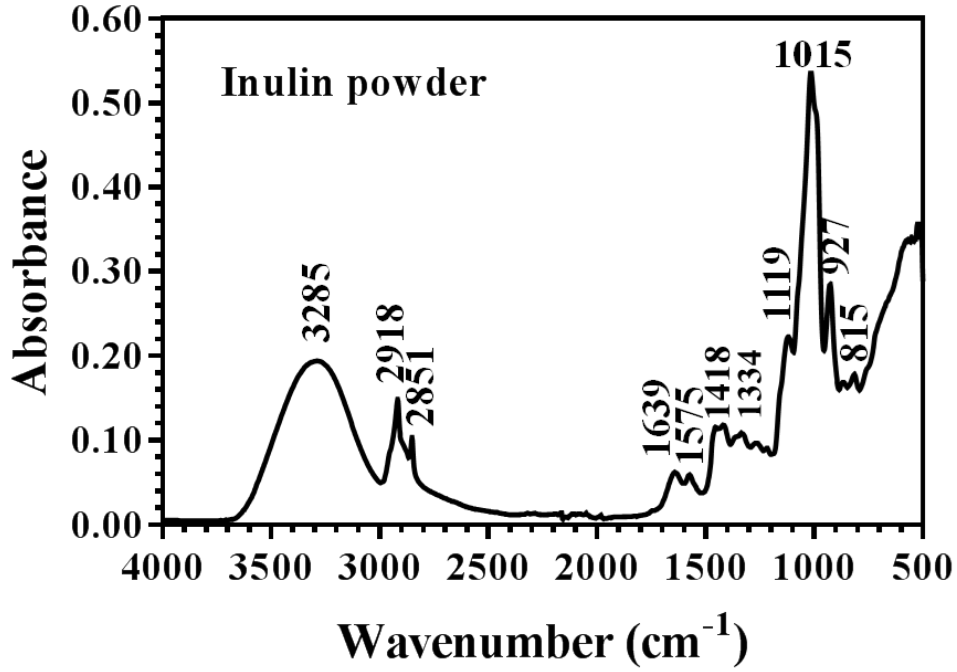


Figure 5-8 FTIR absorption spectrum of IN.

FTIR spectrum of aloe vera gel is shown in Figure 5-9. The broad peak at 3313 cm^{-1} is assigned to the vibration of the O-H group of phenol and carbohydrate monomers [182- 184]. Also, the peak at 1638 cm^{-1} is attributed to the presence of COO stretching of the carboxylic acid group (- COOH) [183]. Finally, the smallest peak at 2100 cm^{-1} could not be assigned.

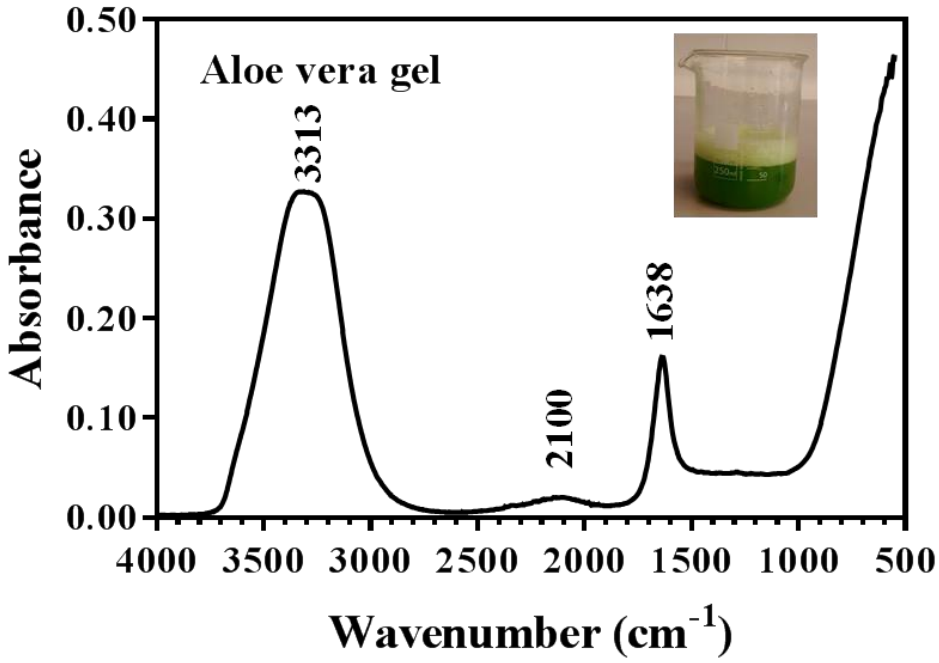


Figure 5-9 FTIR absorption spectrum of AV.

5.4.2 Gas–Chromatography-Mass Spectrometry (GC-MS)

The GC-MS chromatogram presented in Figure 5-10 shows the components that were identified in a hexane extract of IN. The retention times, component names, molecular formula, and percentage peak areas are listed in Table 5-3. As shown in the table, four major components were identified in the hexane extract. These components were hexadecanoic acid (palmitic acid; 52.64%), 2- propenoic acid, 1- methylundecyl ester (methylundecyl acrylate; 23.84%), octadecanoic acid (stearic acid; 16.60%) and 9, 12- octadecadienoic acid (linoleic acid; 2.50%). The molecular structures of these major components are presented in Figure 5-11.

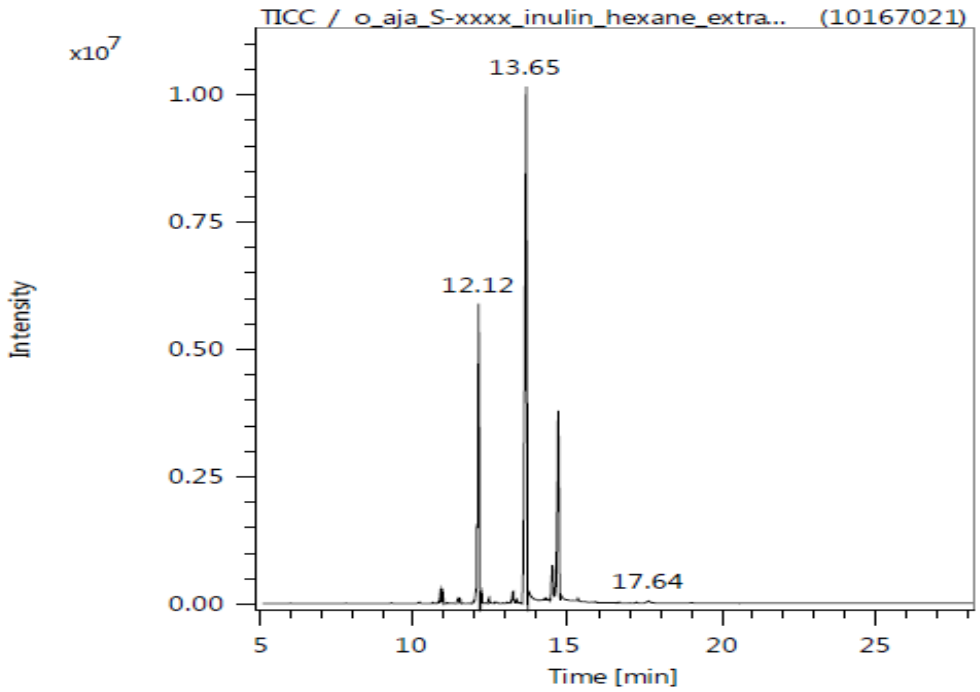


Figure 5-10 GC-MS chromatogram of hexane extract of IN.

Table 5-3 Identified constituents from a hexane extract of IN.

Retention time (min)	Identified compound	Molecular formula	% peak area
10.87	Pentadecane	$C_{15}H_{32}$	0.72
10.94	Butylated Hydroxytoluene	$C_{15}H_{24}O$	0.88
11.50	Hexadecane	$C_{16}H34$	0.30
12.12	2-propenoic acid, 1-methylundecyl ester	$C_{15}H_{28}O_2$	23.84
12.20	Heptadec-8-ene	$C_{17}H_{34}$	0.72
13.24	Nonadecane	$C_{19}H_{40}$	0.82
13.65	Palmitic acid	$C_{16}H_{32}O_2$	52.64
14.50	Linoleic acid	$C_{18}H_{32}O_2$	2.50
14.70	Stearic acid	$C18H_{36}O_2$	16.60

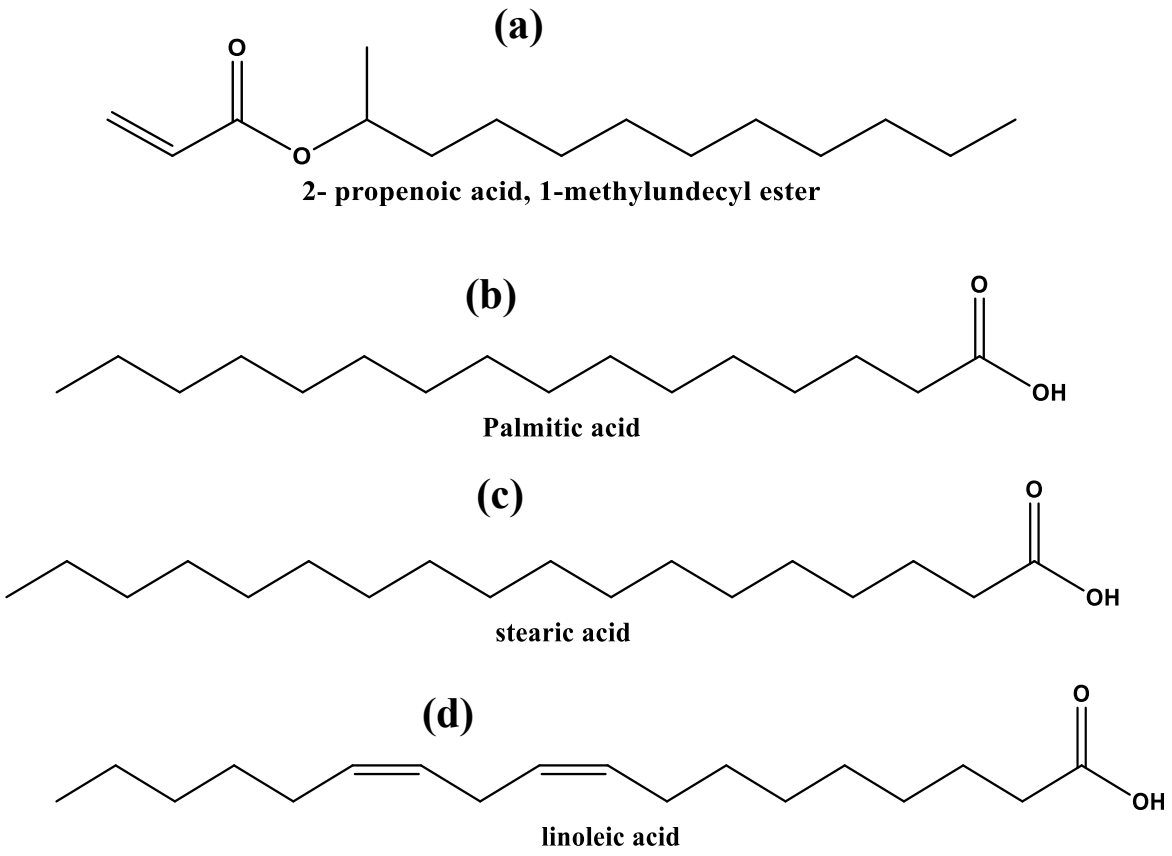


Figure 5-11 Molecular structures of the major components in inulin hexane extract (a) 2- propenoic acid, 1-methylundecyl ester (b) Palmitic acid (c) stearic acid and (d) linoleic acid. Three are fatty acids, the other a fatty acid ester.

Figure 5-12 shows the GC-MS chromatogram of a hexane extract of broccoli. The identified components and their corresponding percentage peak areas are presented in Table 5-4. Six major components were identified, based on retention times and mass spectral comparisons. The types of chemical compounds identified were hydrocarbons, fatty acids, a vitamin, and a sterol. Their chemical structures are shown in Figure 5-13. The most abundant component was linoleic acid (38.42%), followed by nonacosane (26.90%) and n-hexadecanoic acid (15.30%). Other components were, in order of

decreasing chromatographic peak area, vitamin E (7.86%), γ- sitosterol (3.50%) and phytol (1.13%), respectively.

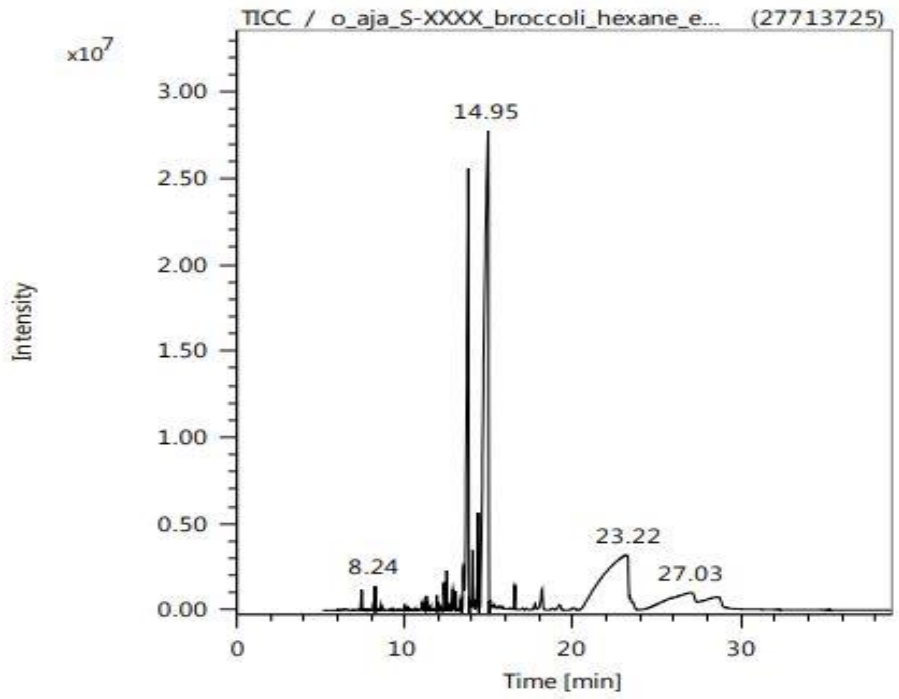


Figure 5-12 GC-MS chromatogram of hexane extract of BC.

Table 5-4 Identified components from a hexane extract of BC

Retention time (min)	Identified compound	Molecular formula	% peak area
7.43	3,4-Furandimethanol	$C_6H_8O_3$	0.39
8.24	4H-Pyran-4-one,23-dihydroxy-6-methyl	C_6H8O_4	0.39
12.34	Propionic acid, 3-(m-aminobenzoyl)-2-methyl-	$C_{11}H_{13}NO_3$	0.46
12.48	Tetradecanoic acid (myristic acid)	$C_{14}H_{28}O_2$	0.59
12.85	α-Ethyl-3-nitrocinnamic acid	$C_{11}H_{11}NO_4$	0.41
13.04	Pentadecanoic acid	$C_{15}H_{30}O_2$	0.24
13.49	5,8,11-Heptadecatrien-1-ol	$C_{17}H_{30}O$	0.82
13.77	n-Hexadecanoic acid	$C_{16}H_{32}O_2$	15.30
14.04	Heptadecanoic acid (margaric acid)	$C_{17}H_{34}O_2$	0.75
14.37	Phytol	$C_{20}H_{40}O$	1.13
14.95	Linoleic acid	$C_{18}H_{32}O_2$	38.42
16.54	Pentacosane	$C_{25}H_{52}$	0.43
18.17	Heptacosane	$C_{27}H_{56}$	0.72
23.22	Nonacosane	$C_{29}H_{60}$	26.90
27.03	Vitamin E	$C_{29}H_{50}O_2$	7.86
28.65	γ-Sitosterol	$C_{29}H_{50}O$	3.50

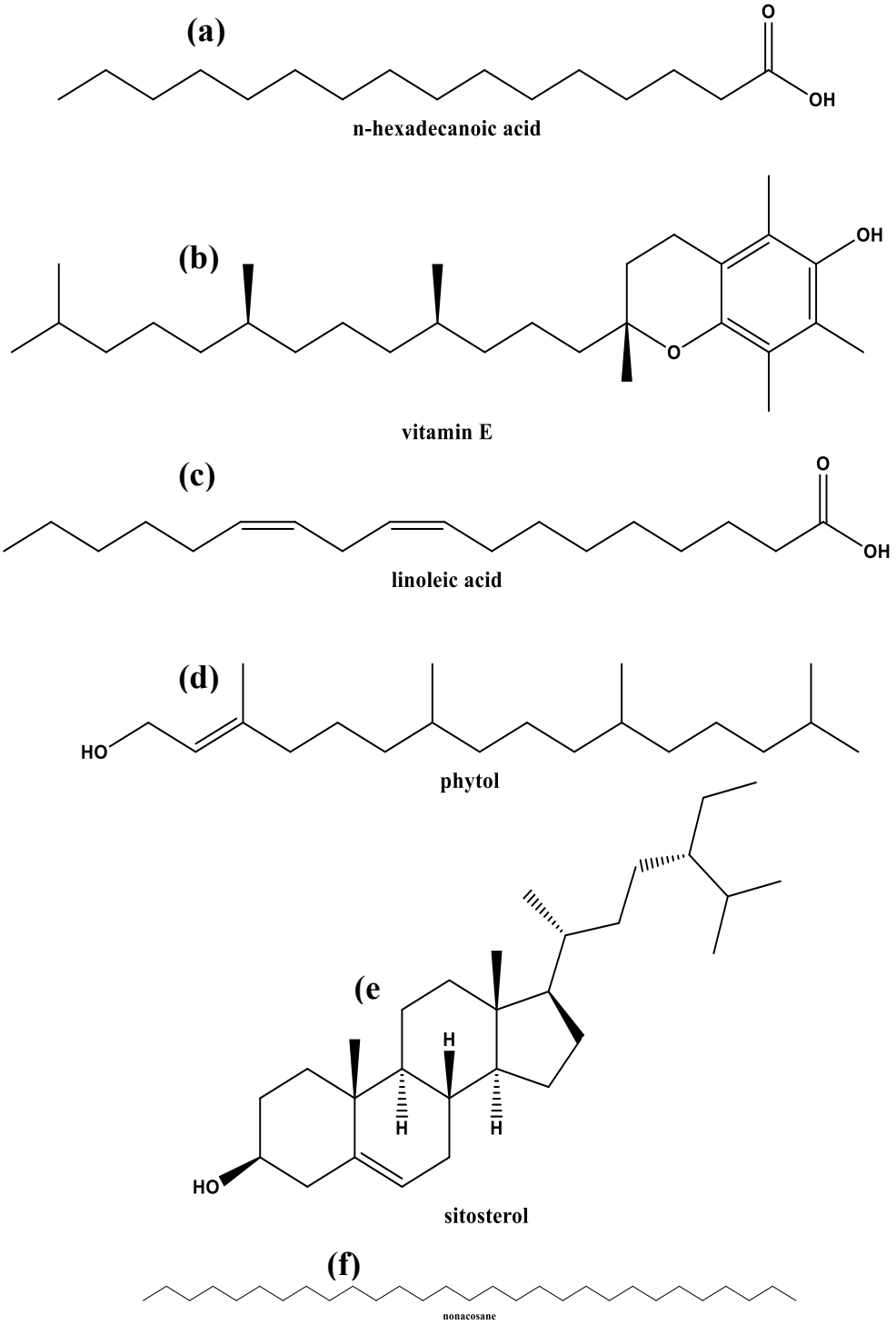


Figure 5-13 Molecular structures of different major constituents in broccoli hexane extract (a) n-hexadecanoic acid (b) vitamin E (c) linoleic acid (d) phytol (e) γ-sitosterol and (e) nonacosane.

Figure 5-14 shows the GC-MS chromatogram of a hexane extract of AV. The identified components that correspond to each peak are shown in Table 5-4, and the molecular structures of the major components are presented in Figure 5-15. The most prominent peak was 2-myristoyl pantetheine (47.32%) at a retention time of 30.03 min. The second largest peak was found to be g-linolenic acid (gamolenic acid; 9.89%) with a retention time of 33.16 min. The third principal constituent was 9- hexadecenoic acid (palmitoleic acid; 9.49%) at a retention time of 29.59 min. Also, the fourth principal constituent that eluted at 33.62 min was octadecanoic acid, 2-(2-hydroxyethoxy) - ethyl ester (diethylene glycol monostearate; 5.59%). Other identified constituents are listed in Table 5-3. GC-MS revealed that aloe vera gel contains vitamin, fatty acids, esters, and hydrocarbons.

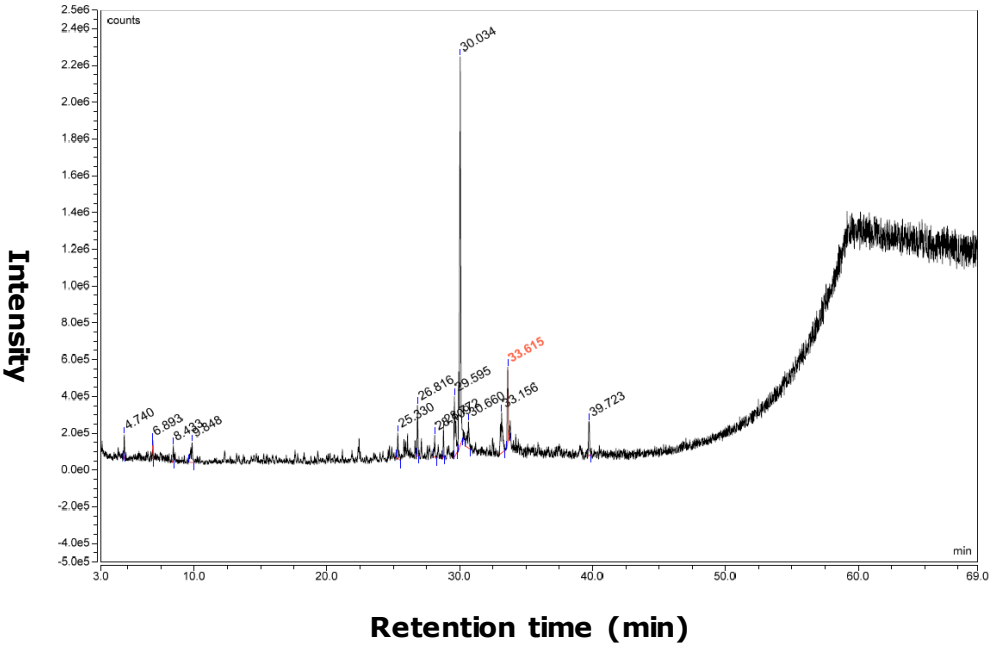


Figure 5-14 GC-MS chromatogram of the hexane extract of AV gel.

Table 5-5 Identified constituents of the hexane extract of AV gel.

Retention time (min)	Identified compound	Molecular formula	% peak area
4.74	4-Carene	$C_{10}H_{16}$	1.19
8.43	Decane	$C_{10}H_{22}$	1.09
9.85	2-Undecenal	$C_{12}H_8S$	4.49
25.33	Napthol (2,3-b) thiophene	$C_{14}H_{28}O_2$	3.19
26.82	Bis (1-chloro-2-propyl) phosphate	$C_6H_{13}ClO_4P$	4.17
28.11	Phthalic acid, isobutyl octadecyl ester	$C_{30}H_{50}O_4$	2.08
28.77	2,6,10-trimethyl- Tetradecane	$C17H_{36}$	2.25
29.59	Palmitoleic acid	$C_{16}H_{30}O_2$	9.49
30.66	2-Myristynoyl pantetheine	$C_{25}H_{44}N_2O_5S$	47.32
33.16	Gamolenic acid	$C_{18}H_{30}O_2$	9.89
33.62	Octadecanoic acid,2-(2-hydroxyethoxy)-ethyl ester	$C_{22}H_{44}O_4$	5.59
39.72	Diisooctyl phthalate	$C_{24}H_{38}O_4$	3.63

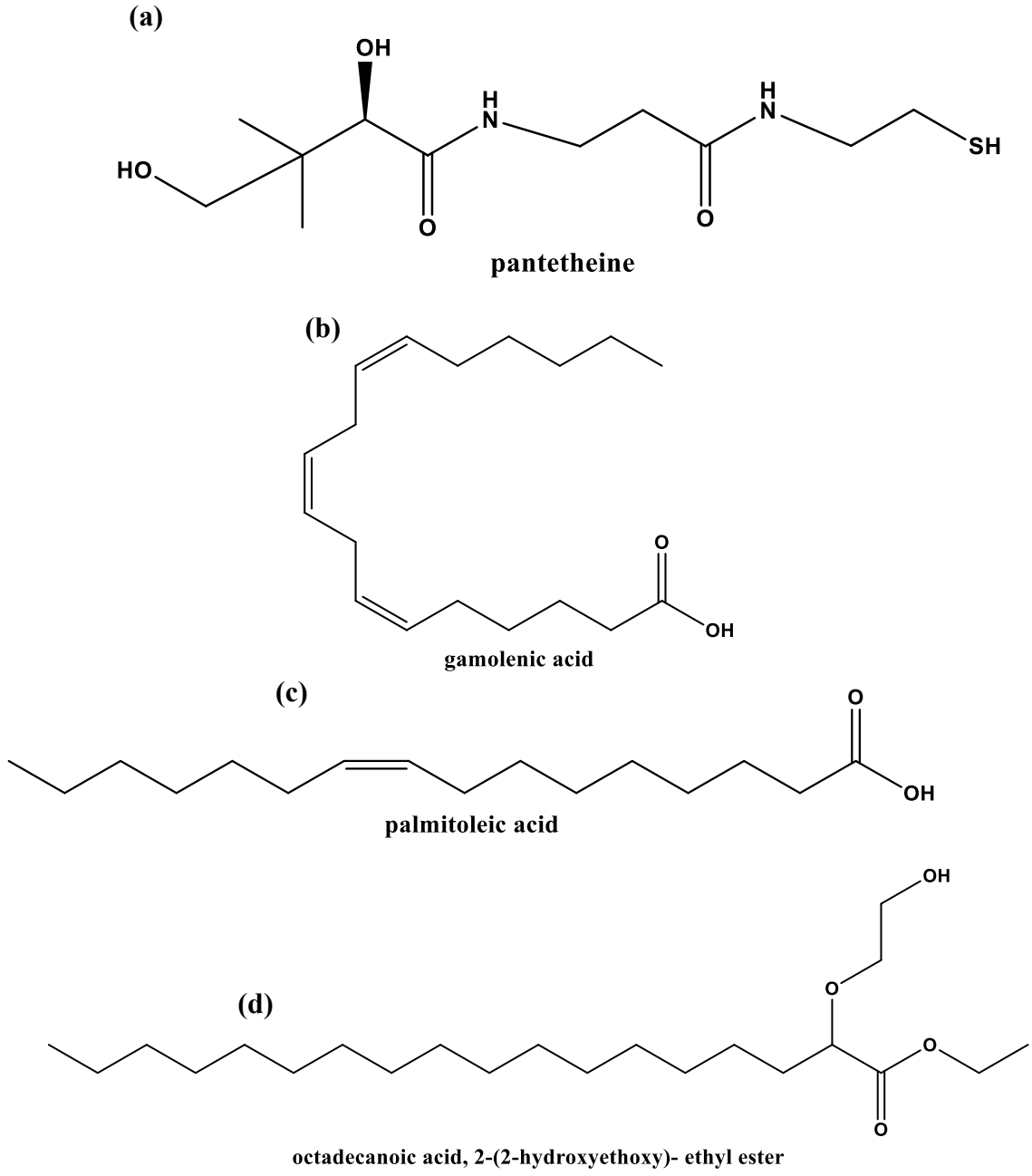


Figure 5-15 Molecular structures of different major constituents in the hexane extract of Aloe Vera gel (a) Pantetheine (b) gamolenic acid (c) palmitoleic acid and (d) octadecanoic acid, 2-(2-hydroxyethoxy)- ethyl ester.

Figure 5-16 shows the GC-MS chromatogram from the analysis of the hexane extract of DW. An enlargement of the baseline around the base of the significant peaks is shown in the inset, to enhance the minor chromatographic peaks present. The identified constituents which correspond to each significant peak in the chromatogram are listed in Table 5-6. The two major constituents that eluted at retention times of 13.84 and 15.15 mins were identified as 9,12-Octadecadienoic acid (Z, Z)- (linoleic acid;71.55%) and hexadecanoic acid, palmitic acid, (26.91%), respectively. The next major constituent was nonadecane (an alkane hydrocarbon;4.17%) at a retention time of 13.23 min, followed by pentadecanoic acid (3.019%) at the retention time of 13.02 min. The molecular structures of these major constituents are shown in Figure 5-17. The results obtained in this work showed that the hexane extract of durum wheat mainly contained saturated and polyunsaturated fatty acids, with other, more trace, constituents, including squalene - a lipid triterpenoid, and a hydrocarbon (nonadecane).

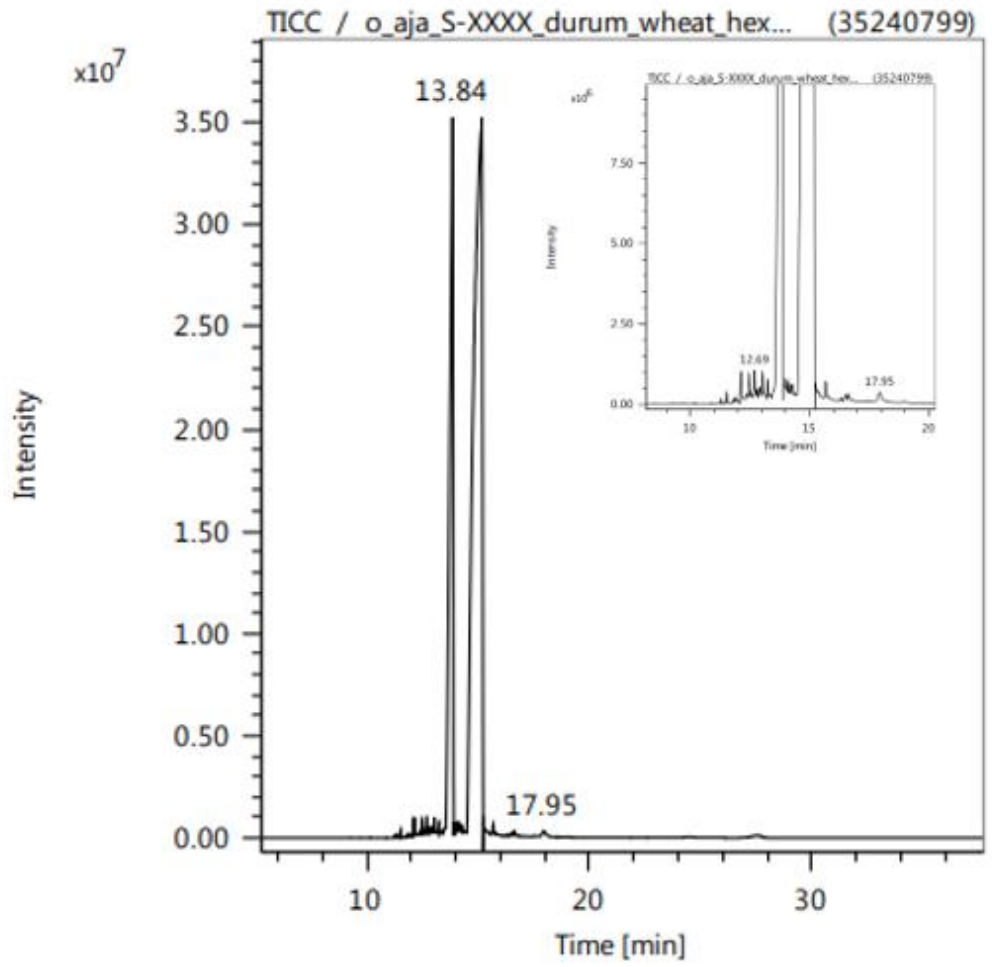


Figure 5-16 GC-MS chromatogram of hexane extract of DW.

Table 5-6 Identified constituents from the hexane extract of DW.

Retention time (min)	Identified compound	Molecular formula	% peak area
12.11	3,7,11-trimethyl-1-Dodecanol	$C_{15}H_{32}O$	0.20
12.69	Octadecane	$C_{18}H_{38}$	0.20
13.02	Pentadecanoic acid	$C_{15}H_{30}O_2$	3.19
13.23	Nonadecane	$C_{19}H_{40}$	4.17
13.84	Hexadecanoic acid (Palmitic acid)	$C_{16}H_{32}O_2$	26.91
15.15	9,12-Octadecadienoic acid (Z, Z)-(linoleic acid)	$C_{18}H_{32}O_2$	71.55
17.95	Squalene	$C_{30}H_{50}$	0.08

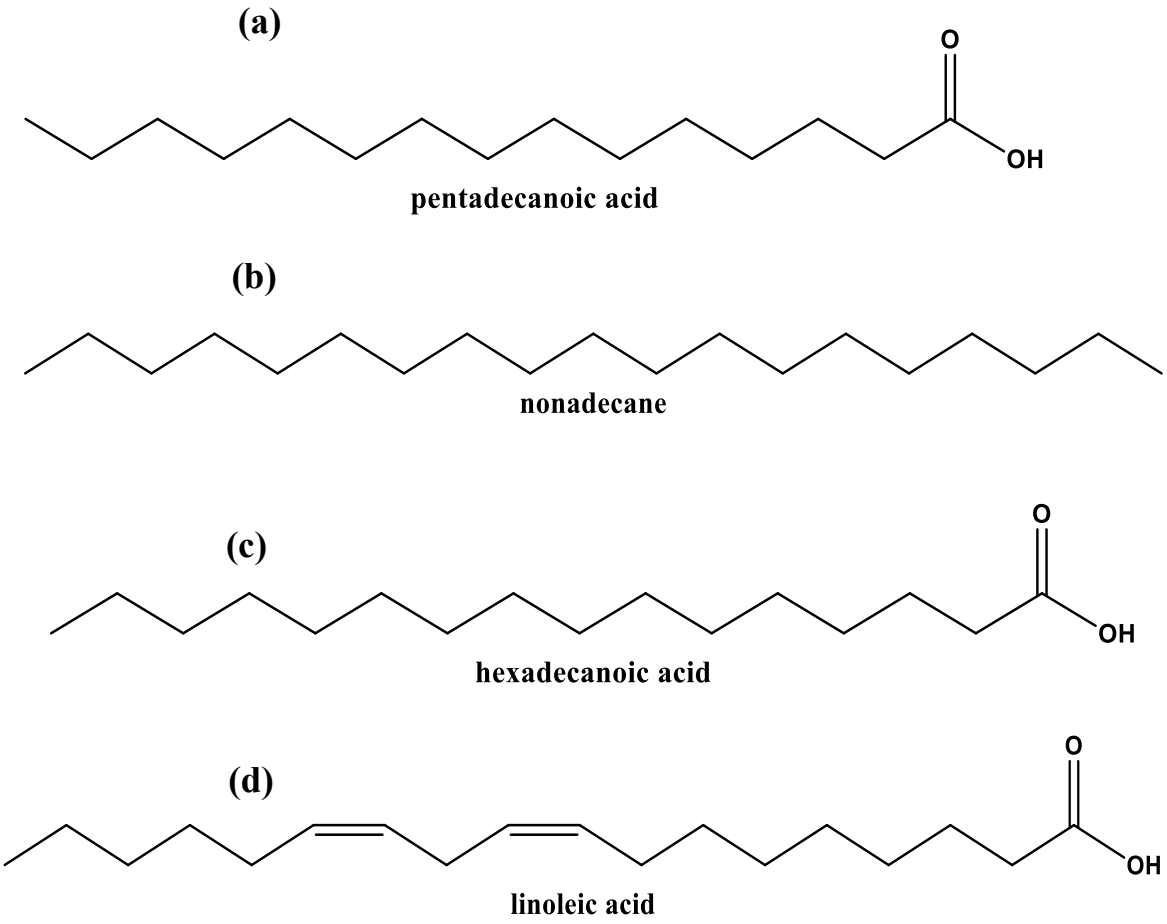


Figure 5-17 Molecular structures of different major constituents in durum wheat hexane extract (a) pentadecanoic acid (b) nonadecane (c) hexadecanoic acid (palmitic acid); (d) 9,12-octadecadienoic acid (Z, Z)- (linoleic acid).

CHAPTER SIX

ANALYSIS OF THE NATURE/COMPOSITION OF THE ADSORBED FILM

6.1 X-ray photoelectron spectroscopy (XPS)

XPS is a surface sensitive technique which measures the elemental composition, chemical state and electronic state of the elements (except hydrogen and helium) within a material [185, 186]. It is sensitive to the chemical state of the atoms in a material's surface up to a depth of ~10 nm. XPS spectra are acquired when a material is irradiated with X-ray beam (e.g., Al Kα x-rays), resulting in the emission of photoelectrons. This technique is applied for many research and industrial applications such as nanoparticle analysis, photovoltaics, corrosion inhibitor/metal interface, identification and measurements of surface contamination, among others. Among other surface techniques, XPS is used continually because of its high surface sensitivity and its ability to provide reliable and most quantitative information about the chemical states of a material surface [187]. It is employed to probe the surface chemistry of a metal surface/inhibitor interface.

In the current study, the inhibitor layers are expected to be a single molecular layer thick, and therefore are likely to be only detectable directly using a surface sensitive technique like XPS. Several authors have used XPS to study the chemistry of the organic inhibitor film formed on metals in corrosive media [8, 102, 188-191].

This chapter presents the chemical nature and composition of films formed on the surfaces of untreated and treated MS in the presence of PA, MI, DW, BC and IN at 20°C after 5 h immersion as analyzed using XPS. XPS studies of MS surface treated with AV were not carried out because of its uneconomical high concentration (100 g/L).

Figure 6-1 and Table 6-1 show the XPS survey spectra and an estimate of the atomic concentrations for MS immersed in 15 wt% HCl solution in the absence and presence

of different inhibitors after 5 h immersion at 20°C by weight loss measurements. From the detected spectra and subsequent quantification of the wide scans, it is clear that photoelectron peaks of Fe 2p, C 1s, O 1s, and Cl 2p were detected on both the uninhibited and inhibited MS surfaces. Also, N 1s signal appeared on MI, DW, BC and IN treated MS surfaces, but was absent in the uninhibited and PA-inhibited surfaces.

As shown in Figure 6-1, C 1s was detected on both untreated and treated MS surfaces. The uninhibited sample shows ~35 at % of carbon (Table 6-1). This is not surprising because some adventitious carbon is expected to be formed on the MS surface due to its exposure to air during sample handling. The amount of carbon in the inhibited samples were ~78, 48, 50, 41 and 52 at% for PA, MI, DW, BC and IN, respectively. It is expected that the C 1s signal would increase in the presence of the inhibitors compared to the uninhibited samples since they all contain carbon, hence forming possibly a thicker layer of the carbon-based material. The sample treated with PA has the highest amount of carbon at its surface, whilst the BC sample had the least. The high amount of carbon may be attributed to the higher coverage of PA on the MS surface.

Fe 2p peak was more intense for the uninhibited sample (~24 at %), while those treated with inhibitors decreased markedly (**Table 6-1**). This is expected since the overlay of carbon is thinner on the uninhibited sample surface. Hence, more Fe photoelectrons can reach the detector. The amount of Fe2p detected in the presence of the inhibitors were 0.8 at%, 8.6 at %, 10 at%, 15.7 at % and 11.2 at% for PA, MI, DW, BC and IN, respectively.

Considering the O 1s peak, MS surface in the uninhibited solution has the highest amount of oxygen (40 at %) compared to the inhibited MS surfaces as shown in

Table 6-1. Also, the amount of oxygen in the presence of PA, MI, DW, BC and IN were 21, 36, 34, 38 and 34 at. %, respectively.

Nitrogen species detected on the surface of samples treated with MI, DW, BC and IN may be due to the nitrogen atoms present in these compounds. The estimated amount of nitrogen species detected on the inhibited samples were 6.5 at. %, 5.8 at. %, 2.9 at. % and 1.7% at. % for MI, DW, BC and IN, respectively.

As shown in **Table 6-1**, the Cl 2p peaks detected on MS surfaces in the absence and presence of all the studied inhibitors. These chloride ions possibly originate from the test environment (15 wt. % HCl). The uninhibited surface had the highest concentration of chloride (above 2 at. %), whilst PA, MI, DW, BC and IN had 0.1, 0.6, 0.9, 1.4 and 0.7 at. %, respectively. The results indicate that more chloride ions are in the film lattice of the uninhibited surface than the inhibited ones.

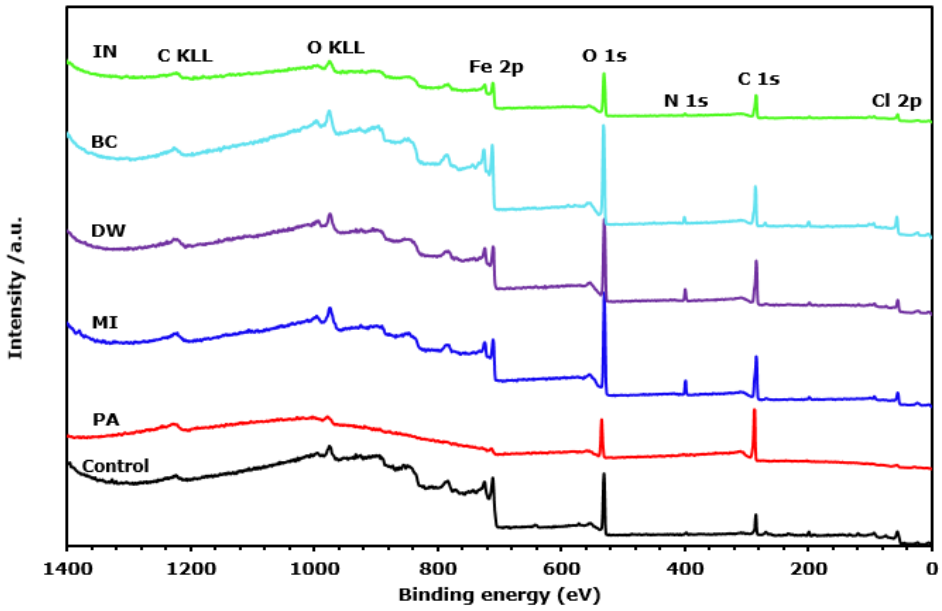


Figure 6-1 XPS survey scan for MS surface after 5 h immersion in 15 wt.% HCl in the absence and presence of optimum concentration of PA, MI, DW, BC and IN at 20°C showing the presence of Fe, O, C, and Cl 2p core levels on all the MS surfaces.

Table 6-1 XPS composition for MS immersed in 15 wt.% HCl in the absence and presence of 7 g/L (PA, MI, DW) and 10 g/L IN at 20°C after 5 h immersion.

Constituents	Control		PA		MI		DW		BC		IN	
	BE	at. %	BE	at. %	BE	at. %	BE	at. %	BE	at. %	BE	at. %
C 1s	285	34.5	287	77.9	285	48.4	285	49.7	286	41.2	285	52.1
O 1s	531	40.0	535	21.1	531	35.9	531	33.6	532	38.8	531	34.4
Fe 2p	711	23.5	713	0.8	710	8.6	710	10.0	712	15.7	710	11.2
N 1s	-	-	-	-	399	6.5	400	5.8	401	2.9	400	1.7
Cl 2p	199	2.1	203	0.1	199	0.6	199	0.9	199	1.4	198	0.7
S 2p	-	-	-	-	-	-	-	-	-	-	-	-

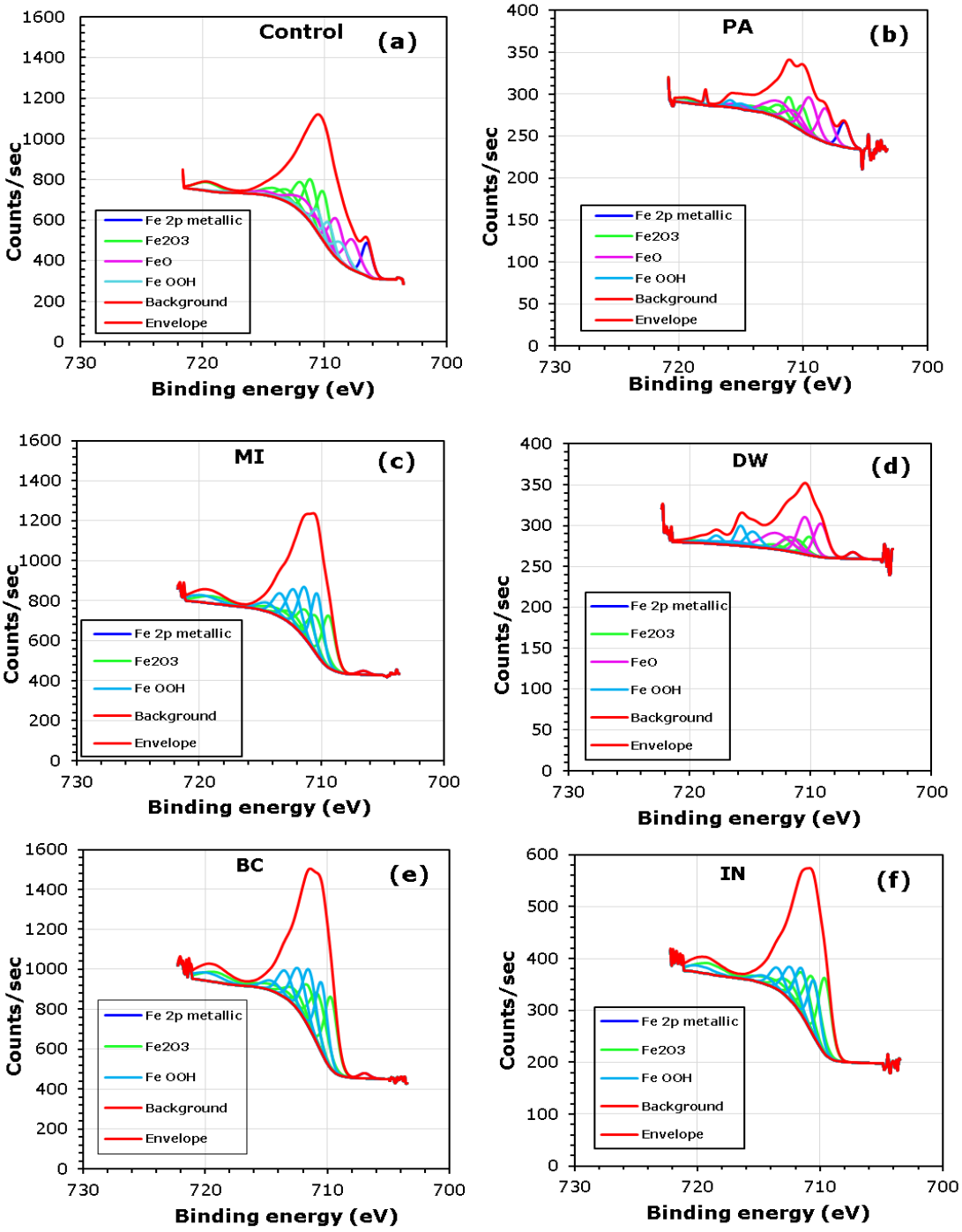


Figure 6-2 XPS deconvoluted profile of Fe 2p core level for MS in 15 wt.% HCl in the absence and presence of inhibitors showing different oxidation states: (a) uninhibited; (b) PA; (c) MI; (d) DW; (e) BC; and (f) IN. The Fe 2p models were performed using the method of Grosvenor et al. [192] and charge corrected to C 1s at 285 eV. Gaussian-Lorentzian (GL) and a Shirley-background were used for the deconvolution of the Fe component.

High-resolution spectra of the Fe2p peaks gives useful information of the chemical states (i.e., metallic and oxide states) of the different core levels detected at the interface of a metal/organic inhibitor. Following the method published in Grosvenor et al.[192] a set of peaks models were built to fit the Fe 2p 3/2 peak. FeO, Fe_2O_3, and FeOOH were detected at the MS surfaces.

The deconvoluted Fe 2p spectra for MS exposed to uninhibited and PA, MI, DW, BC and IN inhibited solutions are shown in Figure 6-2. The relative composition (at %) of the elemental and oxide Fe is summarized in Table 6-2. The untreated MS surface is composed of Fe in both elemental and oxide forms. The amount of the compositions was 1.2 at % elemental iron, 13.9 at % FeO, 20.8 at % FeOOH, and 64.1 at. % Fe_2O_3 layer. Ferric oxide is the main oxide at the uninhibited surface. Turning to the inhibited sample surfaces, both metallic iron and iron oxide/hydroxide were also detected, and the estimate of the concentration are listed in Table 6-2. The PA-treated sample has about 8 at % of metallic Fe, whilst the majority of the Fe was present in the form of an oxide (Table 6-2). MI treated sample has iron oxide-hydroxide (~66 at %), ferric oxide (~31 at %) and the rest elemental Fe. The main oxides visible at the DW treated sample were iron-oxide hydroxide (24 at %), ferric oxide (41 at %) and ferrous oxide (31 at %).

The sample treated with BC shows about 0.6 at% of elemental Fe, ~59 at% iron oxide/hydroxide and ~26 at% ferrous oxide. IN treated sample shows 46 at% iron oxide/hydroxide, 53 at% ferric oxide and about 1.5 at% elemental Fe. It is reasonable to assume that Fe chemical states are layers with FeOOH, FeO, Fe_2O_3 and then metallic Fe below.

Table 6-2 Relative intensity (%) of Fe 2p core level for untreated and treated MS sample.

Sample	Fe metallic (at %)	FeOOH (at %)	Fe_2O_3 (at %)	FeO (at %)
Control	1.19	20.77	64.10	13.94
PA	7.61	14.38	24.35	53.66
MI	0.47	65.65	30.36	-
DW	1.41	24.01	40.88	33.70
BC	0.63	58.56	25.97	-
IN	1.46	45.65	52.93	-

The C 1s spectra for uninhibited and inhibited MS surfaces are shown in Figure 6-3. Carbon is present on both untreated and treated surfaces. However, at% of carbon is higher for inhibited MS surfaces, and this may be due to the formation of a thicker layer. Also, the C 1s spectra observed for treated surfaces contain contributions from both the inhibitors and adventitious species.

The C 1s spectrum for untreated MS surface shown in Figure 6-3(a) composed three chemical components located at binding energies of 285, 286 and 288 eV. These were attributed to C-C, C-O, and O-C=O, respectively and are the features due to adventitious carbon layer [96, 193].

Considering MS surfaces treated with the different inhibitors, the peak positions of the deconvoluted components are almost like the uninhibited surface. Hence, the binding energies at ~285, 286 and 288 eV may be due to features of organic carbon contamination (C-C, C-O, and O-C=O species) as stated for the untreated surface. Also, similar peaks positions and chemical species assigned to adventitious carbon layer were also detected in the presence of PA, DW, BC, and IN. However, the organic inhibitors may also contribute to the surface film lattice as the concentration of carbon increased on surfaces treated with inhibitors compared to the uninhibited layer. The inhibitors

attached to the MS surface from the solution with adventitious carbon in place. The presence of both the inhibitor and adventitious carbon makes interpretation of the C 1s peak complex.

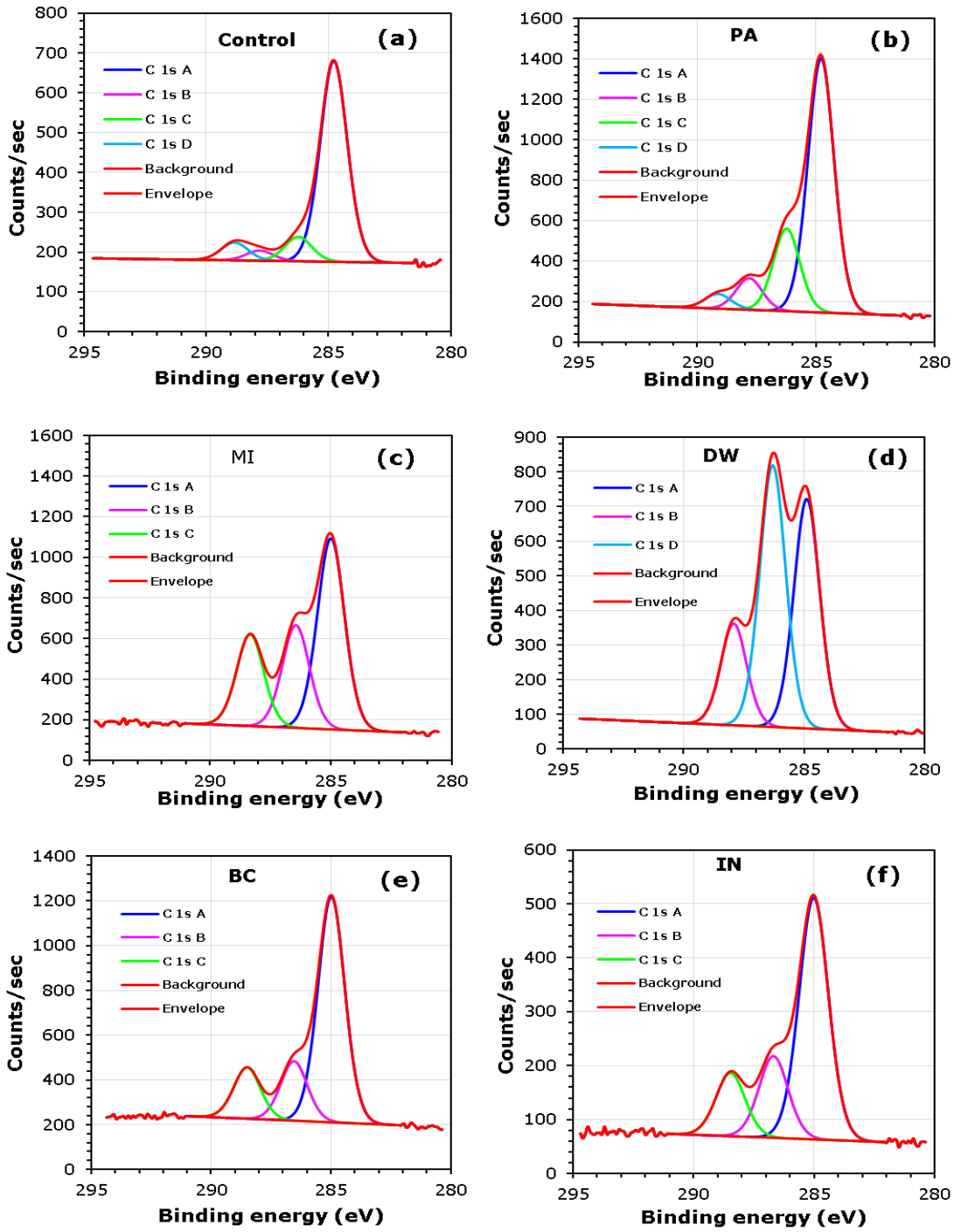


Figure 6-3 XPS deconvoluted profile of C 1s for MS in 15 wt.% HCl in the (a) absence and presence of (b) PA (c) MI (d) DW (e) BC and (f) IN. The C 1s core level was charge corrected at 285 eV. Gaussian-Lorentzian (GL) and a Shirley-background were used for the deconvolution of C 1s

Figure 6-4 and Table 6-3 show the XPS spectra and relative atomic % of O 1s signal derived from the MS surface in the absence and presence of PA, MI, DW, BC and IN, respectively. The oxygen feature present at the MS surface could originate from the surface oxide film and/or organic carbon contamination. Considering the uninhibited and inhibited MS samples, the O 1s envelopes were deconvoluted into three components (i.e., chemical states). Even though the oxygen chemical species detected on both the uninhibited and inhibited surfaces were similar, their atomic concentrations were different (Table 6-3). The oxygen species located at 530-531 eV was assigned to the oxygen (O^{2-}) in FeO and/or Fe_2O_3 oxides, whilst the one located at a binding energy of 532 eV was attributed to oxygen double bonded with carbon (O-C=O), i.e. feature from adventitious carbon and the component at highest binding energy of 533 eV was attributed to the oxygen from the adsorbed water [186, 193].

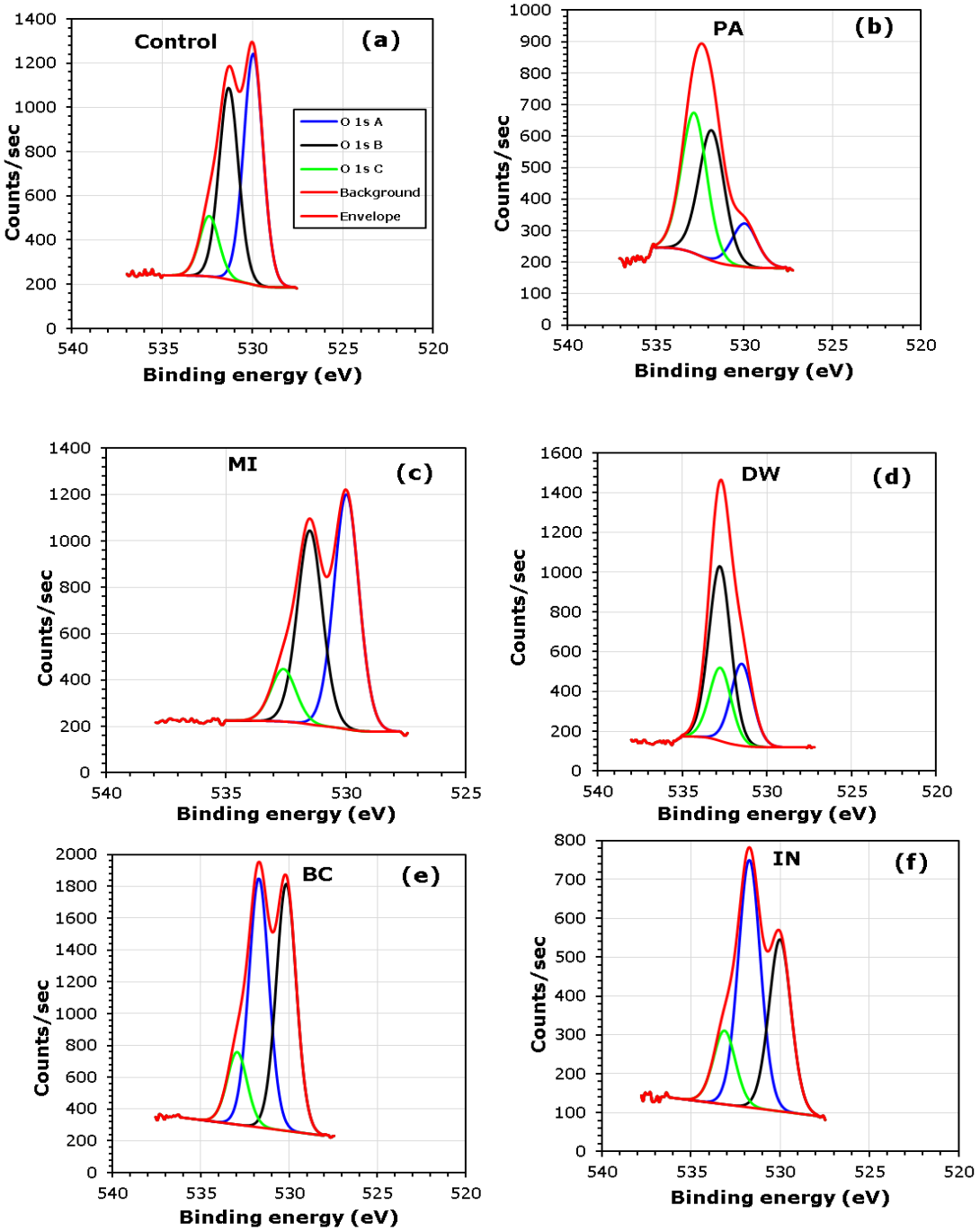


Figure 6-4 XPS deconvoluted profile of O 1s core level for MS in 15 wt% HCl in the (a) absence and presence of (b) PA (c) MI (d) DW (e) BC and (f) IN showing metal oxide at ~530 eV and other species at higher BE. The models were charge corrected to C 1s at 285 eV. Gaussian-Lorentzian (GL) and Shirley-background were used for the deconvolution of each component

Table 6-3 Binding energies (eV), (relative intensity) and their assignment for deconvoluted O 1s profile for MS immersed in 15 wt% HCl in the absence and presence of PA, MI, DW, BC and IN at 20˚C after 5 h of immersion.

Control	PA	MI	DW	BC	IN
530(47.8%)	530 (13.8%)	530 (54.0%)	530 (34.2%)	530 (34.2%)	530 (32.3%)
531(39.7%)	-	-	-	-	-
532(12.5%)	532 (41.5%)	532 (27.12%)	532 (47.3%)	532 (47.29%)	532 (50.3%)
-	533 (44.8%)	533 (18.8%)	533 (18.5%)	533 (18.5%)	533 (17.3%)

Figure 6-5 shows the XPS spectra for deconvoluted N 1s profile for MS surface in 15 wt.% HCl containing MI, DW, BC and IN after 5 h of immersion at 20˚C. The binding energies, relative intensity (%) and their corresponding assignment are listed in Table 6-4. Nitrogen atoms were not detected on MS surface in uninhibited and PA- inhibited solutions and hence XPS spectra not shown in Figure 6-5 for these samples.

Considering MI-inhibited surface, N 1s envelope was fitted into three components as shown in Figure 6-5a. The two components located at binding energies of 399 and 400 eV were attributed to the two chemically distinct N atoms present in MI molecule that are bonded to carbon (C-N) and iron (N-Fe), respectively. The third peak located at 400 eV has the highest concentration of about 90 at. %. The assignment of the third peak at a binding energy of 402 eV is attributed to protonated nitrogen which could be due to surface contamination from the MI solid powder, as it is 98wt% pure [96].

Considering MS surfaces treated with DW, BC and IN, the N 1s envelopes are composed of a single component (chemical species). These components located at 400 eV for DW, BC and IN (Table 6-4) respectively were assigned to the nitrogen atom that is present in each inhibitor, which is bonded to MS surface (-N-Fe)[194].

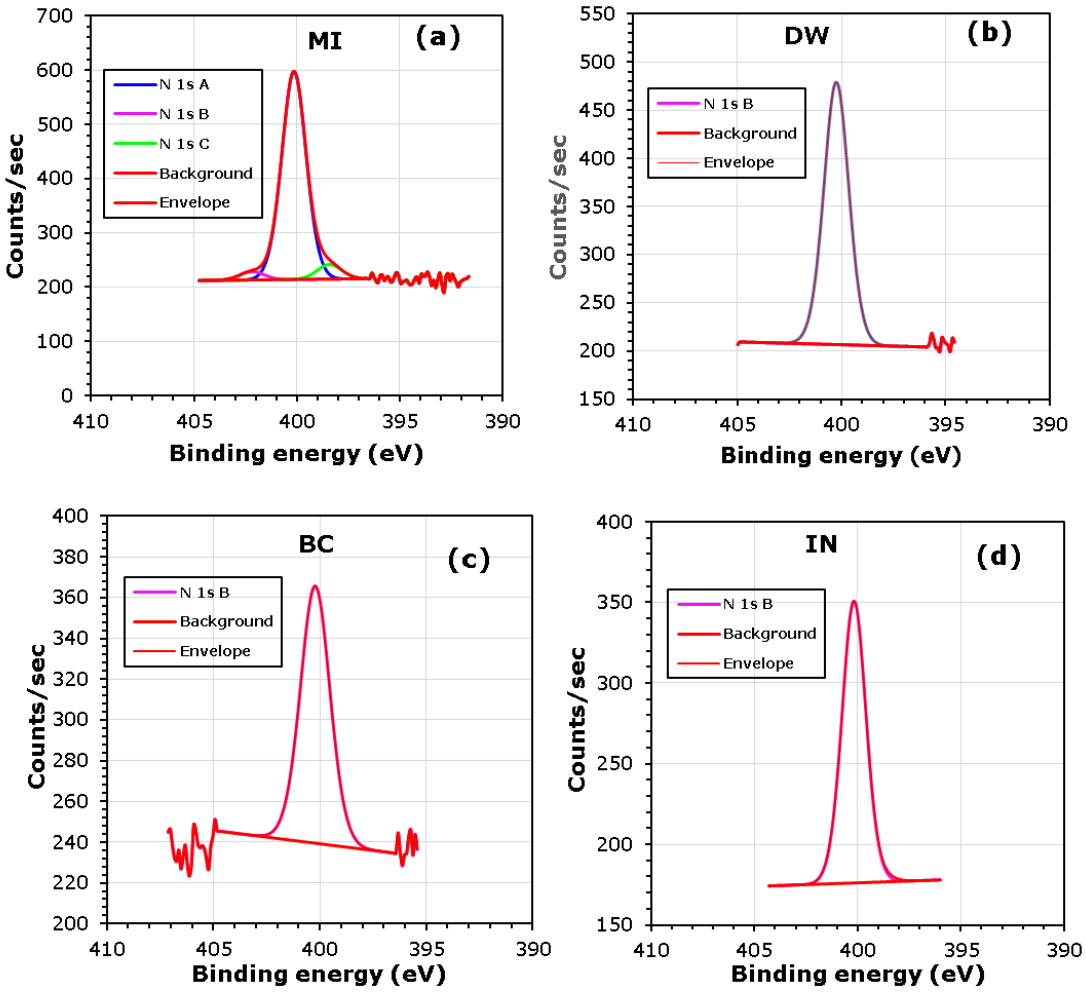


Figure 6-5 XPS deconvoluted profile of N 1s for MS in 15 wt% HCl in the presence of (a) MI (b) DW (c) BC and (d) IN. The background is linear.

Table 6-4 Binding energies, relative intensity and their assignment for deconvoluted N 1s profile for MS immersed in 15 wt% HCl in the absence and presence of PA, MI, DW, BC and IN at 20˚C after 5 h of immersion.

Control	PA	MI	DW	BC	IN
-	-	399 (6.4%)	-		-
-	-	400 (90.0)	400 (100%)	400 (100%)	400 (100%)
-	-	402 (3.6%)			

6.2 FTIR analysis of the adsorbed inhibiting film

Figures 6-6a and 6-6b show the FTIR spectra of the as-received PA inhibitor and the film formed at the MS surface in 15wt% HCl containing 7 g/L PA after 5 h immersion at 60°C by weight loss measurements. It can be seen from the comparison of the FTIR spectra that the acetylenic groups (C≡C) initially present for the as-received PA at 2122 and 638 cm^{-1} were absent at the PA-inhibited MS surface, this could be due to the interaction of the triple bonds of PA molecules with the MS surface. Furthermore, new peaks appeared at 1642, 1598 and 583 cm^{-1} which were not present in the spectrum of the as-received PA and their assignments are C=C, COOFe and FeO species. Hence, the organic film formed at the MS surface treated with PA was composed of OH (3403 cm^{-1}), CH_2 (2976 and 2922 cm^{-1}), C=C (1642 cm^{-1}), COOFe (1598 cm^{-1}) and FeO (583 cm^{-1}) species [68].

Attempts were made to characterize the MS surfaces treated with MI, DW, BC, IN and AV after 5 h immersion using FTIR, but no signal was detected. This is probably due to the thinness of the inhibiting film.

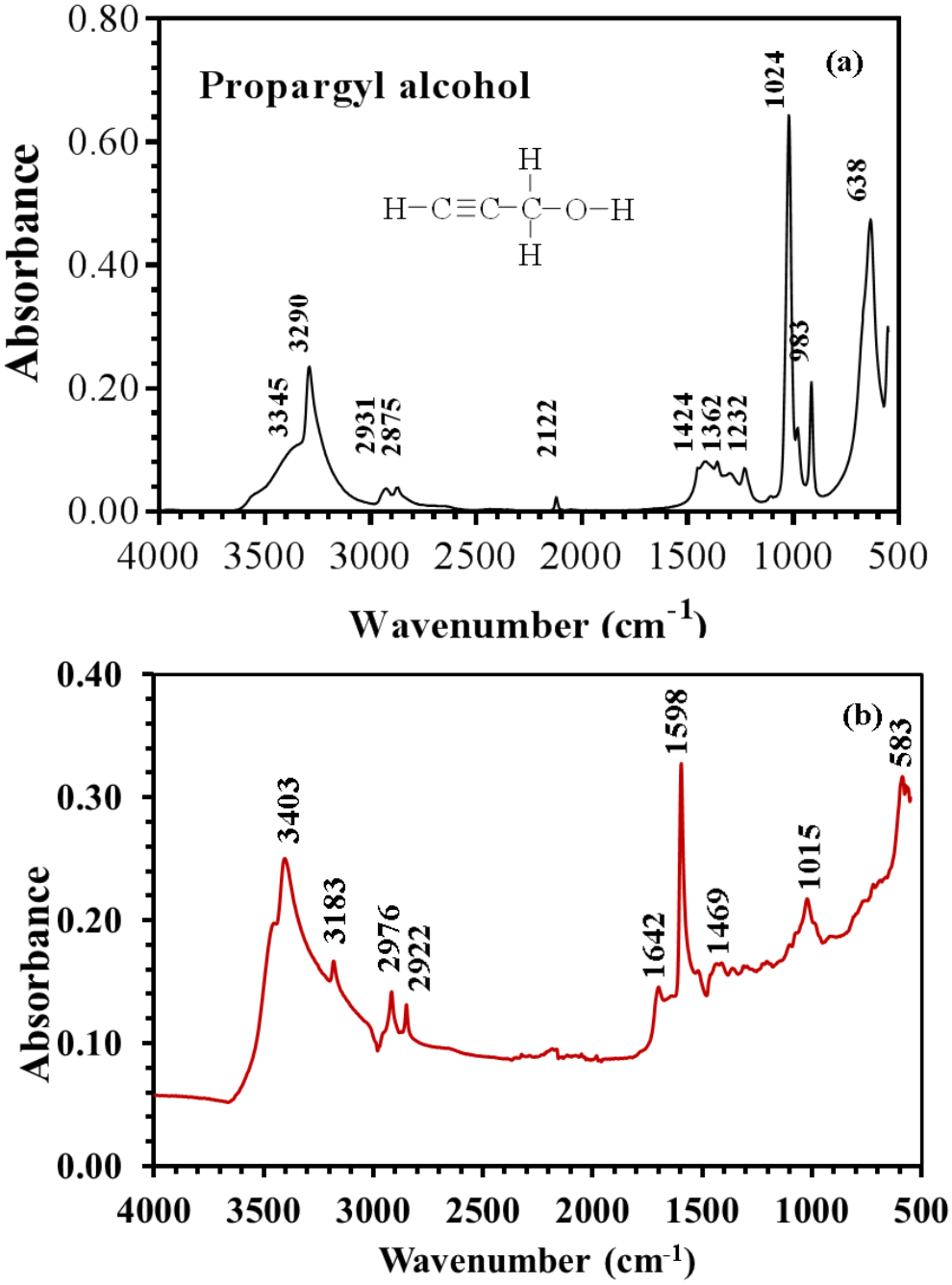


Figure 6-6 FTIR spectra of (a) as-received PA; (b) film formed at the MS immersed in 15wt% HCl containing 7 g/L PA at 60°C after 5 h exposure by weight loss measurements.

Summary

1. XPS data has provided valid information about the surface chemistry of the MS/uninhibited and inhibited interface. The presence of iron oxide/hydroxide films was observed in the film lattice of MS surfaces in the absence and presence of all the studied inhibitors.
2. XPS and FTIR data showed that MS treated PA surface film was composed of Cl, C=C, COOFe, CH.
3. The presence of N 1s peak profile in the presence of MI, DW, BC and IN, respectively confirm the adsorption of these inhibitors on the oxidised MS surfaces, hence forming a protective film against corrosion. This is confirmed by a lower corrosion rate and less Cl attachment.
4. XPS data demonstrated that the adsorbed layer on the MS surface is thin as the metallic Fe was detected. This layer appears to protect the metal surface and leaves the oxides and hydroxides intact.

CHAPTER SEVEN

DISCUSSION OF INDIVIDUAL CORROSION INHIBITOR

7.1 Overview

This section discusses the previously presented results on the inhibitive performance of PA and MI, and later compared with DW, BC, IN and AV as a function of concentration, immersion time and temperature, followed by the description of the proposed mode of adsorption, inhibition mechanisms and nature of the inhibiting film of all the corrosion inhibitors (CIs).

7.2 Propargyl alcohol (PA)

7.2.1 Effect of concentration on PA performance

In this study, the experimental data of the influence of different concentrations of PA on the corrosion behaviour of mild steel (MS) after 5 h of immersion at 20°C (**Table 4- 1**) showed that the corrosion rate of MS decreased from 0.047 mg/cm^{2}h (0.525 mm/y) to 0.009 mg/cm^{2}h (0.100 mm/y) with increasing PA concentration from 1 to 7 g/L. This may be attributed to increase in the adsorption and surface coverage of PA on the MS surface with increasing concentration, leading to the formation of a barrier layer against sample corrosion [36, 51, 64, 65, 72, 195, 196]. This is consistent with the results of Jayaperumal [36], who found that the corrosion rate of MS in 15wt% HCl decreases from 0.9 to 0.4 mm/y with an increase in the concentration of PA from 0.2wt% (2g/L) to 1wt% (10 g/L) at 30°C after 6 h immersion. The percentage decrease of corrosion rate of MS in this present work was about 81% (**Table 4-1**), while that reported by Jayaperumal at the same concentration (1 g/L) decreased by 56%, which means that PA was more effective in the current work.

Further increase in the PA concentration beyond 7 g/L in this work, did not cause a significant change in the corrosion rate, which can be attributed to the formation of strongly adhering protective film on the MS surface [51].

The inhibition efficiency of PA was 99±1% at a concentration of 7g/L in this work. The excellent inhibition performance exhibited by PA has been attributed to the persistent and strong adhering film formed on MS surface, which occurred primarily via the interaction of the pi-electrons of the carbon-carbon triple bonds (highly reactive) and the oxygen atom in the hydroxyl group with the vacant d-orbitals of the iron atom [67, 68, 71]. Similar excellent inhibitive performance of PA has been reported in some previous work for MS in a strongly acidic environment as summarised in **Table 7-1**.

Table 7-1 Comparison of the inhibition efficiency at a different concentration of PA obtained in the present work with those reported in the literature.

Inhibitor	Medium	Material	Inhibitor conc.	Test conditions	Exposure Time (h)	IE (%)	Ref
PA	15wt%HCl	MS	7.0 g/L	WL at 20°C	5.0	99±1%	Present work
PA	15wt%HCl	MS	10 g/L	WL at 30°C	6.0	100%	[36]
PA	15wt%HCl	MS	5.0 g/L	WL at 105°C	0.5	99%	[72]
PA	10wt%HCl	MS	0.2 g/L	WL at 30°C	3.0	95%	[67]

Note: WL means weight loss measurements

XPS result of the adsorbed film formed at the MS surface treated with PA at 20°C after 5 h immersion showed the highest contribution of carbon (over 77 at %) and the lowest amount of Fe (0.8 at%) as presented in **Table 6-1**. The lowest value of Fe detected at the MS/PA interface is a pointer to the fact that the adsorbed layer formed on the MS sample was thick. Also, the MS surface treated with PA appeared to be the smoothest, which could be due to the protective film formed. Hence, it is expected that the inhibition performance would be high. This is confirmed by the excellent inhibition efficiency of over 99% exhibited by PA. Also, the adsorbed species at the MS/PA interface contains C=C, OH, Cl and FeO species as evidenced by FTIR result (**Figure 6-6b**). All these observations demonstrate the formation of an adsorbed layer on the MS surface. Similar inhibiting film products have been reported by Poling et al. [68]. A detailed description of the inhibition mechanism and nature of the inhibiting film formed by PA on MS surface is discussed in **section 7.2.5**.

7.2.2 Effect of immersion time on PA performance

The effect of different immersion times on the inhibition performance of an inhibitor is often investigated in corrosion inhibition studies to determine the stability of the inhibitor as well as the time needed for the inhibitor to achieve maximum inhibition performance [197]. In this work, the inhibition efficiency of PA did not change with increasing immersion times from 5-192 h at 20°C and from 5 to 24 h at 40 and 60°C

(**Figures 4-10, 4-12, and 4-13**). This may be attributed to the stable and adherent inhibiting film formed on the MS surface that was impermeable to the corrosive solution. At all the time intervals investigated, the value of the inhibition efficiency was over 99%. This confirmed that PA is highly effective under the time scale investigated in this work. This is consistent with the results of Podobaev and Avdeev [198], who found that the inhibition efficiency of Armco iron in 1 M HCl containing 2 g/L PA did not change markedly (87.3% IE) with increasing immersion time from 5 to 100 min at 60°C. The inhibition efficiency obtained in the present work was higher than that reported by these authors at the same temperature (60°C), and this could be due to higher PA concentration. In addition, Singh et al. [67] reported the effect of immersion time (4 to 24 h) on the inhibition performance of 200 ppm (0.2 g/L) PA in 10wt% HCl at 90°C and found that the inhibition efficiency increased up to 12 h, then remained unchanged throughout the remaining time. The inhibition efficiency of PA after 12 h was 98%. Although their result did not show optimum inhibition at the onset of the experiment, however, it is still consistent with current work as a point of plateau was achieved and the value of the inhibition efficiency was almost the same.

7.2.3 Effect of temperature on PA performance

In corrosion inhibition studies, investigation of the effect of temperature leads to the understanding of the thermal stability of inhibitors, kinetics of the corrosion process and mechanism of inhibition action [155, 199]. The effect of temperature has a complex effect on corrosion inhibition like decomposition, re-arrangement as well as adsorption and desorption of an inhibitor molecule on the MS surface [29, 155]. In this work, the corrosion rate of MS in the uninhibited 15wt% HCl increased with increasing temperature in the range 20 to 60°C (**Table 4-2 and 4-3**). This is attributed to the acceleration of corrosion reactions with increasing temperature, leading to a higher

dissolution of MS and is consistent with the Arrhenius equation (Eqn 7-1) [36, 200, 201].

Tafel polarisation measurements demonstrated that the corrosion current density (i_{corr}) of MS in 15wt%HCl containing 7 g/L PA increased from 0.013 ±0.002 to 0.127±0.029 mA/cm^2 with increasing temperature from 20°C to 60°C (**Table 4-4**). Linear polarisation resistance agrees with Tafel polarisation measurements (**Table 4- 5**). The increase in corrosion rate with increasing temperature may be attributed to the desorption of the PA molecule from the MS surface. The increase in dissolution of MS with increasing temperature is in-line with the results of Jayaperumal et al.[36], who found that the corrosion current density of MS in the presence of PA increased from 0.052 to 1.2 mA/cm^2 with increase increasing temperature from 30 to 105°C. The corrosion current density reported by these authors is higher that of the present work, which implies that PA was less effective with increasing temperature in their work. The higher corrosion current density may be attributed to the higher temperatures studied. Also, Jayaperumal et al. [202] studied the effect of temperature on the inhibition performance of PA for MS in 5wt% HCl in the presence of 1g/L PA at 30 and 90°C. They found that the corrosion current density of MS increased from 0.030 to 0.100 mA/cm^2 with increasing temperature from 30 to 90°C. Although the concentration of the corrosive solution is not the same as that of the present work, these results are still useful in the discussion of the present results as it indicates the behaviour of the corrosion current density of MS in the presence of PA. The percentage increase of the corrosion current density reported in this thesis was about four times higher than that of the authors, which indicates that PA performed better in their work. The difference in the results could be due to a lower concentration of HCl solution (5wt% HCl). Podobaev and Avdeev [198] also reported that the corrosion current

density of Armco iron in 1 M HCl containing 2 g/L PA after 100 mins increased from 0.093 to 0.160 mA/cm^2 with an increase in temperature from 40 to 60°C.

The stable inhibition efficiency of PA (over 99%) with increasing temperature from 20 to 60°C (**Figures 4-4 and 4-5**) indicated the high protective action of PA under the temperature investigated. According to the studies of Poling [68] and of Avdeev and Kuznetsov [63], the excellent, stable and high inhibition performance offered by PA with increasing temperature is due to the insoluble, thermally stable and strong adhering protective film formed at the MS surface.

7.2.4 Surface characterisation of MS treated with PA

SEM (secondary electron mode) was employed to determine the extent of degradation of MS in both the uninhibited and PA-inhibited solutions and validate the formation of a protective film in the presence of PA. The surface of the uninhibited MS revealed a highly corroded surface (~730 mm/y) as shown in **Figure 4-14b**, which indicates that the sample was damaged severely due to the attack of the aggressive solution. The average surface roughness (S_a) value of the uninhibited surface was 6.55±0.90 µm, which further confirmed the extent of MS corrosion. However, the MS surface treated with PA was less degraded (Figure 4-14c). This is confirmed by the corrosion rate of 0.22 mm/y and the average roughness value (S_a) of 1.43 ± 0.04 µm. The less corroded morphology has been attributed to the formation of a protective layer on the MS surface [109, 119, 129].

7.2.5 Corrosion inhibition mechanism of PA

Generally, the primary step in the inhibition of metal corrosion in acidic solutions is attributed to the adsorption of an inhibitor molecule onto the metal surface, followed inhibition of the corrosion process [45]. The corrosion inhibition mechanism of an organic compound in the acidic medium could occur by an electrostatic attraction between a charged inhibitor molecule and a charged metal surface (physical adsorption) and the interaction between unshared electrons of the heteroatoms of the molecule and the metal (chemical adsorption). Also, the availability of pi-electrons in the multiple bonds of an inhibitor could act as the reaction centre for further adsorption to the metal surface, hence enhancing its inhibition performance [203]. The two basic steps before corrosion inhibition are the transport of the organic compound from the electrolyte to the surface of the metal and the interaction of the inhibitor molecule with the metal surface [44]. The adsorption of an inhibitor molecule from an aqueous solution can be regarded as a substitution process between an inhibitor molecule in an aqueous solution and water molecule on a metal surface [36, 204]. The displacement of water molecules from an electrode surface by the organic compound is due to higher lateral energy between the electrode and the organic compound [47].

One of the ways to understand the adsorption mechanism of PA molecule at the MS/solution interface is by the study of the adsorption isotherm models such as Temkin, Frumkin, Freundlich, Langmuir, and Florry-Huggins.

In the current study, the best fit was obtained for the Langmuir adsorption isotherm among other isotherms in the temperature range from 20-60°C (**Figure 5-1)**, which demonstrates that PA formed a thick layer at the metal/solution interface and subsequently mitigating MS corrosion [205].

Generally, values of Gibbs free energy of adsorption (ΔG_{ads}) between -20 kJ/mol and - 40 kJ/mol are attributed to both physical and chemical (mixed-type) adsorption [6, 9, 50, 150]. In this present study, the calculated values of ΔG_{ads} in the presence of PA were - 26.5, -33.9 and -41.0 kJ/mol at 20, 40 and 60°C, respectively (**Table 5-1**), which means PA molecule interacted with the metal surface via both physical (electrostatic attraction) and chemical adsorption (coordinate covalent bond) mechanism [150]. However, it seems that the adsorption mechanism of PA may change to chemisorption at 60°C as the calculated value of the ΔG_{ads} was above - 40 kJ/mol threshold for mixed adsorption mechanism. This is in line with the results of Jayaperumal [36] who reported the ΔG_{ads} values of -25.76 kJ/mol (physical and chemical adsorption) and - 47.19 kJ/mol (chemisorption) for MS in 15wt% HCl solution containing 1 wt% PA at 30°C and 105°C, respectively. Also, it can be seen from Table 5-1 that the values of ΔG_{ads} increased from 26.50 to 41 kJ/mol with increasing temperature from 20 to 60°C. This demonstrated that the adsorption of PA molecules onto MS became more favourable at a higher temperature. In other words, the bond strength between PA and MS increases with increasing temperature.

To further understand the inhibition mechanism for PA-metal surface interaction, the activation energy for MS-treated with PA was determined (**Table 5-2**). The value of E_a for the MS-treated with PA was lower than that of the inhibitor-free system, indicating that the PA interacted with the MS surface predominantly by chemisorption [157, 206- 208]. This type of interaction is usually associated with the formation of a coordinate type of bond, leading to high inhibitive performance. This is consistent with the high inhibition efficiency over 99% obtained in this present work.

It is noted that the equilibrium constant of the adsorption process (K_{ads}) increases with increase in temperature (Table 5-1), which implied that the adsorption strength of the

PA on the MS surface increases with increases temperature and is suggestive of chemisorption. Also, the K_{ads} value of 2500 L/g obtained at 60°C for PA indicates strong adsorption of PA molecules onto the MS surface (chemisorption). This is validated by the high corrosion inhibition efficiency of over 99% for PA. Several authors have attributed higher values of K_{ads} to stronger adsorption of an organic compound onto a metal surface [150].

Based on the thermodynamic parameters and FTIR studies as well as the findings in the literature [51], the mechanism of corrosion inhibition of PA on the MS surface in 15wt% HCl is proposed:

PA is protonated in the acidic medium by the presence of H^+ from the electrolyte and exists in the cationic form (PA^+) in HCl [36, 67]. The chloride ions in the electrolyte are initially adsorbed on the MS surface, hence creating an excess negative charge on the sample surface. Then, the protonated form of the PA molecule interacted with the pre-adsorbed chloride ions at the MS surface resulting in adsorption of physical character [67]. The presence of chloride ions on MS treated with PA is confirmed by EDS and XPS analyses (**Tables 6-1 and 4-6**). This is consistent with the findings of Fiaud et al.[209] who reported the presence of chloride ions on the steel surface treated with PA.

Also, the highly reactive and electron rich π-electrons in the carbon-carbon triple bonds reinforced by the hydroxyl group interacted with the vacant d-orbitals of the iron atom, leading to the formation of a highly protective film on the MS surface [69, 103, 210]. Fontana and Staehle [211] noted that the chemisorption of acetylenic alcohols results in the formation of the metal-acetylenic surface complex. The disappearance of C≡C after reaction of PA with the MS surface is presumably due to the interaction of

the triple bonds of the PA molecules with the MS surface (**Figure 6-6b**) [67, 68, 212]. This is consistent with the findings of Growcock and Lopp [212], who reported that the disappearance of the -C≡C- peak of PA suggests the interaction of PA with the MS surface. Other authors have reported similar results [66, 68, 71, 209, 212-214].

The following equations represent the mechanism of PA on the MS surface:

$$\mathbf{Fe} + \mathbf{H_2O} \rightleftarrows \mathbf{Fe.H_2O_{ads}} \qquad \text{Eqn 7-2}$$

$$\mathbf{Fe.H_2O_{ads}} + \mathbf{Cl^-} \rightleftarrows \mathbf{Fe.Cl^-_{ads}} + \mathbf{H_2O} \qquad \text{Eqn 7-3}$$

$$\mathbf{Fe.Cl^-_{ads}} + \mathbf{PA^+} \longrightarrow \mathbf{FeCl^-_{ads}.PA^+} \qquad \text{Eqn 7-4}$$

In summary, FTIR results indicated that the inhibiting action of PA is due to the inhibiting film composed of FeO, -COOFe, OH, C=C and CH_2 formed at the MS/solution interface (Figure 4-40) which is consistent with the findings of other authors in the literature [29, 40, 63, 67-69, 77, 215, 216]. They reported that this inhibiting film is polymeric, highly insoluble, thermally stable, hydrophobic and highly protective.

XPS results also showed that the Fe detected on the MS surface treated with PA decreased by 97% and the carbon increased by 125% compared to the uninhibited surface (Table 6-1), which is most likely due to the formation of an adsorbed layer on the MS surface. According to Chan-Rosado and Pech-Canul [217], the carbon intensity increased in the presence of an inhibitor compared to the uninhibited sample which has been attributed to the contribution of carbon from the inhibitor. The schematic

representation of the adsorption and inhibition mechanism of PA onto the MS surface is depicted in **Figure 7-1**.

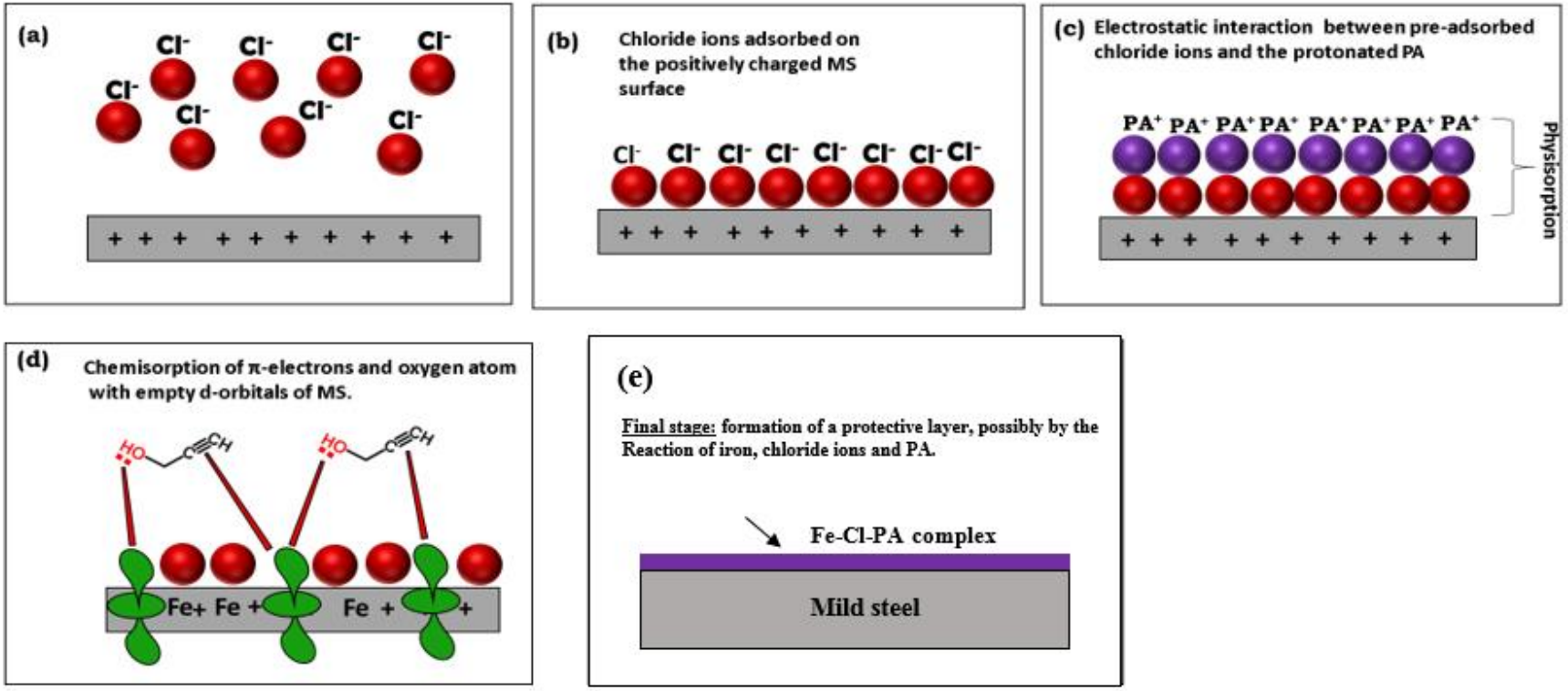


Figure 7-1 Schematic representation of possible corrosion inhibition mechanism for MS in 15wt% HCl solution containing 7 g/L PA: (a) before chloride ions adsorption on MS (b) adsorption of chloride ions on MS surface (c) physisorption of propargyl alcohol on pre-adsorbed chloride ions on MS (d) Chemisorption of triple bond and oxygen atom on MS and (e) film formation by the complex of iron ions, chloride ions with PA.

7.2.6 Summary

The adsorption and inhibition mechanism of MS in the strong, aggressive medium (15wt% HCl) studied in this work is summarised below:

1. PA may inhibit the corrosion of MS in 15wt% HCl by the interaction of its protonated molecules with the positively charged MS surface, which was possibly facilitated by the initially adsorbed chloride ions (physical adsorption); also the pi-electrons of the carbon-carbon triple bonds may interact with the vacant d-orbitals of the iron atoms. This could result in the formation of coordinated covalent bonds (chemical adsorption) at 20 and 40°C, whereas the adsorption inhibition mechanism was mainly chemisorption at 60°C.
2. The adsorbed inhibiting film formed at the MS surface treated with PA is composed of C=C, OH, CH_2, FeO and COOFe species.
3. PA suppressed anodic metal dissolution and retarded cathodic hydrogen evolution reactions with anodic predominance. Hence, PA can be classified as a mixed-type inhibitor.
4. PA is an excellent inhibitor as it maintains its inhibitive action at all the conditions investigated with inhibition efficiency of over 99%.
5. Excellent inhibitive performance of PA (over 99 %) reported in this thesis agrees with the literature, although it should be noted that the concentrations of PA were higher in this study.

7.3 2-Mercaptobenzimidazole (MI)

7.3.1 Effect of MI concentration on MS corrosion inhibition

In the present work, the corrosion rate of MS decreased from 0.171±0.025 (1.91 mm/y) to 0.095±0.010 mg/cm^{2}h (1.06 mm/y) with increasing MI concentration from 1 to 7 g/L at 20°C after 5h as presented in **Table 4-1**. This may be attributed to an increase in the adsorption and greater coverage of MI molecules on the MS surface as the concentration increases, thereby resulting in the formation of more inhibiting film on the electrode surface that acted as an effective barrier against the attack of the corrosive ions from the bulk solution [50, 79, 87-89, 97]. The decrease in corrosion rate with increasing concentration is consistent with the findings of Benabdellah et al.[97] who reported that the corrosion rate of MS in 1 M HCl decreased from 12.86 to 0.29 mm/y with increasing MI concentration from 1.5×10^{-4} to 1.5×10^{-1} g/L at 35°C after 6 h. Also, Morales-Gil et al.[88] reported that the corrosion rate of MS in 1 M HCl decreased from 28 to 0.4 mm/y with increasing MI concentration from 1.5×10^{-4} to 0.3 g/L after 4 h immersion at 25°C. A higher concentration of MI (7 g/L) used in the current study could be due to the stronger HCl solution (5 M HCl).

The corrosion rate of MS did not change with the further increase of MI concentration above 7g/L in the present study. This is attributed to the complete coverage of MI molecules on the MS surface resulting in monolayer formation which is consistent with the findings of Morales-Gil et al.[96] who reported monolayer (one molecule thick) on the MS surface by MI. In other words, the MS surface gets saturated with MI molecules and prevents the ingression of the corrosive solution through the adsorbed protective film.

The possible schematic representation of the increase in adsorption with increasing MI concentration after the displacement of water molecules from the MS surface is presented in **Figure 7-2**.

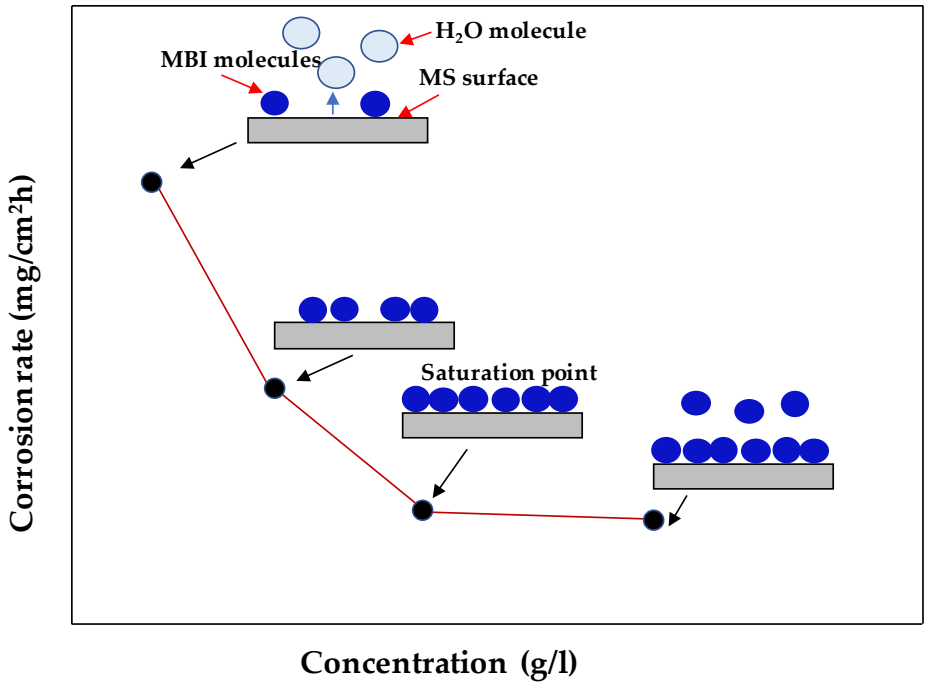


Figure 7-2 possible schematic representation of the effect of concentration on the corrosion rate of MS in 15wt% HCl. The colour and shape in the diagram are not a true representation of MI molecules but are a guide for the eyes.

MI achieved maximum inhibition efficiency of 97±0.4 % at a concentration of 7g/l at 20°C after 5 h of immersion (**Figure 4-2**), which demonstrates that MI effectively inhibited the corrosion of MS in the strong corrosive environment investigated. Interestingly, the excellent inhibitive properties offered by MI in the aggressive solution may be attributed to the interaction of the nitrogen (N) atom of MI with the MS surface

as confirmed by XPS data (Further details about the corrosion inhibition mechanism is discussed in **section 7.3.5**). Other authors have attributed the protective action of MI to the presence of nitrogen and sulphur (S) atoms as well as the pi-electrons in the imidazole and benzene rings which can act as the adsorption centres for binding to the vacant and low energy d-orbitals of MS, hence forming an adsorbed layer against corrosion [218].

The high inhibition efficiency achieved by MI in this present work is consistent with that reported in the literature as shown in **Table 7-2** although the higher concentration of MI is required in the present study because of the stronger corrosive environment (5 M HCl).

Table 7-2 Comparison of the inhibition efficiency of MI obtained in this work with literature.

Inhibitor	Medium	Material	Inhibitor concentration (g/L)	Test conditions	IE (%)	Ref
MI	5 M HCl	MS	1-7	WL at 20°C	93-97%	Present work
MI	1 M HCl	MS	0.30	LPR at 25°C	98%	[88]
MI	0.1 M HCl	MS	0.30	LPR at 25°C	98%	[88]
MI	0.01M HCl	MS	0.30	LPR at 25°C	92%	[88]
MI	1 M HCl	MS	0.25	TP at 25°C	89%	[79]
MI	1 M HCl	API-5L steel	0.20	EIS at 25°C	98%	[90]

Note: WL means weight loss measurements, LPR means linear polarisation resistance and TP= Tafel polarisation measurements.

The formation of a protective inhibiting film by MI on MS surface was confirmed by XPS results (**Table 6-1**) showing the presence of N (6.5 at. %) at the MS surface treated with MI. This validates the interaction of N atom available in MI skeleton ($C_7H_6N_2S$) with the MS surface. Furthermore, the percentage increase (40%) of carbon on the

inhibited surface compared to the uninhibited might be due to the carbon contribution from the MI molecules, and this further supported the adsorption of MI onto the MS surface. These observations are consistent with the findings of Dominguez et al. [219] who reported that increase in the amount of carbon and nitrogen in the presence of MS in the presence of imidazole compared to the uninhibited MS surface was due to the adsorption of this inhibitor (imidazole) on the MS surface. Morale-Gil et al.[88] also reported similar results for the MS treated with MI in 1 M HCl. A detailed description of the inhibition mechanism of MI is discussed in **section 7.3.5** of this thesis.

7.3.2 Effect of immersion time on inhibition performance of MI

As mentioned previously, the influence of time is often investigated in corrosion inhibition studies to determine the stability and adherence of the inhibitor on a metal surface. In the present study, the corrosion inhibition performance of MI was almost unaffected with increasing immersion time from 5 to 192 h at 20°C (**Figure 4-10**). Also, the high inhibition performance of MI was maintained with increasing immersion time from 5 to 24 h at 40 and 60°C (**Figures 4-12 and 4-13**), this indicates that the MI molecules remained on the MS surface throughout the time interval investigated. In other words, the inhibiting film formed on the MS was tightly adsorbed and stable on the MS surface. This is consistent with the results of Espinoza et al. [90] who found that MI maintained an inhibition efficiency of 98% between 3 and 336 h at 20°C for steel in 1 M HCl containing 0.2 g/l MI. Although the authors used a lower acidic solution (1 M HCl), the results still showed that the inhibition efficiency of MI molecules at a metal/solution interface was stable with prolonged immersion times. It is noted that not much work has been done on the effect of immersion time on the inhibition performance of MI in HCl medium.

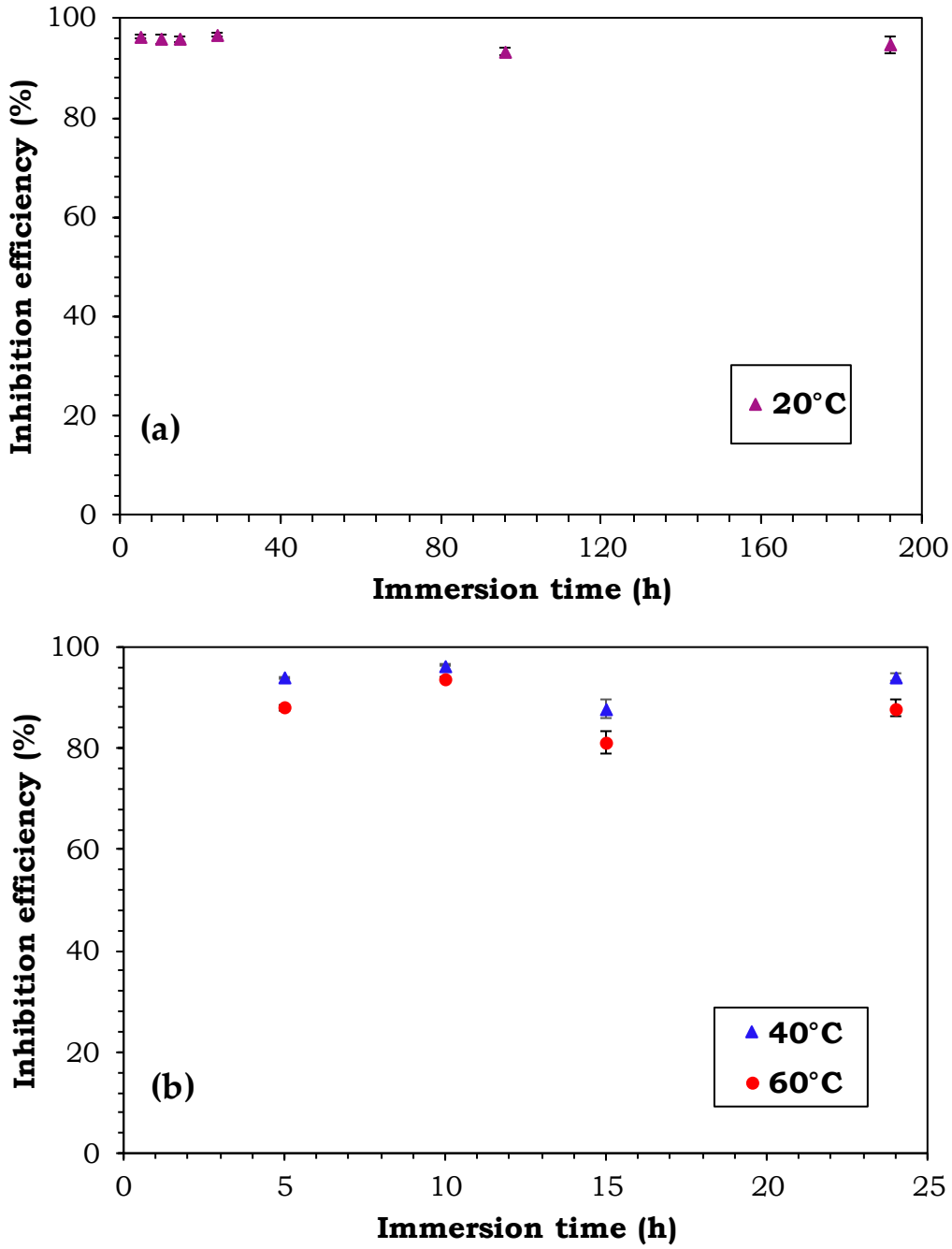


Figure 7-3 Time-dependence of inhibition efficiency of MI for MS in 15wt% HCl solution at (a) 20°C in the time range from 1-192 h and (b) 40 and 60°C in the temperature range from 1-24 h. Error bars represent the standard deviation of three measurements.

7.3.3 Effect of temperature on the inhibition performance of MI

The corrosion rate of MS in the uninhibited solution (15wt% HCl) increased considerably with increase in temperature in the range of 20 to 60°C (Tables 4-2 and 4- 3), indicating that the corrosion reactions (metal dissolution and hydrogen evolution) were accelerated with increasing temperature, and this is in agreement with Arrhenius relation (Eqn 2-1)[155, 157]. A similar increase in the corrosion rate of metals with temperature has been widely reported in the literature for MS in HCl solution [8, 12, 88, 109, 110, 124, 199, 220-222].

Turning to the MI-inhibited solution, the corrosion rate of MS also increased with increasing temperature from 20 to 60°C (**Tables 4-2 and 4-3**), which may be attributed to increased kinetic energy of the system which resulted in the desorption of the MI layer from the sample surface, hence exposing the MS surface to the corrosive solution. In other words, increase in temperature speeds up the thermal movement (diffusion) of MI molecules in the bulk solution, hence weakening the bond between the initially adsorbed MI species and the MS surface, resulting in the desorption of MI protective layer. The decreased adsorption equilibrium constant with increasing temperature (**Table 5-1**) confirmed the desorption of MI molecules from the MS/solution interface.

The increase in corrosion rate with increasing temperature is consistent with the results of Benabdellah et al.[97], who found that the corrosion rate of MS in 1 M HCl containing 0.15 g/L MI increased from 0.026 to 0.521 mg/cm^{2}h with increasing temperature from 35 to 60°C. The corrosion rates obtained in this study (**Tables 4- 2 and 4-3**) are higher than those reported by the authors, which may be attributed to higher HCl concentration and longer immersion time. Other authors have reported increased corrosion rates with increasing temperature for MS in 1 M HCl in the presence of MI [50, 79].

It should be noted that even though the corrosion rate of MS in MI-inhibited solution increased with temperature, the presence of MI significantly decreased the corrosion rate compared to the uninhibited solution at each temperature investigated. For example, the corrosion rate of 48.58 mg/cm^{2}h for MS in uninhibited solution significantly decreased to 5.9 mg/cm^{2}h in the presence of 7 g/L MI after 24 h immersion (this is about 88% decrease) (**Table 4-3**), indicating the corrosion inhibitive effectiveness of MI. The decreased inhibition efficiency of MI with increasing temperature from 20 to 60°C indicates the desorption of MI from the MS surface and is suggestive of the adsorptive inhibitive mechanism of physical (electrostatic) character [79].

It was observed that the inhibition efficiency of MI decreased with increasing temperature from 20 to 60°C (**Figures 4-4 and 4-5**). This is possibly due to the decrease of the strength of the adsorption process of MI onto the MS surface at higher temperatures. In other words, an increase in temperature did not favour MI adsorption onto the MS surface, and this is suggestive of physical adsorption character. MI desorption was validated by the decrease in the value of the adsorption equilibrium constant (K_{ads}) with increasing temperature (**Table 5-1**). Decreased MI inhibition efficiency with an increase in temperature is consistent with the results of Aljourani et al.[79] who found that the inhibition efficiency of MI decreased from 89 to 75 % with increasing solution temperature from 25 to 55°C and they attributed this behaviour to the desorption of MI from the MS surface. Other authors have reported similar results as presented in Table 7-3. As shown in the table, a higher concentration of MI used in this work is compared to that of the previous study. This concentration may be due to the higher HCl solution employed for industrial applications.

It is noted that MI offered a high inhibition efficiency of 88% at 60°C (**Table 7-3**), which indicates that it is an effective inhibitor in the temperature range investigated.

Table 7-3 Comparison of the variation of temperature on the inhibition performance of MI.

Inhibitor	Medium	Material	Inhibitor concentration	Test conditions	IE (%)	Ref
MI	5 M HCl	MS	7 g/l	WL: 20-60°C	97-88%	Present work
MI	1 M HCl	MS	0.75 g/l	WL:35-60°C	96-85%	[97]
MI	1 M HCl	MS	0.25 g/l	TP: 25-55°C	89-75%	[79]
MI	1 M HCl	MS	0.15 g/l	EIS:20-60°C	97-93	[50]

WL means weight loss measurement; EIS means electrochemical impedance spectroscopy and TP means Tafel polarization measurements.

7.3.4 Surface characterisation of MS in the presence of MI

As previously mentioned, the MS surface immersed in the uninhibited solution was severely damaged (corrosion rate of 730 mm/y) with an average surface roughness of 6.55±0.90µm (**Figure 4-14b**), which indicates that the MS surface was attacked severely by the corrosive solution leading to the dissolution of the sample. However, the MS surface immersed in MI-inhibited solution was less corroded (corrosion rate of 90.1 mm/y) as presented in **Figure 4-14d**. The corrosion rate decreased by about 88% in the presence of MI. Also, the average roughness value of the MI-inhibited surface is 2.34 ±0.02 µm, indicating a percentage decrease roughness of about 75%. In other words, a smoother surface morphology was achieved in the presence of MI.

The decreased degradation in the presence of MI can be attributed to the formation of a protective film on the MS surface. This is consistent with the findings of Morales-Gil

et al.[88] who found that a smoother morphology was obtained for MS in 1 M HCl in the presence of 2 mM MI compared to the uninhibited surface.

7.3.5 Corrosion inhibition mechanism of MI

In the present study, the best fit was obtained for Langmuir adsorption isotherm, among all the adsorption isotherms that were graphically fitted to the experimental data temperature range of 20 to 60°C (**Figure 5-1**). This demonstrated that MI interacted with the MS surface by the formation of a monolayer. This is consistent with the findings of Aljourani et al.[79] and Benabdellah et al.[97] who reported that the adsorption of MI onto MS surface in 1 M HCl solution follows Langmuir adsorption isotherm. Also, Langmuir adsorption model has been widely reported in the literature for the adsorption of an inhibitor at a metal/solution interface [8, 12, 87, 140, 146, 150, 168, 189, 223]. Further investigation of MI adsorption mechanism was appraised by the calculation of the Gibbs free energy of adsorption (ΔG_{ads}). Generally, the value of ΔG_{ads} between -20 and – 40 kJ/mol is attributed to both physical and chemical adsorption [8, 12, 223, 224]. In the current study, the calculated values of ΔG_{ads} are -25, -27 and – 18 kJ/mol at 20, 40 and 60°C respectively (**Table 5-1**), which indicates that MI interacted with the MS surface via physical and chemical adsorption at 20 and 40°C, whilst it physically adsorbed onto the MS surface at 60°C. This means adsorption at 60°C occurred solely between the protonated MI and the pre-adsorbed chloride ion on the MS surface. This is in-line with the findings of Aljourani et al.[79] who reported that MI interacted with MS surface in 1 M HCl solution at 25°C by both physical and chemical adsorption. Other authors have reported similar results (**Table 7-4**). Furthermore, Benabdellah et al.[97] reported that the adsorption of MI at 60°C for MS in 1 M HCl was due to both physical and chemical adsorption.

It is noted that the values of ΔG_{ads} increased from 25.31 to 27 kJ/mol with increasing temperature from 20 to 40°C, and subsequently decreased to about 18 kJ/mol at 60°C. This showed that the bond strength between MI molecules and MS increased from 20 to 40°C, and then decreased (i.e., the adsorption became less favourable) at 60°C.

Other proposed adsorption mechanism in the presence of MI is summarised in **Table 7-4**.

Table 7-4 Comparison of the ΔG_{ads} obtained for MI in this work, and that reported in the literature.

System	Temperature (°C)	Metal	ΔG_{ads} (kJ/mol)	Adsorption type	Ref
5 M HCl	20	MS	-25	Physical and chemical	Present work
5M HCl	40	MS	-26	Physical and chemical	Present work
5 M HCl	60	MS	-18	Physical	Present work
1 M HCl	60	MS	-37	Physical and chemical	[97]
1 M HCl	35	MS	-38	Physical and chemical	[97]
1 M HCl	40	MS	-37	Physical and chemical	[97]
1 M HCl	25	MS	-33	Physical and chemical	[79]
1 M HCl	25	MS	-33	Physical and chemical	[87]

The equilibrium adsorption constant (K_{ads}) indicates the adsorption strength of an inhibitor on a metal surface. The decreasing value of K_{ads} 32.47, 29.67 and 0.76 l/g with increasing temperature from 20, 40 and 60°C after 5 h of immersion (**Tables 5-1**) show that increasing temperature resulted in decreased adsorption strength of MI on MS

surface. This phenomenon is corroborated by the decrease of MI inhibition performance from 97 to 88% with an increase in temperature from 20 to 60°C after 5 h (**Figure 4- 3**). which is consistent with the findings of Benabdellah et al. [97] who reported that the value of K_{ads} of MI on MS decreased from 97 to 92% with increasing temperature from 20 to 60°C.

Potentiodynamic polarisation measurements showed that the addition of MI into the electrolyte significantly decreased the anodic and cathodic corrosion current density at each temperature (**Table 4-4**). This demonstrated that the presence of MI suppressed anodic MS dissolution and cathodic hydrogen evolution. Also, the presence of MI shifted the corrosion potential (E_{corr}) to more negative potentials compared to the blank at each temperature. Therefore, MI can be classified as a mixed-type inhibitor with cathodic predominance [79, 88, 97].

XPS data showed the presence of a nitrogen atom (6.5 at. %) at the MS/MI interface, which was undetectable on the uninhibited surface. The presence of this N confirmed that MI bound to the MS surface (**Table 6-1**). This nitrogen atom most likely originates from MI ($C_7H_6N_2S$). The deconvolution of N 1s envelope revealed three peaks. The two peaks at binding energies of 400 eV and 399 eV are due to the two chemically distinct nitrogen atoms of pyrrole and pyridine in MI molecule (**Figure 6-5 and Table 6-4**) [88, 218]. The assignment of the third peak could be due to surface contamination. Sulphur (S) was not detected at the MI/MS interface by XPS, although MI contain S in its molecular structure. Most notably, XPS data confirmed the adsorption of MI onto the MS surface.

The presence of N 1s detected at the inhibited MS/MI interface is consistent with the findings of Morales et al.[88] who found that two distinct nitrogen atoms were detected

at the MS surface treated with MI by XPS. They reported that MI interacted with the MS surface via the nitrogen atoms in the MI ($C_7H_6N_2S$) molecules.

Based on the experimental findings obtained in this work, the corrosion inhibition mechanism of MI/MS interface is discussed below:

MI exists in the molecular as well as cationic form in the acidic solution [225] because it is an organic base that gets protonated by the hydrogen ion (H^+) in the HCl solution as shown in **Figure 7-4** [94]:

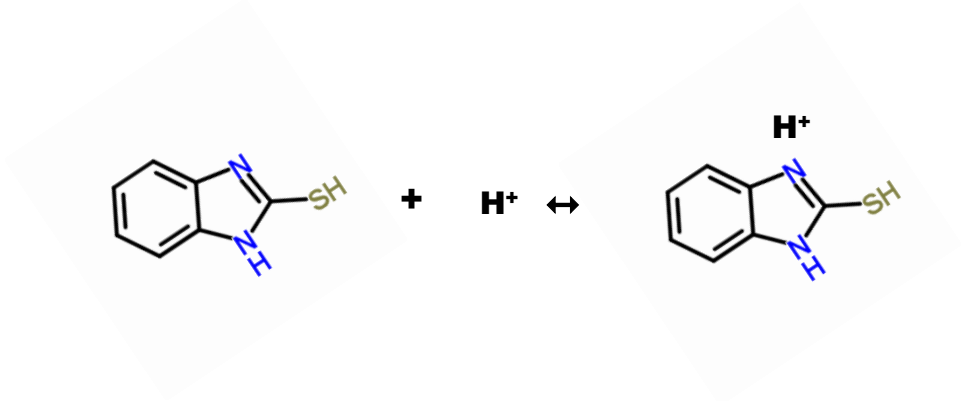


Figure 7-4 Protonation of MI in acidic solution [94].

The hydrogen ion (H^+) anchored on the pyridine nitrogen atom at the 3-position in the molecule and not on the pyrrole nitrogen ring because pyrrole is a weaker base than pyridine. Pyrrole is a weaker base because its nitrogen atom at the 1-position of the molecule is delocalized on all the atoms of the 5-member ring; unlike the pyridine where the lone pair is localized on one atom of the aromatic hexagonal ring (benzene)[94]. The chloride ions in the electrolyte first adsorbed on the oxide/hydroxide film on the MS surface, thereby creating an excess negative charge on the electrode surface [50, 79, 94]. The presence of iron oxide/hydroxide film on the MS surface was confirmed by XPS results (**Table 6-2**). This is in-line with the findings in the literature that the presence of surface oxide facilitates the adsorption of the inhibitor

on a metal surface [166, 226]. The presence of chloride ions on the MS surface treated with MI was confirmed by the XPS results (**Table 6-1**) and EDS data (**Table 4-6**). The protonated MI (MIH^+) interacted with the pre-adsorbed chloride ions due to electrostatic force of attraction (physisorption) [50, 89, 94] (**Figure 7-5a**), followed by the interaction of the unshared electrons of the nitrogen atom of the pyrrole ring of the neutral form of MI with the vacant and low-energy d-orbitals of MS (**Figure 7-5b**).

The schematic representation of both physical and chemical adsorption mechanism of MI on the MS surface is presented in **Figure 7-5**.

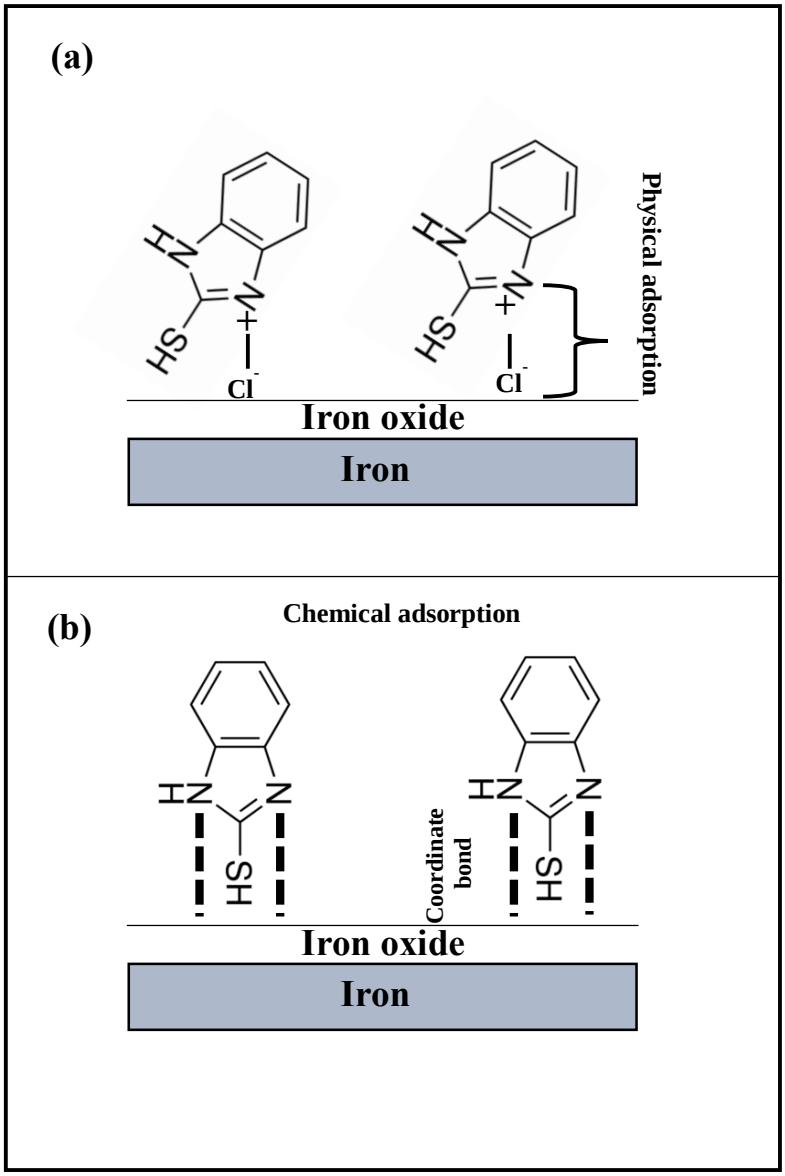


Figure 7-5 Schematic representation of the likely inhibition corrosion mechanism of MS in 15wt% HCl in the presence of MI after 5 h immersion (a) showing interaction of the cationic form of MI and pre-adsorbed chloride ion (b) showing formation of coordinate covalent bond due to the lone pair electrons of N and S atoms. The XPS results showed the formation of iron oxides on the MS surface.

7.3.6 Summary

1. The results obtained in this study were consistent with a mechanism where MS corrosion in the presence of MI at 20 and 40°C could be attributed to the interaction of the protonated MI and the pre-adsorbed chloride ions on the MS surface (physical adsorption), and simultaneously transferring the lone pair electrons available in the nitrogen atom to the vacant d-orbitals of iron.
2. The inhibition of MS corrosion in the presence of MI at 60°C may occur by electrostatic attraction between the pre-adsorbed chloride ions and the MS surface.
3. MI possibly suppressed both the anodic dissolution of MS and cathodic hydrogen evolution (H^+ reduction). Hence, MI can be classified as a mixed-type acidic corrosion inhibitor with cathodic predominance in the conditions investigated.
4. It is possible that MI is as an effective inhibitor against MS corrosion with a variation of the environmental factors (solution temperature and immersion time).
5. XPS results confirmed the adsorption of MI onto the surface oxide of MS (FeOOH and Fe_2O_3) through the two-chemical distinct nitrogen in the MI molecular structure.

7.4 Inulin (IN)

7.4.1 Effect of concentration on IN performance

The corrosion rate of MS decreases, and the inhibition efficiency increases with increasing concentration of inulin (IN) up to 10 g/l at 20°C after 5 h immersion (**Table 4-1 and Figure 4-2**). In other words, the corrosion inhibition performance was enhanced with an increase in IN concentration in the bulk solution. This may be attributed to increase in the adsorption and surface coverage of IN molecules at the MS/HCl solution interface, thereby forming a more protective film which prevents the diffusion of the corrosive solution to the MS surface [53, 115, 121, 171, 227-230]. This is consistent with the results of Choudhary et al. [15] who found that the corrosion rate of N 80 steel decreased from 6.92 to 2.44 mg/cm^{2}h and the inhibition efficiency increased from 55 to 84% with increase in IN concentration from 3.6 g/L to 10 g/L after 6 h immersion at 65°C.

It is noted that further increase in IN concentration beyond 10 g/L, yield little or no change of the inhibition efficiency (80±0.5%) and corrosion rate (0.551±0.023 mg/cm^{2}h). This is probably due to the saturation of the MS surface with IN molecules. The optimum inhibition efficiency achieved by IN in this work is consistent many results, including the findings of Osman and Shalaby [231] and Ji et al. [123], who found that some plant extracts achieved optimum inhibition performance, and they attributed this phenomenon to the complete coverage of the inhibitors onto the metal surface. Other authors have also reported optimum inhibition performance for different plant extracts as shown in **Table 7-5**. A higher concentration of inulin used in this work compared to other authors can be attributed to higher HCl concentration.

Table 7-5 Comparison of inhibition efficiency of IN in this work with previous studies.

Inhibitor	Medium	Material	Inhibitor concentration (g/L)	Temp (°C)	IE (%)	Reference
IN	5 M HCl	MS	10-11	20	79.6-79.1	Present work
IN	5 M HCl	N80 steel	3.6	65	55	[15]
IN	5 M HCl	N80 steel	10	65	84	[15]

Conc- concentration, Temp – temperature and IE- inhibition efficiency.

The confirmation of a protective film on the MS surface is in line with XPS results showing a decreased amount of iron (11.2%) on the IN-treated MS surface compared to the uninhibited MS (23.5%) (**Table 6-1**). Furthermore, the amount of carbon detected on the inulin-inhibited surface increased by 34% compared to the uninhibited MS surface. This could be due to the contribution of the carbon from inulin (**Figure 6-1 and Table 6-1**). These observations validated the formation of a protective layer on the MS surface with the addition of IN into the acidic test solution. A detailed explanation of the inhibition mechanism of MS corrosion by IN molecules is discussed in **section 7.4.5.**

The schematic diagram presented in **Figure 7-6 (a)** shows the initial stage of IN molecules adsorption at MS/solution interface after its addition into 15wt% HCl solution. Further increase in the concentration of IN molecules as presented in **Figure 7-6 (b)** results in the adsorption of more IN species on the MS surface, thereby enhancing its corrosion inhibition performance. Furthermore, increasing the concentration beyond the optimum concentration has little or no influence on the protective ability of inulin molecules as shown in **Figure 7-6(c)**.

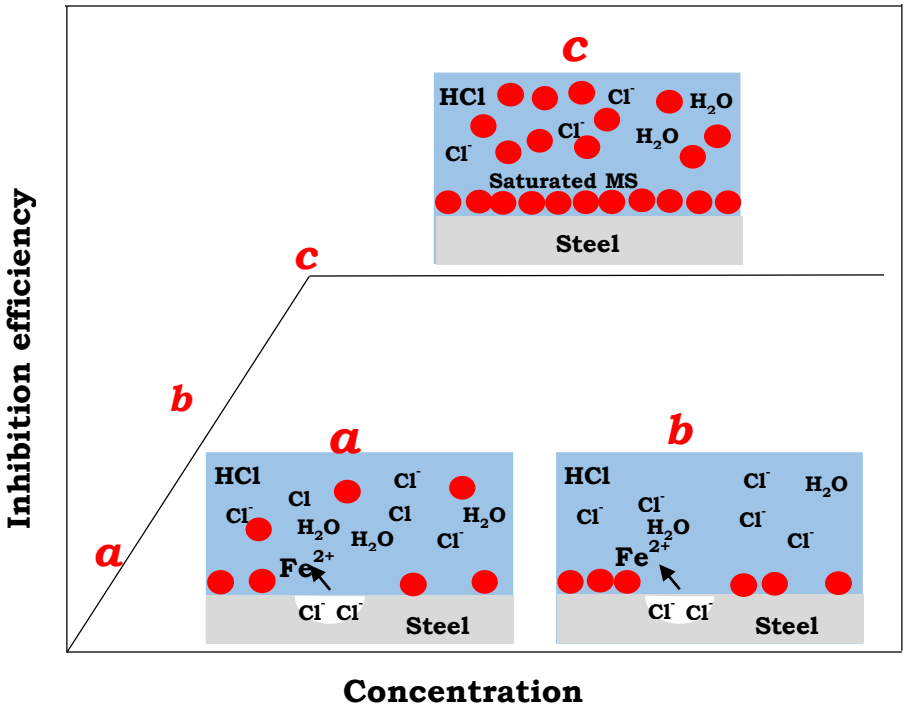


Figure 7-6 Possible schematic representation of the effect of inulin concentration on corrosion inhibition performance: (a) Initial stage of inulin adsorption at MS-solution interface; (b) more inulin adsorption with an increasing concentration on MS surface (c) saturated MS/solution interface at an optimum concentration of inulin. Red circles represent inhibitor molecules.

7.4.2 Effect of immersion time on inulin performance

The corrosion inhibition performance of IN was almost unaffected with increasing immersion times over the range of 5 – 192 h and 5-24 h at 20 and 40°C respectively (**Figures 4-10 and 4-12**), indicating that the adsorbed protective layer was stable on MS surface after displacement of water molecules [7, 62, 189]. This is consistent with the work of Haque et al.[232] who reported that the inhibition efficiency of chitosan (polysaccharide) remained unchanged with increasing immersion time from 12 -30 h for MS in HCl solution.

On the other hand, the corrosion inhibition performance of inulin significantly decreased after 15 h of immersion at 60°C (**Figure 4-13**). This may be attributed to the

hydrolysis of inulin molecules at MS-solution interface, thereby exposing a greater area of the MS to the corrosive solution [197, 233]. This is an agreement with the results obtained by Roy et al.[160], who found that the inhibition efficiency of guar gum (polysaccharide) increases quickly and attains a maximum of 93% after 5h and then decreased drastically. They attributed the decreased behaviour to the hydrolysis of this inhibitor.

7.4.3 Effect of temperature on IN performance

The corrosion rate of MS in the uninhibited and inhibited HCl solutions significantly increased with increasing temperature from 20 to 60°C (**Tables 4-2 and 4-3)**, this behaviour agrees with Arrhenius relation (Eqn 7-1). However, IN decreased the corrosion of MS compared to the uninhibited sample at each temperature studied. This is consistent with previous work [8, 200, 228].

The inhibition efficiency of IN significantly decreased with increase in temperature between 40°C and 60°C after 24 h of immersion (Figure 4-5), this may be attributed to the degradation of IN molecules [79, 222, 234-236]. Similar decreased corrosion inhibition performance with an increase in temperature has been reported by several authors [8, 50, 128, 171, 223, 237, 238].

Degradation tests of IN molecules carried out in this work showed that the inhibition efficiency of MS in 15wt% HCl solution containing IN heated to 60°C for 24 h before weight loss measurements were lower (42.1±2.2%) than that in an unheated inulin-HCl solution (78.2±0.9%), which indicated that inulin degraded at 60°C. Also, a change in the colour of the heated IN-HCl solution provides indirect evidence for its degradation (Figure 7-7). In other words, the increase in temperature caused an irreversible change of IN and not thermally activated desorption.

This is consistent with the findings of Glibowski and Bukowska [239] who reported that increasing the temperature of IN added to a strong acidic environment (pH 1-3) from 40 to 100°C resulted in a significant increase in the amount of inulin's reducing sugar, indicating an increase in its degradation.

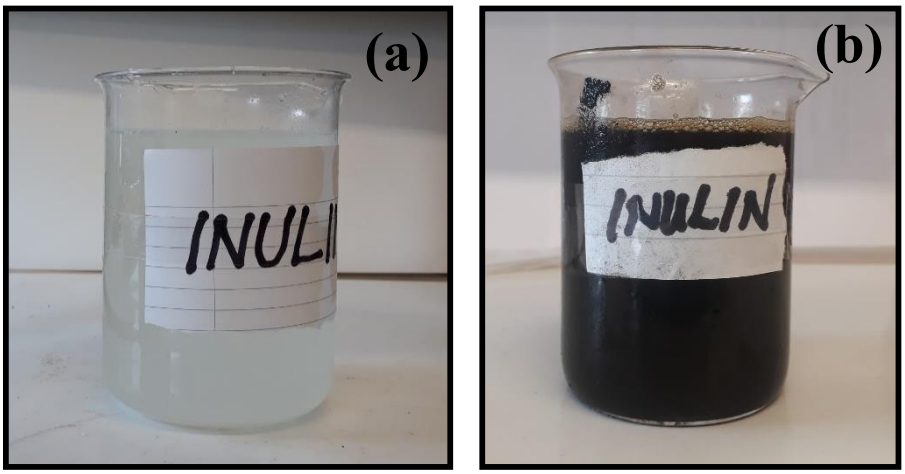


Figure 7-7 Inulin-HCl solution (a) before degradation (b) after the weight loss test at 60°C for 24 h showing a change in colour which could be due to degradation.

On the other hand, the inhibition efficiency of inulin increased with increase in temperature between 20 and 40°C after 5 and 24 h immersion (Figures 4-4 and 4-5). This demonstrated that the adsorption of IN at the conditions is favoured at 20 and 40°C. This is consistent with the results of Torres et al. [127] who found that the inhibition efficiency of 400 mg/l coffee ground extract increased from 76 to 91% with an increase in temperature from 25 to 55°C.

7.4.4 Surface characterisation of MS surface in the presence of IN

The surface morphology of MS immersed in uninhibited 15wt% HCl solution at 60°C after 5 h of immersion exhibits a rough and highly corroded surface (**Figure 4-14b**) with an average surface roughness of 6.55±0.90µm (**Table 4-7**). Also, the corrosion rate of the uninhibited substrate was 730 mm/y. This indicates that the substrate was severely attacked by the corrosive ions in the electrolyte, resulting in the MS dissolution. The 3D profile of the uninhibited surface showed a rough surface (**Figure 4-15b**), which further confirmed the attack of the corrosive ions in the solution. However, the MS surface treated with inulin revealed a less corroded surface (**Figure 4-14e**), with a surface roughness of 2.00±0.02 µm, demonstrating the MS corrosion was inhibited (88 mm/y). The less corroded surface in the presence of IN may be attributed to the formation of a protective layer on the MS surface [6, 113]. The formation of an adsorbed layer on the MS surface is consistent with XPS data showing 52% decrease of the Fe detected at the inulin inhibited MS surface compared to the uninhibited (**Table 6-1**). Furthermore, a higher amount of carbon observed on the inhibited surface compared to the uninhibited could be due to the adsorption of inulin on the MS surface (**Table 6-1**). This is consistent with the findings of Olivares-Xometal et al.[240] who reported that a higher amount of carbon detected on steel treated with amide inhibitor was due to the carbon atoms present in this compound. EDS showed that the chloride ions decreased in the presence of inulin. This also confirmed the overlay of MS by the inhibitive film. Therefore, the characterization results demonstrated that a barrier layer was formed on the MS surface in the presence of inulin, which decreases the diffusion of the corrosive ions in the electrolyte.

7.4.5 Corrosion inhibition mechanism of IN

Generally, the adsorption of an inhibitor molecule at a metal/solution interface occurs after the displacement of water molecules from a metal surface [8, 47, 241-243]. The interaction energy between an inhibitor molecule and the surface of the metal is higher than that between water molecules and the surface of the metal, and that is the reason for adsorption of inhibitor molecules [47]. The higher the interaction energy, the greater the extent of adsorption. In theory, the adsorption of organic inhibitor molecules at a metal-solution interface may occur in one or more of the following ways:

1. Electrostatic interaction between the protonated inhibitor molecules and the charged metal surface (physical adsorption).
2. Interaction of the unshared lone pair electrons of heteroatoms (P, N, S or O) with a metal surface (chemical adsorption).
3. Interaction of π-electrons in the multiple bonds or aromatic rings with a metal surface (chemical adsorption).
4. A combination effect of 1-3 [228, 244].

The adsorption of inulin on MS surface obeys the Langmuir isotherm, indicating that inulin molecules inhibited the corrosion of MS by the formation of a monolayer (one molecule thick) [245], hence preventing the diffusion of aggressive ions to the MS surface [8]. Also, the monolayer adsorption is formed because the metal (adsorbent) surface has a fixed number of active adsorption sites that can only accommodate one adsorbed species (adsorbate), and once these sites are occupied, there will not be further adsorption on the metal surface [237]. This finding is consistent with the results obtained by Azzaoui et al.[8] who found that the adsorption of gum arabic (polymer) on MS in 1 M HCl follows Langmuir adsorption isotherm. Several authors have also reported that the adsorption of plant-based materials on a metal surface follows

Langmuir adsorption isotherm [6, 109, 113]. The adsorption mechanism was further investigated by Gibbs free adsorption energy (ΔG_{ads}), which gives useful information about the interaction of an inhibitor on a metal surface [6]. Generally, values of ΔG_{ads} between -20 kJ/mol and -40 kJ/mol are suggestive of both physisorption and chemisorption [8, 150, 246]. In this work, the values of ΔG_{ads} for inulin between -18 kJ/mol to -21 kJ/mol (Table 5-1) over the temperature range from 20 to 60°C indicates that the adsorption of IN molecules occurred via an electrostatic interaction between the IN molecule and the charged MS surface, known as physisorption [12, 145]. Furthermore, a decrease in the value of Gibbs free energy of adsorption with an increase in temperature suggests physical adsorption between inulin and the MS surface [171]. A physical adsorption mechanism was further confirmed by higher apparent activation energy (71.7±2.5 kJ/mol) obtained for MS in 15wt% HCl in the presence of 10 g/l inulin than the uninhibited sample (61.9±0.1 kJ/mol) (Table 5-2). The addition of IN into the acidic test solution increased the energy barrier of the corrosion process [8, 247].

Several authors have also reported similar increased E_a results for plant extracts as shown in **Table 7-7**.

Table 7-7 Apparent activation energy values and adsorption mechanism obtained in the present work and those reported in the literature.

Inhibitor	Test solution	Ea uninhibited (kJ/mol)	Ea inhibited (kJ/mol)	Adsorption mode	Ref
Inulin	5 M HCl	61.9 ± 0.1	71.7± 2.5	Physical adsorption	Present work
Zenthoxylum plant	5 M HCl	43.07	69.47	Physical adsorption	[109]
Zenthoxylum plant	1.6 M	43.07	69.76	Physical adsorption	[109]
Henna extract	1 M HCl	27.06	77.48	Physical adsorption	[12]
Mange peel	1 M HCl	51.5	65.8	Physical adsorption	[154]
Orange peel	1 M HCl	51.5	74.9	Physical adsorption	[154]
Passion fruit	1 M HCl	51.5	63.9	Physical adsorption	[154]
Cashew peel	1 M HCl	51.5	75.5	Physical adsorption	[154]

Tafel polarization results showed that the polarization curves of MS in 15wt% HCl in the presence of IN were shifted to lower corrosion current density at 20, 40 and 60°C after 1 h OCP (Figure 4-9 and Table 4-4), which indicates that the anodic and cathodic processes which were retarded after the addition of inulin to the corrosive medium. Consequently, IN can be classified as a mixed-type inhibitor in 15wt% HCl solution at all the temperature studied.

Table 5-1 showed that the values of ΔG_{ads} increased -17kJ/mol to 21 kJ/mol with increasing temperature from 20 to 60°C, demonstrating that the bond strength between IN and MS increases with increasing temperature.

Based on the previously discussed results of Gibbs free energy of adsorption and apparent activation energy, the adsorption mechanism of IN molecules at the interface of MS-solution is hypothesized:

In a strong acidic solution, inulin becomes protonated and forms its hydrochlorides [248]. Then, the hydrated chloride ions in the bulk solution are adsorbed on the positively charged MS surface as shown in Figure 7-8b via electrostatic attraction.

The MS surface has been reported to be positively charged in 15wt% HCl solution [55]. Consequently, this process changes the charge towards the solution from positive to negative [9, 145]. EDS data confirmed the adsorption of chloride ions on the metal surface (Table 4-6). Inulin has been reported to protonate in strong acids [248]. The protonated inulin molecules (INH^+) then adsorbed onto the MS surface via electrostatic interaction as shown in Figure 7-8(c) [249, 250]. This type of adsorption mechanism is known as physical adsorption.

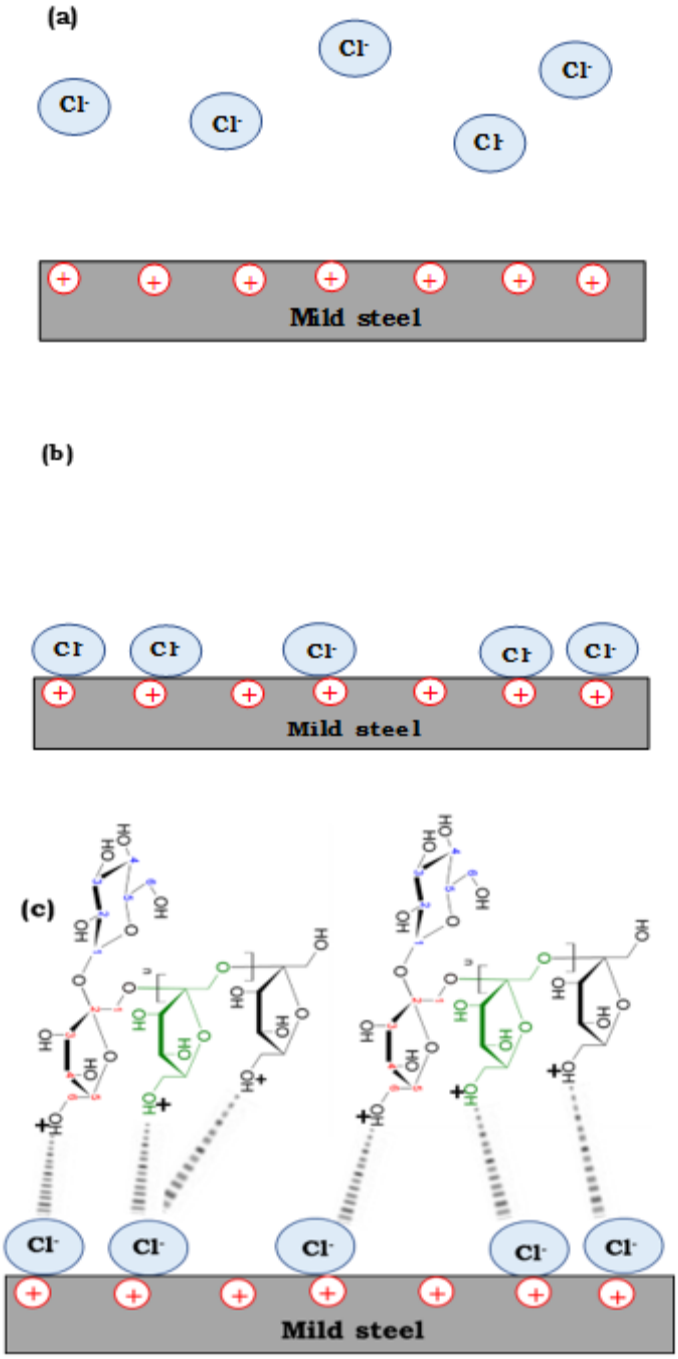


Figure 7-8 Schematic illustration of possible physical adsorption mechanism: (a) Before chloride ion adsorption on the MS surface (b) after chloride adsorption on positively charged MS surface and (c). Adsorption of protonated inulin on the chloride-MS surface [251].

7.4.6 Summary

The mechanism by which inulin acts as a corrosion inhibition can be summarized as follows:

1. The corrosion inhibition of MS in 15 wt% HCl may occur by the electrostatic attraction (Van der Waals forces) between the protonated form of inulin and the pre-adsorbed chloride ions on the MS surface, which forms a protective layer against the attack of the corrosive medium.
2. Inulin compound can be classified as a mixed-type inhibitor as it retarded both anodic and cathodic reactions. However, the cathodic reaction was predominant at 20, and 60°C while the anodic reaction was predominant at 40°C.
3. Increasing the solution temperature caused degradation of inulin and not thermally activated desorption.
4. The corrosion inhibition behaviour of IN agrees with other plant extracts in literature as a monolayer was formed on the MS surface.

7.5 Durum wheat extract

7.5.1 Effect of concentration on durum wheat extract performance

The corrosion rate of MS decreased from 0.351 mg/cm^{2}h (3.92 mm/y) to 0.065 mg/cm^{2}h (0.78 mm/y) with increase in durum wheat extract (DW) concentration from 1 to 7 g/L at 20°C after 5 h immersion (**Table 4-1**). The decrease in corrosion rate may be attributed to an increase in the adsorption and surface coverage of DW on the MS surface [171, 221]. In other words, increasing concentration of DW resulted in the adsorption of more DW onto the electrode surface, thereby isolating the electrode from the corrosive ions and subsequently decreasing metal dissolution. The corrosion inhibition performance of DW has not been reported in the literature.

Similar results of decreasing corrosion rate in the presence of an increasing concentration of plant extracts have been reported by other authors for MS in HCl solution as summarised in **Table 7-8**. The higher corrosion rate of MS reported by these authors compared to the current work may be due to higher solution temperature investigated. It is noted that most of the corrosion inhibition studies by plant extracts were done using low concentrations of HCl solution.

Table 7-8 Comparison of the corrosion rate of the present work with plant corrosion inhibition reported for MS in HCl solution.

Inhibitor	Medium	Material	Conc. (g/L)	Test conditions	CR (mm/y)	Ref
DW	5 M HCl	MS	1-7.0	WL at 20°C	3.92-0.78	Present work
Zenthoxylum alatum	5 M HCl	MS	0.5-3.0	WL at 30°C	15.96-3.99	[109]
Ferula assa-foetida	2 M HCl	MS	0.2-0.8	WL at 30°C	33.29-1.23	[115]
Gum arabic	1 M HCl	MS	0.13-1.0	WL at 30°C	9.16-0.45	[8]

***NOTE**: WL means weight loss measurements*

Further increase in DW concentration above 7 g/L in this work did not affect the corrosion rate of MS markedly, which may be attributed to the saturation of the MS surface with DW.

DW extract achieved a maximum inhibition efficiency of 97±0.3% at a concentration of 7g/L in the strong HCl solution investigated. The high inhibition efficiency offered by DW may be due to the strong interaction between the unshared electrons of nitrogen and oxygen atoms as well as the pi-electrons in the double bonds of the carbonyl group with the low energy d-orbital of the iron atom (Figure 4-25). A detailed explanation of the inhibition mechanism of MS corrosion in the presence of DW is discussed in **section 7.5.5**

7.5.2 Effect of immersion time on DW performance

The influence of immersion time on inhibition performance is usually investigated in corrosion studies to determine the time needed for an inhibitor to reach optimum inhibition efficiency as well as the stability of an inhibitor. In this work, the corrosion rate of MS in DW-inhibited solution at 20°C increased with increasing immersion time up to 15 h and then plateaus from 24 to 192 h (Figure 7-9), which implies that DW formed a stable and adherent protective film at the MS/solution interface after 24 h.

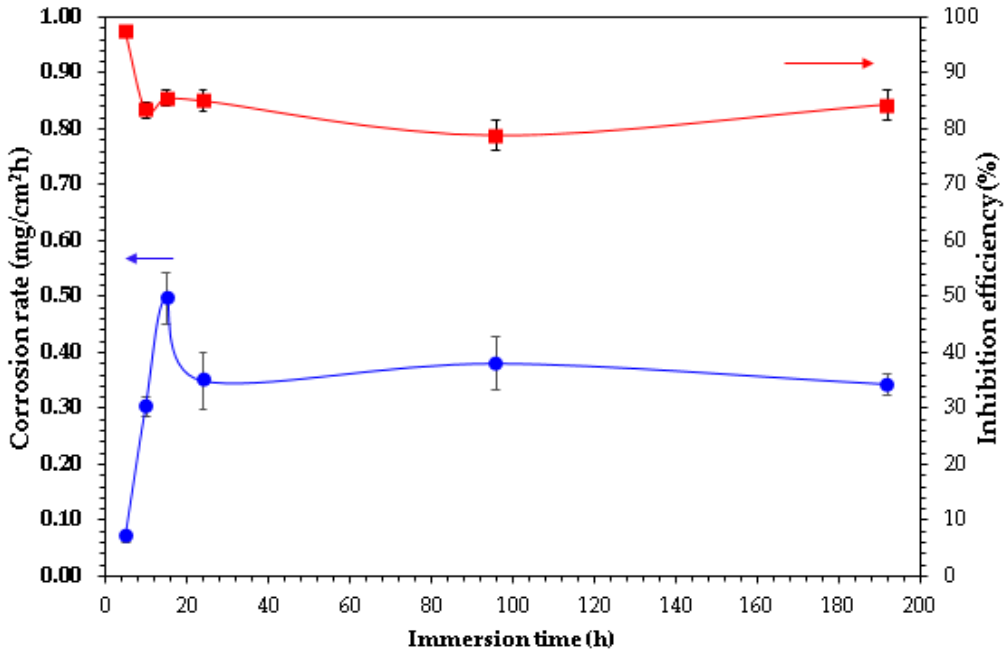


Figure 7-9 Dependence of corrosion rate and inhibition efficiency on immersion time for MS in 15wt% HCl containing 7g/l DW at 20°C.

There is no significant change in the inhibition efficiency of DW between 10 and 192 h immersion, (Figure 4-10). This indicates that the protective layer formed on the MS surface in the presence of DW extract was stable and persistent for long immersion time. This prevented the ingression of the corrosive solution to the adsorbed film [252].

The extract of DW achieved maximum inhibition efficiency of 97±0.3% (Figure 4-10), 91±3% (Figure 4-12) and 88±0.4% (Figure 4-13) after 5 h immersion at 20, 40 and 60°C respectively. Also, the inhibition efficiency of DW was still high after prolonged immersion times. Hence, the extract of DW may act as a good corrosion inhibitor for the acidizing treatment of oil wells and other industrial applications.

7.5.3 Effect of temperature on the inhibition performance of DW

Weight loss measurements showed that the corrosion rate of MS in both uninhibited and DW-inhibited solutions increases with increasing temperature over the range 20°C to 60°C (Tables 4-2 and 4-3). This is due to the acceleration of MS corrosion with increasing temperature and is consistent with the Arrhenius equation (Eqn 7-1). In other words, the increase in temperature enhances the dissolution of MS in HCl solution. This is consistent with the result obtained by Chauhan and Gunasekaran [109] who found that the corrosion rate of MS in 15wt% HCl solution increases with an increase in temperature from 30 to 80°C.

The corrosion rate of MS in the presence of DW significantly decreased at each temperature investigated compared to that of the uninhibited sample (**Tables 4-2 and 4-3**), which is possibly due to the formation of a protective film on the MS surface.

The inhibition efficiency of DW extract decreases with increasing solution temperature from 20 to 60°C after 5 and 24 h immersion (**Figures 4-4 and 4-5**). This is possibly due to the degradation of DW. The degradation of DW was confirmed by higher corrosion rate of MS (20.22 mm/y) immersed in DW/HCl solution heated to 60°C compared to the unheated solution (3.91 mm/y), demonstrating that DW degraded at elevated temperature. Also, the change in the colour of the heated extract of DW solution may be due to its degradation (**Figure 7-10**). Consequently, a decrease in the inhibition performance of DW extract with temperature may be attributed to degradation.

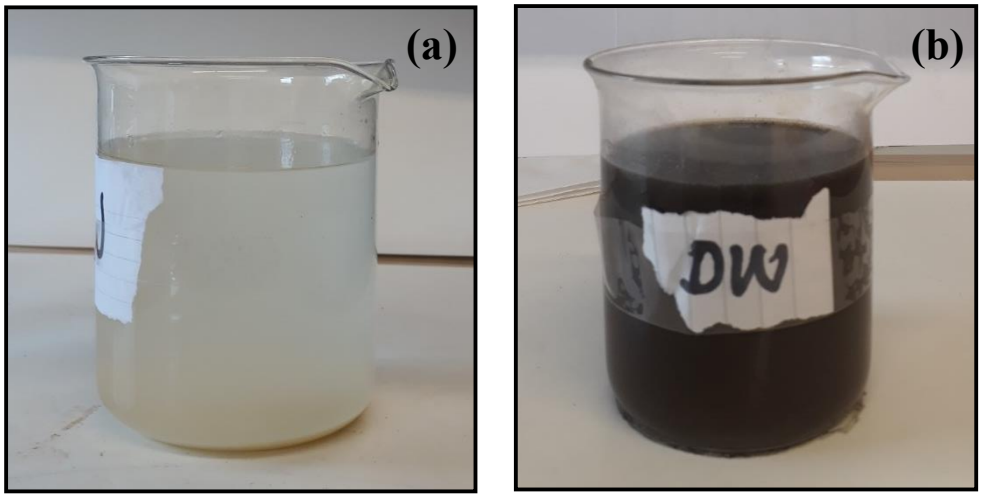


Figure 7-10 DW-HCl solution (a) before heating (b) after heating to 60°C for 24 h.

This is consistent with the results obtained for plant extracts by Ren et al.[229], who found that that the inhibition efficiency of lignin decreased from 97 to 85% as the temperature increased from 25 to 80°C for MS in 10wt% HCl. They attributed the decrease in inhibition efficiency with an increase in temperature to the degradation of lignin on the MS surface. This is in-line with the report of Chauhan and Gunasekaran[109], who found that the inhibition efficiency of Zanthoxylum alatum plant decreased from 98 to 46% as the temperature increased from 30 to 80°C for MS in 15wt% HCl. They attributed the decrease in inhibition efficiency with temperature to the degradation of the extract with increasing temperature.

Despite decreasing inhibition efficiency of DW with temperature, it is noted that at the highest temperature (60°C) and long immersion time (24 h) investigated in this research, DW extracts still achieved 78% protection.

7.5.4 Surface characterisation of MS surface in the presence of DW extracts

The MS surface immersed in uninhibited 15wt% HCl solution at 60°C after 5 h was corroded severely and rough with a corrosion rate of 730 mm/y (Figure 4-14b), which demonstrated that the corrosive solution highly attacked the sample. The presence of the high amount of chloride ions (4.4 %) was confirmed by EDS data revealing the high amount of chloride ions (4.4%) at the uninhibited surface (Table 4- 6). Also, the roughness of the uninhibited sample surface was 6.55±0.90µm (Table 4-7), which further indicated the extent of the MS corrosion. However, the MS surface in 15wt% HCl in the presence of DW was less corroded (Figure 4-14 e) with a corrosion rate of 92 mm/ y. In other words, the decrease of the corrosion rate was about 87%, indicating that the surface was protected from the attack of the corrosive solution, which is most likely due to the formation of a protective layer. XPS results confirmed the formation of an inhibitive film by the presence of nitrogen signal (5.8 at. %) at the MS surface treated with DW (Table 6-1) that was not present on the MS surface exposed to the uninhibited HCl solution, demonstrating that the nitrogen in DW interacted with the MS surface. Also, an increase of carbon signal at the MS surface treated with DW (49.7 at. %) compared to the uninhibited surface (34.5 at. %) could be due to an overlay material formed by DW. It is also noted that the Fe signal was suppressed at the inhibited MS surface, which may be due to the adsorbed layer (Table 6-1). The roughness value of DW-inhibited surface was lower (2.55±0.06 µm) than the uninhibited surface (6.55±0.9 µm) (Table 4-7) which further confirmed the protection of the MS surface against corrosion. Consequently, it can be deduced that the presence of DW extracts in the bulk electrolyte preserve the MS against corrosion by the formation of a protective layer. This is consistent with the widely reported findings that

smoother and less corroded surface morphology is due to the formation of a protective film by an inhibitor [8, 12, 109, 154, 171].

7.5.5 Corrosion inhibition mechanism of DW extracts

As already discussed before in this thesis, the corrosion inhibition mechanism provides a deeper understanding of the interaction between an inhibitor molecule and the electrode/electrolyte interface. The inhibition of metal corrosion occurred by a displacement-adsorption phenomenon that occurred by the displacement of the preadsorbed water molecules from the metal surface and adsorption by an organic molecule [47]. Some of the parameters for evaluating the corrosion inhibition mechanism are apparent activation energy (E_a), Gibbs free energy of adsorption (ΔG_{ads}), equilibrium adsorption constant (K_{ads}), among others. In this work, higher value of activation energy (Ea) of MS in the presence of DW (70.3±2.5 kJ/mol) than that of the uninhibited MS (62.1±0.1 kJ/mol) presented in Table 4-12 indicate that the addition of DW extract into the bulk solution increased the energy barrier to the corrosion process [8, 253], thereby decreasing the dissolution of MS.

Higher Ea in the presence of DW also suggests that the interaction between DW constituents and the MS/solution interface may occur via a physical adsorption mechanism [112, 147, 223, 253, 254]. This is consistent with the results obtained by Azzaoui et al.[8] who found that E_a of MS in HCl solution containing 1 g/L gum arabic (98.04 kJ/mol) was higher than MS in uninhibited solution (66.24 kJ/mol). They reported that the addition of gum arabic into the bulk solution increased the energy barrier of the electrochemical corrosion process and that the interaction is of physical nature. Other results confirming the increase of E_a in the presence of plant extracts reported by different authors are listed in Table 7-9.

Table 7-9 Comparison of the activation energy for DW and other green inhibitors in HCl medium.

System	Inhibitor.	Metal	Ea (uninhibited) kJ/mol	E_a (inhibited) kJ/mol	Temp	Ref
5 M HCl	DW extracts	MS	62.1	70.3	20-60	Present work
1 M HCl	Henna extracts	MS	27.06	77.48	25-80	[12]
1 M HCl	Gum arabic extracts	MS	66.24	98.04	30-60	[8]
5 M HCl	Zethoxylum plant	MS	48.0	69.5	30-80	[109]
1 M	Geisospernum plant	Carbon steel	25.0	40.88	25-55	[119]
1 M HCl	Mango peel	Steel	51.5	65.8	25-60	[154]

To further confirm the adsorption inhibition mechanism of DW extracts, the Gibbs free energy of adsorption (ΔG_{ads}) was calculated. Generally, the values of ΔG_{ads} of an organic compound in the range of -20 kJ/mol and -40 kJ/mol are attributed to both physical and chemical adsorption [6]. In this present work, the values of ΔG_{ads} for DW was between – 22 kJ/mol to – 24 kJ/mol from 20 to 60°C (Table 5-1), which means that DW inhibited the corrosion of MS by both physical and chemical adsorptions. Physical adsorption possibly occurs through the interaction of the cationic form of DW after protonation in the strong acid medium with the pre-adsorbed chloride ions at the MS surface. On the other hand, chemical adsorption may co-occur via the transfer of the unshared electrons in N and O atoms as well as the pi-electrons in the DW constituents with the vacant d-orbital of the MS. The presence of N and O atoms in DW was confirmed by FTIR results (Figure 5-6). Szklarska-Smialowska [195] noted that the presence of a functional group with the elements of the V or VI groups of the periodic table with lone pair of electrons causes the formation of a stronger coordinated bond (chemical adsorption).

The anodic and cathodic corrosion current densities significantly decrease in the presence of DW extracts (Table 4-4). This implies that the introduction of the extracts of DW into the test solution retarded both the anodic dissolution of MS and cathodic hydrogen evolution at all the investigated temperatures. Therefore, DW extracts can be classified as a mixed-type inhibitor.

XPS deconvoluted spectra of the N 1s signal detected on the MS surface treated with DW (Figure 6-1) further revealed that nitrogen atom of DW was bonded to the steel surface (N-Fe) at a binding energy of 400 eV [147, 255, 256]. Also, a higher amount of carbon on DW-inhibited MS (49.7 at. %) compared to the uninhibited surface (34.5 at. %) (Table 6-1) may be due to the contribution of the carbon in the DW, hence forming an overlying carbonaceous film against MS corrosion. This is in agreement with the result obtained by Prakashaiah et al.[257] who reported a higher amount of carbon in the presence of thiosemicarbazide treated sample surface than the uninhibited surface.

Gas chromatography and mass spectrometry (GC-MS) was employed to determine the components in DW extracts. GC-MS results showed that the two most abundant compounds in DW extracts are linoleic acid (72%) and palmitic acid (27%) as presented in Table 5-6. The corrosion inhibition of metals in the presence of palmitic and linoleic acid has not been reported in the literature. Therefore, an assumption is made about the active constituents that are likely to form stronger adsorption on the MS surface based on the number of their reaction centres.

Linoleic acid has carbonyl (C=O) and hydroxyl (OH) groups as well as two double bonds in its molecule, while palmitic acid has C=O and OH functional groups.

It is most likely that linoleic acid could exhibit more inhibitive tendency than palmitic acid because it has more reaction centres which could offer stronger adsorption. However, palmitic acid could also contribute to the inhibition process. Further work is required to investigate the inhibition efficiency of each constituent either by chemical (weight loss) or electrochemical method to certainly determine the active constituent (s) responsible for the inhibition effect of DW extracts for MS in 15wt.% HCl solution.

As shown in table 5-1, the values of ΔG_{ads} was almost unchanged for DW from 20 to 40°C (23 kJ/mol) but decreased to 22 kJ/mol at 60°C. This implies that the adsorption of DW onto the MS sample was less favourable at 60°C (i.e. the bond strength between DW and MS decreased at 60°C).

Based on the experimental results obtained in this current study, the mechanism of adsorption of the constituents of DW extracts at the MS/solution interface is hypothesized:

The components of DW extract, protonate in strong HCl solution and exist in its cationic form [258]. The surface of MS has been reported to be positively charged in 15wt% HCl solution by Yadav et al.[55]. Hence, chloride anions in the aqueous HCl solution first adsorbed on the positively charged MS due to a smaller degree of hydration resulting in the creation of excess negative charge towards the solution [259]. The adsorption of chloride ions onto the inhibited MS surface was confirmed by EDS and XPS data (Tables 4-6 and 6-1). The cationic form of the components of DW extracts may be electrostatically adsorbed on the pre-adsorbed chloride ions.

It is also possible that adsorption mechanism occurred between the unshared lone pair of electrons present on O and N atoms as well as the pi-electrons in the double bonds

of DW with the MS surface resulting in a coordinate type of bond (chemical adsorption).

7.5.6 Summary

The corrosion inhibition mechanism of MS in 15wt% HCl solution containing DW probably occurred via the interaction of the DW and the MS surface as explained below:

1. The mechanism of MS corrosion inhibition may be attributed to both physical and chemical adsorption between the DW and surface of MS. Considering physical adsorption, the chloride ions in 15wt.% HCl solution first adsorbed on the MS surface, thereby causing the MS to be negatively charged. Then, the cationic form of active constituents is adsorbed on the negatively charged MS surface via electrostatic interaction which results in the formation of an adsorbed protective film which once created acts as a barrier against the attack of the corrosive solution. Also, the corrosion inhibitive ability of DW was enhanced probably due to the presence of N and O heteroatoms as well as the pi-electrons in DW which act as additional adsorption sites by donating their lone pair electrons to the vacant d-orbital of the iron atom (chemical adsorption).
2. Durum wheat extract can be classified as a mixed-type corrosion inhibitor in 15wt.% HCl solution because the anodic MS dissolution and cathodic hydrogen evolution processes were suppressed with cathodic predominance at 20°C and anodic at 40 and 60°C.
3. Durum wheat extract degrades at higher temperature leading to its lower corrosion inhibitive performance.
4. The adsorption of durum wheat extract at the MS/solution interface obeyed Langmuir adsorption isotherm.

7.6 Broccoli

7.6.1 Effect of concentration on broccoli performance

The corrosion rate of MS decreased from 1.056±0.039 (11.80 mm/y) to 0.312±0.021 mg/cm^{2}h (3.37 mm/y) with increase in BC concentration from 1 to 10 g/L at 20°C after 5 h immersion (**Table 4-1**). This behaviour may be attributed to an increase in adsorption and surface coverage of BC at the MS/HCl solution interface with BC increasing concentration as presented in Figure 7-11 [223], hence forming a more protective layer which decreases the exposure of the MS surface to the aggressive medium [221, 249]. In other words, the extent of BC adsorption on the MS surface was enhanced with an increase in BC concentration, thereby blocking more active sites of the MS sample exposed to the corrosive solution. This is consistent with many other results, including that obtained by Chauhan and Gunasekaran [109] who found that the corrosion rate of MS in 15wt% HCl containing zanthoxylum alatum extract decreased from 15.96 to 3.99 mm/y with increasing concentration from 0.5 to 2.8 g/L at 30°C.

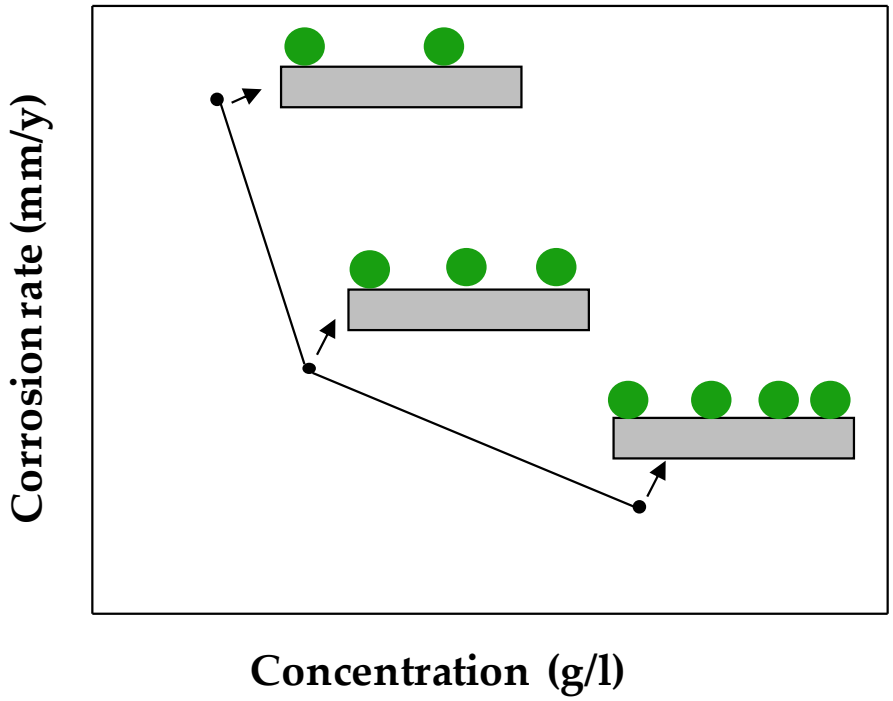


Figure 7-11 Schematic representation of the adsorption strength of BC on the MS surface with increasing concentration resulting in a decrease of the corrosion rate.

The maximum inhibition efficiency of 89±1% was achieved by BC at a concentration of 10 g/L, indicating that the adsorbed layer formed by BC on the MS surface was protective against corrosion. In other words, BC acts as an effective inhibitor for MS corrosion in 15 wt% HCl solution. The interaction of BC with the MS surface is consistent with XPS data showing a decrease in the amount of iron detected on the inhibited surface (15.7 at. %) compared to the uninhibited surface (23.5 at. %) as shown in Table 6-1. This may be due to the overlay of the inhibitor. Also, increase (20%) in the intensity of the carbon signal at the inhibited surface is possibly due to the contribution of carbon atom in the BC constituents (Table 6-1). A detailed description of the nature of the inhibited surface is discussed in **section 7.6.5**.

7.6.2 Effect of immersion time on BC performance

It was evident that the corrosion inhibition efficiency of BC remained unchanged with increasing immersion time from 15 to 192 h at 20°C (**Figure 4-10**), which indicated that the adsorbed protective layer formed at the MS/solution interface was stable and impermeable to the corrosive ions in the electrolyte [189, 256]. The corrosion inhibition efficiency of 83±1% was achieved by BC after 192 h immersion, demonstrating that BC is an effective inhibitor for MS corrosion at prolonged immersion time. This is consistent with the results obtained by Faustin et al.[119] who showed that stable corrosion inhibition efficiency was achieved by geissospermum leaves extract for MS in HCl solution with increasing immersion time from 24-72 h and they attributed this phenomenon to the compact and persistent adsorbed layer formed on the MS surface.

The inhibitive performance behaviour of BC at 40°C was similar to the that at 20°C. The inhibition efficiency of BC did not change markedly from 5 to 24 h of immersion at 40°C (Figure 4-12), demonstrating that the inhibitive film was protective and persistent on MS surface [7, 119]. The maximum inhibition efficiency of 86% was obtained after 24 h immersion.

The inhibition efficiency of BC slightly decreases with an increase in immersion time from 5 to 10 h as well as 15 to 24 h immersion time at 60 °C (**Figure 4-13**). This may be attributed to the desorption of BC from the MS surface as time increased. These results suggested that the inhibitive performance of BC was reduced with increasing immersion at 60°C.

7.6.3 Effect of temperature on BC performance

The corrosion rate of MS increaseed with increasing temperature over the range 20 to 60°C (**Tables 4-2 and 4-3**) which demonstrated that the increase in temperature accelerated MS corrosion and this agrees with Arrhenius equation. This is consistent with many results, including that obtained by Yadav et al.[55] who found that the corrosion rate of MS in 15wt% HCl increased from 20.2 mm/y to 92.69 mm/y with an increase in temperature from 30 to 60°C.

Turning to the BC-inhibited solution, the corrosion rate of MS also increased (**Tables 4- 2 and 4-3**) and the inhibition efficiency of BC decreased with increasing temperature from 20 to 60°C (**Figures 4-4 and 4-5**), which may be attributed to an increase in the kinetic energy of the system leading to desorption and degradation of BC on the electrode surface [79, 222, 234, 260]. This is consistent with the result of Elphick and Voisey [261] who reported that the inhibition efficiency of 4 g/L histidine decreased from 95% to 58% with increasing temperature from 20 to 60°C after 5 h immersion. Several authors have reported a similar decrease in corrosion inhibition performance with an increase in temperature, and they attributed this behaviour to either desorption or degradation of the plant extracts [8, 50, 121, 128, 171, 223, 237, 238].

The degradation of BC with temperature was confirmed by the lower inhibition efficiency (68±1.3%) obtained for BC/HCl solution that was heated to 60°C for 24 h compared to the unheated BC/HCl solution (85±0.7%), which demonstrated that BC degrades at elevated temperature (60°), resulting in weak interaction between BC constituents and the MS surface. This is consistent with the results obtained by Lee et al.[262] who reported percentage loss of 28.8% and 37.2% for kaemferol and quercetin constituents in 4 M HCl containing BC after 120 mins at 90°C, indicating the degradation of BC constituents with temperature. Several authors have also reported

that increasing temperature affects the thermal stability of different phytochemicals such as vitamin C, vitamin E, glucosinolates, phenols, flavonoids, anthocyanins in BC [263-266].

Despite the degradation of BC, the inhibition efficiency of BC is still about 83% and 75% after 5 h, and 24 h immersion at the highest temperature (60°C) studied (**Figures 4-4 and 4-5**), indicating that BC is an effective inhibitor against MS corrosion under the experimental conditions studied.

7.6.4 Surface characterisation of MS in the presence of BC extracts

The surface morphology of the uninhibited MS was severely corroded (730 mm/y) and rough (6.55±0.9 µm) (**Figure 4-14b**), this indicates that the corrosive ions attacked the MS surface in the electrolyte. However, the BC-inhibited MS surface was less corroded (125 mm/y) and surface roughness value of 3.49 ±0.06 µm as presented in Table 4-7, demonstrating that BC formed a protective film. Several authors have attributed smoother morphology of a metal surface in inhibited solution to the formation of an adsorbed protective layer [12, 125, 154, 160, 260].

The formation of an inhibiting film was consistent with XPS data showing an increase of the atomic % of carbon (C) at the inhibited MS compared to the uninhibited sample confirmed the contribution of carbon atom present in BC (Table 6-1). Furthermore, the suppression of iron (Fe) signal in the presence of the additive (BC) compared to the uninhibited sample could be due to the formation of a barrier layer which protects the corrosion of MS. The presence of nitrogen at the BC-treated MS surface film confirmed the interaction between the nitrogen atom of glucosinolates in BC and the MS surface.

7.6.5 Corrosion inhibition mechanism of BC extracts

It has been established by weight loss and electrochemical measurements that BC reduces the corrosion of MS in 15wt% HCl solution. Gas chromatography-mass spectroscopy (GC-MS) was employed to determine the major constituent(s) in BC.

GC-MS results showed that the major chemical components in BC are vitamin E (7.86%), palmitic acid (15.30%), linoleic acid (38.42%), and nonacosane (26.90%) (Table 5-4). Based on the molecular structures of these constituents, the number of adsorption sites for each constituent is presented in **Table 7-13**. From the table, it is clear that linoleic acid had more adsorption sites for binding to the MS surface than other constituents. Consequently, it is plausible that linoleic acid could be the most active constituent responsible for the inhibitive action of BC, hence better corrosion inhibition. However, further work is required to evaluate the inhibition performance of each constituent identified by GC- MS analysis to certainly identify the active constituent(s) responsible for the inhibition action.

Table 7-13 Possible adsorption sites of the major constituents of BC

Major constituent	Adsorption sites	No of active sites
Vitamin E	-OH, O and aromatic ring	3
Palmitic acid	C=O and OH	2
Linoleic acid	C=O, OH and 2 double bonds of C=C	4
Nonacosane	Straight chain	-

The calculated values of Gibbs free energy of adsorption of BC on the MS surface between -18 and -21 kJ/mol over the temperature range 20 to 60°C showed that BC electrostatically adsorbed at the MS/solution interface (physical adsorption)

(Table 5- 1) [6, 8, 132, 155]. This is consistent with the results obtained by Ostovari et al.[12] who found that the Gibbs free energy of adsorption of henna extract for MS is in the range of -14.17 kJ/mol to - 11.36 kJ/mol from 25 to 60°C, and attributed the adsorption process of the henna extract on MS surface to physical adsorption.

Further thermodynamic studies in the present study showed that the calculated value of apparent activation energy (E_a) of MS in 15wt% HCl inhibited with BC was higher (72.5± 0.6 kJ/mol) than that of uninhibited MS (62.1± 0.1 kJ/mol) (Table 5-2). This further demonstrates that the presence of BC in the bulk solution increases the energy barrier of the corrosion process and is suggestive of physical adsorption [112, 147, 155]. This agrees with the results obtained by Chauhan and Gunasekaran [109] who reported that the apparent activation energy of MS in 15wt% HCl containing zanthoxylum alatum plant extracts was higher (69.47 kJ/mol) than the uninhibited MS and attributed the result to the electrostatic interaction between MS and the extract.

It is clear from Table 5-1 that the values of ΔG_{ads} increased from 18 to 21 kJ/mol from 20 to 40°C, and then decreased to 19 kJ/mol at 60°C. This demonstrates that the bond strength between BC and MS increased from 20 to 40°C, and decreased at higher temperatures (60°C). In other words, the adsorption of BC on the MS surface was not favourable at 60°C.

Potentiodynamic polarisation measurements showed that the addition of BC into 15wt% HCl solution decreased the anodic and cathodic current densities of MS (Figure 4-9). This indicated that BC retarded anodic dissolution of MS and cathodic hydrogen evolution. In other words, BC has inhibited both anodic and cathodic reactions. Hence, it can be classified as a mixed-type corrosion inhibitor in 15wt% HCl solution.

Based on the thermodynamic activation parameters studies, the inhibition mechanism of BC is discussed below:

The inhibition mechanism of MS corrosion in 15wt% HCl by BC can be attributed to physical adsorption between the charged BC constituents in the bulk electrolyte and the charged MS surface (physical adsorption). In other words, BC gets protonated in the 15wt% HCl solution and exists in its cationic form. The chloride anions first adsorbed on the positively charged MS surface because of its degree of hydration. Subsequently, the electrode surface becomes negatively charged, and then the cationic form of BC (protonated) interacts with the pre-adsorbed chloride anions on the MS surface via electrostatic attraction. The adsorption and inhibition mechanism of MS corrosion by BC is illustrated schematically in Figure 7-12.

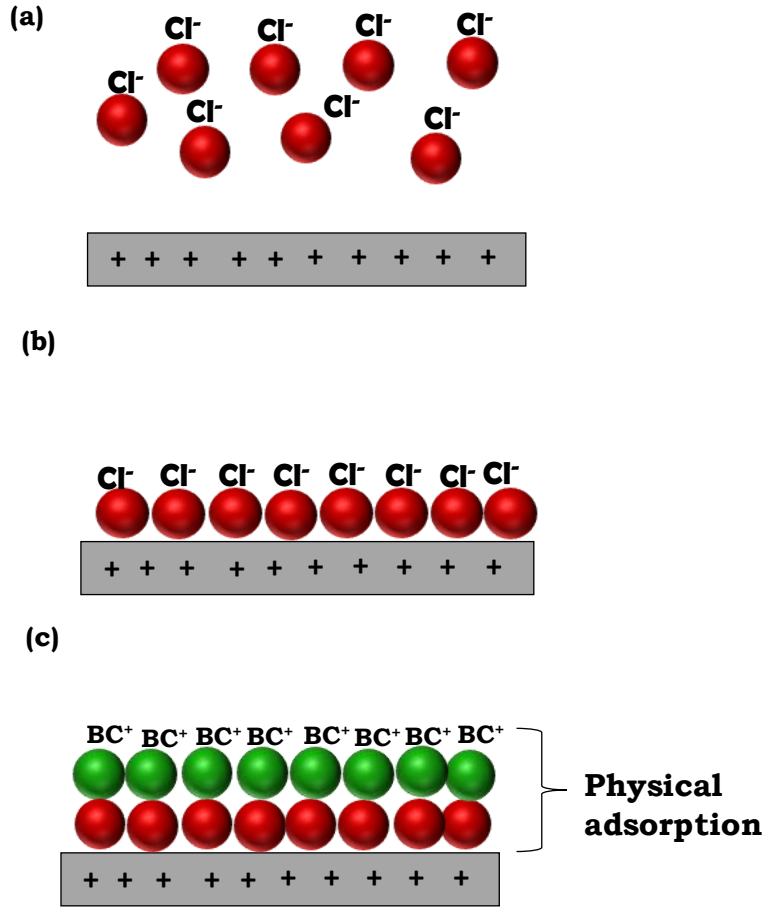


Figure 7-12 Possible adsorption mechanism for the inhibition of MS corrosion. (a) chloride ions in the acidic medium before adsorption (b) Chloride ions adsorbed on the positively charged MS surface and (c) Electrostatic interaction between pre-adsorbed chloride ions and the protonated broccoli constituents (BC^+).

7.6.6 Summary

1. The inhibition of MS corrosion may occur by the physical adsorption of broccoli constituents at the MS/solution interface. In other words, chloride ions adsorb on the positively charged MS surface, thereby creating an excess negative charge on the surface of the substrate. Then, electrostatic interactions can occur between the protonated broccoli constituents and the pre-adsorbed chloride ions on the MS surface. This cooperative effect results in the formation of a protective layer on the MS surface against corrosion.
2. Broccoli suppressed both anodic dissolution of MS and cathodic hydrogen evolution reactions and may be classified as a mixed-type corrosion inhibitor in 15wt% HCl solution with anodic predominance at 20 and 40°C, but the cathodic reaction was predominant at 60°C.
3. Increasing temperature decreased the corrosion inhibition performance of BC due to its degradation.
4. The corrosion inhibition performance of BC was stable at prolonged immersion at 20 and 40°C but was affected at 60°C.
5. The adsorption behaviour of BC on the MS surface follows the Langmuir isotherm model, which indicates monolayer formation on the MS surface.

7.7 Aloe vera gel

7.7.1 Effect concentration on aloe vera gel performance

The corrosion rate of MS decreases, and the inhibition efficiency increases with increasing AV gel constituents (AV) concentration up to 100 g/L in 15 wt% HCl solution at 20°C after 5 h immersion (Table 4-1 and Figure 4-3). This behaviour can be attributed to an increase in the adsorption and surface coverage of AV on the MS surface, thereby leading to the formation of more protective adsorbed layer [114, 140]. In other words, the increase in the concentration of AV leads to an increase in the number of aloe vera gel constituents that adsorb on the active sites of the electrode. This is consistent with the results obtained by Singh et al.[140], who found that the inhibition efficiency increased from 58 to 88% with increasing AV concentration from 0.05 to 0.2 g/L for MS in 1 M HCl at 25°C after 3 h immersion. A higher concentration of AV needed in the current work may be due to stronger HCl solution.

Further increase in AV concentration beyond 100g/L in this present work, offered little or no improvement in the inhibition performance (Figure 4-3), which means AV had achieved an optimum protective performance [123]. AV achieved an optimum inhibition efficiency of 84±2% at 100 g/L. The small calculated value of K_{ads} (0.02 L/g) validated the weak adsorption of AV on the MS surface (Table 5-1) [171]. A detailed explanation of the inhibition mechanism of MS corrosion in the presence of aloe vera gel is discussed in section 7.7.5.

7.7.2 Effect of immersion time on aloe vera gel performance

The inhibition efficiency of aloe vera gel decreased from 84±2 to 75 ±3% with increasing immersion time from 5 to 10 h. This is possibly due to the desorption of the protective film from the MS surface. However, the inhibition efficiency of AV was stable with an increase in immersion time from 10 to 24 h at 20°C (Figure 4-11), and this may be attributed to the persistent inhibitive film formed at the MS/solution interface [140].

The inhibition efficiency decreased markedly from 10 to 15 h at 40°C (Figure 4-12), which may be due to desorption of the adsorbed film after long immersion time [140]. The maximum inhibition efficiency of 76 ± 2% was achieved after 10 h immersion.

At a temperature of 60°C, the inhibition efficiency of aloe vera decreases with the increase of immersion from 5 to 10 h and then remained almost unchanged up to 24 h (Figure 4-13). The decreasing inhibition efficiency behaviour may be attributed to the desorption of the protective film from the MS/solution interface with increasing immersion time [140]. The maximum inhibition efficiency of 78±0.4% was achieved after 5 h immersion. The decreasing corrosion inhibition efficiency with immersion time demonstrated that aloe vera gel is not an effective inhibitor at the elevated temperature investigated in this work.

7.7.3 Effect of temperature on aloe vera gel performance

The corrosion rate of MS increased with increase in temperature from 20 to 60°C after 5 and 24 h (Tables 4-2 and 4-3) both in the uninhibited and AV-inhibited solutions. This showed that the corrosion reaction was accelerated with increasing temperature. However, AV had an inhibitive effect as the corrosion of MS decreased at each temperature compared to the uninhibited sample.

The inhibition efficiency of aloe vera gel decreased with increase in temperature from 20 to 60°C after 24 h (Figures 4-5). It was also observed that the inhibition efficiency of aloe vera decreased with increase in temperature from 20 to 40°C after 5 h of immersion (Figure 4-4). The decreasing inhibition efficiency can be attributed to a decrease in the strength of the adsorption of aloe vera gel (desorption) with a rise in temperature resulting in lower surface coverage [140]. Also, a decrease in inhibition efficiency with increasing temperature demonstrates that AV may physically adsorb at the MS/solution interface [114, 139]. The inhibition performance of AV was significantly affected at the highest temperature (60°C) as shown in Figure 4-5. The decrease in AV performance with the rise in temperature is suggestive of electrostatic interaction between the aloe vera gel and the MS/solution. This is consistent with the results obtained by Singh et al.[140] who reported that the inhibition efficiency of 0.2 g/l aloe vera gel decreased from 90 to 80% with an increase in temperature from 35 to 65°C and attributed this phenomenon to the desorption effect.

7.7.4 Surface characterisation of MS surface treated with aloe vera gel

It is clear that the SEM image of the uninhibited MS surface immersed in 15wt% HCl solution after 5 h immersion at 60°C (Figure 4-14b) revealed a highly corroded and rough morphology having corrosion rate value of 730 mm/y. However, the aloe vera gel inhibited MS surface was less corroded with a corrosion rate value of 162 mm/y as shown in Figure 4-14. Also, EDS data showed that chloride ions were considerably suppressed (about 87% decrease) at the MS surface in the presence of aloe vera (Table 4-6). This observation confirmed the formation of an adsorbed film which suppressed the corrosion of the MS sample.

7.7.5 Corrosion inhibition mechanism of aloe vera gel

The calculated value of E_a obtained for MS immersed in 15wt% HCl solution containing aloe vera gel (84.5±2.1 kJ/mol) was higher than that of the uninhibited solution (62.1±0.1 kJ/mol) as shown in Table 5-2. This demonstrated that the addition of aloe vera gel into the bulk solution increased the energy barrier to the corrosion process [267], hence inhibiting the corrosion of MS. Furthermore, this also demonstrated that adsorption occurred via electrostatic interaction between aloe vera gel constituents and the MS/solution interface [147, 254]. This is consistent with the findings obtained by Abiola and James [114], who found that E_a of MS in 2 M uninhibited HCl solution increased from 2.7 kJ/mol to 17.2 kJ/mol in the presence of 10%v/v aloe vera gel, and attributed this effect to physical adsorption mechanism. Singh et al. [140] also found that E_a in the presence of aloe vera gel was greater than the uninhibited sample.

To further confirm the adsorption mechanism, the Gibbs free energy of adsorption was evaluated. Generally, ΔG_{ads} values $\leq$ -20 kJ/mol is attributed to physical adsorption, whilst those between -20 and -40 kJ/mol are attributed to both physical and chemical adsorption mechanism [145, 146, 150] In the present work, the ΔG_{ads} value obtained for MS-treated with aloe vera gel at 20°C was -7.3 kJ/mol (Table 5-1), indicating that aloe vera gel interacted with the MS surface via physical adsorption. This further corroborated the physical adsorption mode suggested previously. This is consistent with the results obtained by Eddy and Odoemelam[142], who reported that the ΔG_{ads} for MS in acidic medium containing 0.4 g/l aloe vera at 30°C was -8.9 kJ/mol, suggesting physical adsorption.

AV is composed of several naturally occurring phytochemicals [268]. Hence the complex chemical compositions made it difficult to attribute its inhibitive performance

to a particular group or specific constituent. However, an attempt had been made to determine the main constituents in aloe vera gel. Gas chromatography-mass spectrometry (GCMS) results of aloe vera gel showed that it contains 2-myristoyl pantetheine (47.3%), octadecanoic (stearic) acid (5.6%), palmitoleic acid (9.5%) and gamolenic acid (9.9%) as the major constituents (Table 5-5). The corrosion inhibition performance of the identified major compounds has not been studied in the literature. However, further work is required to test the inhibition performance of each of the identified major compounds to identify the active ingredient(s) responsible for the inhibition action.

Aloe vera gets protonated in HCl solution because it is an organic base and it exists in its cationic form [269]. It is possible that chloride ions first adsorbed on the positively MS surface via electrostatic attraction. Consequently, the adsorbed chloride ions facilitate the adsorption of the protonated aloe vera constituents on the electrode surface, hence forming a protective film at the MS/solution interface which inhibits the corrosion of MS.

Summarising the adsorption process of aloe vera onto the MS surfaced is due to physical adsorption mechanism as shown in Figure 7-13.

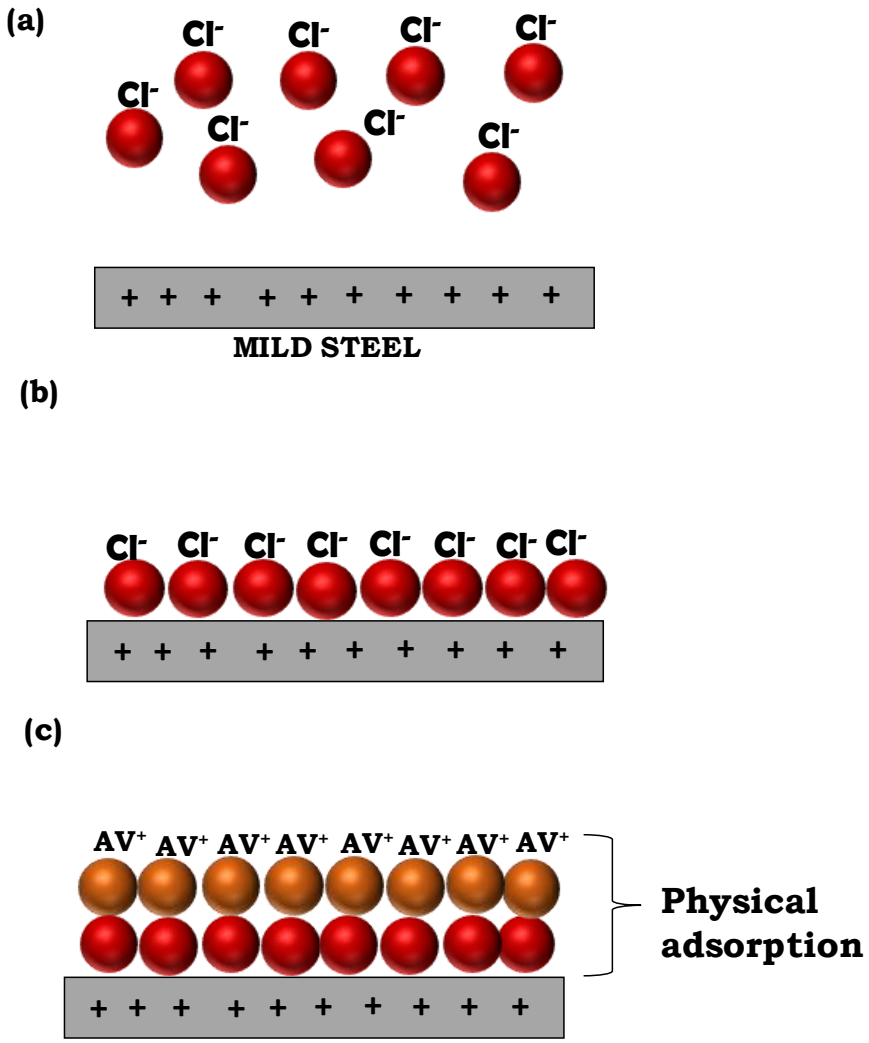


Figure 7-13 Proposed schematic representation of aloe vera gel adsorption mechanism on the MS surface (a) chloride ions before adsorption, (b). Chloride ions adsorbed on the MS surface and (c) AV constituents interacted with the pre-adsorbed chloride ions on the MS surface.

7.7.6 Summary

1. Aloe vera gel inhibited MS corrosion possibly by the interaction of the protonated aloe vera constituents in 15wt% HCl with the pre-adsorbed chloride ions on the MS surface (physical adsorption mechanism).
2. The presence of chloride anions on the MS surface facilitates the adsorption of protonated aloe vera at MS/solution interface.
3. Temperature increase significantly decreased the inhibition efficiency of aloe vera due to its desorption at the MS/solution interface, especially at the highest temperature (60°C) studied.
4. The adsorption process of aloe vera gel on MS surface followed Langmuir adsorption isotherm, and a monolayer of the active constituents is formed on the MS surface.
5. Aloe vera gel acted poorly as a corrosion inhibitor with increasing immersion time from 5 to 24 h at 60°C.

CHAPTER EIGHT

GENERAL DISCUSSION

8.1 Introduction

The possibility of using plant-based materials (DW, BC, IN and AV) as alternative corrosion inhibitors for steel in acid to the toxic commercially available and effective synthetic organic inhibitors such as PA and MI has been investigated in this present study. Also, the influence of temperature and immersion time on the inhibition performance of the studied inhibitors have been investigated.

As expected, it was found that the corrosion rate of MS exposed to the uninhibited solution was the highest. This was attributed to the direct attack of the aggressive solution on the bare metal. On the other hand, the corrosion rate of MS immersed in the inhibited HCl solutions decreased markedly, and the inhibition efficiency increased, with an increase in the concentration of both the commercial inhibitors (PA and MI) and the green alternatives (DW, BC, IN and AV). This was attributed to the adsorption of the inhibitors onto the MS surface, thereby forming a physical barrier/film which prevented the sample against corrosion.

PA outperformed all the inhibitors in the concentration range investigated. This was attributed to the stable adsorbed film formed by the interaction of the lone pairs of electrons in the C≡C triple bond with the vacant d-orbital of MS. The presence of a thicker layer in the presence of PA on the MS was confirmed by the SEM results which showed the least corroded surface of the MS treated surface with PA. Also, FTIR results showed the presence of adsorbed species composed of C=C, OH, CH_2, FeO on the MS surface. This is confirmed by the highest inhibition efficiency (over 99%) achieved by PA.

Table 8-1 Inhibition efficiency obtained from weight loss data of PA, MI, DW, BC, IN and AV for MS immersed in 15% HCl solution at 20°C after 5 h at a concentration of 7 g/L.

S/N	Medium	The inhibition efficiency (%)
1.	PA	99.70
2.	MI	96.50
3.	DW	97.40
4.	BC	84.90
5.	IN	75.78
6.	AV	12.80

As shown in Table 8-1, it is clear that PA inhibited the corrosion of MS the most, while AV performed poorly. MI performed better than BC, IN and AV with the exclusion of DW at 20°C after 5 h immersion at the same concentration of 7 g/L.

It is noted that at the lowest concentration (1 g/l) of the inhibitors, PA and MI performed better than all the green inhibitors (Figure 4-2). However, DW still achieved over 90% protection, demonstrating that DW can effectively act as an acid corrosion inhibitor at low concentration.

Among the plant-based inhibitors, DW achieved the highest inhibition efficiency, while AV was the least effective.

Higher inhibitive performance achieved by DW is most likely due to more reaction centres in its constituents, which is evidenced by the presence of nitrogen and oxygen atoms as well as the pi-electrons available in the double bonds of linoleic acid, (Figure 5-6 and Figure 5-17).

8.2 Effect of Temperature

The effect of temperature on the corrosion behaviour of MS in the absence of inhibitors showed that the corrosion rate of MS was markedly accelerated with increasing temperature from 20 to 60°C. However, the presence of inhibitors in the test solution decreased the corrosion rate at each temperature (Tables 4-2 and 4-3).

The inhibition efficiency of PA was constant (99%) at the temperature range studied. This was attributed to the thermally stable and adherent adsorbed film formed on the metal surface. On the other hand, the inhibition efficiency of MI, DW, BC, IN, and AV decreased with increase in the temperature (Table 8-1). The inhibition efficiency of MI was the least affected after PA, while that of AV significantly dropped significantly at 24 h with increasing temperature from 20 to 60° C (Figure 4-5).

Effect of temperature results showed that the commercial inhibitors (PA and MI) performed better than the plant-based inhibitors (DW, BC, IN, and AV). However, it seems DW and BC are promising candidate inhibitors for further study as they achieved protection efficiency of ~78% and ~75% respectively at 60°C after 24 h immersion. AV behaved poorly with increasing temperature as the inhibition efficiency decreased from 77% to 32% in the temperature range from 20 to 60°C after 24 h immersion, while PA maintained its protection efficiency as shown in Table 8-2.

Table 8-2 Effect of temperature on inhibition performance for different inhibitors after 24 h immersion.

The inhibition efficiency (%)						
Temp (°C)	**PA**	**MI**	**DW**	**BC**	**IN**	**AV**
20	99.72±0.06	96.78±0.16	85.00±1.20	85.00±0.70	78.20±0.90	77.75±2.10
40	99.84±0.06	94.14±0.66	84.50±0.36	86.29±0.27	87.30±1.13	68.59±1.33
60	99.90±0.02	87.90±1.55	77.64±0.29	74.90±1.01	63.88±3.16	32.30±1.37

8.3 Effect of time on inhibition performance

The study of the dependence of inhibition efficiencies of PA, MI, DW, BC, IN and AV on different immersion times from 5 to 24 h at the highest temperature (60°C) gives information about the stability of the adsorbed film in the presence of the studied inhibitors at the metal-solution interface.

Firstly, PA offered the most inhibitive efficiency among all the inhibitors studied within the time scale investigated. Its inhibitive efficiency remained unchanged with immersion time (99% IE). This result was attributed to the adsorbed layer formed by PA molecules at the MS-solution interface which was stable and resistive to the aggressive medium. Also, the excellent MS inhibition exhibited by PA can be attributed to the presence of the highly reactive and electron rich carbon-carbon triple bond in the PA molecule which enhanced its inhibitive properties. Similar high and stable PA inhibition efficiency was obtained by Hackerman and Bartos for iron rod in 1.4 M HCl solution. They found that the corrosion current density of iron remains unchanged (12 $\mu A/cm^2$) in the presence of 10 mM PA from 2 to 24 h immersion [270].

In the case of other inhibitors, the inhibition efficiencies of MI, DW, and BC were relatively stable within the time scale studied. However, MI inhibition efficiency was higher (87.9±1.6%) than DW (77.6±0.3%) and BC (74.9±1%). The higher inhibition performance of MI may be attributed to a greater number of active sites including an aromatic ring, an imidazole ring, a mercapto group, nitrogen and double bond in its molecular structure. The inhibition efficiencies of IN and AV markedly decreased with increasing immersion time (Figure 4-5). This was due to weak bonding to the MS surface, while that of IN could be due to its degradation

Summarising, it is clear from this study that the two commercial inhibitors (PA and MI) performed better than the candidate plant-based inhibitors. However, DW and BC are promising acid corrosion inhibitors in the strong acidic medium studied.

The excellent inhibition performance of PA was attributed to the stable adsorbed layer (composed of FeO, C=C, OH, C-O and C-H species) that was formed on the MS surface [268, 271, 272].

CHAPTER NINE

ECONOMIC AND ENVIRONMENTAL IMPACTS OF GREEN INHIBITORS

9.1 Introduction

This chapter presents the environmental and economic impacts of DW, BC, IN, and AV used as plant-based inhibitors in the present study. Also, the global annual cost of corrosion as well as the estimated cost of each inhibitor.

9.2 Economics of corrosion inhibitors

Most industrialised countries like Canada, Japan, United States, China, and the United Kingdom are affected by the economic problem of corrosion [273-275]. According to the National Association of Corrosion Engineer (NACE), the global annual cost of corrosion was estimated to be US$ 2.5 trillion (2013), which is almost 3.4% of the global Gross Domestic Product (GDP)[275]. It is estimated that between $375-875 billion (USD) could be saved annually by adopting proper corrosion control measures [275]. In the United States, $276 billion was incurred annually on direct corrosion, which was about 3.1% of the US GDP [273]. The application of corrosion inhibitors (CIs) is one of the most economical ways of mitigating corrosion [6, 276]. Among several industrial sectors, the oil and gas industry is one of the largest consumers of CIs [4]. For instance, the total cost consumed on CIs in the United States is about $1.1 billion in 1998. Consequently, one of the factors to consider when selecting organic corrosion inhibitors, especially on an industrial scale is cost-effectiveness.

The advantages of using plant-based materials as inhibitors over the synthetic inhibitors (PA and MI) are due to the simplicity of the extraction procedures, availability of plants, biodegradability and low cost. The cost of the optimum concentration of the plant-based

inhibitors compared to the synthetic alternatives used in this study is presented in Table 9-1.

The data indicated that the price of DW and BC was lower than the commercial inhibitors (PA and MI), but that of IN and AV was higher. Furthermore, the highest concentration (100 ml/L HCl) and the cost of AV are pointers that it was not economically viable on an industrial scale. Even with the unusual higher concentration, the inhibition performance was not effective compared to other plant inhibitors investigated. DW and BC are cost-effective, biodegradable and non-toxic and can be considered as candidate inhibitors on an industrial scale.

Table 9-1 The cost of optimum concentration of inhibitor per litre of 15wt% HCl solution.

Inhibitor	Quantity	Cost/Qty (£)	Cost/ (ml or g)	Cost/optimum concentration
PA	100 ml	20.60	0.206	1.44
MI	100 g	15.50	0.155	1.09
DW	5000 g	5.50	0.0011	0.77
BC	50 g	2.00	0.04	0.40*
IN	24 g	2.99	0.124	1.24
AV	300 ml	5.32	0.0177	1.77**

**The cost of electricity for drying and refluxing sample is not included.*

*** The cost of man-power for extracting aloe vera gel is not included.*

It is worthy of note that the estimated cost for the investigated inhibitors presented in Table 9-1 is for a laboratory scale preparation. It is possible that the cost of the plant-based materials might be cheaper if the quantities are scaled up for industrial-scale production.

In the following section, the environmental and economic impacts of the studied inhibitors are discussed.

9.3 Durum wheat inhibitor

9.3.1 Environmental impact

Durum wheat inhibitor is not a toxic material and does not affect the environment and humans negatively, by ingestion, inhalation, skin or eye contact during its extraction or use. However, dust mask and goggle are to be worn when excessive dust is to be generated during material handling [144]. There is no dangerous effect during storage or transportation of this product. Durum wheat is a source of food products including semolina, bread, and pasta for human consumption[277]. Hence, it does not have a hazardous effect on the environment.

9.3.2 Economic impact

Durum wheat inhibitor was prepared by water-based extraction and did not require any expensive equipment. Another economic benefit of durum wheat as an inhibitor is that it is easy to grow, since it doesn't need rich soil, or much water and is easy to process, because the grain falls away from the chaff, 2.7 million tonnes of durum wheat can be obtained per hectare [277], which implies that durum wheat yield is high. The practice of organic farming by using manure and bone meal as fertilizers and naturally occurring pesticide also have an economic impact [277]. Table 9-1 shows that durum wheat inhibitor used as one of the green corrosion inhibitors for this research was cheaper than the synthetic inhibitors, which may have an economic impact when considering large scale production.

9.4 Inulin

9.4.1 Environmental impact

Inulin belongs to the class of carbohydrate called fibres. It is composed of several fructose moieties joined to a glucose molecule at its terminal end by a β (2,1) bond [278]. Inulin is a natural-based plant product that is biodegradable, environmentally-

friendly, acceptable, and non-toxic to humans. It has several nutritional and health benefits and is used as a prebiotic (i.e., non-digestible food ingredient to stimulate the growth of bacteria), fat and sugar replacer, low caloric food ingredient for diabetic management [279]. Consequently, the discharge of inulin to the environment during its application as a corrosion inhibitor has zero adverse effect on humans and the environment because it is a food grade based product [279]. Inulin satisfies the environmental requirements such as bioaccumulation, biodegradability, biocompatibility, and toxicity of substance being discharged into the environment [279, 280]

9.4.2 Economic impact

The commercial inulin used as a corrosion inhibitor for this study was extracted from Jerusalem artichoke. Some of the positive economic impacts of using inulin extracted from Jerusalem artichoke are summarised as follows [278]:

1. It is resistant to pests and diseases, which saves the cost of agrochemicals.
2. It is tolerant to frost and drought
3. It can be grown on most soils that other food crops cannot survive
4. It has low fertiliser requirements which imply that a great deal of cost will be saved on the purchase of fertiliser
5. The potential yield of inulin from Jerusalem artichoke is about 5 Mg/ha (5 tonnes/ha), and it also has a higher potential dry matter yield of about 4- 35 tonnes/ha.
6. The extraction of inulin is water-based, and that is another economic advantage.

From the cost analysis presented in Table 9-1, it is clear that the cost of IN is lower than PA, while MI is more cost-effective than IN. However, considering the toxicity of PA and MI, IN could be a potential option.

9.5 Broccoli inhibitor

9.5.1 Environmental impact

Broccoli used as one of the green corrosion inhibitors is a food-grade material that has several health benefits such as reducing the risk of lung and colon cancer, improving the health of the bone, aid digestion and natural detoxification, the source of antioxidants, among others [281]. The non-toxicity, biodegradability and environmentally friendly characteristics of broccoli suggest that it meets the environmental regulations for corrosion inhibitor applications. The preparation of broccoli inhibitor and even its application should not pose any hazardous effect on both humans whether by ingestion, inhalation, eye and skin contact. However, personal protective equipment (PPE) must be worn during its applications.

9.5.2 Economic impact

The broccoli extract used as a corrosion inhibitor in this work was extracted in the laboratory using a low-cost apparatus. The estimated cost presented in Table 9-1 showed that broccoli is the most economical inhibitor, but the cost of electricity for drying and refluxing broccoli during its preparation as a corrosion inhibitor was not included. Increase in the demand of broccoli could lead to a rise in its market price because broccoli is already a highly demanded vegetable plant.

9.6 Aloe vera inhibitor

9.6.1 Environmental impact

Aloe vera gel has no toxic effect on both the environment and humans because it is environmentally-friendly and biodegradable [137, 271]. In other words, there are no threats to life and the environment during its extraction via ingestion, inhalation and skin contact as well as during its injection into the oil well as a corrosion inhibitor. It is used for several commercial applications such as laxative, favouring, drinks, and skin care products [137].

9.6.2 Economic impact

The extraction of aloe vera gel inhibitor used for this experimental work did not require special and costly equipment. This makes this inhibitor to be cost-effective; unlike the commercial toxic organic inhibitors that require capital intensive equipment to set up. Also, aloe vera leaves can be grown in a variety of soils (loamy or sandy soil) as well as in low rainfall or dry areas with warm, humid conditions. The fertility of the soil can be improved by adding farmyard manure, which saves the cost of fertilisers [282]. Aloe vera yields start from the second to the fifth year before re-planting, and an average of 40 to 45 tonnes of the output of aloe vera leaves can be obtained from 1- hectare land [137, 282], which implies that the farmland will keep producing for 4 years. However, the unusually high concentration of aloe vera gel required to achieve high inhibition of MS corrosion indicates that it is not economically viable to be used as a corrosion inhibitor.

CHAPTER TEN

CONCLUSIONS AND FUTURE WORK

10.1 CONCLUSIONS

This chapter presents the main conclusions that have been drawn from the present study: corrosion inhibition performance of both the commercial synthetic (PA and MI) and plant-based (DW, BC, IN and AV) inhibitors for MS in 15 wt% HCl solution using weight loss and electrochemical tests as well as surface analysis.

1. The synthetic (PA and MI) and green (DW, BC and IN) inhibitors showed good corrosion protection for MS in the environment/ conditions investigated, while AV performed poorly. PA and MI showed better corrosion inhibition than green inhibitors. PA performed much better than other inhibitors.
2. The effect of optimum concentration studies demonstrated that the inhibition efficiencies of PA and MI were higher than the plant-based inhibitors at room temperature (20 °C) after 5 h immersion, except for DW that competed favourably well with MI at the same conditions. A significant amount of AV concentration is required to achieve adequate corrosion inhibition performance.
3. The effect of temperature results demonstrated that the inhibition efficiencies of PA and MI were better than DW, BC, IN, and AV. PA maintained its stable inhibition performance (99% IE) over the temperature range 20 to 60°C at 5 and 24 h time points. This implies that the inhibition efficiency of PA is not dependent on temperature. The inhibition efficiencies of MI, DW, and BC are temperature dependent. The inhibition efficiency of IN and AV significantly decreased at 60°C after 24 h immersion. Amongst all the green inhibitors, AV performed poorly with increasing solution temperature.
4. The effect of immersion time studies indicated that the corrosion inhibition performance of PA (99% IE) and MI (over 84% IE) remained stable and excellent with prolonged immersion time at 20 °C. However, the corrosion

inhibition efficiencies of DW, BC, and AV slightly decreased at the onset but were later stable throughout the immersion time. The corrosion inhibition performance of IN was stable throughout the immersion time at 20 °C (over 80% IE).

5. Potentiodynamic polarisation results indicated that all the inhibitors could be classified as mixed-type corrosion inhibitors as they suppressed both the anodic dissolution of MS and cathodic hydrogen evolution.
6. The adsorption behaviour of both synthetic and green inhibitors at the MS surface in the strong acid solution (15 wt% HCl) obeyed Langmuir adsorption isotherm model. At 60°C, thermodynamic parameters demonstrated that the adsorption of PA onto the MS surface occurred typically by chemisorption (coordinate covalent bond formation)., while that of MI is solely by physisorption (electrostatic interaction) at the same temperature. For the green inhibitors, adsorption of BC and IN on the MS occurred by physical adsorption that involves electrostatic interaction between the charged inhibitor species and the charged MS surface, except for DW that interacted with the MS surface via physical and chemical adsorption.
7. XPS data revealed that the mechanism of MS corrosion inhibition in 15wt% HCl solution occurred by the adsorption of the inhibitors onto the MS surface. FTIR revealed that the adsorbed film formed on MS treated with PA is composed of C=C, OH, C-O, C-H, and FeO species as well as chloride inclusions. Also, XPS results showed that adsorbed film at the MS surfaces treated with PA, MI, DW, BC and IN contains iron oxide/hydroxide.
8. SEM studies revealed that the uninhibited MS surface was severely corroded with a rough surface after 5 h immersion at 60 °C by weight loss measurements.

However, the MS surfaces exposed to PA, MI, DW, BC, IN, and AV were less corroded due to the inhibiting effect of the adsorbed film formed on the MS surface, which protected MS against corrosion. Also, 3D profilometry confirmed that the synthetic inhibitors performed better than the green inhibitors because of the lower surface roughness value of MS after corrosion. However, the MS surface treated with DW exhibited the lowest surface roughness among the green inhibitors, which confirms its good inhibition action, whereas MS surface immersed in AV-inhibited solution had the highest surface roughness, confirming its weak inhibiting effect.

9. Basic economic analysis of the studied inhibitors indicated that the cost of DW and BC was cheaper (at the optimum concentration found in this study), than the commercial inhibitors (PA and MI), while that of IN and AV was higher. Furthermore, the unusually high concentration (100 ml/L HCl) and the cost of AV are pointers that it is not economically viable on an industrial scale. However, it should be borne in mind that the plant-based inhibitors have little or no negative impact on the environment because they are biodegradable and non-toxic, and full economic costing would need to include the environmental cost.
10. DW and BC are the most promising inhibitors in the environments/conditions investigated amongst all the green inhibitors.

10.2 FUTURE WORK

Other areas of this project to be considered for further investigation (future work), which are beyond the scope of this PhD research have been suggested below:

1) Investigate which of the abundant constituents/components identified by GC- MS are the major **active** constituents responsible for the corrosion inhibition performance of DW, BC, IN and AV by carrying out single component corrosion inhibition tests to investigate the inhibition efficiency of each constituent. (Synergistic effects would also need to be investigated).
2) Investigate whether the plant-based inhibitors could also be used to protect other materials including zinc, aluminium and N80 steel used for other industrial application.
3) Investigate the possibility of using the plant-based inhibitors for corrosion inhibition of MS in lower concentration HCl (1M) and sodium chloride solutions for other applications.
4) Investigate the synergistic inhibition performance of DW and BC for MS in 15wt% HCl solution.
5) Investigate the adsorbed film formed at the MS surface/HCl solution interface to determine the composition of the film as well its thickness during the adsorption-desorption process using ellipsometry.
6) Investigate the effect of persistence tests on the corrosion inhibitors - taking into consideration how long the inhibitors are effective after removal from the solution.
7) Carry out further corrosion tests to determine the effectiveness of the studied corrosion inhibitors in flow condition.

8) Investigate the potential effect of batch variability and extraction methods on the effectiveness of synthetic and green inhibitors.

References

1. McCafferty, E., *Introduction to corrosion science*. New York: Springer.
2. NACE INTERNATIONAL. *Corrosion in the Oil and Gas Industry,* 15th August 2015]; Available from www.nace.org/Corrosion-Central/Industries/Oil-Gas-Production/.
3. Rajeev, P., A. Surendranathan, and C.S. Murthy, *Corrosion mitigation of the oil well steels using organic inhibitors–a review.* J Mater Environ Sci, 2012. **3**(5): p. 856-869.
4. Finšgar, M. and J. Jackson, *Application of corrosion inhibitors for steels in acidic media for the oil and gas industry: A review.* Corrosion Science, 2014. **86**: p. 17-41.
5. Baddini, A.L.d.Q., S.P. Cardoso, E. Hollauer, and J.A.d.C.P. Gomes, *Statistical analysis of a corrosion inhibitor family on three steel surfaces (duplex, super-13, and carbon) in hydrochloric acid solutions.* Electrochimica Acta, 2007. **53**(2): p. 434-446.
6. Fitoz, A., H. Nazır, M. Özgür, E. Emregül, and K.C. Emregül, *An experimental and theoretical approach towards understanding the inhibitive behaviour of a nitrile substituted coumarin compound as an effective acidic media inhibitor.* Corrosion Science, 2018. **133**: p. 451-464.
7. Dutta, A., S.K. Saha, U. Adhikari, P. Banerjee, and D. Sukul, *Effect of substitution on corrosion inhibition properties of 2-(substituted phenyl) benzimidazole derivatives on mild steel in 1M HCl solution: A combined experimental and theoretical approach.* Corrosion Science, 2017. **123**(Supplement C): p. 256-266.
8. Azzaoui, K., E. Mejdoubi, S. Jodeh, A. Lamhamdi, E. Rodriguez-Castellón, M. Algarra, A. Zarrouk, A. Errich, R. Salghi, and H. Lgaz, *Eco-friendly green inhibitor Gum Arabic (GA) for the corrosion control of mild steel in hydrochloric acid medium.* Corrosion Science, 2017. **129**: p. 70-81.
9. Keleş, H., D.M. Emir, and M. Keleş, *A comparative study of the corrosion inhibition of low carbon steel in HCl solution by an imine compound and its cobalt complex.* Corrosion Science, 2015. **101**: p. 19-31.
10. Thakur, S.A., G.P. Flake, G.S. Travlos, J.A. Dill, S.L. Grumbein, S.J. Harbo, and M.J. Hooth, *Evaluation of propargyl alcohol toxicity and carcinogenicity in F344/N rats and B6C3F1/N mice following whole-body inhalation exposure.* Toxicology, 2013. **314**(1): p. 100-111.
11. Gloria, J.H. and H.P. Nick, *Chemical hazards of the workplace* Fifth ed. 2014, New Jersey: Wiley and sons.
12. Ostovari, A., S.M. Hoseinieh, M. Peikari, S.R. Shadizadeh, and S.J. Hashemi, *Corrosion inhibition of mild steel in 1 M HCl solution by henna extract: A comparative study of the inhibition by henna and its constituents (Lawsone, Gallic acid, α-d-Glucose and Tannic acid).* Corrosion Science, 2009. **51**(9): p. 1935-1949.
13. Abdel-Gaber, A.M., B.A. Abd-El-Nabey, I.M. Sidahmed, A.M. El-Zayady, and M. Saadawy, *Inhibitive action of some plant extracts on the corrosion of steel in acidic media.* Corrosion Science, 2006. **48**(9): p. 2765-2779.
14. Shoaib, M., A. Shehzad, M. Omar, A. Rakha, H. Raza, H.R. Sharif, A. Shakeel, A. Ansari, and S. Niazi, *Inulin: Properties, health benefits and food applications.* Carbohydrate Polymers, 2016. **147**: p. 444-454.

15. Choudhary, Y.K., A. Sabhapondit, and A. Kumar, *Application of Chicory as Corrosion Inhibitor for Acidic Environments.* SPE Production & Operations, 2013. **28**(03): p. 268-276.
16. Patel, D.K., K. Patel, and S. Dhanabal, *Phytochemical standardization of Aloe vera extract by HPTLC techniques.* Journal of Acute Disease, 2012. **1**(1): p. 47- 50.
17. Trethewey, K.R. and J. Chamberlain, *Corrosion for science and engineering*. Second ed. 1995, England: Longman.
18. Fontana, M.G., *Corrosion Engineering*. Third ed. 1986, New YorkMcGraw-Hill.
19. Nimmo, B. and G. Hinds, *Beginners guide to corrosion.* NPL, Teddington, 2003.
20. Frankel, G.S. and N. Sridhar, *Understanding localized corrosion.* Materials Today, 2008. **11**(10): p. 38-44.
21. Papavinasam, S., *Chapter 1 - The Oil and Gas Industry*, in *Corrosion Control in the Oil and Gas Industry*, S. Papavinasam, Editor. 2014, Gulf Professional Publishing: Boston. p. 1-39.
22. Roberge, P.R., *Handbook of Corrosion Engineering*. 2012, McGraw-Hill Inc.: New York.
23. Revie, R.W., *Uhlig's Corrosion Handbook*. Second ed. 2000, New York: John Wiley and Sons Inc.
24. Brondel, D., R. Edwards, A. Hayman, D. Hill, S. Mehta, and T. Semerad, *Corrosion in the oil industry.* Oilfield review, 1994. **6**(2): p. 4-18.
25. Videm, K., J. Kvarekval, T.E. Perez, and G. Fitzsimons, *Surface Effects on the Electrochemistry of Iron and Carbon Steel Electrodes in Aqueous CO_2 Solutions*, in *CORROSION 96*. 1996, NACE International: Denver, Colorado. p. 19.
26. Dugstad, A., *Fundamental Aspects of CO_2 Metal Loss Corrosion - Part 1: Mechanism*, in *CORROSION 2006*. 2006, NACE International: San Diego, California. p. 18.
27. Smith, S.N., B. Brown, and W. Sun, *Corrosion at higher H_2S concentrations and moderate temperatures*, in *Corrosion Expo*. 2011, NACE: Houston.
28. Sun, W. and S. Nesic, *A mechanistic model of H_2S corrosion of mild steel* in *Corrosion 2007*. 2007, NACE. p. 1-26.
29. Sastri, V.S., *Corrosion inhibitors: principles and applications*. 1998, England: John Wiley & Sons.
30. Ahmad, Z., *Principles of corrosion engineering and corrosion control*. 2006: Butterworth-Heinemann.
31. Frasch, H., *Increasing the flow of oil wells*, U.S. patent office, Editor. 1896: United States.
32. Bazin, B., *From Matrix Acidizing to Acid Fracturing: A Laboratory Evaluation of Acid/Rock Interactions.* SPE Production & Facilities, 2001. **16**(01): p. 22-29.
33. American Petroleum Institute, *Acidizing-treatment in Oil and Gas.* 2014: p. 1- 5.
34. Migahed, M.A. and I.F. Nassar, *Corrosion inhibition of Tubing steel during acidization of oil and gas wells.* Electrochimica Acta, 2008. **53**(6): p. 2877-2882.

35. Frenier, W.W., F.B. Growcock, V.R. Lopp, and B. Dixon, *Process and Composition for Inhibiting High-Temperature Iron and Steel Corrosion* D.S. Incorporated, Editor. 1990: US.
36. Jayaperumal, D., *Effects of alcohol-based inhibitors on corrosion of mild steel in hydrochloric acid.* Materials Chemistry and Physics, 2010. **119**(3): p. 478-484.
37. Smith, C.F., F.E. Dollarhide, and N.J. Byth, *Acid Corrosion Inhibitors - Are We Getting What We Need?* Journal of Petroleum Technology, 1978. **30**(05): p. 737-746.
38. Cramer, S.D. and B.S. Covino, *Environment and Industries*. Vol. 13. 2006, Ohio: ASM International.
39. El-Sherik, *Trends in Oil and Gas Corrosion research and Technologies*. 2017, Duxton: Elsevier.
40. Schmitt, G., *Application of inhibitors for acid media: report prepared for the European Federation of corrosion working party on inhibitors.* British Corrosion Journal, 1984. **19**(4): p. 165-176.
41. Davis, J.R., *Corrosion: understanding the basics*. 2000: ASM International.
42. Schweitzer, P.A., *Corrosion of Linings and coatings*. Second ed. 2006, Florida, U.S.: CRC Press.
43. J., B., *The use of molasses and vegetable oils to inhibit corrosion of pickling sheet steel in acids*. 1895: England.
44. Sastri, V.S., *Green corrosion inhibitors: Theory and practice*. Vol. 10. 2012: John Wiley & Sons.
45. Shreir, L., R.A. Jarman, and G.T. Burstein, *Corrosion Control*. Vol. 2. 1994, Oxford: Elsevier.
46. Transparency Market Research. *Global Corrosion Inhibitors Market to be Worth US$7.14 Billion by 2019*. 2015 [cited 2015 July 18]; Available from: http://www.transparencymarketresearch.com/pressrelease/corrosion-inhibitors.htm.
47. Mansfeld, F., *Corrosion mechanisms*. 1987, New York: Marcel Dekker Inc. 1-454.
48. Olajire, A.A., *Corrosion inhibition of offshore oil and gas production facilities using organic compound inhibitors - A review.* Journal of Molecular Liquids, 2017. **248**: p. 775-808.
49. Groysman, A., *Corrosion for everybody*. 2009: Springer Science & Business Media.
50. Popova, A., E. Sokolova, S. Raicheva, and M. Christov, *AC and DC study of the temperature effect on mild steel corrosion in acid media in the presence of benzimidazole derivatives.* Corrosion Science, 2003. **45**(1): p. 33-58.
51. Podobaev, N.I. and Y.G. Avdeev, *A Review of Acetylene Compounds as Inhibitors of Acid Corrosion of Iron.* Protection of Metals, 2004. **40**(1): p. 7-13.
52. Tang, L., G. Mu, and G. Liu, *The effect of neutral red on the corrosion inhibition of cold rolled steel in 1.0 M hydrochloric acid.* Corrosion Science, 2003. **45**(10): p. 2251-2262.
53. Okafor, P.C., M.E. Ikpi, I.E. Uwah, E.E. Ebenso, U.J. Ekpe, and S.A. Umoren, *Inhibitory action of Phyllanthus amarus extracts on the corrosion of mild steel in acidic media.* Corrosion Science, 2008. **50**(8): p. 2310-2317.
54. Li, X., S. Deng, and H. Fu, *Inhibition effect of methyl violet on the corrosion of cold rolled steel in 1.0 M HCl solution.* Corrosion Science, 2010. **52**(10): p. 3413-3420.

55. Yadav, M., R.R. Sinha, S. Kumar, and T.K. Sarkar, *Corrosion inhibition effect of spiropyrimidinethiones on mild steel in 15% HCl solution: insight from electrochemical and quantum studies.* RSC Advances, 2015. **5**(87): p. 70832-70848.
56. Vishwanatham, S. and N. Haldar, *Corrosion inhibition of N80 steel in hydrochloric acid by phenol derivatives.* Indian Journal of Chemical Technology, 2007. **14**: p. 501-506.
57. Priya, A.R.S., V.S. Muralidharan, and A. Subramania, *Development of Novel Acidizing Inhibitors for Carbon Steel Corrosion in 15% Boiling Hydrochloric Acid.* CORROSION, 2008. **64**(6): p. 541-552.
58. Yadav, M., D. Behera, and U. Sharma, *Nontoxic corrosion inhibitors for N80 steel in hydrochloric acid.* Arabian Journal of Chemistry, 2016. **9**: p. S1487-S1495.
59. Yadav, M., S. Kumar, and D. Behera, *Inhibition Effect of Substituted Thiadiazoles on Corrosion Activity of N80 Steel in HCl Solution.* Journal of Metallurgy, 2013. **2013**: p. 14.
60. Gao, J., Y. Weng, L. Feng, and H. Yue, *Corrosion inhibition of α, β-unsaturated carbonyl compounds on steel in acid medium.* Petroleum Science, 2009. **6**(2): p. 201-207.
61. Quraishi, M. and D. Jamal, *Fatty acid triazole:Novel corrosion inhibitors for oil well steel(N80) and mild steel.* J. Am. Oil Chem. Soc., 2000. **77**: p. 1107-1111.
62. Quraishi, M.A., N. Sardar, and H. Ali, *A Study of Some New Acidizing Inhibitors on Corrosion of N-80 Alloy in 15% Boiling Hydrochloric Acid.* CORROSION, 2002. **58**(4): p. 317-321.
63. Avdeev, Y.G. and Y.I. Kuznetsov, *Physicochemical aspects of inhibition of acid corrosion of metals by unsaturated organic compounds.* Russian Chemical Reviews, 2012. **81**(12): p. 1133.
64. Subramania, A., S. Kalyana, S. P, Muralidhran, and T. Vasudevan, *Polymeric corrosion inhibitor - An overview.* Bulletin of Electrochemistry 2004. **20**(2): p. 49-58.
65. Funkhouser, J.G., *Acid Corrosion Inhibition With Secondary Acetylenic Alcohols.* CORROSION, 1961. **17**(6): p. 283-287.
66. Aramaki, K. and E. Fujioka, *Spectroscopic investigations on the inhibition mechanism of propargyl alcohol for iron corrosion in hydrochloric acid at elevated temperatures.* Corrosion, 1997. **53**(4): p. 319-326.
67. Pati, B.B., P. Chatterjee, T.B. Singh, and D.D.N. Singh, *Effect of Propargyl Alcohol on Corrosion and Hydrogenation of Steel in Hydrochloric Acid Solution.* CORROSION, 1990. **46**(5): p. 354-359.
68. Poling, G., *Infrared studies of protective films formed by acetylenic corrosion inhibitors.* Journal of The Electrochemical Society, 1967. **114**(12): p. 1209-1214.
69. Frignani, A., C. Monticelli, F. Zucchi, and G. Trabanelli, *Acetylenic alcohols as inhibitors of iron acid corrosion. Improvement of the inhibition efficiency of a class of substances based on their action mechanism.* Int. J. Corros. Scale Inhib, 2014. **3**(2): p. 105-119.
70. Avdeev, Y.G., Y.I. Kuznetsov, and A.K. Buryak, *Inhibition of steel corrosion by unsaturated aldehydes in solutions of mineral acids.* Corrosion Science, 2013. **69**: p. 50-60.

71. Aramaki, K. and E. Fujioka, *Surface-enhanced Raman scattering spectroscopy studies on the inhibition mechanism of propargyl alcohol for iron corrosion in hydrochloric acid.* Corrosion, 1996. **52**(2): p. 83-91.
72. Quraishi, M.A. and D. Jamal, *Technical Note: CAHMT—A New and Eco- Friendly Acidizing Corrosion Inhibitor.* CORROSION, 2000. **56**(10): p. 983-985.
73. Mohammed-Dabo, I.A., Yaro, S.A., Abubakar, G., Ayilara, S.I., Apugo-Nwosu, T.U., Akuso, S.A., *Corrosion Inhibition of Oil Well Steel in Hydrochloric Acid Pickling Solution by the Extract of Ficus Abutilofolia and Propargyl Alcohol.* J. Basic Appl. Sci. Res., 2011. **1**(11): p. 1989-2011.
74. Jayaperumal, D., Muralidharan, P., Subramanian, G., Venkatachari, S., Senthivel, *Propargyl alcohol as hydrochloric acid inhibitor for mild steel-temperature dependence of critical concentration.* 1997. **44**(4): p. 265-268.
75. Morad, M., *Influence of propargyl alcohol on the corrosion behaviour of mild steel in H_3PO_4 solutions.* Materials chemistry and physics, 1999. **60**(2): p. 188- 195.
76. Quraishi, M.A., Ahmad, S. A., Venkatchari, G., *Synergistic effect of 2-Amino-6-Chloro-benozothiazole on inhibitive performance of Propargyl alcohol during corrosion of mild steel in boiling hydrochloric acid solution.* Bulletin of Electrochemistry, 1997. **13**(6): p. 829-852.
77. Chen, Z., L. Li, G. Zhang, Y. Qiu, and X. Guo, *Inhibition effect of propargyl alcohol on the stress corrosion cracking of super 13Cr steel in a completion fluid.* Corrosion Science, 2013. **69**: p. 205-210.
78. Ravari, F.B., M. Heydari, and A. Dadgarineghad, *Corrosion Inhibition Propargyl Alcohol on Low Alloy Cr Steel in 0.5 M H2SO4 in the Absence and Presence of Potassium Iodide.* Gazi University Journal of Science, 2011. **24**(3): p. 507-515.
79. Aljourani, J., K. Raeissi, and M. Golozar, *Benzimidazole and its derivatives as corrosion inhibitors for mild steel in 1M HCl solution.* Corrosion Science, 2009. **51**(8): p. 1836-1843.
80. Abd El-Maksoud, S.A. and A.S. Fouda, *Some pyridine derivatives as corrosion inhibitors for carbon steel in acidic medium.* Materials Chemistry and Physics, 2005. **93**(1): p. 84-90.
81. Machnikova, E., K.H. Whitmire, and N. Hackerman, *Corrosion inhibition of carbon steel in hydrochloric acid by furan derivatives.* Electrochimica Acta, 2008. **53**(20): p. 6024-6032.
82. Fenelon, A.M. and C.B. Breslin, *The electropolymerization of pyrrole at a CuNi electrode: corrosion protection properties.* Corrosion Science, 2003. **45**(12): p. 2837-2850.
83. Al-Mulla, A., *A review: Biological Importance of Heterocyclic Compounds.* Der Pharma Chemica, 2017. **9**(13): p. 141-147.
84. Popova, A., M. Christov, and A. Zwetanova, *Effect of the molecular structure on the inhibitor properties of azoles on mild steel corrosion in 1 M hydrochloric acid.* Corrosion Science, 2007. **49**(5): p. 2131-2143.
85. Wang, L., *Evaluation of 2-mercaptobenzimidazole as corrosion inhibitor for mild steel in phosphoric acid.* Corrosion Science, 2001. **43**(12): p. 2281-2289.
86. Wang, L., J.-X. Pu, and H.-C. Luo, *Corrosion inhibition of zinc in phosphoric acid solution by 2-mercaptobenzimidazole.* Corrosion Science, 2003. **45**(4): p. 677-683.

87. Aljourani, J., M.A. Golozar, and K. Raeissi, *The inhibition of carbon steel corrosion in hydrochloric and sulfuric acid media using some benzimidazole derivatives.* Materials Chemistry and Physics, 2010. **121**(1): p. 320-325.
88. Morales-Gil, P., M.S. Walczak, C.R. Camargo, R.A. Cottis, J.M. Romero, and R. Lindsay, *Corrosion inhibition of carbon-steel with 2-mercaptobenzimidazole in hydrochloric acid.* Corrosion Science, 2015. **101**: p. 47-55.
89. Mahdavian, M. and S. Ashhari, *Corrosion inhibition performance of 2- mercaptobenzimidazole and 2-mercaptobenzoxazole compounds for protection of mild steel in hydrochloric acid solution.* Electrochimica Acta, 2010. **55**(5): p. 1720-1724.
90. Espinoza, A., G. Negrón, M. Palomar-Pardavé, M.A. Romero-Romo, I. Rodríguez-Torres, and H. Herrera-Hernández, *Electrochemical Impedance Spectroscopy Analysis of 2-Mercaptobenzimidazole (2MBI) as Corrosion Inhibitor in HCl 1M.* ECS Transactions, 2009. **20**(1): p. 543-553.
91. Amar, H., A. Tounsi, A. Makayssi, A. Derja, J. Benzakour, and A. Outzourhit, *Corrosion inhibition of Armco iron by 2-mercaptobenzimidazole in sodium chloride 3% media.* Corrosion science, 2007. **49**(7): p. 2936-2945.
92. Anandarajagopal, K., R.N. Tiwari, K. Bothara, J.A.J. Sunilson, C. Dineshkumar, and P. Promwichit, *2-Mercaptobenzimidazole derivatives: synthesis and anticonvulsant activity.* Advances in Applied Science Research, 2010. **1**(2): p. 132-138.
93. Swayze, E.E., S.M. Peiris, L.S. Kucera, E.L. White, D.S. Wise, J.C. Drach, and L.B. Townsend, *Synthesis of 1-(2-aminopropyl) benzimidazoles, structurally related to the TIBO derivative R82150, with activity against human immunodeficiency virus.* Bioorganic & Medicinal Chemistry Letters, 1993. **3**(4): p. 543-546.
94. Popova, A., M. Christov, S. Raicheva, and E. Sokolova, *Adsorption and inhibitive properties of benzimidazole derivatives in acid mild steel corrosion.* Corrosion Science, 2004. **46**(6): p. 1333-1350.
95. Popova, A., M. Christov, and T. Deligeorgiev, *Influence of the Molecular Structure on the Inhibitor Properties of Benzimidazole Derivatives on Mild Steel Corrosion in 1 M Hydrochloric Acid.* CORROSION, 2003. **59**(9): p. 756- 764.
96. Morales-Gil, P., M.S. Walczak, R.A. Cottis, J.M. Romero, and R. Lindsay, *Corrosion inhibitor binding in an acidic medium: Interaction of 2- mercaptobenizmidazole with carbon-steel in hydrochloric acid.* Corrosion Science, 2014. **85**(Supplement C): p. 109-114.
97. Benabdellah, M., A. Tounsi, K.F. Khaled, and B. Hammouti, *Thermodynamic, chemical and electrochemical investigations of 2-mercapto benzimidazole as corrosion inhibitor for mild steel in hydrochloric acid solutions.* Arabian Journal of Chemistry, 2011. **4**(1): p. 17-24.
98. Álvarez-Bustamante, R., G. Negrón-Silva, M. Abreu-Quijano, H. Herrera-Hernández, M. Romero-Romo, A. Cuán, and M. Palomar-Pardavé, *Electrochemical study of 2-mercaptoimidazole as a novel corrosion inhibitor for steels.* Electrochimica Acta, 2009. **54**(23): p. 5393-5399.
99. Morales-Gil, P., G. Negrón-Silva, M. Romero-Romo, C. Ángeles-Chávez, and M. Palomar-Pardavé, *Corrosion inhibition of pipeline steel grade API 5L X52 immersed in a 1 M H2SO4 aqueous solution using heterocyclic organic molecules.* Electrochimica Acta, 2004. **49**(26): p. 4733-4741.

100. Zhang, D.-q., L.-x. Gao, and G.-d. Zhou, *Inhibition of copper corrosion in aerated hydrochloric acid solution by heterocyclic compounds containing a mercapto group.* Corrosion Science, 2004. **46**(12): p. 3031-3040.
101. Niamien, P.M., F.K. Essy, A. Trokourey, A. Yapi, H.K. Aka, and D. Diabate, *Correlation between the molecular structure and the inhibiting effect of some benzimidazole derivatives.* Materials Chemistry and Physics, 2012. **136**(1): p. 59-65.
102. Zhang, C. and J. Zhao, *Synergistic inhibition effects of octadecylamine and tetradecyl trimethyl ammonium bromide on carbon steel corrosion in the H_2S and CO2 brine solution.* Corrosion Science, 2017. **126**: p. 247-254.
103. Heydari, M. and M. Javidi, *Corrosion inhibition and adsorption behaviour of an amido-imidazoline derivative on API 5L X52 steel in CO 2-saturated solution and synergistic effect of iodide ions.* Corrosion Science, 2012. **61**: p. 148-155.
104. Zhang, D.-Q., L.-X. Gao, and G.-D. Zhou, *Synergistic effect of 2-mercapto benzimidazole and KI on copper corrosion inhibition in aerated sulfuric acid solution.* Journal of Applied Electrochemistry, 2003. **33**(5): p. 361-366.
105. Larabi, L., Y. Harek, M. Traisnel, and A. Mansri, *Synergistic Influence of Poly(4-Vinylpyridine) and Potassium Iodide on Inhibition of Corrosion of Mild Steel in 1M HCl.* Journal of Applied Electrochemistry, 2004. **34**(8): p. 833-839.
106. Abiola, O.K., J.O.E. Otaigbe, and O.J. Kio, *Gossipium hirsutum L. extracts as green corrosion inhibitor for aluminum in NaOH solution.* Corrosion Science, 2009. **51**(8): p. 1879-1881.
107. Abiola, O.K. and J.O.E. Otaigbe, *The effects of Phyllanthus amarus extract on corrosion and kinetics of corrosion process of aluminium in alkaline solution.* Corrosion Science, 2009. **51**(11): p. 2790-2793.
108. Raja, P.B. and M.G. Sethuraman, *Natural products as corrosion inhibitor for metals in corrosive media — A review.* Materials Letters, 2008. **62**(1): p. 113-116.
109. Chauhan, L.R. and G. Gunasekaran, *Corrosion inhibition of mild steel by plant extract in dilute HCl medium.* Corrosion Science, 2007. **49**(3): p. 1143-1161.
110. Deng, S. and X. Li, *Inhibition by Ginkgo leaves extract of the corrosion of steel in HCl and H 2 SO 4 solutions.* Corrosion Science, 2012. **55**: p. 407-415.
111. El-Etre, A.Y., *Inhibition of acid corrosion of carbon steel using aqueous extract of olive leaves.* Journal of Colloid and Interface Science, 2007. **314**(2): p. 578- 583.
112. Da Rocha, J.C., J.A.d.C.P. Gomes, and E. D'Elia, *Corrosion inhibition of carbon steel in hydrochloric acid solution by fruit peel aqueous extracts.* Corrosion Science, 2010. **52**(7): p. 2341-2348.
113. de Assunção Araújo Pereira, S.S., M.M. Pêgas, T.L. Fernández, M. Magalhães, T.G. Schöntag, D.C. Lago, L.F. de Senna, and E. D'Elia, *Inhibitory action of aqueous garlic peel extract on the corrosion of carbon steel in HCl solution.* Corrosion Science, 2012. **65**: p. 360-366.
114. Abiola, O.K. and A.O. James, *The effects of Aloe vera extract on corrosion and kinetics of corrosion process of zinc in HCl solution.* Corrosion Science, 2010. **52**(2): p. 661-664.
115. Behpour, M., S.M. Ghoreishi, M. Khayatkashani, and N. Soltani, *The effect of two oleo-gum resin exudate from Ferula assa-foetida and Dorema ammoniacum on mild steel corrosion in acidic media.* Corrosion Science, 2011. **53**(8): p. 2489-2501.

116. Aouniti, A., K.F. Khaled, and B. Hammouti, *Correlation between inhibition efficiency and chemical structure of some amino acids on the corrosion of Armco iron in 1 M HCl.* Int. J. Electrochem. Sci., 2013(8): p. 5925-5943.
117. Amin, M.A., K.F. Khaled, Q. Mohsen, and H.A. Arida, *A study of the inhibition of iron corrosion in HCl solutions by some amino acids.* Corrosion Science, 2010. **52**(5): p. 1684-1695.
118. Bentrah, H., Y. Rahali, and A. Chala, *Gum Arabic as an eco-friendly inhibitor for API 5L X42 pipeline steel in HCl medium.* Corrosion Science, 2014. **82**: p. 426-431.
119. Faustin, M., A. Maciuk, P. Salvin, C. Roos, and M. Lebrini, *Corrosion inhibition of C38 steel by alkaloids extract of Geissospermum leave in 1 M hydrochloric acid: Electrochemical and phytochemical studies.* Corrosion Science, 2015. **92**: p. 287-300.
120. Soltani, N., N. Tavakkoli, M. Khayatkashani, M.R. Jalali, and A. Mosavizade, *Green approach to corrosion inhibition of 304 stainless steel in hydrochloric acid solution by the extract of Salvia officinalis leaves.* Corrosion Science, 2012. **62**: p. 122-135.
121. Satapathy, A.K., G. Gunasekaran, S.C. Sahoo, K. Amit, and P.V. Rodrigues, *Corrosion inhibition by Justicia gendarussa plant extract in hydrochloric acid solution.* Corrosion Science, 2009. **51**(12): p. 2848-2856.
122. Oguzie, E.E., *Evaluation of the inhibitive effect of some plant extracts on the acid corrosion of mild steel.* Corrosion Science, 2008. **50**(11): p. 2993-2998.
123. Ji, G., S. Anjum, S. Sundaram, and R. Prakash, *Musa paradisica peel extract as a green corrosion inhibitor for mild steel in HCl solution.* Corrosion Science, 2015. **90**: p. 107-117.
124. Odewunmi, N.A., S.A. Umoren, and Z.M. Gasem, *Watermelon waste products as green corrosion inhibitors for mild steel in HCl solution.* Journal of Environmental Chemical Engineering, 2015. **3**(1): p. 286-296.
125. Fiori-Bimbi, M.V., P.E. Alvarez, H. Vaca, and C.A. Gervasi, *Corrosion inhibition of mild steel in HCl solution by pectin.* Corrosion Science, 2015. **92**: p. 192-199.
126. Deng, S. and X. Li, *Inhibition by Jasminum nudiflorum Lindl. leaves extract of the corrosion of aluminium in HCl solution.* Corrosion Science, 2012. **64**(Supplement C): p. 253-262.
127. Torres, V.V., R.S. Amado, C.F. de Sá, T.L. Fernandez, C.A.d.S. Riehl, A.G. Torres, and E. D'Elia, *Inhibitory action of aqueous coffee ground extracts on the corrosion of carbon steel in HCl solution.* Corrosion Science, 2011. **53**(7): p. 2385-2392.
128. Lebrini, M., F. Robert, A. Lecante, and C. Roos, *Corrosion inhibition of C38 steel in 1M hydrochloric acid medium by alkaloids extract from Oxandra asbeckii plant.* Corrosion Science, 2011. **53**(2): p. 687-695.
129. Raja, P.B., A.K. Qureshi, A. Abdul Rahim, H. Osman, and K. Awang, *Neolamarckia cadamba alkaloids as eco-friendly corrosion inhibitors for mild steel in 1 M HCl media.* Corrosion Science, 2013. **69**: p. 292-301.
130. Li, X., S. Deng, and H. Fu, *Inhibition of the corrosion of steel in HCl, H2SO4 solutions by bamboo leaf extract.* Corrosion Science, 2012. **62**(Supplement C): p. 163-175.
131. Li, X. and S. Deng, *Inhibition effect of Dendrocalamus brandisii leaves extract on aluminium in HCl, H_3PO_4 solutions.* Corrosion Science, 2012. **65**(Supplement C): p. 299-308.

132. Chevalier, M., F. Robert, N. Amusant, M. Traisnel, C. Roos, and M. Lebrini, *Enhanced corrosion resistance of mild steel in 1M hydrochloric acid solution by alkaloids extract from Aniba rosaeodora plant: Electrochemical, phytochemical and XPS studies.* Electrochimica Acta, 2014. **131**(Supplement C): p. 96-105.
133. Gadow, H.S. and M.M. Motawea, *Investigation of the corrosion inhibition of carbon steel in hydrochloric acid solution by using ginger roots extract.* RSC Advances, 2017. **7**(40): p. 24576-24588.
134. Li, L., X. Zhang, J. Lei, J. He, S. Zhang, and F. Pan, *Adsorption and corrosion inhibition of Osmanthus fragran leaves extract on carbon steel.* Corrosion Science, 2012. **63**: p. 82-90.
135. Bachiega, P., J.M. Salgado, J.E. de Carvalho, A.L.T.G. Ruiz, K. Schwarz, T. Tezotto, and M.C. Morzelle, *Antioxidant and antiproliferative activities in different maturation stages of broccoli (Brassica oleracea Italica) biofortified with selenium.* Food Chemistry, 2016. **190**: p. 771-776.
136. Shapiro, T.A., J.W. Fahey, K.L. Wade, K.K. Stephenson, and P. Talalay, *Chemoprotective glucosinolates and isothiocyanates of broccoli sprouts metabolism and excretion in humans.* Cancer Epidemiology Biomarkers & Prevention, 2001. **10**(5): p. 501-508.
137. Eshun, K. and Q. He, *Aloe Vera: A Valuable Ingredient for the Food, Pharmaceutical and Cosmetic Industries—A Review.* Critical Reviews in Food Science and Nutrition, 2004. **44**(2): p. 91-96.
138. Ahlawat, K.S. and B.S. Khatkar, *Processing, food applications and safety of aloe vera products: a review.* Journal of Food Science and Technology, 2011. **48**(5): p. 525-533.
139. Hart, K. and A. James, *The inhibitive effect of aloe vera barbadensis gel on copper in hydrochloric acid medium.* Journal of Emerging Trends in Engineering and Applied Sciences, 2014. **5**(1): p. 24-29.
140. Singh, A.K., S. Mohapatra, and B. Pani, the *Corrosion inhibition effect of Aloe Vera gel: Gravimetric and electrochemical study.* Journal of Industrial and Engineering Chemistry, 2016. **33**: p. 288-297.
141. N.O., E. and O. S.A., *Inhibition of corrosion of mild steel in acidic medium using ethanol extract of Aloe vera.* Pigment & Resin Technology, 2009. **38**(2): p. 111-115.
142. Eddy, N. and S. Odoemelam, *Inhibition of corrosion of mild steel in acidic medium using ethanol extract of Aloe vera.* Pigment & Resin Technology, 2009. **38**(2): p. 111-115.
143. Sladana, Z., B. Miroljub, P. Mirjana, D. Dejan, and D. I., *Characterization of proteins from grain of different bread and durum wheat genotypes.* Int. J. Mol. Sci., 2011. **12**(9): p. 5878-5894.
144. Mike, S., A. Joel, M. Brian, and C. Marina, *Durum wheat: Chemistry and Technology*. 2012, Minnesota, U.S.A.: AACC International Inc.
145. Quartarone, G., L. Ronchin, A. Vavasori, C. Tortato, and L. Bonaldo, *Inhibitive action of gramine towards corrosion of mild steel in deaerated 1.0 M hydrochloric acid solutions.* Corrosion Science, 2012. **64**: p. 82-89.
146. Sığırcık, G., D. Yildirim, and T. Tüken, *Synthesis and inhibitory effect of N,N'-bis(1-phenylethanol)ethylenediamine against steel corrosion in HCl Media.* Corrosion Science, 2017. **120**(Supplement C): p. 184-193.
147. Tang, Y., F. Zhang, S. Hu, Z. Cao, Z. Wu, and W. Jing, *Novel benzimidazole derivatives as corrosion inhibitors of mild steel in the acidic media. Part I:*

Gravimetric, electrochemical, SEM and XPS studies. Corrosion Science, 2013. **74**(0): p. 271-282.
148. Mohagheghi Samarin, A., H. Poor Azarang, H. Akhlaghi, A. Elhami Rad, and N. Hematyar, *Antioxidant activity of potato (Solanum tuberosum, raja) peel extract.* Iranian Journal of Nutrition Sciences & Food Technology, 2008. **3**(3): p. 23-32.
149. Mourya, P., S. Banerjee, and M.M. Singh, *Corrosion inhibition of mild steel in acidic solution by Tagetes erecta (Marigold flower) extract as a green inhibitor.* Corrosion Science, 2014. **85**: p. 352-363.
150. Qiang, Y., S. Zhang, B. Tan, and S. Chen, *Evaluation of Ginkgo leaf extract as an eco-friendly corrosion inhibitor of X70 steel in HCl solution.* Corrosion Science, 2018. **133**: p. 6-16.
151. Ghareba, S. and S. Omanovic, *12-Aminododecanoic acid as a corrosion inhibitor for carbon steel.* Electrochimica Acta, 2011. **56**(11): p. 3890-3898.
152. Solomon, M.M., S.A. Umoren, I.I. Udosoro, and A.P. Udoh, *Inhibitive and adsorption behaviour of carboxymethyl cellulose on mild steel corrosion in sulphuric acid solution.* Corrosion Science, 2010. **52**(4): p. 1317-1325.
153. Arockiasamy, P., X.Q.R. Sheela, G. Thenmozhi, M. Franco, J.W. Sahayaraj, and R.J. Santhi, *Evaluation of Corrosion Inhibition of Mild Steel in 1 M Hydrochloric Acid Solution by Mollugo cerviana.* International Journal of Corrosion, 2014. **2014**: p. 7.
154. Da Rocha, J.C., J.A. Da Cunha Ponciano Gomes, and E. D'Elia, *Corrosion inhibition of carbon steel in hydrochloric acid solution by fruit peel aqueous extracts.* Corrosion Science, 2010. **52**(7): p. 2341-2348.
155. Desimone, M.P., G. Gordillo, and S.N. Simison, *The effect of temperature and concentration on the corrosion inhibition mechanism of an amphiphilic amido-amine in CO2 saturated solution.* Corrosion Science, 2011. **53**(12): p. 4033-4043.
156. Rahuma, M.N., H. Amer, and M. Alfergani, *Corrosion inhibition of mild steel in 11% hydrochloric acid solutions by using black pepper (Piper nigrum).* Chemical Science Transactions, 2014. **3**(2): p. 764-72.
157. Popova, A., *Temperature effect on mild steel corrosion in acid media in the the presence of azoles.* Corrosion Science, 2007. **49**(5): p. 2144-2158.
158. Labjar, N., F. Bentiss, M. Lebrini, C. Jama, and S. El hajjaji, *Study of Temperature Effect on the Corrosion Inhibition of C38 Carbon Steel Using Amino-tris(Methylenephosphonic) Acid in Hydrochloric Acid Solution.* International Journal of Corrosion, 2011. **2011**.
159. Mourya, P., P. Singh, A.K. Tewari, R.B. Rastogi, and M.M. Singh, *Relationship between structure and inhibition behaviour of quinolinium salts for mild steel corrosion: Experimental and theoretical approach.* Corrosion Science, 2015. **95**: p. 71-87.
160. Roy, P., P. Karfa, U. Adhikari, and D. Sukul, *Corrosion inhibition of mild steel in acidic medium by polyacrylamide grafted Guar gum with various grafting percentage: Effect of intramolecular synergism.* Corrosion Science, 2014. **88**: p. 246-253.
161. Goldstein, J.I., D.E. Newbury, J.R. Michael, N.W. Ritchie, J.H. Scott, and D.C. Joy, *Scanning electron microscopy and X-ray microanalysis*. Fourth ed. 2018, New York: Springer.
162. Sparkman, O.D., Z.E. Penton, and F.G. Kitson, *Gas Chromatography and Mass Spectrometry*. Second ed. 2011, Calfornia, USA: Elsevier.

163. Swamy, M.K., G. Arumugam, R. Kaur, A. Ghasemzadeh, M.M. Yusoff, and U.R. Sinniah, *GC-MS Based Metabolite Profiling, Antioxidant and Antimicrobial Properties of Different Solvent Extracts of Malaysian Plectranthus amboinicus Leaves.* Evidence-Based Complementary and Alternative Medicine, 2017. **2017**: p. 10.
164. Casuga, F.P., A.L. Castillo, and M.J.-A.T. Corpuz, *GC–MS analysis of bioactive compounds present in different extracts of an endemic plant Broussonetia luzonica (Blanco) (Moraceae) leaves.* Asian Pacific Journal of Tropical Biomedicine, 2016. **6**(11): p. 957-961.
165. Shai, Y., *ATR-FTIR studies in pore-forming and membrane induced fusion peptides.* Biochimica et Biophysica Acta (BBA) - Biomembranes, 2013. **1828**(10): p. 2306-2313.
166. Olivares-Xometl, O., N. Likhanova, R. Martínez-Palou, and M. Domínguez-Aguilar, *Electrochemistry and XPS study of an imidazoline as corrosion inhibitor of mild steel in an acidic environment.* Materials and Corrosion, 2009. **60**(1): p. 14-21.
167. Yang, Z., F. Zhan, Y. Pan, Z. Lyu, C. Han, Y. Hu, P. Ding, T. Gao, X. Zhou, and Y. Jiang, *Structure of a novel Benzyl Quinolinium Chloride derivative and its effective corrosion inhibition in 15 wt.% hydrochloric acid.* Corrosion Science, 2015. **99**: p. 281-294.
168. Bentiss, F., M. Bouanis, B. Mernari, M. Traisnel, H. Vezin, and M. Lagrenée, *Understanding the adsorption of 4H-1,2,4-triazole derivatives on mild steel surface in molar hydrochloric acid.* Applied Surface Science, 2007. **253**(7): p. 3696-3704.
169. Li, X., S. Deng, X. Xie, and H. Fu, *Inhibition effect of bamboo leaves' extract on steel and zinc in citric acid solution.* Corrosion Science, 2014. **87**: p. 15-26.
170. Kumar, S.H. and S. Karthikeyan, *Torsemide and Furosemide as Green Inhibitors for the Corrosion of Mild Steel in Hydrochloric Acid Medium.* Industrial & Engineering Chemistry Research, 2013. **52**(22): p. 7457-7469.
171. Amin, M.A., O.A. Hazzazi, F. Kandemirli, and M. Saracoglu, *Inhibition Performance and Adsorptive Behavior of Three Amino Acids on Cold-Rolled Steel in 1.0 M HCl—Chemical, Electrochemical, and Morphological Studies.* CORROSION, 2012. **68**(8): p. 688-698.
172. Wan Ngah, W.S. and M.A.K.M. Hanafiah, *Adsorption of copper on rubber (Hevea brasiliensis) leaf powder: Kinetic, equilibrium and thermodynamic studies.* Biochemical Engineering Journal, 2008. **39**(3): p. 521-530.
173. Ahamad, M.R., Narren, S. F., Sadiq, A. S., *Synthesis of 2- Mercaptobenzimidazole and some of its Derivatives.* Journal of Al-Nahraim University, 2013. **16**(2): p. 77 - 83.
174. Kamil, M.M., M.S. Hussien, G.H. Ragab, and S.K. Khalil, *Detecting adulteration of durum wheat by FT-IR spectroscopy.* Journal of American Science, 2011. **7**(6): p. 573-578.
175. García-Saldaña, J.S., O.N. Campas-Baypoli, J. López-Cervantes, D.I. Sánchez-Machado, E.U. Cantú-Soto, and R. Rodríguez-Ramírez, *Microencapsulation of sulforaphane from broccoli seed extracts by gelatin/gum arabic and gelatin/pectin complexes.* Food Chemistry, 2016. **201**: p. 94-100.
176. Melanie, H., A. Susilowati, Y.M. Iskandar, P.D. Lotulung, and D.G.S. Andayani, *Characterization of Inulin from Local Red Dahlia (Dahlia sp. L) Tubers by Infrared Spectroscopy.* Procedia Chemistry, 2015. **16**: p. 78-84.

177. Apolinário, A.C., E.M. de Carvalho, B.P.G. de Lima Damasceno, P.C.D. Da Silva, A. Converti, A. Pessoa, and J.A. da Silva, *Extraction, isolation and characterization of inulin from Agave sisalana boles.* Industrial Crops and Products, 2017. **108**: p. 355-362.
178. Grube, M., M. Bekers, D. Upite, and E. Kaminska, *Infrared spectra of some fructans.* Spectroscopy, 2002. **16**(3-4).
179. Ibrahim, M., M. Alaam, H. El-Haes, A.F. Jalbout, and A.d. Leon, *Analysis of the structure and vibrational spectra of glucose and fructose.* Eclética Química, 2006. **31**: p. 15-21.
180. Gunnarsson, I.B., S.E. Svensson, E. Johansson, D. Karakashev, and I. Angelidaki, *Potential of Jerusalem artichoke (Helianthus tuberosus L.) as a biorefinery crop.* Industrial Crops and Products, 2014. **56**: p. 231-240.
181. Nadezhda, P. and D. Panteley. *Methods for determination of inulin*. in *Food, Technologies and Health*. 2015. Bulgaria: Agricultural Academy.
182. Nejatzadeh-Barandozi, F. and S.T. Enferadi, *FT-IR study of the polysaccharides isolated from the skin juice, gel juice, and flower of Aloe vera tissues affected by fertilizer treatment.* Organic and Medicinal Chemistry Letters, 2012. **2**: p. 33-33.
183. Jha, R., R. Dagar, and N. Sharma, *Ale vera gel mediated green synthesis of Fe_2O_3 nanoparticles* Int. J. of Innovation in engineering and Technology, 2016. **7**(1): p. 663-668.
184. Ravi, S., P. Kabilar, S. Velmurugan, R.a. Kumar, and M. Gayathiri, *Spectroscopy studies of the status of aloin in aloe vera and commercial samples.* Journal of experimental sciences, 2011. **2**(8): p. 10-13.
185. Johanna, M.W., *X-Ray Photoelectron Spectroscopy*. 2010, Nova Science Publishers, Inc.: United Kingdom. p. 1-290
186. Biesinger, M.C., B.P. Payne, A.P. Grosvenor, L.W.M. Lau, A.R. Gerson, and R.S.C. Smart, *Resolving surface chemical states in XPS analysis of first-row transition metals, oxides and hydroxides: Cr, Mn, Fe, Co and Ni.* Applied Surface Science, 2011. **257**(7): p. 2717-2730.
187. Andrade, J.D., *X-ray Photoelectron Spectroscopy (XPS)*, in *Surface and Interfacial Aspects of Biomedical Polymers: Volume 1 Surface Chemistry and Physics*, J.D. Andrade, Editor. 1985, Springer US: Boston, MA. p. 105-195.
188. Tian, H., W. Li, A. Liu, X. Gao, P. Han, R. Ding, C. Yang, and D. Wang, *Controlled delivery of multi-substituted triazole by a metal-organic framework for efficient inhibition of mild steel corrosion in neutral chloride solution.* Corrosion Science, 2018. **131**: p. 1-16.
189. Luo, X., X. Pan, S. Yuan, S. Du, C. Zhang, and Y. Liu, *Corrosion inhibition of mild steel in simulated seawater solution by a green eco-friendly mixture of glucomannan (GL) and bis-quaternary ammonium salt (BQAS).* Corrosion Science, 2017. **125**: p. 139-151.
190. Barmatov, E. and T.L. Hughes, *Effect of corrosion products and turbulent flow on inhibition efficiency of propargyl alcohol on AISI 1018 mild carbon steel in 4M hydrochloric acid.* Corrosion Science, 2017. **123**: p. 170-181.
191. Finšgar, M. and D.K. Merl, *2-Mercaptobenzoxazole as a copper corrosion inhibitor in chloride solution: Electrochemistry, 3D-profilometry, and XPS surface analysis.* Corrosion Science, 2014. **80**: p. 82-95.
192. Grosvenor, A.P., B.A. Kobe, M.C. Biesinger, and N.S. McIntyre, *Investigation of multiplet splitting of Fe 2p XPS spectra and bonding in iron compounds.* Surface and Interface Analysis, 2004. **36**(12): p. 1564-1574.

193. Mantel, M., Wightman, J.P., *Influence of the surface chemistry on the wettability of stainless steel* Surface and Interface Analysis, 1994. **33**(7): p. 591-594.
194. Meng, Y., W. Ning, B. Xu, W. Yang, K. Zhang, Y. Chen, L. Li, X. Liu, J. Zheng, and Y. Zhang, *Inhibition of mild steel corrosion in hydrochloric acid using two novel pyridine Schiff base derivatives: a comparative study of experimental and theoretical results.* RSC Advances, 2017. **7**(68): p. 43014-43029.
195. Szklarska-Smialowska, Z., *Pitting and corrosion*. 2005, Texas: NACE International.
196. Ravari, F.B. and D. Athareh, *Synergistic influence of propargyl alcohol and zinc sulphate on inhibition of corrosion of aluminium in 0.5 m H_2SO_4* J. Chil. Chem. Soc., 2013. **58**(3): p. 1853-1857.
197. El Hamdani, N., R. Fdil, M. Tourabi, C. Jama, and F. Bentiss, *Alkaloids extract of Retama monosperma (L.) Boiss. seeds used as a novel eco-friendly inhibitor for carbon steel corrosion in 1M HCl solution: Electrochemical and surface studies.* Applied Surface Science, 2015. **357**: p. 1294-1305.
198. Podobaev, N.I. and Y.G. Avdeev, *Temperature and Time Effects on the Acid Corrosion of Steel in the Presence of Acetylenic Inhibitors.* Protection of Metals, 2001. **37**(6): p. 529-533.
199. Amin, M.A., M.A. Ahmed, H.A. Arida, T. Arslan, M. Saracoglu, and F. Kandemirli, *Monitoring corrosion and corrosion control of iron in HCl by non-ionic surfactants of the TRITON-X series – Part II. Temperature effect, activation energies and thermodynamics of adsorption.* Corrosion Science, 2011. **53**(2): p. 540-548.
200. Noor, E., *Temperature effects on the corrosion inhibition of mild steel in acidic solutions by aqueous extract of fenugreek leaves.* Int. J. of Electrochem. Sci., 2007. **2**: p. 996-1017.
201. Nascimento, R.C., L.B. Furtado, M.J.O.C. Guimarães, P.R. Seidl, J.C. Rocha, J.A.C. Ponciano, and M.T.M. Cruz, *Synergistic effect of propargyl alcohol, octadecylamine, and 1,3-dibutyl thiourea for API P110 alloys in acetic and formic acidic solutions used in oil well acidizing.* Journal of Molecular Liquids, 2018. **256**: p. 548-557.
202. D., J., M. S., S. P., V. G., and S. S., *Propargyl alcohol as hydrochloric acid inhibitor for mild steel - temperature dependence of critical concentration.* Anti-Corrosion Methods and Materials, 1997. **44**(4): p. 265-268.
203. Vinutha, M.R. and T.V. Venkatesha, *Review on mechanistic action of inhibitors on steel corrosion in acidic media.* Portugaliae Electrochimica Acta, 2016. **34**: p. 157-184.
204. Gopiraman, M., N. Selvakumaran, D. Kesavan, and R. Karvembu, *Adsorption and corrosion inhibition behaviour of N-(phenylcarbamothioyl)benzamide on mild steel in acidic medium.* Progress in Organic Coatings, 2012. **73**(1): p. 104-111.
205. Popova, A., M. Christov, and A. Vasilev, *Inhibitive properties of quaternary ammonium bromides of N-containing heterocycles on acid, mild steel corrosion. Part I: Gravimetric and voltammetric results.* Corrosion Science, 2007. **49**(8): p. 3276-3289.
206. Szauer, T. and A. Brandt, *Adsorption of oleates of various amines on iron in acidic solution.* Electrochimica Acta, 1981. **26**(9): p. 1253-1256.

207. Szauer, T. and A. Brandt, *On the role of fatty acid in adsorption and corrosion inhibition of iron by amine—fatty acid salts in acidic solution.* Electrochimica Acta, 1981. **26**(9): p. 1257-1260.
208. Riggs, O.L. and R.M. Hurd, *Temperature Coefficient of Corrosion Inhibition.* CORROSION, 1967. **23**(8): p. 252-260.
209. Fiaud, C., A. Harch, D. Mallouh, and M. Tzinmann, *The inhibition of iron corrosion by acetylenic alcohols in acid solutions at high temperature.* Corrosion Science, 1993. **35**(5): p. 1437-1444.
210. Feng, Y., K.S. Siow, W.K. Teo, and A.K. Hsieh, *The synergistic effects of propargyl alcohol and potassium iodide on the inhibition of mild steel in 0.5 M sulfuric acid solution.* Corrosion Science, 1999. **41**(5): p. 829-852.
211. Mars, G.F. and W.S. Roger, *Advances in corrosion science and technology*. Vol. 1. 1970, New York: Plenum
212. Growcock, F. and U. Lopp, *The inhibition of steel corrosion in hydrochloric acid with 3-phenyl-2-propyn-1-ol.* Corro Sci, 1988. **28**: p. 397 - 410.
213. Bartos, M., S.D. Kapusta, and N. Hackerman, *A Study of Polymerization of Propargyl Alcohol on Steel.* Journal of The Electrochemical Society, 1993. **140**(9): p. 2604-2605.
214. Yang, B., N.G. Smart, and J.O.M. Bockris, *Ellipsometric investigation of the adsorption of acetylenic alcohols on iron.* Electrochimica Acta, 1992. **37**(2): p. 317-326.
215. Tedeschi, R., *Acetylenic corrosion inhibitors.* Corrosion, 1975. **31**(4): p. 130-134.
216. Duwell, E.J., J.W. Todd, and H.C. Butzke, *The mechanism of corrosion inhibition of steel by ethynylcyclohexanol in acid solution.* Corrosion Science, 1964. **4**(1): p. 435-441.
217. Chan-Rosado, G. and M.A. Pech-Canul, *The Inhibition Effect of Sodium Glutarate towards Carbon Steel Corrosion in Neutral Aqueous Solutions.* International Journal of Corrosion, 2016: p. 1-12.
218. Finšgar, M., *2-Mercaptobenzimidazole as a copper corrosion inhibitor: Part II. Surface analysis using X-ray photoelectron spectroscopy.* Corrosion Science, 2013. **72**(Supplement C): p. 90-98.
219. O., O.X., L.N. V., M.P. R., and D.A.M. A., *Electrochemistry and XPS study of an imidazoline as corrosion inhibitor of mild steel in an acidic environment.* Materials and Corrosion, 2009. **60**(1): p. 14-21.
220. Ekanem, U.F., S.A. Umoren, I.I. Udousoro, and A.P. Udoh, *Inhibition of mild steel corrosion in HCl using pineapple leaves (Ananas comosus L.) extract.* Journal of Materials Science, 2010. **45**(20): p. 5558-5566.
221. Amin, M.A., S.S. Abd El-Rehim, E.E.F. El-Sherbini, and R.S. Bayoumi, *The inhibition of low carbon steel corrosion in hydrochloric acid solutions by succinic acid: Part I. Weight loss, polarization, EIS, PZC, EDX and SEM studies.* Electrochimica Acta, 2007. **52**(11): p. 3588-3600.
222. Bentiss, F., M. Lebrini, and M. Lagrenée, *Thermodynamic characterization of metal dissolution and inhibitor adsorption processes in mild steel/2,5-bis(n- thienyl)-1,3,4-thiadiazoles/hydrochloric acid system.* Corrosion Science, 2005. **47**(12): p. 2915-2931.
223. Soltani, N., M. Behpour, S.M. Ghoreishi, and H. Naeimi, *Corrosion inhibition of mild steel in hydrochloric acid solution by some double Schiff bases.* Corrosion Science, 2010. **52**(4): p. 1351-1361.

224. Yilmaz, N., A. Fitoz, ÿ. Ergun, and K.C. Emregül, *A combined electrochemical and theoretical study into the effect of 2-((thiazole-2-ylimino)methyl)phenol as a corrosion inhibitor for mild steel in a highly acidic environment.* Corrosion Science, 2016. **111**: p. 110-120.
225. Obot, I.B. and N.O. Obi-Egbedi, *Theoretical study of benzimidazole and its derivatives and their potential activity as corrosion inhibitors.* Corrosion Science, 2010. **52**(2): p. 657-660.
226. Zarrok, H., A. Zarrouk, B. Hammouti, R. Salghi, C. Jama, and F. Bentiss, *Corrosion control of carbon steel in phosphoric acid by purpald – Weight loss, electrochemical and XPS studies.* Corrosion Science, 2012. **64**: p. 243-252.
227. Negm, N.A., M.F. Zaki, M.M. Said, and S.M. Morsy, *Inhibitory action of biodegradable modified vanillin on the corrosion of carbon steel in 1M HCl.* Corrosion Science, 2011. **53**(12): p. 4233-4240.
228. Ahamad, I., R. Prasad, and M.A. Quraishi, *Adsorption and inhibitive properties of some new Mannich bases of Isatin derivatives on corrosion of mild steel in acidic media.* Corrosion Science, 2010. **52**(4): p. 1472-1481.
229. Rehim, S.S.A., O.A. Hazzazi, M.A. Amin, and K.F. Khaled, *On the corrosion inhibition of low carbon steel in concentrated sulphuric acid solutions. Part I: Chemical and electrochemical (AC and DC) studies.* Corrosion Science, 2008. **50**(8): p. 2258-2271.
230. Liao, L.L., S. Mo, H.Q. Luo, Y.J. Feng, H.Y. Yin, and N.B. Li, *Relationship between inhibition performance of melamine derivatives and molecular structure for mild steel in acid solution.* Corrosion Science, 2017. **124**: p. 167- 177.
231. Osman, M.M. and M.N. Shalaby, *Some ethoxylated fatty acids as corrosion inhibitors for low carbon steel in formation water.* Materials Chemistry and Physics, 2003. **77**(1): p. 261-269.
232. Haque, J., V. Srivastava, D.S. Chauhan, H. Lgaz, and M.A. Quraishi, *Microwave-Induced Synthesis of Chitosan Schiff Bases and Their Application as Novel and Green Corrosion Inhibitors: Experimental and Theoretical Approach.* ACS Omega, 2018. **3**(5): p. 5654-5668.
233. Shukla, S.K. and M.A. Quraishi, *4-Substituted anilinomethylpropionate: New and efficient corrosion inhibitors for mild steel in hydrochloric acid solution.* Corrosion Science, 2009. **51**(9): p. 1990-1997.
234. Herrag, L., B. Hammouti, S. Elkadiri, A. Aouniti, C. Jama, H. Vezin, and F. Bentiss, *Adsorption properties and inhibition of mild steel corrosion in hydrochloric solution by some newly synthesized diamine derivatives: Experimental and theoretical investigations.* Corrosion Science, 2010. **52**(9): p. 3042-3051.
235. Pun, A.F. and J.P. Zheng, *Utilizing gallium arsenide sacrificial films to inhibit surface roughening during the thermal desorption of gallium arsenide.* Electrochemical and Solid State Letters, 2007. **10**(6): p. H189-H192.
236. Hassan, H.H., *Inhibition of mild steel corrosion in hydrochloric acid solution by triazole derivatives: Part II: Time and temperature effects and thermodynamic treatments.* Electrochimica Acta, 2007. **53**(4): p. 1722-1730.
237. Daoud, D., T. Douadi, H. Hamani, S. Chafaa, and M. Al-Noaimi, *Corrosion inhibition of mild steel by two new S-heterocyclic compounds in 1 M HCl: Experimental and computational study.* Corrosion Science, 2015. **94**: p. 21-37.
238. Ostovari, A., S.M. Hoseinieh, M. Peikari, S.R. Shadizadeh, and S.J. Hashemi, *Corrosion inhibition of mild steel in 1M HCl solution by henna extract:*

A comparative study of the inhibition by henna and its constituents (Lawsone, Gallic acid, α-d-Glucose and Tannic acid). Corrosion Science, 2009. **51**(9): p. 1935-1949.

239. Glibowski, P. and A. Bukowska, *The effect of pH, temperature and heating time on inulin chemical stability.* Acta Sci. Pol., Technol. Aliment, 2011. **10**(2): p. 189-196.
240. Olivares-Xometl, O., N.V. Likhanova, M.A. Domínguez-Aguilar, J.M. Hallen, L.S. Zamudio, and E. Arce, *Surface analysis of inhibitor films formed by imidazolines and amides on mild steel in an acidic environment.* Applied Surface Science, 2006. **252**(6): p. 2139-2152.
241. Solmaz, R., *Investigation of corrosion inhibition mechanism and stability of Vitamin B1 on mild steel in 0.5M HCl solution.* Corrosion Science, 2014. **81**: p. 75-84.
242. Bockris, J.O.M. and D.A.J. Swinkels, *Adsorption of n-Decylamine on Solid Metal Electrodes.* Journal of The Electrochemical Society, 1964. **111**(6): p. 736- 743.
243. Bockris, J.O.M., M. Green, and D.A.J. Swinkels, *Adsorption of Naphthalene on Solid Metal Electrodes.* Journal of The Electrochemical Society, 1964. **111**(6): p. 743-748.
244. Shokry, H., M. Yuasa, I. Sekine, R.M. Issa, H.Y. El-baradie, and G.K. Gomma, *Corrosion inhibition of mild steel by Schiff base compounds in various aqueous solutions: part 1.* Corrosion Science, 1998. **40**(12): p. 2173-2186.
245. Saha, S.K., A. Dutta, P. Ghosh, D. Sukul, and P. Banerjee, *Adsorption and corrosion inhibition effect of Schiff base molecules on the mild steel surface in 1 M HCl medium: a combined experimental and theoretical approach.* Physical Chemistry Chemical Physics, 2015. **17**(8): p. 5679-5690.
246. Garai, S., S. Garai, P. Jaisankar, J.K. Singh, and A. Elango, *A comprehensive study on crude methanolic extract of Artemisia pallens (Asteraceae) and its active component as effective corrosion inhibitors of mild steel in acid solution.* Corrosion Science, 2012. **60**: p. 193-204.
247. Torres, V.V., V.A. Rayol, M. Magalhaes, G.M. Viana, L.C.S. Aguiar, S.P. Machado, H. Orofino, and E. D'Elia, *Study of thioureas derivatives synthesized from a green route as corrosion inhibitors for mild steel in HCl solution.* Corrosion Science, 2014. **79**: p. 108-118.
248. Thomas, B., M. Milena, C. Peter, and P. Nikolai, *Inulin- a versatile polysaccharide with multiple pharmaceutical and food chemical users.* J. Experimental and Food Chem., 2010. **1**(3): p. 27-50.
249. Deng, S., X. Li, and H. Fu, *Acid violet 6B as a novel corrosion inhibitor for cold rolled steel in hydrochloric acid solution.* Corrosion Science, 2011. **53**(2): p. 760-768.
250. Bentiss, F., M. Traisnel, and M. Lagrenee, *The substituted 1,3,4-oxadiazoles: a new class of corrosion inhibitors of mild steel in acidic media.* Corrosion Science, 2000. **42**(1): p. 127-146.
251. Bio-Tech, X.A. *3W supply Inulin Powder, 90% Inulin Powder (Chicory Extract, Natural Plant Extract)*. 2016 [cited 14/6/2016]; Available from: http://www.extractsupplier.com/3w-supply-inulin-powder-90-inulin-powder-chicory-extract-natural-plant-extract-28460/.
252. Li, X., S. Deng, H. Fu, and G. Mu, *Inhibition effect of 6-benzylaminopurine on the corrosion of cold rolled steel in H_2SO_4 solution.* Corrosion Science, 2009. **51**(3): p. 620-634.

253. He, X., Y. Jiang, C. Li, W. Wang, B. Hou, and L. Wu, *Inhibition properties and adsorption behaviour of imidazole and 2-phenyl-2-imidazoline on AA5052 in 1.0M HCl solution.* Corrosion Science, 2014. **83**: p. 124-136.
254. Xu, B., W. Yang, Y. Liu, X. Yin, W. Gong, and Y. Chen, *Experimental and theoretical evaluation of two pyridinecarboxaldehyde thiosemicarbazone compounds as corrosion inhibitors for mild steel in hydrochloric acid solution.* Corrosion Science, 2014. **78**: p. 260-268.
255. Bentiss, F., C. Jama, B. Mernari, H.E. Attari, L.E. Kadi, M. Lebrini, M. Traisnel, and M. Lagrenée, *Corrosion control of mild steel using 3,5-bis(4-methoxyphenyl)-4-amino-1,2,4-triazole in normal hydrochloric acid medium.* Corrosion Science, 2009. **51**(8): p. 1628-1635.
256. Bentiss, F., M. Lagrenée, and M. Traisnel, *2,5-Bis(n-Pyridyl)-1,3,4-Oxadiazoles as Corrosion Inhibitors for Mild Steel in Acidic Media.* CORROSION, 2000. **56**(7): p. 733-742.
257. Prakashaiah, B.G., D. Vinaya Kumara, A. Anup Pandith, A. Nityananda Shetty, and B.E. Amitha Rani, *Corrosion inhibition of 2024-T3 aluminium alloy in 3.5% NaCl by thiosemicarbazone derivatives.* Corrosion Science, 2018. **136**: p. 326-338.
258. Giannetti, V., M.B. Mariani, and P. Mannino, *Furosine as a Pasta Quality Marker: Evaluation by an Innovative and Fast Chromatographic Approach.* Journal of Food Science, 2013. **78**(7): p. 994-999.
259. *Corrosion Inhibition of Carbon Steel in HCl Solution by Some Plant Extracts.* International Journal of Corrosion, 2012. **2012**.
260. Kosari, A., M. Momeni, R. Parvizi, M. Zakeri, M.H. Moayed, A. Davoodi, and H. Eshghi, *Theoretical and electrochemical assessment of inhibitive behaviour of some thiophenol derivatives on mild steel in HCl.* Corrosion Science, 2011. **53**(10): p. 3058-3067.
261. Elphick, D. and K. Voisey, *Experimental investigation of green corrosion inhibitors for the application of acidization*. 2015, University of Nottingham. p. 1-9.
262. Lee, I.S.L., M.C. Boyce, and M.C. Breadmore, *Extraction and on-line concentration of flavonoids in Brassica oleracea by capillary electrophoresis using large volume sample stacking.* Food Chemistry, 2012. **133**(1): p. 205-211.
263. Francisco, M., P. Velasco, D.A. Moreno, C. García-Viguera, and M.E. Cartea, *Cooking methods of Brassica rapa affect the preservation of glucosinolates, phenolics and vitamin C.* Food Research International, 2010. **43**(5): p. 1455-1463.
264. Yvette and Porter, *Antioxidant properties of green broccoli and purple-sprouting broccoli under different cooking conditions* Bioscience Horizons, 2012. **5**: p. 1-11.
265. Zhang, D. and Y. Hamauzu, *Phenolics, ascorbic acid, carotenoids and antioxidant activity of broccoli and their changes during conventional and microwave cooking.* Food Chemistry, 2004. **88**(4): p. 503-509.
266. Wachtel-Galor, S., K.W. Wong, and I.F.F. Benzie, *The effect of cooking on Brassica vegetables.* Food Chemistry, 2008. **110**(3): p. 706-710.
267. Khamis, E., *The Effect of Temperature on the Acidic Dissolution of Steel in the Presence of Inhibitors.* CORROSION, 1990. **46**(6): p. 476-484.
268. Josias, H.H., *Composition and applications of aloe vera leaf gel.* Molecules, 2008. **13**(8): p. 1599-1616.

269. Shama, S., *Green Corrosion Chemistry and Engineering: opportunities and challenges*. 2009, Germany: Wiley-VCH.
270. Bartos, M. and N. Hackerman, *A study of inhibition action of propargyl alcohol during the anodic dissolution of iron in hydrochloric acid.* Journal of the Electrochemical Society, 1992. **139**(12): p. 3428-3433.
271. Benítez, S., I. Achaerandio, M. Pujolà, and F. Sepulcre, *Aloe vera as an alternative to traditional edible coatings used in fresh-cut fruits: A case of study with kiwifruit slices.* LWT - Food Science and Technology, 2015. **61**(1): p. 184- 193.
272. Boudreau, M.D. and F.A. Beland, *An Evaluation of the Biological and Toxicological Properties of Aloe Barbadensis (Miller), Aloe Vera.* Journal of Environmental Science and Health, Part C, 2006. **24**(1): p. 103-154.
273. Tiu, B.D.B. and R.C. Advincula, *Polymeric corrosion inhibitors for the oil and gas industry: Design principles and mechanism.* Reactive and Functional Polymers, 2015. **95**: p. 25-45.
274. Reza, J., *How corrosion affects industry and life.* Anti-Corrosion Methods and Materials, 2000. **47**(1): p. 30-34.
275. Koch, G., J. Varney, N. Thompson, O. Moghissi, G. M., and J. Payer. *International measures of prevention, application, and economics of corrosion technologiesstudy*.[cited30/05/2018]; Availablefrom http://impact.nace.org/documents/Nace-International-report.pdf.
276. Dwivedi, D., K. Lepkova, and T. Becker, *Carbon steel corrosion: a review of key surface properties and characterization methods.* RSC Advances, 2017. **7**(8): p. 4580-4610.
277. Calzarano, F., F. Stagnari, S. D'Egidio, G. Pagnani, A. Galieni, S. Di Marco, E. Metruccio, and M. Pisante, *Durum Wheat Quality, Yield and Sanitary Status under Conservation Agriculture.* Agriculture, 2018. **8**(9): p. 140.
278. Johansson, E., T. Prade, I. Angelidaki, S.-E. Svensson, W.R. Newson, I.B. Gunnarsson, and H.P. Hovmalm, *Economically Viable Components from Jerusalem Artichoke (Helianthus tuberosus L.) in a Biorefinery Concept.* International Journal of Molecular Sciences, 2015. **16**(4): p. 8997-9016.
279. Mensink, M.A., H.W. Frijlink, K. van der Voort Maarschalk, and W.L.J. Hinrichs, *Inulin, a flexible oligosaccharide I: Review of its physicochemical characteristics.* Carbohydrate Polymers, 2015. **130**: p. 405-419.
280. Cerezuela, R., A. Cuesta, J. Meseguer, and M.A. Esteban, *Effect of dietary inulin and heat-inactivated Bacillus subtillis on gilthead seabream (Sparus aurata L.) innate immune parameters.* Beneficial microbes, 2012. **3**(1): p. 77- 81.
281. Latté, K.P., K.E. Appel, and A. Lampen, *Health benefits and possible risks of broccoli – An overview.* Food and Chemical Toxicology, 2011. **49**(12): p. 3287- 3309.
282. AgriFarming. *Cost and Profit of Aloe Vera Farming*. 2015 [cited 12th December, 2016]; Available from: http://www.agrifarming.in/aloe-vera-farming.